TECHNICAL UNIVERSITY OF CATALONIA

DEPARTMENT OF GEOTECHNICAL ENGINEERING AND GEOSCIENCES

SCHOOL OF CIVIL ENGINEERING

THERMO-HYDRO-MECHANICAL BEHAVIOUR OF EXPANSIVE CLAYS UNDER HIGH TEMPERATURES

Application to the Temperature Buffer Test Project

PhD Thesis

by:

Abel Carlos Jacinto

Supervised by:

Alberto Ledesma Villalba

Barcelona, May 2010

A Fátima, Santiago y Martina

A la memoria de mi madre, Sara

Abstract

This Thesis presents the results of the research carried out in the framework of the Temperature Buffer Test (TBT) project. The overall objective of this project is to investigate how well the bentonite used in engineered barriers can endure the high temperatures expected to be found around vitrified waste canisters. Within the project, a full-scale field test that simulates the deposition of high level radioactive waste has been implemented. Additionally, laboratory experiments were carried out to evaluate the response of the bentonite used in the project under different external actions.

Coupled formulations used to analyse the behaviour of an engineered clay barrier are written in terms of the state variables by using constitutive relations. Among these laws the soil water retention curve (SWRC) defines the constitutive relationship between the amount of water in the soil and its energy status. Traditionally, the influence of external variables like temperature and soil fabric on the water retention capacity of soils has been analysed using concepts derived from the capillary model. However, theses analyses systematically failed to explain the experimental observations. In this Thesis, experimental data obtained on bentonite samples tested at different temperatures and densities were evaluated using an approach derived from concepts of thermodynamic of adsorption. This approach also gives a tool to introduce in a simple way the effect of temperature and sample porosity in numerical simulations.

It is generally accepted that the interaction between smectite, which is the main mineral of bentonite, and water changes the properties of the water retained in the soil. In particular, values of the water density higher than 1.0 Mg/m^3 (i.e. the density of the free water) have been suggested by experiments at mineralogical level as well as by data obtained on compacted samples of expansive clays. From a practical point of view this effect traduces in values of degree of saturation higher than one at lower values of suction. This is important when a numerical analysis is being performed, as balance equations are based on the degree of saturation as the main variable to indicate the water content within the porous medium. In this Thesis a methodology that defines the water density as a function of the energy of the water within the soil pores was developed. This method was applied to analyse published data about the water retention capacity for compacted samples of different bentonites.

The analysis of the mechanical response of expansive clays under external actions as those typically found in engineered barriers is a complex task. Constitutive models used in numerical calculations have to be able to simulate the main aspects of the material response. Models previously developed to simulate the behaviour of compacted samples made up of expansive clay were adopted in this Thesis. Parameters in these models were calibrated using experimental data corresponding to compacted samples of MX-80 bentonite, the material adopted as reference in the TBT project.

Concepts developed in the Thesis were included in a numerical code able to solve coupled problems in deformable porous media. This code was then applied to the analysis of a mock-up experiment and to the simulation of the in situ test carried out within the framework of the TBT project. Theses numerical simulations showed the capabilities of the code to capture the general tendency of the experimental data. Additionally, the analysis of numerical results enhanced the understanding of the different phenomena that take place in coupled processes as well as the interaction mechanisms between them.

Resumen

Esta Tesis presenta los resultados de la investigación desarrollada en el marco del proyecto Temperature Buffer Test (TBT). El objetivo general de este proyecto es investigar el desempeño de la bentonita usada en barreras de ingeniería bajo la acción de las altas temperaturas que se esperan alrededor de los contenedores con residuos vitrificados. Dentro del proyecto, se ha implementado un ensayo de campo a escala real que simula el almacenamiento de residuos radioactivos de alta actividad. Adicionalmente, se realizaron experimentos en laboratorio para evaluar la respuesta de la bentonita usada en el proyecto bajo diferentes acciones externas.

Las formulaciones que se usan para analizar el comportamiento de barreras de ingeniería de arcillas se escriben en términos de las variables de estado usando relaciones constitutivas. Entre esas leyes la curva de retención define la relación constitutiva entre la cantidad de agua en el suelo y su nivel de energía. Tradicionalmente, la influencia de variables externas como la temperatura y la fábrica del suelo sobre la capacidad de retención de agua del suelo se analiza utilizando conceptos derivados del modelo capilar. Sin embargo, estos análisis sistemáticamente fallaron para explicar las observaciones experimentales. En esta Tesis, se han evaluado los datos experimentales obtenidos en muestras de bentonita ensayadas a diferentes temperaturas y densidades usando una aproximación derivada a partir de conceptos de termodinámica de adsorción. Esta aproximación también define una herramienta para introducir en una manera simple el efecto de temperatura y densidad de la muestra en las simulaciones numéricas.

En general se supone que la interacción entre la esmectita, que es el principal mineral de la bentonita, y el agua cambia las propiedades del agua retenida en el suelo. En particular, experimentos a nivel mineralógico así como los datos obtenidos en muestras compactadas de arcilla expansiva sugieren valores de la densidad del agua mayores que 1.0 Mg/m^3 (es decir, la densidad del agua libre). Desde un punto de vista práctico, este efecto se traduce en valores calculados del grado de saturación mayor que uno para valores bajos de succión. Este aspecto es importante cuando se realizan análisis numéricos, debido a que las ecuaciones de balance se basan en el grado de saturación como la principal variable para indicar el contenido de agua en el medio poroso. En esta Tesis se ha desarrollado una metodología que define la densidad del agua como una función de la energía del agua en los poros del suelo.

Este método fue usado para analizar datos publicados de la capacidad de retención de agua de muestras compactadas de diferentes bentonitas.

El análisis de la respuesta mecánica de arcillas expansivas bajo acciones externas como aquellas típicamente encontradas en barreras de ingeniería es una tarea compleja. Los modelos constitutivos usados en los cálculos numéricos deben ser capaces de simular los principales aspectos de la respuesta material. En esta Tesis se han adoptado modelos previamente desarrollados para simular el comportamiento de muestras compactadas de arcilla expansiva. Los parámetros de estos modelos se calibraron usando datos experimentales que corresponden a muestras compactadas de bentonita MX-80, el material adoptado como referencia en el proyecto TBT.

Los conceptos desarrollados en esta Tesis se incorporaron en un código numérico capaz de resolver problemas acoplados en medios porosos deformables. Este código fue aplicado tanto para el análisis de un ensayo de maqueta como para la simulación del ensayo in situ, ambos desarrollados en el marco del proyecto TBT. Las simulaciones numéricas demostraron las capacidades del código para capturar la tendencia general de los datos experimentales. Además, el análisis de los resultados numéricos puso de manifiesto los diferentes fenómenos que tienen lugar en los procesos acoplados así como los mecanismos de interacción entre ellos.

Agradecimientos

Deseo expresar mi agradecimiento al Profesor Alberto Ledesma Villalba por la dirección de esta tesis, y especialmente por sus palabras de apoyo y ánimo en momentos difíciles durante el desarrollo de la misma. Su predisposición a escuchar propuestas y el aporte de sus ideas han sido fundamentales durante este trabajo de investigación. Agradezco también a los miembros del Departamento que han colaborado de manera incondicional durante la elaboración de este trabajo. Mi estancia junto al grupo humano que conforma este Departamento ha sido una experiencia sumamente enriquecedora. A los miembros administrativos gracias por su colaboración en las distintas instancias del doctorado.

Agradezco a los miembros del Instituto de Estructuras de la Universidad Nacional de Tucumán su apoyo y estímulo durante estos años. A la Facultad de Ciencias Exactas y Tecnología el haberme esperado pacientemente durante mi formación en Barcelona.

Este trabajo ha sido posible gracias al apoyo económico recibido por parte de diferentes instituciones. En primer lugar mi gratitud a la Comisión Europea quien inicialmente financió mis estudios a través del programa Alβan. También quiero agradecer el apoyo económico recibido durante estos años, a través del CIMNE, por parte de ANDRA, ENRESA y SKB.

Agradezco también a aquellas personas con las que he interactuado más activamente por aspectos relacionados al proyecto TBT. Mi reconocimiento a Mattias Åkesson de Clay Technology AB y a María Victoria Villar del CIEMAT por el interés que han tenido en este trabajo y por las valiosas sugerencias realizadas. Agradezco a Marcelo Sánchez su colaboración y dedicación durante mi estancia en Glasgow.

A mis compañeros de doctorado les agradezco los buenos momentos compartidos a lo largo de estos años como así también las discusiones de las que tanto he aprendido. Espero que las vueltas de la vida nos permitan re-encontrarnos en otros sitios alguna vez.

A los amigos que hemos hecho durante nuestro paso por Barcelona: los Ardanás, Malet, Marinelli, Sombra Matiasich, Mayugo, Montenegro, Muñoz, Pérez, Riera Vallejan, Sánchez, Soto, Segura Serra, Varese. Me llevo el recuerdo de los buenos

Table of contents

Notation

A_α : coefficient in the relative permeability law

A^e : Helmholtz free energy of the adsorbed phase

D_0 : diffusivity

D_m^w : coefficient of water molecular diffusion in gas

$\mathbf{D}_g^w$: effective diffusion coefficient of water in the gas phase

e : void ratio

e_w : water ratio

f_β : interaction functions between micro and macrostructure

f_i : fugacity of the i component

$\mathbf{g}$, g : gravity

G^a : Gibbs free energy of the adsorbed phase per unit mass of adsorbent

G^e : Gibbs free energy of the adsorbed phase

G_s : relation between solid density and water density

G_t : Gibbs free energy of soil water

h_t : soil water potential head

H^e : enthalpy of the adsorbed phase

$\mathbf{i}_c$: conductive flux of heat

$\mathbf{I}$: identity matrix

$k_{r\alpha}$: relative permeability of the α phase

$\mathbf{k}$: tensor of intrinsic permeability

$\mathbf{k}_0$: tensor of reference intrinsic permeability

K_m : microstructural bulk modulus

m : coefficients in the expression of the soil water retention curve

m : mass of solid adsorbent

n_α : coefficient in the relative permeability law

M_w : molar mass of water

n_j : amount of moles of the j component in the system

n_i^a, n_i^e : amount adsorbed of the i component per unit mass of adsorbent

p : net mean stress

p_0^* : pre-consolidation stress for a saturated state

p_0 : net mean pre-consolidation stress at suction s

p^c : reference stress

$\hat{p}$: microstructural mean effective stress

P_α : pressure in the α phase

P_c : capillary pressure

P_0 : coefficients in the expression of the soil water retention curve

P_v : vapour pressure at temperature T

P_v^0 : saturated vapour pressure at temperature T

P_v^{ref} : saturated vapour pressure at reference temperature T^{ref}

P_g^0 : reference pressure

$\mathbf{q}_\alpha$: advective flow of the α phase

r : radius of the capillary, material parameter (BBM)

R : universal gas constant

s : soil suction

$S_{\alpha e}$: effective degree of saturation of the α phase

S^a : entropy of the adsorbed phase per unit mass of adsorbent

S^e : entropy of the adsorbed phase

S_{lr} : minimum degree of saturation

S_{ls} : maximum degree of saturation

S_w : specific entropy of water in soil

T : absolute temperature

T^{ref}, T_0 : absolute reference temperature

U : total energy of the system

U^e : excess energy

U^g : energy of the gas phase

U^s : energy of the clean solid adsorbent

V^e : excess volume

V^g : volume of the gas phase

V^s : volume of the solid phase

V_w : specific volume of water in soil

w : gravimetric water content

x_i : generic thermodynamic state variable

y_i : mole fraction of the i component in the gas phase

z_0, z : reference elevation, elevation

∇ : gradient operator

α_m : material parameters of the microstructure (BExM)

β : material parameter (BBM)

β_m : material parameter of the microstructure (BExM)

Δg^e, $\Delta \overline{g}^e$: molar, differential Gibbs free energy of the adsorbed phase

ΔH_{vap} : enthalpy of vaporization

Δh^e, $\Delta \overline{h}^e$: molar, differential enthalpy of the adsorbed phase

Δs^e, $\Delta \overline{s}^e$: molar, differential entropy of the adsorbed phase

$\dot{\varepsilon}_v^p$: volumetric plastic strain increment

ϕ : porosity

ϕ_0 : reference porosity

Φ : surface potential of the solid adsorbent relative to its pure standard state

γ_g : leakage coefficient

γ_{gl} : liquid-gas interfacial tension

γ_{s0} : free surface energy of the clean surface of a solid

γ_{sf} : free surface energy when the surface of a solid is covered by a film

γ_{sv} : solid-vapour interfacial tension

φ : moisture ratio, spreading pressure

κ_i : slope of the unloading-reloading line in an $e - \ln(p)$ diagram

κ_s : slope of the reversible wetting-drying line in an $e - \ln(s)$ diagram

λ_T : soil thermal conductivity

λ_{dry} : soil thermal conductivity in dry state

λ_{sat} : soil thermal conductivity in saturated state

λ_0 : slope of the virgin saturated consolidation line

λ_s : slope of the virgin consolidation line at suction s

μ : chemical potential of the solid adsorbent defined on a mass basis

μ_α : dynamic viscosity of the α phase

μ_c : capillary potential on mass basis

μ_g : gas potential expressed on mass basis

μ_i : chemical potential of the i component in the gas phase

μ_m : matric potential expressed on mass basis

μ_p : pressure potential expressed on mass basis

Π : osmotic pressure

θ : volumetric water content

θ_{sl} : contact angle

ρ_α : density of the α phase

ρ_d : dry density of the soil sample

ρ^g : molar density of the bulk gas phase

Σ : specific surface area of the adsorbent

τ : tortuosity

ω_α^β : mass fraction of the β component in the α phase

Ω : total grand potential

Ω^e : excess free energy change

Ω^s : grand potential of the clean adsorbent in vacuo

ψ_b : oberburden pressure potential expressed on volume basis

ψ_g : gas pressure potential expressed on volume basis

ψ_h : hydrostatic pressure potential expressed on volume basis

ψ_m : matric potential expressed on volume basis

ψ_p : pressure potential expressed on volume basis

ψ_s : solute or osmotic potential expressed on volume basis

ψ_t : soil water potential expressed on volume basis

ψ_z : gravitational potential expressed on volume basis

Abbreviations and acronyms

ANDRA: French National Agency for Radioactive Waste Management

BBM: Barcelona Basic Model

BExM: Barcelona Expansive Model

CEA: French Atomic Energy Commission

CIEMAT: Research Centre for Energy, Environment and Technology

CODE_BRIGHT: COupled DEformation, BRlne, Gas and Heat Transport

ENRESA: Spanish Agency for Management of Radioactive Waste

ESEM: Environmental Scanning Electron Microscopy

FEBEX: Full-scale Engineered Barriers Experiment

GHG: GreenHouse Gases

IAEA: International Atomic Energy Agency

MIP: Mercury Intrusion Porosimetry

SKB: Swedish Nuclear Fuel and Waste Management Co.

SWRC: Soil Water Retention Curve

TBT: Temperature Buffer Test

THM: Thermo-Hydro-Mechanical

URLs: Underground Research Laboratories

Chapter 1

Introduction

Summary

A general overview on the scope and topics studied along the Thesis is given in this opening Chapter. The objectives of the research carried out and a layout of the overall document are also given.

1.1 Preface

According to the IAEA (International Atomic Energy Agency), in 2007 nuclear power accounted for an electricity production of 372 GW(e), about 14 % of the total electricity generated in the world. This proportion has remained basically constant since the late eighties. Every year since 1981 the IAEA has published two updated projections for the world's nuclear power generating capacity, a low projection and a high projection. In 2008, the low projection scenario of nuclear power capacity in 2030 is 27 % higher than today's capacity while in the high projection scenario is double today's capacity (MacDonald et al., 2008).

The increased use of nuclear power would help to meet the increase in energy demand, enhance the security of energy supplies and mitigate carbon emissions (ElBaradei, 2007). There are several reasons for renewed interest in nuclear power. For many countries, nuclear power is a way to enhance the security and diversity of their energy supplies. Another factor driving the interest in nuclear power is that it emits almost no greenhouse gases (GHG). The complete nuclear power chain - from mining the uranium and manufacturing the fuel to constructing and operating the reactor and disposing of the waste - emits only 1.6 grams of carbon equivalent per kW/h. This is about the same negligible emission rate as wind and hydropower and many times less than coal, oil and natural gas. An important factor is also the significant improvements in nuclear power plant reliability as well as lower operating costs and a progressively improved safety record.

The production of nuclear power and associated activities give rise to radioactive wastes. Significant amounts of radioactive waste also arise from dismantling nuclear reactors, an activity that will increase sharply in coming years due to the achievement of the planned lifetimes of power plants. Additional sources of nuclear waste are military nuclear activities and the use of radionuclides in medicine, research and industry. Those wastes must be disposed in an adequate manner (Gens, 2003). For waste management purposes, it is usual to distinguish different waste types. Geotechnical engineering has an important role to play in the area of waste management of all types of nuclear waste.

High level radioactive waste primarily consists of spent nuclear fuel. This waste is sufficiently hot and it has to be cooled. Some of the radioactive substances present in spent nuclear fuel have an extremely long half-life and this highly radioactive, long-lived

waste must therefore be stored safely over a very long period of time. Deep geological disposal is by far the possibility most likely to be implemented for the safe disposal of high level radioactive waste. Crystalline rock, natural clay, and salt have been considered as suitable host media in which a repository can be built. Figure 1.1 shows a typical scheme for an underground repository. It involves the sinking of deep shafts down to a depth of several hundred meters. The shafts provide access to a network of horizontal drifts that constitute the main repository area. Part of those drifts will be access tunnels and part will be devoted to nuclear waste disposal. Many options are contemplated regarding canister emplacement. A possibility is to place them in the horizontal drift itself but other options put them inside boreholes drilled from the main access tunnels. The boreholes may be vertical (as shown in Figure 1.1) or horizontal.
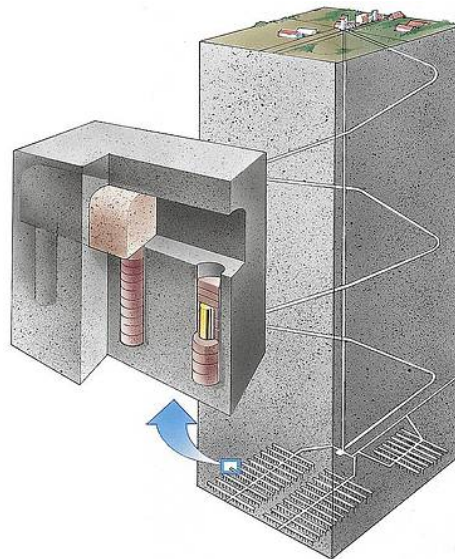
Figure 1.1. Sketch of a deep repository (http://www.skb.se).

The repository is built according to the multiple barrier principle which guarantees safety (Figure 1.2). This is based on placing several barriers, both natural and artificial, between the potentially harmful radionuclides and the biosphere. Nearest the fuel is the canister whose function is to isolate the fuel from the environment. The canister is surrounded by a buffer, often constructed using blocks of compacted expansive clay. Bentonite has generally been chosen because of its high swelling capacity, low permeability and favourable retardation properties. The rock constitutes the natural barrier and its primary purpose is to protect the canister and the buffer from mechanical damage and to offer a stable chemical environment.
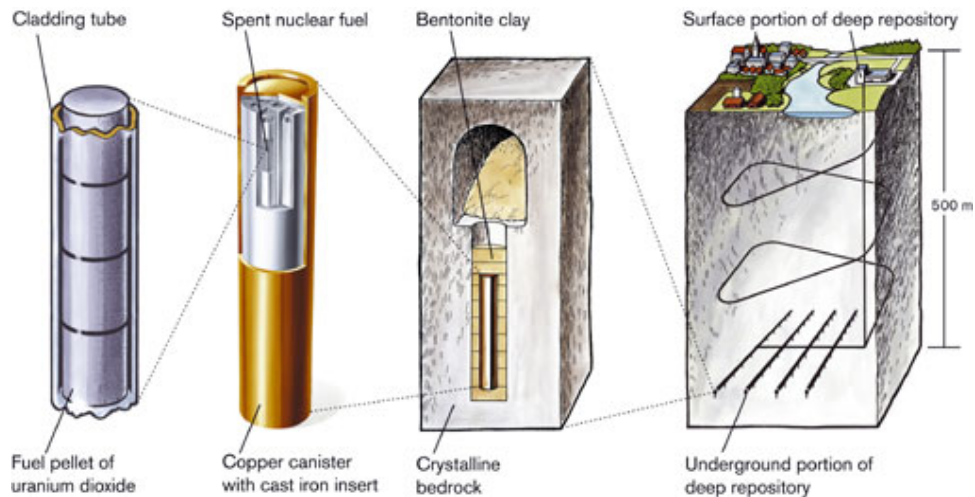
Figure 1.2. Sketch of the multiple barrier principle (http://www.skb.se).

To study the problem of high level nuclear waste disposal under conditions similar to those that will prevail in the real disposal facilities, underground research laboratories (URLs) have been built in different countries. They were excavated in rock types considered to be suitable for repository construction and, typically, they are located a few hundred meters below the surface. URLs are a key tool to integrate the various hydrologic, thermal, mechanical, chemical and biological phenomena and coupled processes in a realistic geological setting (Gens, 2003). The global behaviour of the repository systems tested in URLs must be complemented by means of carefully controlled laboratory experiments. The basic aim of the laboratory work is to determine the hydraulic and mechanical behaviour of the materials involved in a deep geological repository under controlled conditions of suction and temperature.

To improve the understanding of the various thermal, hydraulic and mechanical phenomena that take place in the buffer materials and adjacent host rock, different large-scale and medium-scale heating tests simulating repository conditions were implemented in underground laboratories around the world (Dixon et al., 2002; Chen & Ledesma, 2008; Gens et al., 2009). Additionally, coupled thermo-hydro-mechanical (THM) formulations have been developed (Pollock, 1986; Olivella et al., 1994; Gawin et al., 1995; Thomas et al., 1998). They are a useful tool to understand and interpret experimental results using suitable numerical models able to reproduce the main features of those experiments. In situ tests in underground laboratories are generally intensively instrumented, and often include a large amount of the independent data required to define the parameters of the coupled THM numerical model adequately.

1.2 Background

Compacted expansive clay is often the material of choice for constructing barriers in repositories located in natural clays or crystalline rocks. It plays an important role in the general performance of the engineering barrier. At the beginning, the main actions that affect the bentonite barrier are the heating arising from the canisters and the hydration from the surrounding rock. Its low hydraulic conductivity, micro-porous structure, good sorption properties and plasticity make this material an effective barrier. It is expected that the bentonite protects the canister and restricts the movement of radionuclides released from the waste packages after canister failure. This material is initially in an unsaturated state and to analyse its thermo-hydro-mechanical behaviour it will be necessary to consider a solid, liquid and gas phase.

Figure 1.3 shows, in a schematic way, some of the thermo-hydraulic processes occurring in the barrier and immediate adjacent rock (Gens, 2003; Gens et al., 2009). The heat flux from the canister is transferred by conduction through the three phases of the material. A temperature gradient will therefore develop in the near field and heat dissipation will be basically controlled by the thermal conductivity of the barrier and host rock. Degree of saturation and water pressure will reduce in the inner zone of the barrier due to the heat supplied by the waste. Vapour arising in this part will diffuse outwards until finding a cooler region where it will condense, causing a local increase in water saturation. Hydration will take place with water moving from the host rock to the barrier. Drying of the bentonite will cause shrinking of the material whereas hydration will produce swelling which in turn results in the development of swelling pressures. The main feature in this problem is that all those phenomena are strongly coupled, interacting with each other in a complex manner.

In order to obtain an improved understanding of the behaviour of an engineered clay barrier, partial differential equations that govern coupled processes (i.e., balance of mass, energy, and momentum) must be solved. There are different coupled thermo-hydro-mechanical (THM) formulations applicable to deformable porous media (Pollock, 1986; Olivella et al., 1994; Gawin et al., 1995; Thomas et al., 1998). These formulations are written in terms of the state variables by using constitutive relations. In the case of unsaturated soil, direct experimental assessment of unsaturated properties of the medium may be extremely demanding. However, the soil water retention curve (SWRC) seems as a practical and sufficient estimation tool from which to derive unsaturated soil property functions (Barbour, 1998; Fredlung, 2006). The SWRC

defines the constitutive relationship between the amount of water in the soil and the suction.
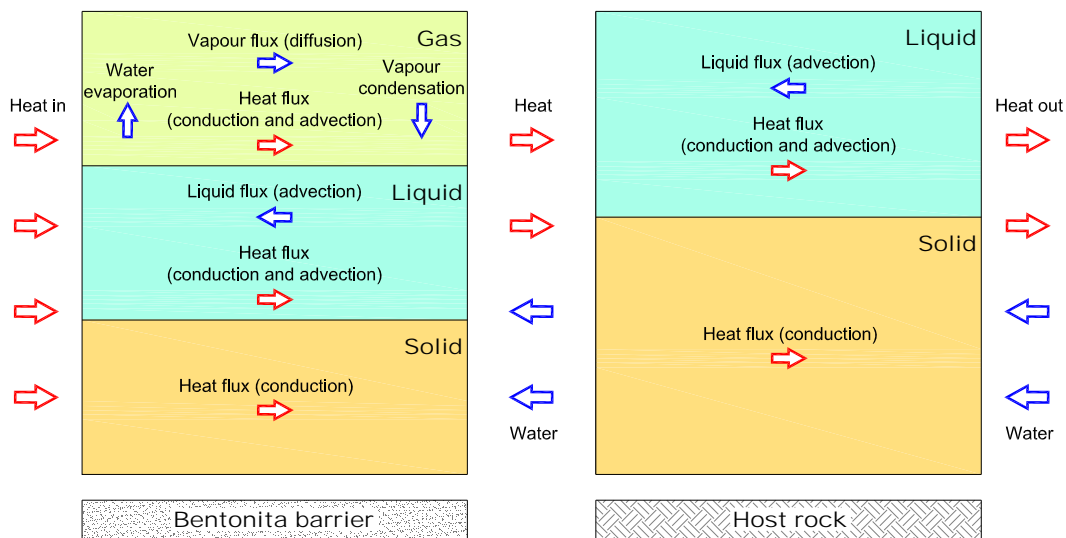
Figure 1.3. Scheme of the thermo-hydraulic processes in the near field [from Gens et al. (2009)].

The pores of a soil are of many different kinds and vary in size and in shape. Microstructural observations (e.g. electron microscope, gas and mercury porosimeters) of the fabric of bentonite samples statically compacted at different dry densities show that it is possible to consider a double structure defined by the clay aggregates and the pores between them. Each range of pore size is associated with a characteristic adsorptive behaviour of water to the solid matrix (Gregg & Sing, 1967). Their dependence on distance is such that the first layer of adsorbed molecules will be strongly held whereas higher layers will be more weakly adsorbed. Because of the complex mechanisms by which water is held in soil pores, the equations used to represent the SWRC still remain in essence empirical.

As suggested by experimental results, for low and medium values of suction, water retention in soil is affected by changes in the soil fabric (Taylor & Box, 1960; Box & Taylor, 1962; Assouline et al, 1997; Al-Mukhtar et al., 1999; Vanapalli et al., 1999; Ng & Pang, 2000; Startsev & McNabb, 2001; Rao & Revanasiddappa, 2005). The density (or void ratio) can be assumed as a first order approximation to the description of the soil fabric. Additionally, it is one of the variables used in the formulation of codes used to solve THM coupled problems. Consequently, the void ratio has been generally the variable adopted to incorporate, at least partially, the influence of changes within the

soil fabric in expressions proposed for the SWRC (Stange & Horn, 2005; Mbonimpa et al., 2006; Assouline, 2006; Jacinto et al., 2009).

The water retention capacity of soil also depends on the temperature. Phillips & de Vries (1957) suggested that changes with temperature were due entirely to changes in interfacial tension of liquid water against its vapour. However, this correction has consistently failed to account for measured temperature induced changes in the water retention capacity (Gardner, 1955; Chahal, 1964, 1965; Haridasan & Jensen, 1972; Hopmans & Dane, 1986; Nimmo & Miller, 1986; Constantz, 1991; She & Sleep, 1998; Romero et al., 2001; Bachmann et al., 2002; Villar & Lloret, 2004; Villar et al., 2005; Tang & Cui, 2005; Villar & Gómez-Espina, 2007).

A way to analyse the effect of variables like temperature and sample density on the water retention capacity of soil is throughout the capillary model. Although very intuitive, this model only explains partially the effect of those variables on the retention capacity. A more useful tool to interpret experimental observations can be obtained by using thermodynamic of interfacial phenomena. Within the thermodynamic of adsorption it seems that solution thermodynamics is better than adsorption thermodynamics to analyse the physical adsorption of water by soils (Hill, 1950; Myers, 2002; Myers & Monson, 2002).

The interaction between layers of smectite, which is the main mineral of bentonite, and water has been the object of studies during many years (Mooney et al., 1952a-b; Keren & Shainberg, 1975, 1979; Kraehenbuehl et al., 1987; Cases et al., 1992; Cuadros, 1997; Dios Cancela et al., 1997; Tournassat et al., 2003). Experimental results suggest that the water confined in small pores or in the proximity of the clay layers of expansive materials presents properties that differ from those of bulk water (Low, 1979; Hawkins & Egelstaff, 1980; Cariati et al., 1981; Derjaguin et al., 1986; Pusch et al., 1990; Skipper et al., 1991; Swenson et al., 2000; Villar & Lloret, 2004; Fernández & Rivas, 2005).

In many applications the water retention curve is presented as suction against degree of saturation, which can be directly evaluated from the gravimetric water content. In the case of highly expansive soils, it is systematically observed that, close to saturation (nil suction), the degree of saturation calculated from the water content is bigger than one (Villar, 2002; Marcial, 2003). It is generally accepted that this error comes from the value assigned to the density of the water in the bentonite, which must be well above 1.0 Mg/m^3.

Experimental works have been carried out to evaluate the temperature influence on different aspects of the stress-strain response of clay samples tested in saturated state (Demars & Charles, 1982; Hueckel & Baldi; 1990; Kuntiwattanakul et al., 1995; Tanaka et al., 1997; Burghignoli et al., 1999; Delage et al., 2000; Abu-Zreig et al., 2001; Sultan et al., 2002; Cekerevac & Laloui; 2004). A pioneering work to include the temperature influence into a mechanical model for saturated clay is due to Hueckel & Borsetto (1990). This thermo-elasto-plastic model has been the basis for the development of improved models (Robinet et al., 1996; Modaressi & Laloui, 1997; Graham et al., 2001; Cui et al., 2000; Abuel-Naga et al., 2007).

More recently the experimental study of the mechanical behaviour of unsaturated samples under temperature changes has become a matter of interest (Romero et al., 2003; Villar & Lloret, 2004; Lloret et al., 2004; Villar, 2005; Tang et al., 2008). Pusch & Karnland (1988) and Pusch & Güven (1990) present results of the effect of temperature on the fabric of expansive clay. In the case of unsaturated soils, the Barcelona Basic Model (BBM) proposed by Alonso et al. (1990) was then extended to incorporate the temperature effect (Gens, 1995). Bolzon & Schrefler (2005) also propose a model that includes the effect of temperature and suction on the mechanical response of the material.

The BBM is an elasto-plastic model appropriate to simulate the hydro-mechanical behaviour of low and moderate expansive soils. In recent years the fabric of compacted expansive clays has been studied in detail, and a double structure made up of clay aggregates and large macrostructural pores has been recognised. From these observations, a new conceptual framework called Barcelona Expansive Model (BExM) was put forward (Gens & Alonso, 1992). Using these ideas, a model based on generalized plasticity was implemented to solve boundary value problems (Sánchez, 2004; Sánchez et al., 2005). Tang & Cui (2008) propose a similar model that includes the effect of temperature.

Most of the organizations responsible for the management of high level radioactive waste are currently working on the design of a concept for geological disposal. As a part of that work, ANDRA (French National Agency for Radioactive Waste Management) and SKB (Swedish Nuclear Fuel and Waste Management Co) are involved in the development of the Temperature Buffer Test (TBT) project. The overall objective of the project is to investigate how well the bentonite buffer can endure the high temperatures expected to be found around vitrified waste canisters. In the framework of the project a large scale field test was running at the Äspö Hard Rock

Laboratory (Sweden) since March 2003 and some laboratory test were performed at CIEMAT (Spain) and CEA (France). In this Thesis, both laboratory and field tests have been analysed using a numerical code able to solve coupled THM processes (Olivella et al., 1996). The specific developments carried out in the context of this research work have been considered in those analyses. Important conclusions could be obtained when experimental and simulated results were compared.

1.3 Objectives of the Thesis

The Thesis has been developed within the framework of the Temperature Buffer Test project. Research works were principally oriented to understand the influence of different factors on the interaction mechanisms between expansive clays (bentonites) and water. From this point of view, the effect of the sample density and temperatures higher than 100 ºC on the hydraulic response of bentonites as those used in the engineering barriers was analysed. The influence of those mechanisms on the properties of the pore water was also studied. All these effects have been considered in the simulation of laboratory and in situ tests carried out using a numerical code developed to solve coupled thermo-hydro-mechanical problems.

Specific objectives of the Thesis are the following:

- Review of the different tools that can be used to analyse the interaction mechanisms between expansive clays and the water inside the pores of samples made up of this material.

- Study of the effects of variables like temperature and sample density on the soil water retention curve of bentonites and to propose a mechanism to quantify these influences.

- Define a methodology to obtain the soil water retention curve in terms of suction against degree of saturation taking into account the changes in water properties, in particular its density, due to the interaction with the clay particles.

- Simulation of laboratory experiments and field test (TBT) applying the theoretical concepts previously developed.

1.4 Layout of the Thesis

This Thesis has been organized in seven Chapters and each one contains its own summary, background and conclusions. The present one gives an overview of the motivation and objectives of this work. Chapter two summarizes the formulation used along the Thesis and introduces thermodynamics concepts which are then used to interpret the effect of different variables on the water retention capacity of soils. Aspects related to temperature and density influence on the water retention capacity of bentonites are considered in Chapter three. The incorporation of these effects into SWRC equations to be used in numerical simulation is also discussed in this Chapter. The interaction between the clay layers of expansive materials as those used in engineering barriers and the water is addressed in Chapter four. The influence of that interaction on the density of the pore water and how it can be included in the SWRC is also analysed. Chapter five describes the coupled thermo-hydro-mechanical analysis of a laboratory experiment carried out in the framework of the TBT project. Concepts developed in previous Chapters are used in this analysis. In Chapter six the main characteristics of a full-scale field test (TBT) are described. A discussion of experimental results and its interpretation aided by numerical simulations is carried out. The main conclusions and possible areas for future researches are addressed in Chapter seven. The Thesis ends up with a list of the quoted references and two Appendixes.

Chapter 2

Fundamentals of the soil-water interaction

Summary

Analysis and prediction of the response of an engineering barrier requires the solution of the equations that govern coupled thermo-hydro-mechanical (THM) processes. These equations are written in terms of state variables using constitutive relations that simulate the behaviour of the different materials which form the barrier. Among these laws, the soil water retention curve (SWRC) permits to define many aspects of the material response under unsaturated conditions. Therefore, it is important to understand how different actions influence this constitutive law. Many theories have been used to explain experimental results about the influence of variables like temperature and density on the SWRC. Those data could be partially justified although it is evident that additional effects should be considered. Concepts derived from thermodynamics of interfacial phenomena seem to be a useful tool to explain those experimental data.

This Chapter presents the concept of potential of water in soil and its traditional thermodynamic treatment. The relation between the soil water pontential and the water retenion curve is highlighted. Pertinent concepts of interfacial phenomena are introduced and its use in the analysis of the physical adsorption of water by soils is shown. An interpretation of the capillary model using these concepts is given. The relation between the expression for the water chemical potential derived using the traditional thermodynamic treatment and that obtained using solution thermodynamic is shown. Finally, an overview of the governing equations used to solve THM problems is presented.

2.1 Preface

A comprehensive analysis of coupled heat and moisture transfer in a deformable unsaturated soil is a problem of interest in different areas of research. In particular, in order to obtain an improved understanding of the behaviour of an engineered clay barrier, heat transfer, moisture migration, air transfer, stress equilibrium and stress-strain relation need to be considered (Thomas et al., 1998a).

Partial differential equations that govern coupled processes (i.e., balance of mass, energy, and momentum) are derived for a representative element volume (REV). Exact analytical solutions are only possible for simplified cases since the interrelated effects of the various phenomena are too complicated. Therefore, an effective numerical approach has to be employed for the modelling work (Feddes et al., 1988; Fredlund, 2006). This can be achieved applying the physics of the REV to an element of the continuum called a finite element. Combining the finite elements eventually allows an entire continuum to be modeled. Boundaries or limits must be placed on the region considered to make the problem manageable and this gives rise to a boundary value problem.

Different coupled thermo-hydro-mechanical (THM) formulations applicable to deformable porous media have been proposed in the literature (Pollock, 1986; Olivella et al., 1994; Gawin et al., 1995; Thomas et al., 1998b). In these formulations, the governing equations are written in terms of state variables (unknowns) by using constitutive relations. Every constitutive relationship defines a physical property of the medium and may be linear or nonlinear in nature. Direct experimental assessment of unsaturated properties of the medium (e.g., permeability, shear strength, volume change) may be extremely demanding and therefore constitutive relations are usually empirical or semiempirical (Fredlund, 2006).

The introduction of the notion of capillary potential of soil water and its later generalization in terms of water potential provided the basis for an understanding of the different forces acting in the water present within the soil pores (Groenevelt & Bolt, 1972). The concept of energy or potential within the water to do work has been historically used to solve coupled problems in Soil Physics. One of the components of the water potential is related to the affinity of water by soil and it is called the soil water matric potential. It depends on changes in the water content as well as any additional

contributions that might arise from physical changes of the soil matrix (Box & Taylor, 1962). It is a measure of the soil capacity to hold water in its pores against forces resulting from external actions as those due to the gravity field, gradients of pressure or concentration, among others (Groenevelt & Bolt, 1972).

In Geotechnical Engineering, the affinity of water by soil has been traditionally called suction s, which has unit of stress (energy per unit volume). The soil water retention curve (SWRC) defines the constitutive relationship between the amount of water in the soil and the suction. The amount of water in the soil can be given in terms of gravimetric water content w, volumetric water content θ, or degree of saturation S_l. SWRC has emerged as a practical and sufficient estimation tool from which to derive unsaturated soil property functions (Barbour, 1998; Fredlund, 2006).

To be useful in modeling processes, a continuous representation of the SWRC is required and needs to be incorporated in predictive models. Several mathematical equations have been proposed to describe the soil water retention curve. In general, they provide a reasonable fit of experimental data in the low and intermediate suction ranges (Leong & Rahardjo, 1997; Cornelis et al., 2005). However, these equations are not forced through zero water content at high suction values and new models have been developed to solve this limitation (Fedlung & Xing, 1994; Romero et al., 2001; Gitirana & Fredlund, 2004; Groenevelt & Grant, 2004; Pham & Fredlund, 2008).

Many expressions proposed for the SWRC are mainly based on pore size distribution functions in combination with the concept of bundle of capillaries, in which the pores are represented by cylindrical capillary tubes obeying the Young and Laplace equation. The capillary model, although very intuitive, gives only a first approximation to interpret the effect of variables like temperature and soil structure on the matric suction, as capillarity only represents one of the mechanisms by which soil is able to hold water in its voids. A more powerful tool is obtained when thermodynamic concepts of interfacial phenomena are considered to analyse the physical adsorption of water by soils. Surface thermodynamics is able to explain the physical adsorption of thin films on solid surface but its application to porous materials is of very limited utility because of the complex geometry of the interfaces in the case of soils. On the other hand, the thermodynamics of adsorption can be treated as a special case of solution thermodynamics for which the adsorbates are the solutes and the adsorbent is the solvent (Hill, 1950; Myers, 2002; Myers & Monson, 2002).

In the first part of this Chapter aspects related to retention mechanisms of water by soil and their representation throughout the water retention curve are briefly discussed. The Chapter continues with a description of the different potential that can be defined in the soil water together with the thermodynamic treatment traditionally used. Then, pertinent thermodynamics concepts of interfacial phenomena are introduced. A reference to the well knows capillary model and its interpretation using thermodynamics are carried out. The Chapter ends up with a description of the partial differential equations that govern thermo-hydro-mechanical processes as those analysed in this Thesis.

2.2 Water retention in soils

Soils consist of a solid skeleton (matrix) with pores in between. The pores have different sizes, shapes and spatial distributions and provide the space for storage and transport of liquid and gas. In dealing with the analysis of coupled thermo-hydro-mechanical problems in unsaturated soils, it is necessary a relationship between the water fraction in the soil and a measure of the soil capacity to hold water in its pores against forces resulting from external actions as those due to the gravity field, gradients of pressure or concentration, among others (Groenevelt & Bolt, 1972). Storage or retention of water by soils depends on attractive forces (matric forces). There are different mechanisms for binding of water to the solid matrix like direct adhesion of water molecules to solid surfaces, osmotic binding of water in double layers and capillary binding of water.

When a solid is exposed in a closed space to a gas (or vapour) at some definite pressure or is in contact with a liquid, the solid begins to adsorb the fluid. The adsorption is a consequence of the force field at the surface of the solid (the adsorbent), which attracts the molecules of the gas or liquid (the adsorbate). When the forces of attraction from a solid are of physical nature, they give rise to physical adsorption.

The forces involved in physical adsorption include dispersion forces (which are attractive in nature) and short-range repulsive forces (Gregg & Sing, 1967). In addition there may be forces due to permanent dipoles within the adsorbed molecules, as in the case of water. All these forces define the total energy of adsorption. Their dependence on distance is such that the first layer of adsorbed molecules will be strongly held;

higher layers will be more weakly adsorbed with energy not much in excess of the enthalpy of vaporization. The physical adsorption is the main mechanism of binding of water in fine soils.

Adhesion is the attraction of dissimilar substances for each other while cohesion is the mutual attraction of particles of the same substance. The adhesive forces together with the cohesive forces between water molecules form the basis for capillary binding of soil water. This is the most important mechanism of binding of water in coarse soils.

The pores of a solid skeleton are of many different kinds and may vary in size and in shape within a given solid and between a solid and another. A classification has been proposed according to the width of the pores (e.g. the diameter of a cylindrical pore or the distance between sides of slit-shaped pores). Pores of widths below 20 Å are described as micropores, those with widths above 200 Å as macropores, and those in between as transitional (or intermediate) pores. Each range of pore size is associated with a characteristic adsorptive behaviour (Gregg & Sing, 1967).

When a sorbate (gas or vapour) is in contact with sorbent (solid), the amount adsorbed per gram of solid depends on the equilibrium pressure, the temperature, and also on the nature of the gas and of the solid. Equilibrium pressure refers to the pressure of the vapour in thermodynamic equilibrium with the adsorbed liquid. For a given gas adsorbed on a given solid at a fixed temperature, the adsorption is only a function of the pressure. The relation between the amount adsorbed and the pressure is called the adsorption isotherm. It is expected that a mathematical expression for the isotherm involves important parameters characterizing the solid, like its specific surface or pore volume. However, any theory to be mathematically tractable has to be based on simplified models (e.g. a system of cylindrical pores of equal diameter, or a planar surface even on the molecular scale) which are far removed from the actual solids encountered in practice. Because of that, the equations used to represent the isotherm still remain in essence empirical (Gregg & Sing, 1967).

In a porous solid the thickness of the adsorbed layer is necessarily limited by the width of the pores. In solid containing micropores the potential fields from opposite walls will overlap so that the attractive force acting on adsorbate molecules will be increased as compared with that on an open surface. This increase in field may originate, even at low pressures, a filling of the pores with adsorbate molecules packed as in the liquid form. Other aspect that defines the adsorption behaviour is the

presence in the pores of constrictions narrow enough to hinder the free passage of molecules through them.

Capillary condensation of the adsorbate to a liquid occurs in pores within the transitional range. The most widely accepted mechanism is that a multilayer is gradually built up as the pressure increases till a value were the pores are completely filled with adsorbate in a liquid-like condition; thereafter adsorption increases very slowly. This process defines the adsorption branch of the isotherm. When the adsorbate is withdrawn from the system, the liquid begins to evaporate from the pores and the desorption branch of the isotherm is traversed. The mechanism of desorption and adsorption are different and it is the basis of the existence of the hysteresis loop in the isotherm.

In Geotechnical Engineering, the adsorption isotherm for a given soil is called the soil water retention curve (SWRC). SWRC has emerged as a practical and sufficient estimation tool from which to derive unsaturated soil property functions (Barbour, 1998; Fredlund, 2006). In fact, methods have been proposed to predict volume change, shear strength, permeability, diffusion, adsorption, thermal conductivity, and a variety of other properties for unsaturated soil based in part on the information provided in the soil water retention curve.

The measurement of the SWRC can be obtained by a variety of methods and consists of determining the water content at given suction values (Taylor, 1965; Fredlund & Rahardjo, 1993; Barbour, 1998). These methods may be tedious, time-consuming, and expensive to use. The basis for all of them is that the moisture within the soil is brought to thermodynamic equilibrium with water or vapour at a known reference energy. The form of reference energy does have implications for interpretation of soil behaviour. Thus, in some cases it is only possible to measure the matric suction (pressure plate apparatus), whereas in other cases what is measured is the total suction within the soil water (osmotic desiccator). In the case of soils where volume changes can be assumed negligible, measurements are somewhat simplified because the initial void ratio e is assumed to remain constant (independent of the suction) so that values of S_l associated with measured water content can be easily obtained for different suction values. In the case of deformable soils, on the other hand, a suction variation may induce a volume change, so void ratio becomes dependent on suction values. Experimental procedures to obtain the SWRC in this kind of soil involve

the simultaneous measurement of water content and specimen volume at different suctions if a drying path is adopted in the experiment. Other option is to determine the SWRC under confined conditions by using a wetting path.

Empirical expressions proposed for the SWRC can be divided into categories of two and three parameter equations (Fredlund, 2006). These parameters are determined by fitting the equations to laboratory data. Each of the proposed equations has one variable that bears a relationship to the air entry value of the soil (i.e., suction value to which the biggest pores in the soil start to desaturate) and a second variable that is related to the rate at which the soil desaturates. The third variable, when used, allows the low suction range near the air entry value to have a shape that is independent of the high suction range near residual conditions.

As suggested by experimental results, for low and medium values of suction, water retention in soil is affected by changes in the soil fabric (Taylor & Box, 1960; Box & Taylor, 1962; Assouline et al, 1997; Al-Mukhtar et al., 1999; Vanapalli et al., 1999; Ng & Pang, 2000; Startsev & McNabb, 2001; Rao & Revanasiddappa, 2005). Recently, some theories have been developed which intent to predict the retention capacity of soils from the pore geometry (Reeves & Celia, 1996; Tuller et al., 1999; Or & Tuller, 1999). However, due to the complexity of the soil fabric of compacted samples, the application of those models to practical problems seems to be not an easy task. The density (or void ratio) can be assumed as a first order approximation to the description of soil fabric. Additionally, it is one of the variables used in the formulation of codes developed to solve coupled problems. Consequently, the void ratio has been generally the variable adopted to incorporate the influence of changes within the soil fabric in the expressions proposed for the SWRC (Stange & Horn, 2005; Mbonimpa et al., 2006; Assouline, 2006; Jacinto et al., 2009).

The water retention capacity of soil also depends on the temperature. Phillips & de Vries (1957) suggested that changes with temperature were due entirely to changes in interfacial tension of liquid water against its vapour. However, this correction has consistently failed to account for measured temperature induced changes in the water retention capacity (Gardner, 1955; Chahal, 1964, 1965; Haridasan & Jensen, 1972; Hopmans & Dane, 1986; Nimmo & Miller, 1986; Constantz, 1991; She & Sleep, 1998; Romero et al., 2001; Bachmann et al., 2002; Villar & Lloret, 2004; Villar et al., 2005; Tang & Cui, 2005; Villar & Gómez-Espina, 2007).

A way to analyse the effect of variables like temperature and sample density on the water retention capacity of soil is throughout the capillary model. Although very intuitive, this model only explains partially the effect of those variables on the retention capacity. A more useful tool to interpret experimental observations can be obtained by using concepts of solution thermodynamics or adsorption thermodynamics (Hill, 1950; Myers, 2002; Myers & Monson, 2002). These concepts and the relation between them are treated in this Chapter.

2.3 Potential energy of water in soil

Soil water can contain energy in different forms and quantities. Since the movement of water in soil is quite slow, its kinetics energy is generally considered negligible. On the other hand, the potential energy, which is due to position or internal condition, is of primary importance in determining the state and movement of water in soil. The energy state characterizes the effects of the forces exerted on soil water by its surroundings.

Potential energy is the energy that a body has in virtue of its position in a force field (Koorevaar et al., 1983). Water molecules experience many different forces in a porous material such as soil. The variety of forces and the directions in which they act make it all but possible to characterize the force field in a real soil. However, it is possible to calculate the potential energy of a unit quantity of water as a consequence of the forces acting upon it. Differences in potential energy from point to point in a system determine both the direction of water flow and the net force driving it (Hillel, 1980; Tindall & Kunkel, 1999; Jury & Horton, 2004).

The potential energy of water in soil must be defined relative to a reference or standard state, since there is no absolute scale of energy. The standard state is customarily defined to be the state of pure (no solutes), free (no external forces other than gravity) water at a reference pressure P_g^0, reference temperature T_0, and reference elevation z_0 and is arbitrarily given the value zero. The soil water potential is defined as the difference in energy per unit quantity of water compared to the reference state.

The total potential of the constituent water in soil at temperature T_0 is the amount of useful work per unit quantity of pure water that must be done by means of externally

applied forces to transfer reversibly and isothermally an infinitesimal amount of water from the standard state to the soil liquid phase at the point under consideration (Hillel, 1980; Jury & Horton, 2004).

There are several systems of units in which the total potential may be described, depending on whether the quantity of pure water mentioned in the preceding definition is expressed as a mass, a volume, or a weight (Table 2.1).

Units	Symbol	Name	Dimensions	SI units
Energy / mass	G_t	Gibbs free energy of soil water	L^2 / T^2	J / kg
Energy / volume	ψ_t	Soil water potential	$M / (L \cdot T^2)$	N / m^2
Energy / weight	h_t	Soil water potential head	L	m

Table 2.1. System of units of the total water potential in soil.

The potential can be defined as energy divided by volume; in that case it has units of pressure and because of that it is also called pressure equivalent. It is sometimes used to work with potential on mass basis instead on volume basis. The former is obtained from the latter by dividing by the density ρ. Other possibility is to express potential on weight basis and it is obtained dividing the potential on mass basis by the gravity g. The units correspond to a length and it can be indicated as head equivalent.

2.3.1 Components of the soil water potential

The transformation of water from the reference state to the soil water state may be broken up into a series of steps, each of which partially converts water to the final state. As long as each step is performed reversibly and isothermally, the total change in potential energy of the water may be set equal to the sum of the potential energy changes corresponding to each of the steps. These sequential potential energy changes will be called components of the total water potential. The transition from the reference pool to the soil water state can be defined in three steps. The different components of the total water potential are defined below (Hillel, 1980; Koorevaar et al., 1983; Tindall & Kunkel, 1999; Jury & Horton, 2004).

Gravitational potential

It is indicated as ψ_z and is the energy per unit volume of water required to move an infinitesimal amount of pure, free water from the reference elevation z_0 to the soil water elevation z. It has the value

$$\psi_z = \rho_w g (z - z_0) \tag{2.1}$$

with ρ_w the water density.

Solute or osmotic potential

It is indicated as ψ_s and represents the change in energy per unit volume of water when solutes, identical in composition to the soil solution at the point of interest, are added to pure, free water at the elevation of the soil.

Pressure potential

The pressure potential ψ_p, is the energy per unit volume required to transfer an infinitesimal amount of solution containing solutes (which are identical in composition to the soil water) from a reservoir of solution (which is at the reference pressure and located at the elevation of the soil) to the point of interest in the soil.

This component describes the effects of all forces on soil water other than gravity and solutes. Its influence may include the effects of binding to soil solids, interfacial curvature, air pressure, weight of overlaying soil solid material, and hydrostatic water pressure in saturated soil. Traditionally, the pressure potential energy has been divided in several other components. This division, however, must be made carefully because the various forces on a soil water element can interact with each other (Hillel, 1980; Koorevaar et al., 1983).

Matric potential

Indicated as ψ_m, represent the energy per unit volume of water required to transfer an infinitesimal quantity of water from a reference pool of soil water at the elevation of the soil to the point of interest in the soil at reference pressure. Thus, this potential

differs from the pressure potential in that the gas pressure is maintained at reference pressure.

The transition to the final state is achieved with the following definitions, depending on whether the soil is unsaturated and has a gas phase that can exert pressure on the water or it is saturated and water experiences hydrostatic pressure from an overlying liquid phase.

Gas pressure potential

It is defined as the change in energy per unit volume of water when the gas pressure is changed from the pressure P_g^0 of the reference state to the pressure P_g of the soil. If this change does not alter the geometry of the liquid phase then

$$\psi_g \approx P_g - P_g^0 \tag{2.2}$$

which is the pressure of the gas phase relative to the standard state gas pressure.

Hydrostatic pressure potential

It is defined as the water pressure exerted by overlying unsupported (saturated) water on the point of interest in the soil. By definition, it is

$$\psi_h = \rho_w g (z - z_{wt}) \tag{2.3}$$

which is the water pressure exerted by the height of water between the point of interest z, and the water table (saturated-unsaturated soil interface) z_{wt}.

The potentials described above are sufficient to describe soil water energy states whenever the soil solid matrix is rigid and self-supporting. For these soils the weight of soil solid material above the point of interest is borne entirely by the rigid matrix. The situation is more complex in swelling and compressible soils. Since the soil particles are not in complete contact with each other, part or all of the weight of the overlying solid material and external loads may be exerted on an element of soil water. In this case, an additional component of the pressure potential to those previously defined is considered (Philip, 1969; Iwata et al., 1995).

<u>Overburden pressure potential</u>

It is defined as the change in energy per unit volume of soil water when the soil changes its bulk volume and it is under the action of gravity and external loads. It is generally indicated as ψ_b.

2.3.2 Total soil water potential and Gibbs free energy

The Gibbs free energy of water in soil, referenced to the Gibbs free energy of pure water, at a chosen temperature and pressure, is equivalent to the total potential of water in soil (Iwata et al., 1995). The osmotic potential of water in soil corresponds to a component of the soil free energy related to solutes existing in the soil solution while the pressure potential is related to a component which depends on the interaction mechanisms between the water and the soil particles as well as on the soil fabric.

When the water in soil is treated thermodynamically, the different components of the total potential indicated in section 2.3.1 should be considered. In that case, the differential expression for the Gibbs free energy of water in soil, G_t, could be expressed by (Box & Taylor, 1962)

$$dG_t = -S_w\, dT + V_w\, dP_g + \sum_{j=1}^{k}\left(\frac{\partial G_t}{\partial n_j}\right)dn_j + \sum_{i=1}^{n}\left(\frac{\partial G_t}{\partial x_i}\right)dx_i \qquad (2.4)$$

where S_w and V_w represent the specific entropy and the specific volume of water in soil respectively, T the absolute temperature, P_g the pressure in the gaseous phase, n_j is the amount of moles of the j component, and k is the number of components in the soil solution. The last terms in equation (2.4) represents the change in the free energy of the water in soil because of the change in the x_i state variable, with n the number of state variables (other than T, P_g and n_j) that define the state of the water in the soil.

The first term on the right hand side of equation (2.4) shows the dependence of the free energy on temperature; the second one describes the effect of the gas pressure at the liquid-gas interface and can be related to the gas pressure potential defined

previously. The third term represents the changes in the Gibbs free energy of soil water when the concentrations of the chemical species present in the soil solution are changed; this term is associated with the osmotic potential.

In the last term it is possible to include the contribution of the gravity and the interaction forces between the water and the solid particles. The contribution of the gravity field on the free energy can be obtained by dividing equation (2.1) by the density. It is clear that the state variable in this case is the z coordinate. Therefore, one of the terms in the last summation in equation (2.4) is given by

$$\frac{\partial G_t}{\partial z} dz = g \; dz \tag{2.5}$$

The contribution of the potential fields associated to the interaction forces between the water and the solid particles depend on the soil deformability. If the soil matrix is rigid, the influence on the Gibbs free energy can be considered through the change in the water content of the soil. A suitable state variable to be considered is the volumetric water content θ, or the gravimetric water content w. Thus, considering equation (2.5) and the new state variable, equation (2.4) becomes

$$dG_t = -S_w \; dT + V_w \; dP_g + g \; dz + \sum_{j=1}^{k}\left(\frac{\partial G_t}{\partial n_j}\right)dn_j + \frac{\partial G_t}{\partial w} \; dw \tag{2.6}$$

When the soil is deformable the Gibbs free energy of water depends on additional variables. Taylor & Box (1961) presented results on the influence of confining pressure and bulk density on the soil water potential. Box & Taylor (1962) analysed different alternatives proposed by other researchers to include the soil deformability in the total potential of soil water. Finally, they concluded that the dry density ρ_d is the state variable that seems appropriate to describe that effect. Philip (1969) introduced the concept of overburden potential associated to the soil deformation, which is included in the Gibbs free energy through the moisture ratio φ, defined by

$$\varphi = (1+e)\theta \tag{2.7}$$

with e the void ratio of the soil. The same concept was further elaborated by Groenevelt & Bolt (1972), which used the same state variable adopted by Romero &

Vaunat (2000). These authors adopted the water ratio e_w (volume of water respect to volume of solids) as the thermodynamic variable associated with the matric component of the free energy and defined as

$$e_w = G_s w \tag{2.8}$$

where G_s is the relation between the solid density and water density. By using again equation (2.5) and this last state variable, equation (2.4) becomes

$$dG_t = -S_w\, dT + V_w\, dP_g + g\, dz + \sum_{j=1}^{k}\left(\frac{\partial G_t}{\partial n_j}\right) dn_j + \frac{\partial G_t}{\partial e_w}\, de_w \tag{2.9}$$

Equation (2.9) defines the differential of the Gibbs free energy of water in a soil which can undergo deformations. Using equation (2.8) and operating, yields

$$dG_t = -S_w\, dT + V_w\, dP_g + g\, dz + \sum_{j=1}^{k}\left(\frac{\partial G_t}{\partial n_j}\right) dn_j + \frac{\partial G_t}{\partial w}\, dw + \frac{\partial G_t}{\partial e}\, de \tag{2.10}$$

If the volume of the soil matrix is constant the last term in equation (2.10) disappears and the expression reduces to equation (2.6). This last term is associated with the envelope pressure potential defined by Philip (1969). Equation (2.10) is similar to the expression proposed by Box & Taylor (1962). As suggested by these authors, it seems more adequate to divide the effect of the soil matric forces on the water potential between those originated by changes in the water content and those due to changes in the amount of solid material per unit volume.

2.3.3 Soil suction and soil water potential

In unsaturated soil, the pressure potential is defined by two components; the matric potential ψ_m, resulting exclusively from the soil matrix, and the gas potential ψ_g, due to the gas pressure in excess of atmospheric pressure

$$\psi_p = \psi_m + \psi_g \tag{2.11}$$

Equation (2.11) suggests that under normal atmospheric conditions the pressure potential is equal to the matric potential. This equation can be expressed on mass basis as

$$\mu_p = \mu_m + \mu_g \qquad (2.12)$$

where μ_p, μ_m and μ_g mean respectively, pressure potential, matric potential and gas potential, all expressed on mass basis. The soil water matric potential is defined as the affinity of the soil matrix for water (Box & Taylor, 1962). It depends on the water content variable and any additional contributions that might arise from physical changes of the matrix. The matric potential, therefore, represents the contribution of the soil water content combined with any changes in the soil matrix, to the total potential of the soil water.

Equation (2.10) can be rewritten in the following form

$$dG_t = -S_w dT + g\,dz + \sum_{j=1}^{k}\left(\frac{\partial G_t}{\partial n_j}\right) dn_j + d\mu_p \qquad (2.13)$$

where

$$d\mu_p = V_w\,dP_g + \frac{\partial G_t}{\partial w}\,dw + \frac{\partial G_t}{\partial e}\,de \qquad (2.14)$$

The first term in equation (2.14) is related to the gas pressure potential. Therefore, that equation yields

$$d\mu_m = \frac{\partial G_t}{\partial w}\,dw + \frac{\partial G_t}{\partial e}\,de = \mu_w\,dw + \frac{\partial G_t}{\partial e}\,de \qquad (2.15)$$

where μ_w is called the chemical potential of water in soil. The chemical potential defines the relationship between the fraction of water in a soil and the matric potential when all the variables, except the water content, are held constant. In addition, equation (2.15) suggests that the matric potential also depends on density changes. The variation of the soil water potential with the soil density was designated structural affinity by Taylor & Box (1961).

In Soil Mechanics, the equivalent of the water potential expressed on volume basis and with opposite sign is called suction s (Yong, 1999; Gens & Olivella, 2001). As it was already indicated, the functional relationship between the suction and the water content (with the other variables held constant) is characteristic for a given soil and is called the soil water retention curve (SWRC). This relation could be considered as a physical fingerprint of the soil (Groenevelt & Bolt, 1972).

2.4 Thermodynamics of interfacial phenomena

The process by which certain porous solids bind large numbers of molecules to their surfaces is known as adsorption. The nature of the adsorbing surface is a determining factor in adsorption. Surfaces of such solids are irregular at the molecular level, and they contain sites of particular attraction for adsorbing molecules.

In the adsorption of gases, the number of molecules attracted to a solid surface depends on conditions in the gas phase. For very low pressures, relatively few molecules are adsorbed, and only a fraction of the solid surface is covered. As the gas pressure increases at a given temperature, surface coverage increases. When all sites become occupied, the adsorbed molecules are said to form a monolayer. Further increase in pressure promotes multilayer adsorption. It is also possible for multilayer adsorption to occur on one part of a porous surface when vacant sites still remain on another part (Gregg & Sing, 1967; Adamson, 1990).

The complexity of solid surfaces and the inability to characterize exactly their interactions with adsorbed molecules limits the understanding of the adsorption process. However, it is possible to develop a thermodynamic description of adsorption equilibrium, applicable equally to monolayer and multilayer adsorption.

The force field of the solid adsorbent influences properties in the adjacent gas phase, but its effect decreases rapidly with distance. Thus the properties of the gas change rapidly in the immediate neighborhood of the solid surface, but they do not change abruptly. A region of change exists which contains gradients in the properties of the gas, but the distance into the gas phase that the solid makes its influence felt cannot be precisely established (Tolman, 1948).

The problem of defining a boundary between the two phases can be solved as proposed by Gibbs (Tolman, 1948; Adamson, 1990). A system with two phases at equilibrium can be regard as composed of two phases which have substantially uniform distribution of matter throughout their interiors but which meet in a thin layer of physical inhomogeneity where a transition takes place from the distribution in one phase to that in the other (Tolman, 1948). To simplify the treatment of the thermodynamic properties of such a system, it is assumed that the actual interface is replaced by an imaginary geometrical surface, which lies within the layer of physical inhomogeneity, and which passes through points within that transition layer where the fluid is locally in some given specific condition (the same for all points). Such a surface was called by Gibbs a dividing surface. A variety of choices for such a dividing surface can be made, according to which condition of the neighboring matter is selected for the construction of that surface. Hence the properties of the whole transition layer are determined by the area and configuration of the particular dividing surface (Tolman, 1948).

Thermodynamics of adsorption gives a tool to analyse the physical adsorption of water by soils. Surface thermodynamics is able to explain the physical adsorption of thin films on solid surface but its application to porous materials is of very limited utility because of the complex geometry of the interfaces in the systems. On the other hand, the thermodynamics of adsorption can be treated as a special case of solution thermodynamics for which the adsorbates are the solutes and the adsorbent is the solvent (Hill, 1950; Myers, 2002; Myers & Monson, 2002).

2.4.1 Adsorption thermodynamics

In the case of gas-adsorbate equilibrium, it is assumed that the properties of the gas phase extend unchanged up to the solid surface. Differences between the actual and the unchanged properties can then be attributed to the mathematical surface, treated as a two-dimensional phase with its own thermodynamic properties. This provides not only a precisely defined surface phase to account for the singularities of the interfacial region, but it also extracts them from the three-dimensional gas phase so that it too may be treated precisely (Smith et al., 2001). The solid, despite the influence of its force field, is assumed inert and for purposes of thermodynamic analysis is treated as a two-dimensional phase. It is assumed that the surface area and structure of the adsorbent are independent of temperature and pressure (Hill, 1949).

The Gibbs free energy for a two-dimensional phase in an open system can be written by analogy with a three-dimensional system (Smith et al., 2001). This equation is written on the basis of a unit mass of solid adsorbent

$$dG^a = -S^a dT + \Sigma d\varphi + \sum_{i=1}^{c} \mu_i dn_i^a \tag{2.16}$$

where S^a is the entropy of the adsorbed phase per unit mass of adsorbent, T the absolute temperature, Σ the specific surface area of the adsorbent (a quantity characteristic of a particular adsorbent), φ the spreading pressure, μ_i the chemical potential of the i component presents in the gas phase, and n_i^a is the amount adsorbed of that component per unit mass of adsorbent.

The spreading pressure is the two-dimensional analog of pressure, having units of force per unit length, akin to surface tension. The spreading pressure is the difference between the free surface energy of the clean solid (in a vacuum) and the free surface energy when in equilibrium with a chemically dissimilar fluid component (gas or liquid). The value of φ is given by the equation (Boyd & Livingston, 1942)

$$\varphi = \gamma_{s0} - \gamma_{sf} \tag{2.17}$$

in which γ_{s0} is the free surface energy of the clean surface of a solid, and γ_{sf} is the same quantity when the surface is covered by a film. The free surface energy is the same quantity as the surface tension, which in the case of a liquid may be determined directly, whereas with a solid some other type of experimental method needs to be employed (Jura & Harkins, 1944).

The Gibbs free energy can be also written as (Hill, 1949; Smith et al., 2001)

$$G^a = \sum_{i=1}^{c} n_i^a \mu_i \tag{2.18}$$

Differentiation of equation (2.18) and comparison with equation (2.16) gives

$$S^a dT - \Sigma d\varphi + \sum_{i=1}^{c} n_i^a d\mu_i = 0 \tag{2.19}$$

which is the Gibbs – Duhem relation for the adsorbate.

The condition of equilibrium between adsorbate and gas phase at constant gas pressure and temperature requires that the chemical potential of the component i in the adsorbed phase is equal to the chemical potential of that component in the gas phase (Guggenheim, 1967; Myers, 2002). Therefore, the chemical potential of the i component in the adsorbed phase is equal to the chemical potential of that component in the gas phase. At constant temperature, equation (2.19) reduces to the Gibbs adsorption isotherm

$$\Sigma d\varphi = \sum_{i=1}^{c} n_i^a d\mu_i = RT \sum_{i=1}^{c} \frac{n_i^a}{f_i} df_i \qquad (2.20)$$

where the chemical potential μ_i has been written as a function of the fugacity f_i. For the adsorption of a pure perfect gas component the fugacity coincides with the gas pressure, and integrating from zero pressure (where $\varphi = 0$) results

$$\varphi = -\frac{RT}{\Sigma} \int_0^p \frac{n^a}{p} dp \qquad (2.21)$$

with p the equilibrium vapour pressure. This expression represents the integral of the adsorption isotherm, which defines the relationship between the amounts adsorbed and the gas pressure, for a given gas and a given solid at a fixed temperature. Approximations in equation (2.21) include the consideration of perfect gas and to ignore the usually negligible volume of the adsorbed phase (Hill, 1949).

The adsorption thermodynamic approach is based upon surface area. The concept of area is useful when the only perturbations of the adsorbent by the sorbate are non-structural (Hill, 1950); that is, the volume of the sorbent and its equilibrium molecular structure are essentially constant. Other limitation of this theory is that there is not a simple way to measure the surface area in porous materials.

2.4.2 Solution thermodynamics

Solution thermodynamics applied to adsorption systems treats all the components in a symmetric way. This aspect constitutes a difference over the adsorption

thermodynamics which considers the components of the systems in an asymmetric way (Hill, 1950).

Analysis of results using adsorption thermodynamics is based in a series of different heats of adsorption whose definition is not completely clear. Confusion over the meaning of those thermodynamics quantities is eliminated by the solution thermodynamics approach (Myers, 2002).

Hill (1950) presents a comparison between the solution thermodynamics and adsorption thermodynamics approaches to the problem of gas adsorption on deformable porous solids. Myers (2002) and Myers & Monson (2002) present a detailed treatment of the subject and its application to experimental results.

The adsorption mechanism in a soil can be analysed from the interaction between a gas phase and a solid phase (Myers, 2002). For an adsorbent such as clay, adsorption occurs in the different pores present in the material. In order to divide the adsorbate molecules and their properties into two phases, it is necessary to distinguish adsorbed molecules from those in the gas phase.

In general, any extensive thermodynamic function in the adsorption system may be written as (Myers, 2002; Myers & Monson, 2002)

$$Z = Z^e + Z^g + Z^s \tag{2.22}$$

where Z represents the total extensive thermodynamic function under consideration, while Z^e, Z^g and Z^s represent that function, respectively, in the adsorbed phase, bulk gas phase and in the solid adsorbent in its pure standard state.

The amount adsorbed n_i^e of the i component presents in the gas phase is

$$n_i^e = n_i - V^g \rho^g y_i \tag{2.23}$$

with n_i the total amount of the i component introduced in the system, V^g the volume of the gas phase, ρ^g the molar density of the bulk gas phase, and y_i the mole fraction of the i component in the gas phase. Equation (2.23) is called Gibbs excess adsorption and is the total amount of gas in the pores minus the amount that would be present if the pores were filled with gas at the equilibrium bulk density. Equation (2.23)

is defined the same way as equation (2.22) but the term for the amount of i component in the clean solid is zero.

The equations for bulk solutions are extended to adsorption by adding an additional term for the solid adsorbent, which in a sense can be viewed as a solvent (Myers & Monson, 2002). The differential of the internal energy becomes

$$dU = TdS - PdV + \sum_{i=1}^{c} \mu_i dn_i + \mu dm \tag{2.24}$$

where the intensive variables are the absolute temperature T, the external pressure P, the chemical potential of the adsorbates μ_i, and the chemical potential of the solid adsorbent μ defined on a mass basis. The extensive variables are the internal energy U, the entropy S, the amount of moles of each adsorbate n_i, and the mass of solid adsorbent m. Equation (2.24) applies to the solid phase containing c species of solutes (adsorbates) inside the pores of the adsorbent. The chemical potential of the adsorbent changes with the amount of material adsorbed. The total volume of the system V, is divided into the gas phase volume and the solid phase volume V^s.

A porous medium can be assumed as composed of a matrix and a porous space (Coussy, 2004). In this approach it is assumed that the connected porous space (the space through which two points can be joined by a path lying entirely within it) coincides with the gas phase volume, V^g. The matrix is composed of both a solid part and a possible occluded porosity, whether saturated or not, and its volume is given by V^s. Therefore, both volumes can undergo changes when the thermodynamic variables are changed.

A useful thermodynamic function in the case of adsorption is the grand potential Ω, which is defined as (Myers & Monson, 2002)

$$\Omega = U - TS - \sum_{i=1}^{c} \mu_i n_i = -PV + \mu m \tag{2.25}$$

and represents the thermodynamic potential for a system with fixed volume, chemical potentials, and temperature. Using equation (2.25), equation (2.24) can be rewritten

$$dU = TdS + \frac{\Omega}{m}dm + \sum_{i=1}^{c}\mu_i dn_i + \frac{Pm}{\rho_d^2}d\rho_d \qquad\qquad \rho_d = \frac{m}{V} \qquad\qquad (2.26)$$

where ρ_d is the dry density of the porous solid. Equation (2.26) can be applied to flexible adsorbents for which the density varies with the amount adsorbed (as it is the case of swelling clays) or under the application of external loads.

In what follows, all the extensive variables (U, S, n_i, and so on) are written per unit mass of adsorbent and called mass extensive variables (Myers, 2002; Myers & Monson, 2002). However, because of simplification in the notation, no distinction is made between the symbols used to indicate variables on solid mass basis. In the case of adsorption systems with constant mass, the differential of the grand potential becomes

$$d\Omega = -SdT - \sum_{i=1}^{c}n_i d\mu_i + \frac{P}{\rho_d^2}d\rho_d \qquad\qquad (2.27)$$

The grand potential can be obtained by isothermal integration of equation (2.27)

$$\Delta\Omega = \Omega - \Omega^s = -RT\sum_{i=1}^{c}\int_0^{f_i}\frac{n_i}{f_i}df_i + \int_{\rho_d^0}^{\rho_d}\frac{P}{\rho_d^2}d\rho_d \qquad\qquad (2.28)$$

where the reference for the grand potential is the clean adsorbent in vacuo ($\Omega^s = \mu_0^s$), and the chemical potential μ_i has been replaced by the fugacity f_i. For adsorption of a single perfect gas, by using equation (2.23), results

$$\Delta\Omega = -RT\int_0^p\frac{n^e}{p}dp + \int_{\rho_d^0}^{\rho_d}\frac{P}{\rho_d^2}d\rho_d - P^g V^g \qquad\qquad (2.29)$$

where the fugacity has been replaced by the equilibrium pressure p.

Ω^e is the excess free energy change associated with isothermal immersion of the clean adsorbent in the bulk fluid. From equations (2.22) and (2.29) an expression for the excess grand potential is obtained

$$\Omega^e = \Delta\Omega - \Omega^g = -RT\int_0^p \frac{n^e}{p}dp + \int_{\rho_d^0}^{\rho_d} \frac{P}{\rho_d^2}d\rho_d \tag{2.30}$$

The calculation of Ω^e from experimental data alone is not able to give any information about the existence or magnitude of matrix perturbation. If it is present, it will automatically be included in the thermodynamic functions (Hill, 1950).

Because all of natural variables of the internal energy are extensive quantities, it is possible to apply the Euler's homogeneous function theorem to equation (2.24) and results

$$U = TS - PV + \sum_{i=1}^c \mu_i n_i + \mu \tag{2.31}$$

The excess energy U^e is given by

$$U^e = U - U^g - U^s \tag{2.32}$$

The excess energy is the total energy of the system (gas phase plus solid phase) minus the energy of the gas phase (U^g) minus the energy of the clean solid adsorbent (U^s) at the equilibrium temperature and pressure.

The total volume is assumed equal to the matrix plus gas phase volume. Therefore, the excess volume V^e results

$$V^e = V - V^g - V^s = 0 \tag{2.33}$$

From equations (2.31) and (2.32), the internal energy of the adsorbed phase U^e is

$$U^e = TS^e + \sum_{i=1}^c \mu_i n_i^e + \Phi \tag{2.34}$$

where S^e is the entropy of the adsorbed phase, and Φ the surface potential or chemical potential of the solid adsorbent relative to its pure standard state at the equilibrium pressure and temperature. They are given by

$$S^e = S - S^g - S^s \qquad\qquad \Phi = \mu - \mu^s \tag{2.35}$$

If not adsorption occurs, then μ is equal to μ^s and the surface potential is zero. Using the Legendre transformations for the auxiliary functions in the adsorbed phase results (Myers, 2002)

$$U^e = H^e \tag{2.36a}$$

$$G^e = A^e = H^e - TS^e = \sum_{i=1}^{c} \mu_i n_i^e + \Phi \tag{2.36b}$$

$$\Omega^e = G^e - \sum_{i=1}^{c} \mu_i n_i^e = \Phi \tag{2.36c}$$

where H^e, A^e, and G^e mean enthalpy, Helmholtz free energy, and Gibbs free energy, respectively. The free energy of the adsorbed phase consists of the free energy of n_i^e moles of each species in equilibrium with the gaseous phase plus the surface potential, Φ, which is zero if no adsorption takes place. The excess grand potential coincides with the surface potential.

The excess integral functions for the adsorbed phase [eqs. (2.36)] are defined relative to the perfect gas reference state at the same temperature (Myers, 2002; Myers & Monson, 2002)

$$\Delta G^e = \Delta H^e - T\Delta S^e = \sum_{i=1}^{c} n_i^e \left(\overline{\mu}_i - \mu_i^0 \right) + \Omega^e = \Delta G^{comp} + \Delta G^{imm} \tag{2.37a}$$

$$\Delta H^e = \sum_{i=1}^{c} n_i^e \left(\overline{h}_i - h_i^0 \right) - T^2 \frac{\partial}{\partial T} \left[\frac{\Omega^e}{T} \right]_{P, y_i} = \Delta H^{comp} + \Delta H^{imm} \tag{2.37b}$$

$$\Delta S^e = \sum_{i=1}^{c} n_i^e \left(\overline{s}_i - s_i^0 \right) - \left[\frac{\partial \Omega^e}{\partial T} \right]_{P, y_i} = \Delta S^{comp} + \Delta S^{imm} \tag{2.37c}$$

The quantities μ_i^0, s_i^0, and h_i^0 refer to the molar values in the perfect gas reference state. The overline notation means partial molar variables in the bulk gas phase. The derivatives are at constant pressure P, and constant molar fraction of the i adsorbate in the gas phase y_i. Equations (2.37) show that adsorption may be decomposed into

an isothermal compression of n_i^e moles of each gas from its perfect gas reference state to the equilibrium pressure, and an isothermal, isobaric immersion of clean adsorbent in the compressed gas (Myers, 2002; Myers and Monson, 2002).

The functions in equations (2.37) are converted to molar excess functions by dividing each function by the total amount adsorbed n_t^e

$$\Delta g^e = \frac{\Delta G^e}{n_t^e} = \Delta h^e - T\Delta s^e \tag{2.38a}$$

$$\Delta h^e = \frac{\Delta H^e}{n_t^e} \tag{2.38b}$$

$$\Delta s^e = \frac{\Delta S^e}{n_t^e} \tag{2.38b}$$

Differentiation of equations (2.37) gives the differential functions for a component i in the adsorbed phase (Myers, 2002; Myers & Monson, 2002)

$$\Delta \overline{g}_i^e = \left[\frac{\partial \Delta G^e}{\partial n_i^e} \right]_{T,n_j^e} = \overline{\mu}_i - \mu_i^0 = RT\ln\left(\frac{f_i}{f_i^0} \right) \tag{2.39a}$$

$$\Delta \overline{h}_i^e = \left[\frac{\partial \Delta H^e}{\partial n_i^e} \right]_{T,n_j^e} = \overline{h}_i - h_i^0 = -RT^2\left[\frac{\partial \ln f_i}{\partial T} \right]_{n_i^e,n_j^e} = R\left[\frac{\partial \ln f_i}{\partial(1/T)} \right]_{n_i^e,n_j^e} \tag{2.39b}$$

$$\Delta \overline{s}_i^e = \left[\frac{\partial \Delta S^e}{\partial n_i^e} \right]_{T,n_j^e} = \overline{s}_i - s_i^0 = -\frac{\partial}{\partial T}\left[RT\ln\left(\frac{f_i}{f_i^0} \right) \right]_{n_i^e,n_j^e} \tag{2.39c}$$

The differential molar functions are based on the perfect gas reference state and are obtained at constant molar fractions of the components. The independent variables for the differential functions are temperature and mol numbers. f_i^0 is the standard-state fugacity. The overline notation in these functions is used to distinguish differential functions from molar integral functions. The partial molar and molar functions are equal for a pure bulk fluid. The molar and differential functions for the adsorbed phase are unequal, even for a pure adsorbate.

The differential enthalpy for adsorption of a pure, perfect gas is given by

$$\Delta \bar{h}^e = -RT^2 \left[\frac{\partial \ln p}{\partial T} \right]_{n^e}$$ (2.40)

This equation, with a plus sign, is identical with the isosteric heat of adsorption (Hill, 1949, 1950). Differential enthalpy as defined by equation (2.40) is a state function which can be measured either by calorimetry or by differentiating a series of adsorption isotherms at constant loading (Myers, 2002). The differential enthalpy contains less thermodynamic information than the molar enthalpy (Hill, 1950). This is related to the fact that more work is involved in using equation (2.38b) than equation (2.40), as Ω^e must first be calculated by integration from equation (2.30).

The equation of state for the adsorbed phase is the surface potential, which for a given density can be expressed as a function of the temperature, pressure and mol fraction of each component in the gas phase. From equation (2.30), the adsorption isotherm for a pure, perfect gas is

$$n^e = -\frac{p}{RT} \left[\frac{\partial \Omega^e}{\partial p} \right]_T$$ (2.41)

In general, no equation of state is known that leads to an adsorption isotherm which fits experimental data over the entire range of gas pressure considered.

2.4.3 Adsorption against solution thermodynamics

In the framework of adsorption thermodynamics, the differential of internal energy for the adsorbed phase can be written as (Hill, 1949, 1950)

$$dU^a = TdS^a + \sum_{i=1}^{c} \mu_i dn_i^a + \varphi d\Sigma$$ (2.42)

while from solution thermodynamics, the following expression is obtained (Myers, 2002)

$$dU^e = TdS^e + \sum_{i=1}^{c} \mu_i dn_i^e + \Phi dm$$ (2.43)

Comparing these equations the point at which adsorption thermodynamics diverges from solution thermodynamics can be clearly understood. Adsorption thermodynamics assumes an inert adsorbent; that is, all its thermodynamic properties are the same in the presence as in the absence of adsorbate molecules. The interaction between the adsorbed molecules and the adsorbate are included in the spreading pressure, φ (energy by unit area). Additionally, the surface area and structure of the adsorbent are independent of temperature and pressure (Hill, 1949, 1950).

From the perspective of solution thermodynamics, on the other hand, it is assumed that the intimate contact of the adsorbate molecules with the atoms of the porous material alters the surface potential of the solid phase, Φ (energy on mass basis). That is, the chemical potential of the solid phase changes with the amount adsorbed. Adsorbent that swell can be included in the analysis (Hill, 1949, 1950; Myers, 2002).

Adsorption thermodynamics is valid when the surface area can be measured experimentally. In this case, the model of an inert adsorbent with adsorption occurring in a film on its external surface is realistic. However, the physics of adsorption in porous solids is best described within the framework of solution thermodynamics because spreading pressure in a micropore is undefined and the surface area can not be well defined in these cases (Myers, 2002).

For the case of an inert adsorbent with a well defined surface area, a relationship between the spreading pressure and the surface potential of a solid phase results (Hill, 1950; Myers, 2002)

$$\varphi \Sigma = \Phi m \tag{2.44}$$

2.4.4 Surface potential and osmotic pressure

Hill (1950) discusses the relation between the surface potential of the solid phase Φ and the osmotic pressure Π. It is assumed that a pure solid phase at a pressure P and temperature T is separated from a solution (gas plus solid phase), at the same pressure and temperature, by a kind of semi-permeable piston. This piston is impermeable to sorbate but sorbent can pass through it; that is, the piston prevents the sorbate from spreading over the entire sorbent. The chemical potential of pure sorbent is μ^s and of sorbent in the solution is μ. The osmotic pressure is defined as the

excess hydrostatic pressure on the solution needed in order to increase μ up to the value μ^s (at constant temperature and composition)

$$\mu^s - \mu = -\Phi = -\Omega^e = \int_P^{P+\Pi} V^s dP \tag{2.45}$$

For an inert adsorbent, the volume of the solid phase (V^s) as well as the area (Σ) are constant, and equation (2.45) yields

$$\Phi m = \varphi \Sigma = -\Pi V^s \tag{2.46}$$

By using equations (2.45) and (2.46) it is possible to write

$$\Omega = \Omega^e + \Omega^s - P^g V^g = \mu - \mu^s + \mu_0^s - P^g V^g \tag{2.47}$$

The chemical potential of the solid phase μ^s depends on the chemical potential in vacuo and on the pressure in the solid phase, which can be obtained from equation (2.46)

$$\mu^s = \mu_0^s + \Pi V^s \tag{2.48}$$

By replacing this last expression in equation (2.47) yields

$$\Omega = \mu - \Pi V^s - P^g V^g \tag{2.49}$$

Finally, by considering the definition of the grand potential [eq. (2.25)] and equation (2.49) the following equality results

$$PV = \Pi V^s + P^g V^g \tag{2.50}$$

which defines a relationship between the applied pressure and the pressure in the solid and gas phase, respectively.

2.5 The capillary model

As it was previously indicated the water retention capacity in soils is not exclusively a capillary process. However, the capillary model is a simple and intuitive tool to analyse

the water retention capacity of soils, although it has a limited application because the model is only able to reproduce part of the complex mechanisms that hold water in soils.

In clayey soils that assumption could be considered valid in the zone of low suctions where the main mechanism of water retention in compacted samples is attributed to capillarity (Romero et al., 2001). However, in the region of high suction values, soil water retention capacity is mainly related to physico-chemical interactions between the clay particles and the water tightly attached to them. On the other hand, this approximation is more appropriate for the analysis of the retention capacity in granular soils.

2.5.1 The capillary principle

When a capillary tube is dipped in a free water reservoir a meniscus results as a consequence of the interaction between the water and the walls of the tube. The curvature of this meniscus will be greater the narrower the tube. The occurrence of curvature causes a pressure difference to develop across the liquid-gas interface. In the case of water, the meniscus will be concave toward the gas phase, and the liquid pressure under the meniscus P_l will be smaller than the gas pressure P_g. For this reason, the water inside the tube and the meniscus will be driven up the tube until the pressure difference between the water inside the tube and the water under the flat surface outside the tube is entirely countered by the hydrostatic pressure of the water column in the capillary tube.

The equation of Young and Laplace relates the difference between the pressures in the liquid and in the gas phases throughout the following relationship (Gregg & Sing, 1967)

$$P_c = P_g - P_l = \frac{2\gamma_{gl}\cos\theta_{sl}}{r} \tag{2.51}$$

where P_c is capillary pressure, γ_{gl} is the surface tension between fluids (liquid and gas), θ_{sl} is the angle at which the liquid meets the capillary, and r is the radius of the

capillary tube. Equation (2.51) corresponds to energy on volume basis. If this energy is expressed in terms of mass basis that equation becomes

$$\mu_c = \frac{2\gamma_{gl}\cos\theta_{sl}}{\rho_l r} \tag{2.52}$$

with μ_c the capillary potential on mass basis, and ρ_l the liquid density.

2.5.2 Capillary in soils

Equation (2.51) is a good first approximation to explain the water retention capacity in soils. However, the limited range of applicability of the capillary model when used in the analysis of the water retention capacity by soils can be partially explained using the concept of spreading pressure. This pressure was already defined by equation (2.17) within the framework of adsorption thermodynamics.

The spreading pressure of a liquid on a solid is the increase in the Gibbs free surface energy of phase transfer of a solid from a liquid into its vapour. It is given by (Harkins & Livingston, 1942)

$$\varphi_{l/s'} = \gamma_{sv} - \gamma_{sl} \tag{2.53}$$

where γ_{sv} and γ_{sl} are the solid-vapour and solid-liquid interfacial tension respectively, and the subscript s' represents the solid covered by a film which is in equilibrium with the liquid l. An additional relation which expresses equation (2.53) can be obtained when the equilibrium between a lens of the liquid and the surface of the solid in equilibrium with the saturated vapour of the liquid is considered

$$\gamma_{sv} - \gamma_{sl} = \gamma_{lv}\cos\theta_{sl} \tag{2.54}$$

with γ_{lv} the liquid-vapour interfacial tension and θ_{sl} the equilibrium angle between the solid and the liquid lens.

On the other hand, the spreading pressure of a liquid on a clean surface of a solid is given by

$$\varphi_{l/s} = \gamma_{s0} - \gamma_{sl} \tag{2.55}$$

where γ_{s0} is the interfacial tension of the solid in a vacuum (note that the subscript s does not have the prime symbol).

Solids that exhibit a zero contact angle with water are classed as hydrophilic while others which give a finite contact angle are designated as hydrophobic. In the case of soils, which can be included in the former group ($\theta_{sl} = 0$), the final spreading pressure ($\varphi_{l/s'}$) is equal to γ_{lv} [see eqs. (2.53) and (2.54)]. Experimental results about the interaction between water and different solids indicate that the initial spreading pressure ($\varphi_{l/s}$) is very much larger than $\varphi_{l/s'}$.

It is deduced from precedent equations that it is not possible to express the initial spreading pressure ($\varphi_{l/s}$) by equation (2.54) whether the equilibrium angle (θ_{sl}) is equal to or larger than zero. The equilibrium value of the contact angle is obtained when the surface of the solid is covered by a film of the material of the liquid, and this film has the same vapour pressure as the pure liquid (Harkins & Livingston, 1942).

Now, recalling equation (2.51) it is clear that the capillary pressure only considers part of the total energy of interaction between the solid particles and the water. This constitutes a limitation of the capillary model when applied to the quantitative analysis of water retention data by soils.

2.6 Gibbs free energy of the adsorbed phase and water matric potential

The differential of the matric potential of water in soil is given by equation (2.15)

$$d\mu_m = \mu_w \, dw + \frac{\partial G_t}{\partial e} de \tag{2.56}$$

It is interesting to relate the above expression with the results obtained using the solution thermodynamics approach. Applying equations (2.24), (2.32) and (2.50) to the adsorption of a single component yields

$$dU^e = -TdS^e + \mu^e dn^e - PdV + \Pi dV^s + P^g dV^g \qquad (2.57)$$

where the symbol μ^e has been used to emphasize that it refers to the chemical potential of the adsorbed phase. Combining the differential of the excess Gibbs free energy [eq. (2.36b)] and equation (2.57) the following expression is obtained

$$dG^e = -S^e dT + \mu^e dn^e - PdV + \Pi dV^s + P^g dV^g \qquad (2.58)$$

From the definition of the total volume, the differential of the gas phase volume is

$$dV^g = dV - dV^s \qquad (2.59)$$

Using this equality in equation (2.58) yields

$$dG^e = -S^e dT + \mu^e dn^e - (P^g - \Pi)dV^s - (P - P^g)dV \qquad (2.60)$$

As it was indicated, the porous space within the porous medium is given by the connected porous space (which is assumed equal to V^g) and the occluded porous space. If the total volume of the porous space is indicated as V_v and that of the occluded porosity as V_{vm}, the following relationships can be defined

$$dV^s = dV_{vm} = V_s de_m \qquad (2.61a)$$

$$dV = dV_v = V_s de \qquad (2.61b)$$

where V_s is the particle solid volume and e_m is the void ratio of the matrix. Replacing in equation (2.60) yields (for a constant temperature)

$$dG^e\big|_T = \mu^e dn^e - (P^g - \Pi)V_s de_m - (P - P^g)V_s de \qquad (2.62)$$

Now, equations (2.56) and (2.62) can be compared remembering that the former represents energy per unit mass of the liquid while the latter is energy referred to the mass of the solid phase.

In the case of swelling soils, under a condition of constant volume ($de = 0$), the water chemical potential in equation (2.56) includes the water chemical potential

corresponding to the adsorption on an inert adsorbent plus a term which takes into account the effect due to the matrix deformability.

2.7 Thermo-hydro-mechanical processes

So far, the soil and water interaction has been considered the be at static equilibrium. This interaction, however, depends on factors like liquid and gas pressures, solute concentration, temperature, external loads. In nature, conditions change continually due to influences from within, as well as from outside the soil. Disturbances of equilibrium conditions tend to be dissipated until new equilibrium is attained. A way to describe and predict these processes is using coupled thermo-hydro-mechanical formulations which consider simultaneously all the phenomena occurring within the porous media.

The coupled thermo-hydro-mechanical (THM) formulation used in this Thesis has been described elsewhere (Olivella et al., 1994, 1996) and it will only be outlined herein. A representative element volume (REV) of the porous medium under consideration is shown in Figure 2.1.
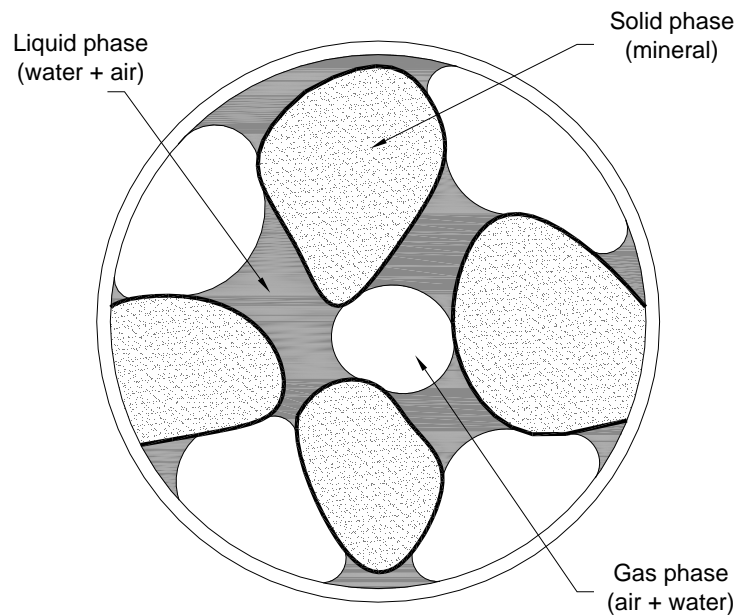
Figure 2.1. Schematic representation of a representative element volume (REV) of the porous medium.

To establish the balance equations, the compositional approach is adopted, consisting of balancing the species (mineral, water and air) rather than the phases (solid, liquid and gas). In this way, phase change terms do not appear explicitly in the equations, which is particularly useful when equilibrium conditions are assumed. The following convention is established for writing the equations defining the formulation: superscripts refer to species (w for water and a for air) and subscripts refer to phases (s for solid, l for liquid and g for gas). Dry air is considered as a single species. No symbol is attributed to the mineral species, because it has been assumed that it coincides with the solid phase.

In this approach, the macroscopic balance of any thermodynamic property per unit mass ψ is expressed by

$$\frac{\partial}{\partial t}(\rho\psi) + \nabla \cdot (\mathbf{j}_\psi) - f^\psi = 0 \tag{2.63}$$

where ρ is the mass density of the species per unit volume containing ψ, $\mathbf{j}_\psi$ is the total flux of ψ with respect to the reference system, and f^ψ is the rate of production/removal of ψ per unit of volume. The total flux $\mathbf{j}_\psi$ can be decomposed into an advective component (phase motion) and a nonadvective component (motion of the species inside the phase)

$$\mathbf{j}_\psi = \rho\psi\mathbf{v}_\psi + \mathbf{i}_\psi \tag{2.64}$$

where $\mathbf{v}_\psi$ is the mass weighted mean velocity and $\mathbf{i}_\psi$ represents the nonadvective flux. The total flux is expressed in relation to a fixed reference system and therefore it is necessary to account for the fact that the solid indeed moves (Olivella et al., 1994).

2.7.1 Mass balance of solid

Mass balance of solid in the medium is written as

$$\frac{\partial}{\partial t}[\rho_s(1+\phi)] + \nabla \cdot [\rho_s(1+\phi)\dot{\mathbf{u}}] = 0 \tag{2.65}$$

where ρ_s is the mass of solid per unit volume of solid, ϕ is the porosity of the medium, and $\mathbf{u}$ is the solid displacement vector. The dot symbol indicates time derivative. Using the material derivative with respect to the solid, defined as

$$\frac{D_s(\bullet)}{Dt} = \frac{\partial(\bullet)}{\partial t} + \dot{\mathbf{u}} \cdot \nabla(\bullet)$$
(2.66)

it is possible to obtain an expression for the porosity variation from equation (2.65)

$$\frac{D_s\phi}{Dt} = \frac{1-\phi}{\rho_s}\frac{D\rho_s}{Dt} + (1-\phi)\nabla \cdot \dot{\mathbf{u}}$$
(2.67)

2.7.2 Mass balance of water

Water is present in liquid and gas phases. The total mass balance is expressed as

$$\frac{\partial}{\partial t}\left(\theta_l^w S_l \phi + \theta_g^w S_g \phi\right) + \nabla \cdot \left(\mathbf{j}_l^w + \mathbf{j}_g^w\right) = f^w$$
(2.68)

where θ_α^w is the mass of water per unit volume of the α phase, S_α is the volumetric fraction of pores occupied by the α phase, $\mathbf{j}_\alpha^w$ is the flux of water in the α phase, and f^w is a water supply. Using equations (2.66) and (2.67), and considering that ρ_s is constant, expression (2.68) yields to

$$\phi\frac{D_s}{Dt}\left(\theta_l^w S_l + \theta_g^w S_g\right) + \left(\theta_l^w S_l + \theta_g^w S_g\right)\nabla \cdot \dot{\mathbf{u}} + \nabla \cdot \left(\mathbf{j}_l'^w + \mathbf{j}_g'^w\right) = f^w$$
(2.69)

In this expression, $\mathbf{j}_\alpha'^w$ represents the flux of water in the α phase with respect to the solid phase. That term can be written as

$$\mathbf{j}_\alpha^w = \mathbf{j}_\alpha'^w + \theta_\alpha^w S_\alpha \phi\, \dot{\mathbf{u}} \qquad\qquad \mathbf{j}_\alpha'^w = \mathbf{i}_\alpha^w + \theta_\alpha^w \mathbf{q}_\alpha$$
(2.70)

where $\mathbf{i}_\alpha^w$ is the nonadvective flux of water in the α phase and $\mathbf{q}_\alpha$ is the advective volumetric flux of the α phase with respect to the solid phase.

2.7.3 Mass balance of air

The procedure to obtain the mass balance of air is similar to that applied for water. It is considered that the air is the main component of the gas phase and that it may be also present as dissolved air in the liquid phase. The final expression is similar to that in equation (2.69), but the superscript w is changed by a.

2.7.4 Momentum balance for the medium

The inertial terms are not considered and the momentum balance reduces to

$$\nabla \cdot \boldsymbol{\sigma} + \mathbf{b} = \mathbf{0} \tag{2.71}$$

where $\boldsymbol{\sigma}$ is the stress tensor and $\mathbf{b}$ is the vector of body forces.

2.7.5 Internal energy balance for the medium

Considering the internal energy of each phase, the equation of internal energy balance for the porous media is

$$\frac{\partial}{\partial t}\left[E_s\rho_s(1-\phi) + E_l\rho_l S_l\phi + E_g\rho_g S_g\phi\right] + \nabla \cdot \left(\mathbf{i}_c + \mathbf{j}_{Es} + \mathbf{j}_{El} + \mathbf{j}_{Eg}\right) = f^E \tag{2.72}$$

where E_α is the specific internal energy (internal energy per unit mass of phase) and ρ_α the density corresponding to each α phase. $\mathbf{i}_c$ is energy flux due to conduction through the porous medium, $\mathbf{j}_{E\alpha}$ are advectives fluxes caused by mass motion and f^E is an energy supply.

2.7.6 Constitutive equations and equilibrium restrictions

To solve a general problem, the dependent variables in the balance equations presented above have to be related to the state variables (unknowns). This is achieved through constitutive and constrain equations as well as equilibrium restrictions (Olivella et al., 1994, 1996). In this formulation, the selected unknowns are the solid

displacement vector $\mathbf{u}$, the liquid phase pressure P_l, the gas phase pressure P_g, and the temperature T.

The conductive flux of heat is simulated using the Fourier´s law

$$\mathbf{i}_c = -\lambda_T \nabla T \qquad\qquad \lambda_T = f\left(\lambda_{dry}, \lambda_{sat}, S_l\right) \qquad\qquad (2.73)$$

where λ_T is the current soil thermal conductivity that depends on the thermal conductivity in dry and saturated state, λ_{dry} and λ_{sat} respectively, and on the liquid degree of saturation S_l.

The advective flow of the α phase is given by the generalized Darcy´s law (Bear, 1972)

$$\mathbf{q}_\alpha = -\frac{\mathbf{k} k_{r\alpha}}{\mu_\alpha}(\nabla P_\alpha - \rho_\alpha \mathbf{g}) \qquad\qquad (2.74)$$

with $\mathbf{k}$ the tensor of intrinsic permeability that depends on pore structure of the medium, $k_{r\alpha}$ the relative permeability of the α phase, which controls the permeability in unsaturated state, μ_α the dynamic viscosity, P_α the pressure in the α phase, and $\mathbf{g}$ the gravity vector.

The relative permeability of the α phase depends on the effective degree of saturation $S_{\alpha e}$

$$k_{r\alpha} = f\left(S_{\alpha e}\right) \qquad\qquad (2.75)$$

The Fick´s law defines the nonadvective flux of species inside the fluid phases. It defines the flux in terms of gradients of mass fraction of species ω_α^i and a hydrodynamic dispersion tensor $\mathbf{D}_\alpha^i$

$$\mathbf{i}_\alpha^i = -\mathbf{D}_\alpha^i \cdot \nabla \omega_\alpha^i \qquad\qquad (2.76)$$

The dispersion tensor includes nonadvectives fluxes caused by molecular diffusion and mechanical dispersion. It depends on porosity, degree of saturation and advective phase flux (Olivella & Gens, 2000).

The hydraulic constitutive law (soil water retention curve) defines the relationship between the effective liquid degree of saturation S_{le} and the suction s, which is a stress variable related to fluid pressures

$$S_{le} = f(s) \tag{2.77}$$

A general expression for the mechanical constitutive law can be written as

$$\dot{\boldsymbol{\sigma}} = \mathbf{D} \cdot \dot{\boldsymbol{\varepsilon}} + \mathbf{f}\dot{s} + \mathbf{t}\dot{T} \tag{2.78}$$

where $\boldsymbol{\sigma}$ is the stress vector, $\boldsymbol{\varepsilon}$ is the strain vector, $\mathbf{D}$ is the constitutive stiffness matrix, $\mathbf{f}$ is a constitutive vector relating changes in the fluid pressures and stresses, and $\mathbf{t}$ is a constitutive vector relating stresses and temperature changes.

The properties of the fluid phases appearing in the balance equations and in the constitutive law depend on the composition of the phases and on the state variables (temperature and fluid pressures).

The formulation assumes that phase changes are rapid in relation to the characteristic times typical of these types of problems (Olivella et al., 1994). Therefore, they can be considered in local equilibrium, giving rise to a set of equilibrium restrictions that must be satisfied at all times. Thus, an equilibrium restriction defines the concentration of dissolved air in liquid phase, which is evaluated by means of Henry's law. Other restriction is given for the concentration of water vapour in gas phase, which is computed through the psychometric law.

Table 2.2 is a summary of the constitutive laws and equilibrium restrictions incorporated in the general formulation. This table also includes the dependent variables that are computed using each one of the adopted laws. Thus, for example, the retention curve (hydraulic constitutive law) relates the degree of saturation of the liquid phase (dependent variable) with the liquid and gas pressure (state variables).

Constitutive equation	Variable name	Symbol
Darcy´s law	Liquid and gas advective flux	$\mathbf{q}_l , \mathbf{q}_g$
Fick´s law	Water nonadvective flux in gas phase	$\mathbf{i}_g^w$
Fourier´s law	Conductive heat flux	$\mathbf{i}_c$
Hydraulic model (retention curve)	Liquid phase degree of saturation	S_l
Mechanical model	Stress tensor	$\boldsymbol{\sigma}$
Phase density	Liquid phase density	ρ_l
Ideal gas law	Gas phase density	ρ_g
Equilibrium restriction	Variable name	Symbol
Henry´s law	Air mass fraction in liquid phase	ω_l^a
Psychrometric law	Water mass fraction in gas phase	ω_g^w
Constrain equation	Variable name	Symbol
$\boldsymbol{\varepsilon} = \dfrac{1}{2}\left[(\nabla \cdot \mathbf{u}) + (\nabla \cdot \mathbf{u})^T \right]$	Deformation tensor	$\boldsymbol{\varepsilon}$
$S_l + S_g = 1$	Gas phase degree of saturation	S_g
$\omega_l^w + \omega_l^a = 1$	Water mass fraction in liquid phase	ω_l^w
$\omega_g^w + \omega_g^a = 1$	Air mass fraction in gas phase	ω_g^a
$\mathbf{i}_l^w + \mathbf{i}_l^a = \mathbf{0}$	Water nonadvective flux in liquid phase	$\mathbf{i}_l^w$
$\mathbf{i}_g^w + \mathbf{i}_g^a = \mathbf{0}$	Air nonadvective flux in gas phase	$\mathbf{i}_g^a$

Table 2.2. Constitutive equations, equilibrium restrictions, constrain equations, and associated dependent variables used in the formulation.

2.8 Concluding remarks

The different components of the total potential of the water in soil were introduced. Moreover, how they have been traditionally considered from a thermodynamic point of view was discussed. From this analysis an expression for the free energy of the soil water results. Also, an expression for the free energy of the adsorbed phase could be deduced by using concepts of thermodynamic of adsorption. The comparison of both expressions permits to conclude that in the case of swelling soils the matric potential of water in soils also depends on the changes at the microstructural level.

Thermodynamic of interfacial phenomena introduces two definitions associated to the free energy of the solid phase. When the solid is assumed inert this is called the spreading pressure while in deformable solids it is called the surface potential of the solid phase. These variables change as the adsorption progress and they represent a quantity similar to the surface tension. Moreover, a relation between both variables and the more familiar osmotic pressure could be established. Thus, for the case of an inert adsorbent a relation between the applied pressure, the gas pressure and the pressure in the solid phase is deduced.

The limitation of the capillary model to describe the retention capacity of water by fine-graded soils could be explained by using the definition of spreading pressure. Thus, the capillary model represents the energy of adhesion of the water with the surface of the solid particles already covered with a film in equilibrium with the saturated vapor of the liquid. This energy is a very much smaller value than the real adhesion energy between the clean particles of clayey soils and the liquid water.

Chapter 3

Effect of temperature and density on the water retention capacity of expansive clays

Summary

The Chapter presents the analysis of experimental data of the retention capacity of MX-80 bentonite samples obtained under isochoric conditions at different dry densities and temperatures. The influence of dry density on the water retention capacity depends on the suction range. For suctions above a threshold value, the retention capacity in terms of water content is almost independent of the dry density, whereas for lower suctions, the lower the dry density the higher the water content for a particular suction. The retention capacity decreases with temperature, more than predicted by the change in interfacial tension of water in equilibrium with its vapour.

The water retention capacity of soils is included in the analysis of thermo-hydro-mechanical problems through the soil water retention curve. In this Chapter, some modifications to the law proposed by van Genuchten (1980) have been put forward to fit experimental values. Effects of temperature and void ratio on the water retention capacity (other than the traditionally included in the air entry value coefficient) were incorporated throughout empirical laws that resemble the experimental evidences. By a fitting process, values of the coefficients in those laws were determined for the material used in this work.

Finally, one-dimensional THM simulations using the finite element program CODE_BRIGHT have been performed in order to analyse the consequences of considering or not temperature and density influences on the water retention curve.

3.1 Preface

A current design for engineered barriers in the context of high level radioactive waste disposal includes bentonite compacted blocks initially unsaturated. The heat released by the waste may induce high temperatures in the bentonite barrier. As an example, in the Temperature Buffer Test (TBT) values well above 100 ºC are reached in the bentonite rings surrounding the heaters in order to simulate real conditions in a particular disposal concept (Hökmark et al., 2007). The work presented in this Chapter investigates a fundamental issue concerning the influence of high temperatures on the retention capacity of compacted bentonite. Traditionally, water retention capacity of bentonite was measured under free volume conditions. It has been shown, however, that the experiments should be performed under constant volume conditions in order to simulate the confinement of the barrier (Lloret et al., 2004; Lloret & Villar, 2007). In addition to that, the temperature should be considered as an independent variable. Thus retention properties depend not only on density but also on temperature.

Although it is generally acknowledged that suction in soils is not exclusively a capillary process, a first analysis of experimental results can be carried out if it is assumed that the soil suction s, coincides with the capillary pressure given by equation (2.51)

$$s \equiv P_c = P_g - P_l = \frac{2\gamma_{gl}\cos\theta_{sl}}{r} \tag{3.1}$$

In clayey soils that assumption could be considered valid in the zone of low suctions where the main mechanism of water retention in compacted samples is attributed to capillary (Romero et al., 2001). However, in the region of high suction values, soil retention capacity is mainly related to physico-chemical interactions between the clay particles and the water tightly attached to them. On the other hand, it is expected that this approximation has a lower influence in the analysis of experimental results of sandy soils.

Philip & de Vries (1957) assume that the surface tension is the only temperature dependent parameter in equation (3.1) when analysing the moisture movement in porous media induced by temperature gradients. By mathematical derivation of this equation it is possible to obtain the variation of soil suction with respect to temperature, for constant water content, as

$$\left.\frac{\partial s}{\partial T}\right|_w = \frac{s}{\gamma_{gl}}\frac{\partial \gamma_{gl}}{\partial T} \qquad\qquad (3.2)$$

where w is the gravimetric water content. In deriving this equation it is assumed that the contact angle θ_{sl} is independent of the temperature.

Equation (3.2) suggests that suction decreases with temperature, as it occurs with the surface tension. However, experimental data indicate that suction decreases more rapidly than predicted by equation (3.2). Experimental results of temperature effects on water retention capacity in sand and silt loam described in the literature could not be explained from changes in the surface tension (Gardner, 1955; Chahal, 1964, 1965; Haridasan & Jensen, 1972; Hopmans & Dane, 1986; Nimmo & Miller, 1986; Constantz, 1991; She & Sleep, 1998; Bachmann et al., 2002). Generally, temperature effects were larger than those predicted by using the proposal of Philip & de Vries (1957).

Different alternatives have been suggested to explain the larger than expected changes in the water retention capacity due to temperature increase. Chahal (1964, 1965) attributed the discrepances to the effect of the thermal expansion of the entrapped air with increasing temperature. Hopmans & Dane (1986) suggest that the combined effect of entrapped air volume and surface tension should minimize the temperature influence on the water retention curve. Nimmo & Miller (1986) suggest that another origin for these differences can be the presence of organic substances that increase the temperature dependence of the surface tension.

Grant & Salehzadeh (1996) present a modification of equation (3.2) that incorporates changes in the contact angle induced by temperature. They fit experimental data of water retention in soils and a glass-beads sample at different temperatures and show that the temperature sensitivity of the contact angle has effects on the retention capacity. Grant (2003) analyses the applicability of that extension to the zone of low water content. She & Sleep (1998) used the model proposed by Grant & Salehzadeh (1996) and conclude that the contact angle in silica sand samples depends not only on the temperature but also on the water content. A similar conclusion was obtained by Bachmann et al. (2002) when analysing three different soils.

Lui & Dane (1993) suggest that in soils, water appears as a continuous phase and as isolated packets. Their model supposes that an increase in temperature produces a flow from isolated packets to the continuous phase and it results in an additional temperature effect on the retention capacity.

The temperature influence on the water retention capacity of clayey soils has received special attention in the last decades (Romero et al., 2001; Villar & Lloret, 2004; Villar et al., 2005; Tang & Cui, 2005; Villar & Gómez-Espina, 2007). In compacted samples of clayey soils, it is assumed that temperature dependence of surface tension is the main mechanism affecting the soil water retention capacity when capillary effects dominate, that is, for high water contents (Romero et al., 2001). However, for low water contents, the main temperature effects on the water retention capacity are due to changes in the interaction mechanisms between clay particles and water (Romero et al., 2001; Villar & Lloret, 2004; Villar et al., 2005).

Furthermore, it is accepted that the soil fabric influences the water retention capacity of fine-graded soils in the low suction zone whereas no major effects are observed in the range of high suction values (Taylor & Box, 1960; Box & Taylor, 1962; Assouline et al, 1997; Al-Mukhtar et al., 1999; Vanapalli et al., 1999; Ng & Pang, 2000; Startsev & McNabb, 2001; Rao & Revanasiddappa, 2005). The density of the sample can be assumed as a first order approximation to the description of the soil fabric. At high suctions, the influence of porosity is negligible because the retention capacity depends mainly on the clay mineralogy and on the intra-aggregate structure which shows minor changes for samples of the same material compacted at different densities. On the other hand, at low suctions, the reduction in porosity when density increases, affects the water volume that can be retained by the soil. Al-Mukhtar et al. (1999), Vanapalli et al. (1999) and Ng & Pang (2000) conclude that in compacted samples showing a double structure fabric, the air entry value (i.e. the suction value when desaturation begins in a drying path) increases as the applied compaction pressure increases.

Experimental evidences indicate that temperature and density are variables which affect the water retention capacity of soils. In addition, the temperature influence on the soil water retention capacity is more important than that defined by the dependence of the water surface tension on the temperature. Villar et al. (2005, 2006) and Villar & Gómez-Espina (2007) presented experimental results about retention capacity of compacted samples of MX-80 bentonite. Samples were compacted at different densities and tested at temperatures ranging from 20 to 100 °C. The analysis of those experimental data using concepts already presented in Chapter 2 as well as the methodology proposed by Philip & de Vries (1957) is carried out in the present Chapter.

3.2 Experimental results

3.2.1 Material and experimental method

The MX-80 bentonite is extracted from Wyoming (USA). It is a worldwide known commercial material, of quite variable characteristics, supplied in the form of powder homoionised to sodium. The MX-80 bentonite consists mainly of montmorillonite (65-82 %). It also contains quartz (4-12 %), feldspars (5-8 %), and smaller quantities of cristobalite, calcite and pyrite. The bentonite of the batch used in the analysed experiments has a CEC of 74 meq / 100 g, and the major exchangeable cations are Na (61 meq / 100 g), Ca (10 meq / 100 g) and Mg (3 meq / 100 g). The equilibrium water content of the clay under laboratory conditions is 9.0 % (Villar et al., 2006).

A method to determine the retention curve at constant volume and at different temperatures, the sensor/cell method, was developed by Villar et al. (2005, 2006). Essentially it consists on measuring the relative humidity (RH) of clay blocks at particular water contents while they are kept inside stainless steel hermetic cells whose temperature can be regulated. Initially the clay is mixed with a given quantity of deionised water and kept for two days in a plastic bag to allow homogenisation of the moisture. Afterwards, a block of this mixture is compacted to the desired density. The dimensions of the block are equal to the internal dimensions of the cell, which are 7 cm diameter and 10 cm height. A hole is drilled in the central, upper part of the block to insert a capacitive sensor and the cell is closed. The external wall of the cell is covered with a silicone-rubber laminated heater that fixes the temperature all over the cell. After measuring the RH of the bentonite corresponding to the laboratory temperature, the temperature of the external heating mat is increased to 120 °C in intervals of 20 °C. Each target temperature is kept for about two days. The accuracy of the humidity sensor is ± 1 % over the range 0-90 % RH and ± 2 % over the range 90-100 % RH. The results obtained for dry densities of 1.60 and 1.75 Mg/m^3 are presented in this section.

Some of the results presented here were obtained following a methodology developed previously, in which the water retention curve at constant volume is determined in special cells designed to avoid the swelling of the clay in wetting paths (Villar, 2002; Villar & Lloret, 2004). The cells consist of a stainless steel cylindrical body with two perforated covers joined by bolts. The powdered clay is compacted directly inside the cell ring at room temperature using static uniaxial compaction. The length of the

specimen is 1.2 cm and its cross section area is 11.34 cm^2. The cells are placed in desiccators with a sulphuric acid solution or with a NaCl solution (i.e. the suction is imposed controlling the relative humidity). The cells allow the exchange of water between the clay and the atmosphere of the desiccators. Once the water content of the clay is stabilized (approximately after 2 to 3 months, depending on the dry density), the solution in the desiccators is changed in order to apply a different suction. To determine the curve at different temperatures, the desiccators are placed inside ovens. There are temperature dependent experimental relations between the concentration of the solution and its water activity. The drawback of the cell method is the duration of the tests, because the time to reach equilibrium at a given suction is very long.

The calculation of the chemical potential of soil water (or soil suction) on the basis of relative humidity is accomplished through the thermodynamics relationship (Edlefsen & Anderson, 1943)

$$RH = \exp\left[\frac{M_w \Delta\mu_w}{\rho_l RT}\right] = \exp\left[-\frac{M_w s}{\rho_l RT}\right] \tag{3.3}$$

with M_w the molar mass of water, R the gas constant and μ_w the water potential. The symbol Δ is used here to indicate that the chemical potential of soil water is defined relative to the perfect gas reference state at the same temperature.

The results obtained with both methodologies, despite the fact that their theoretical principles are different, have been found to be coherent (Villar et al., 2005, 2006; Villar & Gómez-Espina, 2007).

3.2.2 Test results

In Figure 3.1 some of the results obtained with both methodologies are plotted. They present the relation between the soil suction and the water content in samples tested under isochoric conditions and at different temperatures. The difference among the curves in Figure 3.1 is more important in the high water content zone and the trend indicates that near saturation the water content decreases when the temperature increases. It can be partially attributed to the water dilation and as suggested by different authors to the transference of interlayer water to the macropores as a consequence of the temperature increase (Ma & Hueckel, 1992, 1993; Villar & Lloret, 2004).
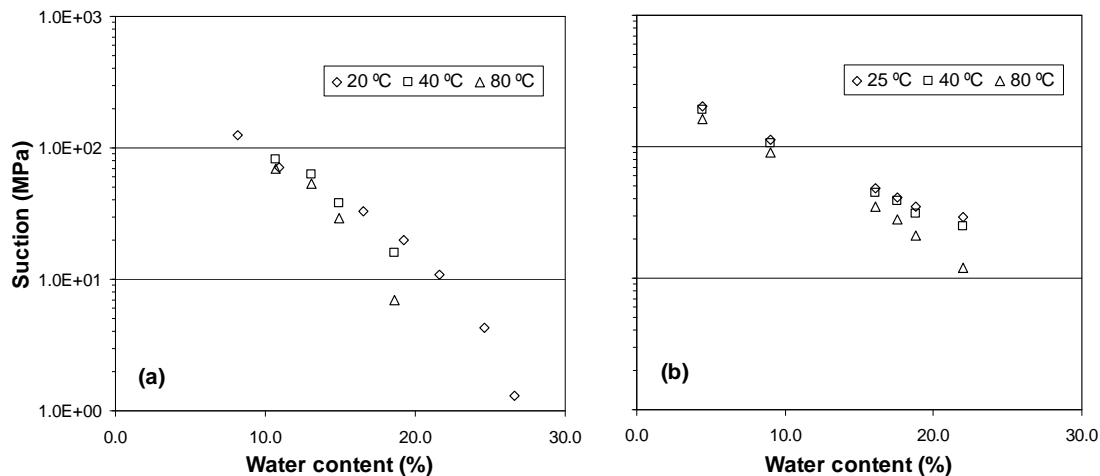
Figure 3.1. Experimental values of soil suction against water content for MX-80 bentonite samples tested at different temperatures and dry densities. (a) 1.60 Mg/m^3 (cell method for T = 20 ºC, sensor/cell method for T = 40 and 80 ºC); (b) 1.75 Mg/m^3 (sensor/cell method).

The properties of the water confined in small pores or in the proximity of the clay platelets have been investigated by many researchers (Low, 1979; Hawkins & Egelstaff, 1980; Sposito & Prost, 1980; Cariati et al., 1981; Skipper et al., 1991; Swenson et al., 2000; Fernández & Rivas, 2005; among others). The experimental results have shown that the water into the interlamellar space of smectite-like materials has properties that differ from those of the free water. In particular, the results suggest that its density is higher than 1.0 Mg/m^3. Experimental results of compacted bentonite samples also indicate that the water density is a function of the specimen density and water content, and values higher than 1.05 Mg/m^3 have been determined (Pusch et al., 1990; Villar & Lloret, 2004). Koster van Gross & Guggenheim (1984, 1986) and Huang et al. (1994) observed that, at low pressures and depending on the exchangeable cations, there exists a range of temperatures between 80 and 150 ºC in which the water content between the clay platelets decreases. Keren & Shainberg (1980) obtained a similar conclusion from results of sorption isotherms on montmorillonite powder determined at different temperatures. Ma & Hueckel (1992, 1993) suggest that an increase in temperature produces a transfer of water from the interlayer region to the pores between the clay aggregates (macropores). If the volume of the sample does not change very much and the interlayer water density is higher than one, then the volume occupied by the transferred water to the macropores increases and the sample becomes saturated earlier when temperature is increased (Villar & Lloret, 2004).

Figure 3.2 shows retention values of MX-80 bentonite samples compacted at two dry densities (1.30 y 1.80 Mg/m^3) and tested at 60 ºC using the cell method (Villar, 2005). The values correspond to a wetting path in the case of dry density 1.30 Mg/m^3 and to a wetting after drying path in the case of dry density 1.80 Mg/m^3. At high suctions the influence of the initial dry density is negligible, which means that the retention capacity mainly depends on the clay mineralogy and the intra-aggregate structure. At low suctions more water can be retained in the low density sample because of its higher total porosity. These results suggest that the water retention capacity of samples tested in confined conditions depends on its dry density. Similar results were obtained by Romero et al. (1999) and Lloret et al. (2004).
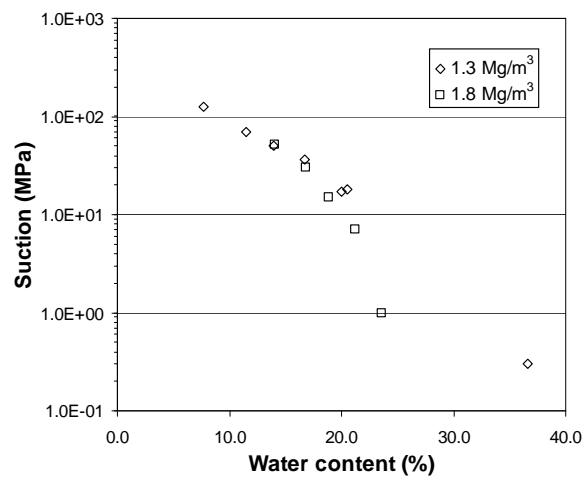
Figure 3.2. Suction against water content for compacted samples of MX-80 bentonite tested at 60 ºC under isochoric conditions with the cell method [from Villar (2005)].

3.3 Analysis of experimental results

An analysis of the experimental results using the concepts presented in Chapter 2 and the methods developed by Philip & de Vries (1957) is carried out in this section. However, previous to this analysis some aspects need to be addressed. As it was indicated, two methods were used to obtain the experimental data which have different theoretical principles.

In the cell method, the soil water potential is fixed and once equilibrium is attained, the water content is determined weighing the sample before and after it is placed in an oven at 105 ºC. On the other hand, in the sensor/cell method the total water content is initially defined and then the water potential determined at different temperatures. In

the latter case, although the total water content is constant, as the temperature increases more liquid water becomes vapour (water in the gas phase). This aspect has to be considered when experimental results from the sensor/cell method are analysed.

For the analysis of the temperature effect on the water retention capacity using the concepts described in Chapter 2, it will be preferable to express the energy of water in soil on a mass basis. In that case, the negative of the suction values expressed in MPa are numerically equal to the water potential values expressed in kJ/kg.

3.3.1 Total and liquid water content

An unsaturated soil can be considered as a porous medium where it is possible to indentify a solid, liquid and gaseous phase. The liquid degree of saturation, commonly referred to as degree of saturation, is defined by the following expression

$$S_l = \frac{\rho_d w}{\rho_l \phi}$$ (3.4)

where ϕ is the porosity, ρ_d the soil dry density, and ρ_l the liquid density. Strictly, the liquid phase is composed of water and dissolved air. But, because of the differences between the densities of the two species, it is commonly accepted that the liquid density is equal to the water density.

The initial water content in a soil (corresponding to a given temperature and pressure) defines a suction value (soil water potential). This suction can be evaluated through the relative humidity measured in the soil pores by using equation (3.3). At ambient temperature, the water content in the soil is defined by the mass of liquid water. However, if a soil sample is heated liquid water evaporates until a dynamic equilibrium is obtained between this and the water in the gas phase (vapour). If the sample is in a closed recipient the water content will be constant but, as more liquid water becomes vapour, the liquid degree of saturation will decrease.

By considering the initial liquid degree of saturation and porosity of a soil sample, it is possible to define the initial volume occupies respectively by the liquid phase V_l and gas phase V_g. From the initial conditions, the moles of vapour and air can also be determined.

It is assumed that the gas phase behaves as an ideal gas. Therefore, it is possible to determine the variation of the saturated vapour density ρ_v^0 with the temperature using equations (A.1) and (A.2). Then, if the relative humidity at different temperatures is determined experimentally it is possible to calculate the vapour density ρ_v using the relation

$$RH = \frac{\rho_v}{\rho_v^0} \qquad (3.5)$$

The gas phase volume and vapour density define the mass of water in the gaseous phase (vapour mass) m_g^w [see eq. (A.4)]. Finally, the water mass in the liquid phase m_l^w is calculated as

$$m_l^w = m_w - m_g^w \qquad (3.6)$$

where m_w is the total mass of water in the sample.

The vapour mass is calculated using the volume of the gas phase. If it is assumed that the temperature increment does not affect the porosity of the sample then the void volume is constant when the test is carried out in confined conditions. The volume of the water in bulk changes because its density decreases as the temperature increases. However, it is well known that in compacted samples of expansive soils the water density depends, among others, on the water potential, sample density, and kind of soil (see Chapter 4). Unfortunately, until most experimental results become available it is not possible to define a law which contemplates the effect of all those variables in the values of the soil water density. Because of that, the volume of the gas phase determined from the initial conditions was considered constant during the test. It is thought that this approximation might introduce some error at higher water contents and high temperatures (low suctions).

Appendix A presents the results obtained when the concepts described above are applied to the experiments on compacted samples of MX-80 bentonite with different initial water contents and dry densities of 1.60 and 1.75 Mg/m^3 (Villar et al., 2006; Villar & Gómez-Espina, 2007). Figure 3.3 shows calculated values of liquid water content and the corresponding values of suction for different temperatures and sample dry density. Straight lines in the figures were used to define suction values at intermediate liquid water contents.
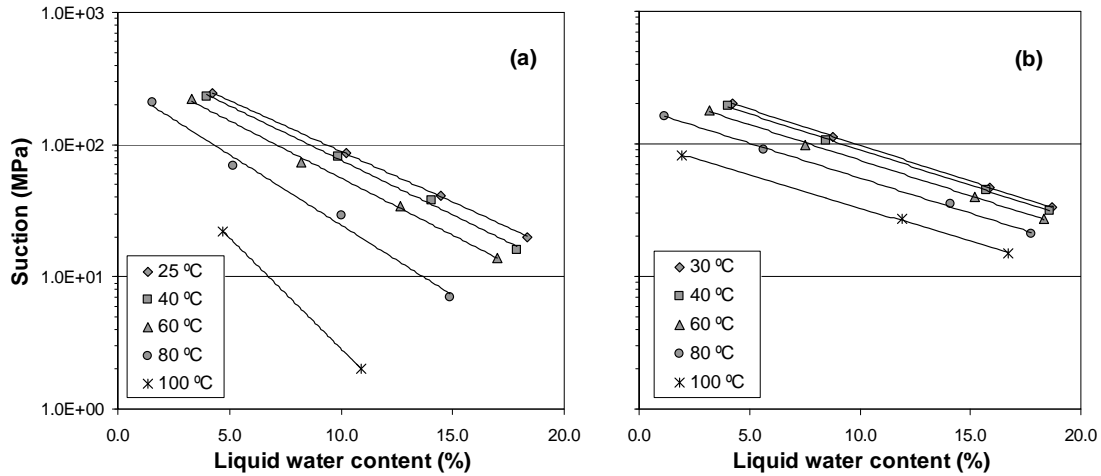
Figure 3.3. Experimental values of suction against calculated liquid water content for MX-80 bentonite samples tested at different temperatures and dry density equal to (a) 1.60 Mg/m^3 and (b) 1.75 Mg/m^3.

3.3.2 Analysis using solution thermodynamics

Using the solution thermodynamic approach, the following expression for the potential of soil water can be deduced [eq. (2.39a)]

$$\Delta\mu_w \equiv \Delta\overline{g}^e = \Delta\overline{h}^e - T\Delta\overline{s}^e \tag{3.7}$$

where $\Delta\overline{g}^e$, $\Delta\overline{h}^e$, and $\Delta\overline{s}^e$ are the differential Gibbs free energy, enthalpy, and entropy respectively, and T is the absolute temperature.

The differential entropy can be calculated as [eq. (2.39c)]

$$\Delta\overline{s}^e = -\left[\frac{\partial\Delta\overline{g}^e}{\partial T}\right]_{n^e} \tag{3.8}$$

with n^e the amount adsorbed. The differential entropy is the slope in a plot of the water potential as a function of the temperature (at constant amount adsorbed).

The differential enthalpy can be obtained dividing equation (3.7) by T^2 and rearranging terms, which gives (Taylor & Stewart, 1960)

$$\Delta \overline{h}^e = -T^2 \frac{\partial}{\partial T} \left[\frac{\Delta \overline{g}^e}{T} \right]_{n^e} \tag{3.9}$$

When the potential of soil water is determined through the relative humidity RH, it is more convenient to use these data to estimate the differential enthalpy. Writing the differential free energy as a function of the relative humidity in equation (3.9) and after some algebra, the following expression results

$$\Delta \overline{h}^e = R \left[\frac{\partial \ln(RH)}{\partial(1/T)} \right]_{n^e} \tag{3.10}$$

By use of equation (3.10) and the slope in a plot of $\ln(RH)$ as a function of $(1/T)$ it is possible to calculate the differential enthalpy.

Figure 3.4 is a plot of the water chemical potential as a function of temperature, at different liquid water contents and for each dry density considered in the experiments. Figure 3.5 presents values of $\ln(RH)$ as a function of the inverse of temperature for the same cases considered before. In both figures and within the range of water contents considered, the experimental results can be well fitted by straight lines.
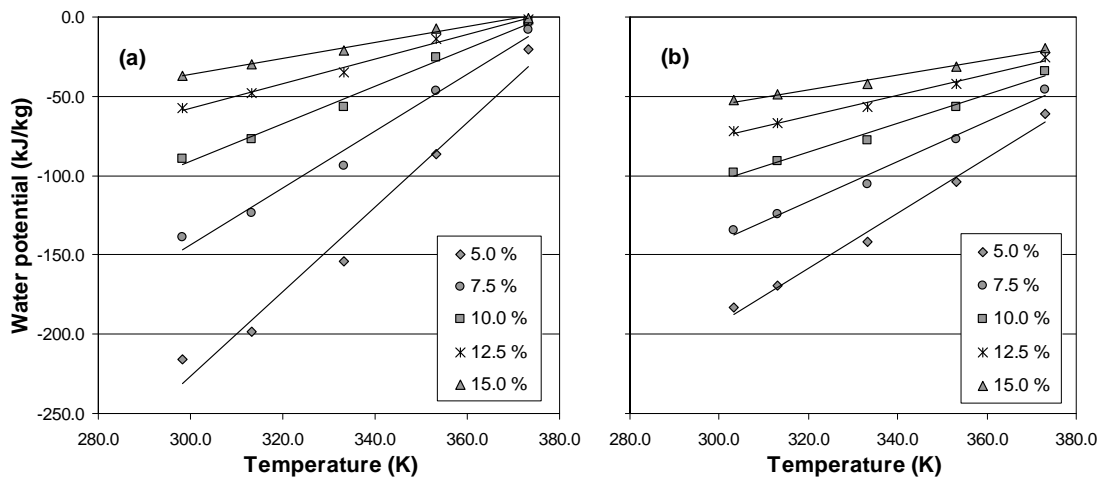
Figure 3.4. Water chemical potential against temperature at different water content for compacted bentonite samples at a dry density of (a) 1.60 Mg/m³ and (b) 1.75 Mg/m³. Continuous lines correspond to a linear fitting of experimental results.
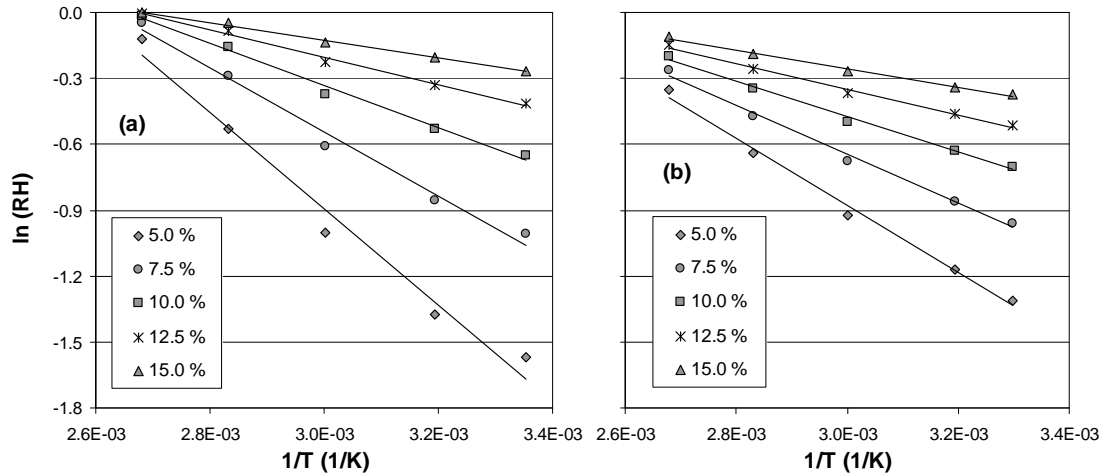
Figure 3.5. ln(RH) against 1/T at different water content for compacted bentonite samples at a dry density of (a) 1.60 Mg/m³ and (b) 1.75 Mg/m³. Continuous lines correspond to a linear fitting of experimental results.

The slopes of straight lines in Figure 3.4 with changed sign represent the value of the differential entropy at a given water content. On the other hand, from the slopes in Figure 3.5 the differential enthalpy can be calculated using equation (3.10). The values obtained are independent of the temperature, but vary with the water content. The values of these energies for each water content and dry density are indicated in Table 3.1.

Water content	Dry density (Mg/m³)			
	1.60		1.75	
	$\Delta \overline{s}^e$	$\Delta \overline{h}^e$	$\Delta \overline{s}^e$	$\Delta \overline{h}^e$
(%)	[kJ/(K·kg)]	(kJ/kg)	[kJ/(K·kg)]	(kJ/kg)
5.0	- 2.7	- 1008.5	- 1.7	- 706.8
7.5	- 1.8	- 672.1	- 1.3	- 512.7
10.0	- 1.2	- 441.7	- 0.9	- 371.8
12.5	- 0.8	- 287.8	- 0.7	- 269.5
15.0	- 0.5	- 186.4	- 0.5	- 195.3

Table 3.1. Values of the differential entropy and enthalpy as a function of the liquid water content for different dry densities.

3.3.3 Analysis using the capillary model

The capillary potential of water in soil expressed on mass basis $\Delta \mu_c$ is [eq. (2.52)]

$$\Delta\mu_c = \frac{2\gamma_{gl}\cos\theta_{sl}}{\rho_l r}$$

(3.11)

with ρ_l the liquid density.

Since this model assumes that the capillary potential coincides with the water potential (i.e. $\Delta\mu_c \equiv \Delta\mu_w$). Then, an expression similar to equation (3.2) can be written for the dependence of the water potential with respect to temperature changes (the contact angle is assumed temperature independent)

$$\left[\frac{\partial\Delta\mu_w}{\partial T}\right]_w = \frac{\Delta\mu_w}{\gamma_{gl}}\frac{\partial\gamma_{gl}}{\partial T}$$

(3.12)

The surface tension of most liquid-gas interfaces decreases with increasing temperature in a nearly linear fashion (Adamson, 1990). In the case of water, it is commonly assumed that the dependence of the surface tension with temperature is given by

$$\gamma_{gl} = a + bT$$

(3.13)

where a and b are constant to be determined by fitting experimental results.

From equations (3.12) and (3.13) a relation between the water potential and temperature changes is obtained

$$\frac{d\Delta\mu_w}{\mu_w} = \frac{b}{a+bT}dT$$

(3.14)

Then, integrating the above expression yields

$$\Delta\mu_w = \Delta\mu_w^r\frac{\gamma_{gl}}{\gamma_{gl}^r}$$

(3.15)

with $\Delta\mu_w$ and $\Delta\mu_w^r$ being the water potentials, and γ_{gl} and γ_{gl}^r the surface tensions respectively, at temperature T and at reference temperature T_r. Given a value of water potential and temperature, equation (3.15) defines the evolution of the potential of soil water as the temperature is changed.

Considering the expression adopted for the surface tension [eq. (3.13)], equation (3.15) can be rewritten in a form similar to equation (3.7)

$$\Delta\mu_w = \beta_0 - T\beta_1 \qquad (3.16)$$

with the coefficients β_0 and β_1 defined as

$$\beta_0 = \frac{\Delta\mu_w^r}{\gamma_{gl}^r}a \qquad\qquad \beta_1 = -\frac{\Delta\mu_w^r}{\gamma_{gl}^r}b \qquad (3.17)$$

Table 3.2 indicates the values corresponding to the coefficients β_0 and β_1 defined above. These coefficients were calculated considering a reference value of the water potential ($\Delta\mu_w^r$) at each water content and for a reference temperature (T_r) equal to 25 ⁰C. Coefficients a and b were assumed equal to 0.118 N/m and -1.54×10^{-4} N/(K·m) respectively (Grant & Salehzadeh, 1996).

Water content	Dry density (Mg/m^3)			
	1.60		1.75	
	β_1	β_0	β_1	β_0
(%)	[kJ/(K·kg)]	(kJ/kg)	[kJ/(K·kg)]	(kJ/kg)
5.0	- 0.5	- 353.7	- 0.4	- 303.4
7.5	- 0.3	- 227.3	- 0.3	- 221.9
10.0	- 0.2	- 146.1	- 0.2	- 162.3
12.5	- 0.1	- 93.9	- 0.2	- 118.7
15.0	- 0.1	- 60.4	- 0.1	- 86.8

Table 3.2. Values of the coefficients β_0 and β_1 as a function of the liquid water content for different dry densities.

3.3.4 Comparison of results

Figure 3.6(a) shows the variation of the differential enthalpy (filled symbols) and that of the coefficient β_0 (empty symbols) as a function of the adsorbed water content at each density considered. Figure 3.6(b) compares values of the differential entropy (filled symbols) with those of the coefficient β_1 (empty symbols), also at different water contents and dry densities.
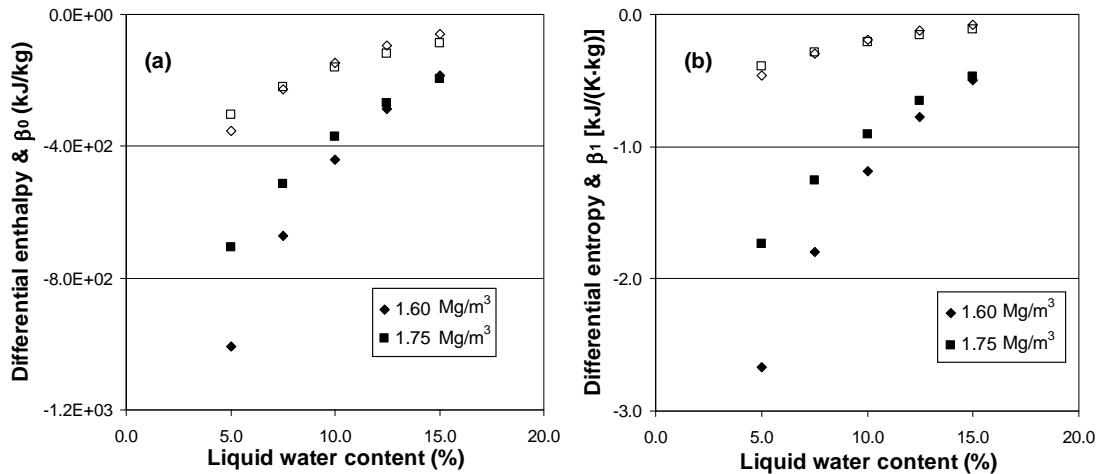
Figure 3.6. (a) Differential enthalpy of soil water and coefficient β_0 against water content; (b) differential entropy of soil water and coefficient β_1 as a function of the water content. Filled symbols are values obtained using the solution thermodynamic approach whereas empty symbols are results from the capillary model.

The differences between the results presented in Figure 3.6 can be partially explained by comparing equations (3.7) and (3.16). Although they are formally similar, coefficients in equation (3.16) are obtained from the capillary model and, because of that, they only consider the change in the surface tension with temperature. On the other hand, coefficients in equation (3.7) were deduced using concepts of thermodynamics of adsorption which also has into account the interaction between the adsorbed water and the soil. This last interaction is considered through the chemical potential of the solid phase, which varies as a function of the amount adsorbed (Chapter 2). It seems therefore that there would be additional mechanisms, other than that due to the reduction in surface tension, responsible of the changes observed in the water retention capacity when temperature is increased.

Recalling equation (3.8) and (3.17), it is possible to write

$$\frac{\Delta\mu_w}{\left[\dfrac{\partial\Delta\mu_w}{\partial T}\right]_w} = \chi + T \tag{3.18}$$

where the expression of the coefficient χ depends on the case considered. Thus, when results are analysed using adsorption thermodynamics the following expression is obtained for this coefficient

$$\chi = -\frac{\Delta \bar{h}^e}{\Delta \bar{s}^e} \tag{3.19}$$

Values of χ were calculated for the two densities analysed in this work. Although both $\Delta \bar{h}^e$ and $\Delta \bar{s}^e$ depend on the water content there is not a clear tendency about the dependence of χ with that variable. For the low density samples a value of -374.3 ± 2.1 K was obtained whereas in the case of the high density samples the value is -410.0 ± 1.9 K.

When the capillary model is considered

$$\chi = -\frac{\beta_1}{\beta_0} = \frac{a}{b} \tag{3.20}$$

and in this case χ will be a constant, as the coefficients a and b are independent of the water content. Replacing the values adopted for a and b in equation (3.20) a value of χ equal to -766.2 K is obtained.

3.4 Discussion and modifications proposed to the soil water retention curve

As it was already commented, in Soil Mechanics the concept of suction is often used as an alternative to the potential of water in soil. As both are related by the density of the soil water, it is possible to write an expression similar to equation (3.18) in terms of suction instead of water potential

$$\frac{s}{\left[\dfrac{\partial s}{\partial T}\right]_w} = \chi + T \tag{3.21}$$

with s the soil suction. It is important to note that the definitions of the coefficient χ given by equations (3.19) and (3.20) are still valid. In equation (3.21) the variation of the soil water density with the temperature has been neglected.

Rewriting equation (3.21) and integrating on each side between a reference temperature T_r and a temperature T yields

$$s = s_r \frac{\chi + T}{\chi + T_r} \tag{3.22}$$

where s_r is the suction at the reference temperature.

In general, the experimental data of suction at different water contents in the soil sample are fitted through an empiric expression which defines the soil water retention curve (SWRC). There are many expressions for the SWRC in the literature and each one has its advantages and drawbacks when applied to a particular soil. An analysis of different expressions is presented by Fredlund & Xing (1994) and Leong & Rahardjo (1997). Because the objective of this work is not to analyse the capabilities of the different SWRC models it was decided to adopt the equation proposed by van Genuchten (1980). This model has been successfully applied to fit experimental results for a wide variety of soils. The equation relates the water content and the suction values in the soil through the following expression

$$\Theta = \frac{w - w_r}{w_s - w_r} = \left[\frac{1}{1 + (\alpha s)^n} \right]^m \tag{3.23}$$

where Θ is the normalized water content, w_s is the saturated water content, w_r is the residual water content, and α, n and m are parameters to be determined by fitting experimental results.

Parameters n and m control the slope of the soil water retention curve. An alternative proposed by van Genuchten (1980) is to relate both parameters through the following equation

$$m = 1 - \frac{1}{n} \tag{3.24}$$

This approach simplifies the fitting process, but reduces the flexibility of equation (3.23).

To use equation (3.23) over the entire suction range, the water content is referenced to zero water content as the normalized water content becomes negative if w is less than w_r (Fredlund & Xing, 1994). Therefore, equation (3.23) yields

$$w = w_s \left[\frac{1}{1 + (\alpha s)^n} \right]^m \tag{3.25}$$

In this equation, w becomes equal to w_s when suction is zero, and w becomes zero when suction goes to infinite.

The parameter α in equation (3.25), which is associated (inversely) with the air-entry value of the soil, is like that in the original expression of van Genuchten (1980). However, this parameter permits to include, in a natural way, the effect of temperature and sample density into the SWRC given by equation (3.25). By using equation (3.22) an expression for α results

$$\alpha = \alpha_r \frac{\chi + T_r}{\chi + T} \tag{3.26}$$

where α_r is the value determined at the reference temperature.

Traditionally, the temperature effect on the SWRC was incorporated following the idea proposed by Philip & de Vries (1957). In this case, α is given by

$$\alpha = \alpha_r \frac{\gamma_{gl}^r}{\gamma_{gl}} \tag{3.27}$$

The same result is obtained from equation (3.26) when χ is replaced by equation (3.20).

It is important to highlight that equation (3.27) has been obtained using the equation of Young and Laplace. Hence, in this way, only the temperature effect on the capillary part of the soil suction is incorporated into equation (3.25). However, in soils like those analysed in this Chapter, part of the suction is attributed to the physico-chemical interaction between the water and the clay platelets. In addition to that, experimental evidences indicate that the capillary model is not able to completely represent the influence of the temperature on the retention capacity of the soil (Haridasan & Jensen, 1972; Hopmans & Dane, 1986; Nimmo & Miller, 1986; Constantz, 1991; She & Sleep, 1998; Bachmann et al., 2002; Romero et al., 2001; Villar & Lloret, 2004; Villar et al., 2005; Tang & Cui, 2005; Villar & Gómez-Espina, 2007). Therefore, it is clear that additional mechanisms are present and must be considered in SWRC equations if the

thermo-hydro-mechanical response of the soil under temperature effects is going to be analysed.

Experimental results also suggest that, for a given temperature and close to saturation, the relationship between the water content and the suction values depends on the density (void ratio) of the tested sample. In the equation proposed by van Genuchten (1980) this aspect could be included through the parameter α, whose value varies as the sample porosity changes (Al-Mukhtar et al., 1999; Romero & Vaunat, 1999; Vanapalli et al., 1999; Ng & Pang, 2000; Jacinto et al., 2009).

Experiments also indicate that the water content for nil suction w_s, at a given density, depends on temperature (Figure 3.1). This value also changes with the density (void ratio) of the tested sample (Figure 3.2). An estimated value of the saturated water content as a function of temperature and void ratio can be obtained using the following expression (Appendix A)

$$w_s = w_s^r \frac{e}{e_r}\left[1-\left(\alpha_w + \frac{\alpha_s}{e}\right)(T-T_r)\right]$$
(3.28)

where w_s^r is the saturated water content at reference temperature T_r and void ratio e_r, α_w and α_s are the coefficients of thermal expansion of pore water and soil grains respectively, T is the temperature, and e is the void ratio.

Test results shown in Figure 3.3 have been fitted using equation (3.25). For simplicity in the fitting process and following the reasoning applied by Romero et al. (2001), it was assumed that temperature only affects the parameter α and the water storage capacity w_s whereas parameters n and m were considered temperature independent. Values of w_s for the two soil densities and different temperatures were estimated using equation (3.28), whereas parameters α, α_r, n and m were determined by fitting experimental results. Table 3.3 indicates the values of the different parameters and Figure 3.7 shows the results obtained for each density considered.

Values of α_r for the low and high density samples were adopted equal to those determined at 25 ºC and 30 ºC respectively. Then, using equation (3.26) it is possible to calculate a value of the coefficient χ at each density considered. An average value of -385.2 ± 8.4 K was obtained for a dry density of 1.60 Mg/m³ and -435.9 ± 12.6 K for 1.75 Mg/m³, which are higher than the surface tension prediction (−766.2 K). These

values are similar to those obtained previously in section 3.3.4. Therefore, the parameter α could be considered as an empirical fitting parameter that is able to include the temperature and density influence on the soil water retention curve of compacted bentonite samples.

	Dry density (Mg/m³)							
	1.60				1.75			
	Temperature (ºC)							
Parameter	25	40	60	80	30	40	60	80
α (MPa⁻¹)	0.025	0.029	0.040	0.092	0.013	0.014	0.017	0.023
w_s (%)	27.0	26.8	26.6	26.2	21.6	21.5	21.3	21.0
n	0.98				1.82			
m	0.90				0.83			

Table 3.3. Parameters of the soil water retention curves for different temperatures and dry densities.
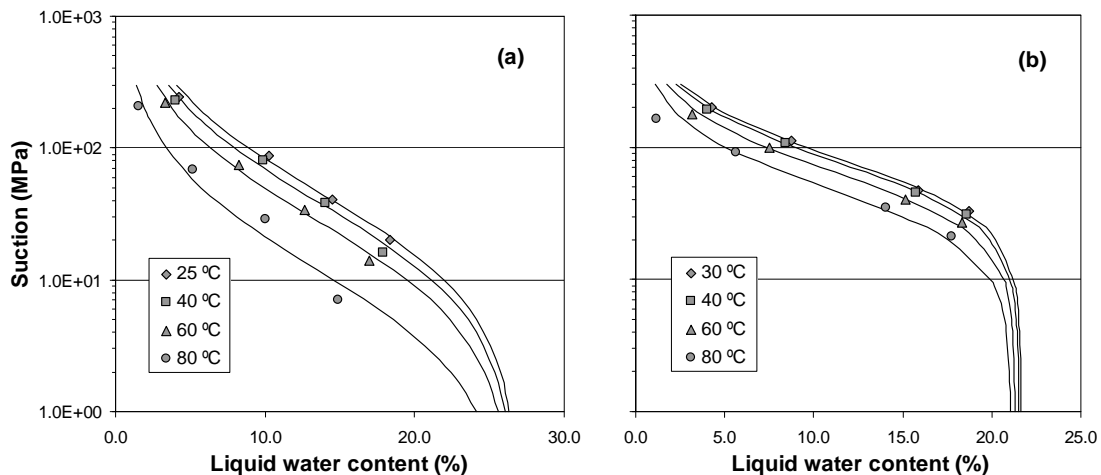
Figure 3.7. Soil water retention curves for different temperatures at fixed dry densities; (a) 1.60 Mg/m³ and (b) 1.75 Mg/m³.

3.5 Applications

The soil water retention curve relates the water content and suction in a soil. This relationships is one of the constitutive laws which must be defined when coupled thermo-hydro-mechanical processes are to be analysed. Results presented above indicate that changes in temperature and void ratio affect the retention capacity of soils. Therefore, some modifications to the original equation proposed by van Genuchten

(1980) have been considered in this section to incorporate these effects into the calculations.

Many numerical codes used to solve THM coupled problems adopt the degree of saturation as the measure to indicate the amount of water contained within the pores of the soil. Considering the equality given by equation (3.24) and using the degree of saturation S_l instead of the water content w, equation (3.25) can be rewritten as

$$S_l = S_{ls} \left[\frac{1}{1 + (\alpha s)^{\frac{1}{1-m}}} \right]^m \tag{3.29}$$

where S_{ls} is the degree of saturation at zero suction. Equation (3.29) contains three independent parameters, which can be estimated by fitting experimental data.

As it can be seen in Table 3.3, parameter α depends on temperature and density. Its evolution with temperature can be directly obtained from equation (3.26) if the coefficients α_r and χ are defined. With respect to the latter, although values obtained in section 3.4 for each density considered show some difference between them, until more experimental data become available, it can be assumed that χ is independent of temperature and void ratio. Romero et al. (2001) determine a unique value for an equivalent parameter when analysing the retention capacity of a low expansive clay (Boom clay) at different temperatures and sample densities.

The value of α_r, on the other hand, increases as the void ratio increases. Unfortunately, there is not enough experimental data of retention capacity at a reference temperature and different dry densities. Consequently, only a tentative law can be postulated for the variation of this coefficient with void ratio. As a first approximation, the following relationships is suggested

$$\alpha_r = \zeta_\alpha \exp(\eta_\alpha e) \tag{3.30}$$

with ζ_α and η_α coefficients to be defined.

Other parameter that must be determined to use equation (3.29) is m. In the analysis presented in section 3.4 it was assumed that this parameter is independent on temperature. Results indicate some dependence of this coefficient on void ratio.

However, because of the limited quantity of available experimental data it was assumed that this coefficient is constant.

Finally, an expression to predict the parameter S_{ls} can be deduced using the reasoning followed in Appendix A

$$S_{ls} = S_{ls}^r \left[1 - \left(\alpha_w + \frac{\alpha_s}{e} \right)(T - T_r) \right] \tag{3.31}$$

where S_{ls}^r is the degree of saturation at the reference temperature T_r and void ratio e. By default, it was assumed that S_{ls}^r is equal to 1.0.

Experimental results for compacted samples of MX-80 bentonite shown in section 3.4 have been interpreted in terms of suction against degree of saturation. Data for a temperature of 25 ºC at a dry density of 1.60 Mg/m^3 and those corresponding to 30 ºC at the higher density (1.75 Mg/m^3) were fitted using equation (3.29). By this process parameters α_r and m corresponding to each density were determined. Additionally, values of the parameters α were obtained for each density at different temperatures. Then, using equation (3.26) an average value for the coefficient χ equal to -415.5 ± 32.0 K was calculated. Parameter m was calculated as an average between the values obtained for each density. Finally, using values of α_r for each density tested and at a reference temperature (25 ºC), coefficients in equation (3.30) were determined (Table 3.4).

ζ_α (MPa^{-1})	η_α
0.006	2.961

Table 3.4. Coefficients used in equation (3.30) and obtained from experimental results.

The finite element program CODE_BRIGHT (Olivella et al., 1996) is a suitable tool to solve thermo-hydro-mechanical coupled problems. The above expressions were implemented in this code. Then, theoretical examples were analysed to evaluate the influence on the results obtained when the effects of temperature and density are incorporated into the expression of the soil water retention curve.

A one-dimensional geometry has been considered in the analyses. It was assumed that the sample is made up of MX-80 bentonite compacted at a dry density of 1.6 Mg/m^3. An initial suction of 20 MPa was adopted, which corresponds to a degree of

saturation of 74.0 % according to the water retention curve used in the analyses. In the calculation the gas phase was included, and an initial temperature of 20 °C was considered. The mechanical behaviour has been simulated using the Barcelona Basic Model which is described elsewhere (Alonso et al., 1990; Gens, 1995). Main material parameters used in the calculations have been obtained from independent tests (Villar, 2005; Villar et al., 2006) and they have been used in other simulations as well (Jacinto et al., 2009). Their values are presented in Tables 3.5 and 3.6.

Thermal conductivity		Intrinsic permeability	
λ_{dry} [W/(K·m)]	λ_{sat} [W/(K·m)]	$\mathbf{k}_0$ (m^2)	ϕ_0
0.3	1.3	3.0x10^{-21}	0.43

Table 3.5. Basic parameters for the thermal and hydraulic models used in the analyses.

κ_{i0}	0.032	κ_{s0}	0.20
α_{ss}	-0.04	λ_0	0.244
r	0.75	β	0.05

Table 3.6. Basic parameters for the mechanical model (BBM) used in the analyses.

Traditionally, it is assumed that the effect of temperature on the water retention curve is only due to changes in surface tension as temperature varies. This effect is incorporated into equation (3.29) through the dependence of the parameter α with temperature [eq. (3.27)]. In examples described below, Case 1 simulates a situation where the water retention curve considered in the analysis incorporates the changes proposed in this Chapter. Case 2, on the other hand, represents a case where the effect of temperature on the water retention curve is included using the traditional methodology.

3.5.1 Influence of temperature (TH analysis)

This example permits to evaluate the effect of temperature on the water retention capacity (void ratio is constant). The temperature on one end of the soil sample is fixed to 20 ºC (initial value) while on the opposite side it is increased from 20 ºC to 80 ºC. The sample is considered impervious to liquid and gas phases.

Figure 3.8(a) shows the distribution of degree of saturation along the sample at different days whereas Figure 3.8(b) presents the water retention curves at different temperatures for each case considered.

Figure 3.8. (a) Distribution of degree of saturation along the sample at different times (in days) for Case 1 (empty symbols) and Case 2 (filled symbols); (b) retention curves at different temperatures for each case analysed.

As temperature increases water redistribution takes place along the sample. As it can be seen, differences between the distributions of the degree of saturation obtained in each case appeared when steady state conditions were reached. These differences are a consequence of the water retention curve used in each case [Figure 3.8(b)]. Thus, degree of saturation on the hot side of the sample is lower in Case 1 than in Case 2. However, as the total mass of water is constant, the lower water content on the hot side in Case 1 is compensated by the slight increment in water content with respect to Case 2 toward the cold side of the sample.

3.5.2 Influence of temperature and density (THM analysis)

The example intents to show how temperature and void ratio affect the results obtained when they are incorporated within the parameters that define the water retention curve of the soil. As before, on one end of the sample the initial temperature (20 ºC) is fixed and on the opposite side the temperature is increased until 80 ºC. The sample was assumed liquid- and gas-tight, and the test was carried out at constant volume (isochoric condition).

Figure 3.9(a) shows the distribution of degree of saturation at different times whereas Figure 3.9(b) indicates the water retention curves for different temperatures and void ratios. Curves used in Case 2 are those for 20 ºC and 80 ºC corresponding to a void ratio of 0.763 (the initial one). In Case 1, the curve at 20 ºC and void ratio 0.852 is valid at the cold side whereas that at 80 ºC and 0.678 is the corresponding one on the opposite side.
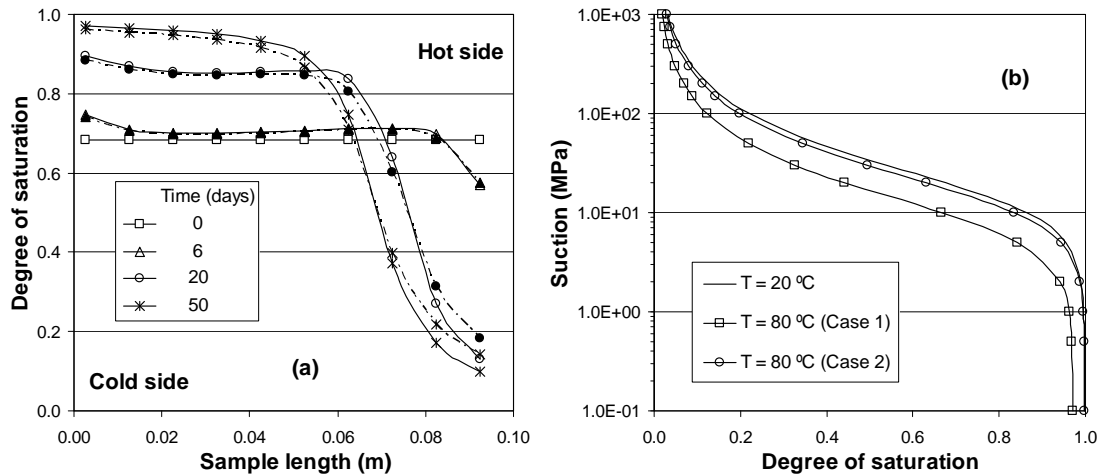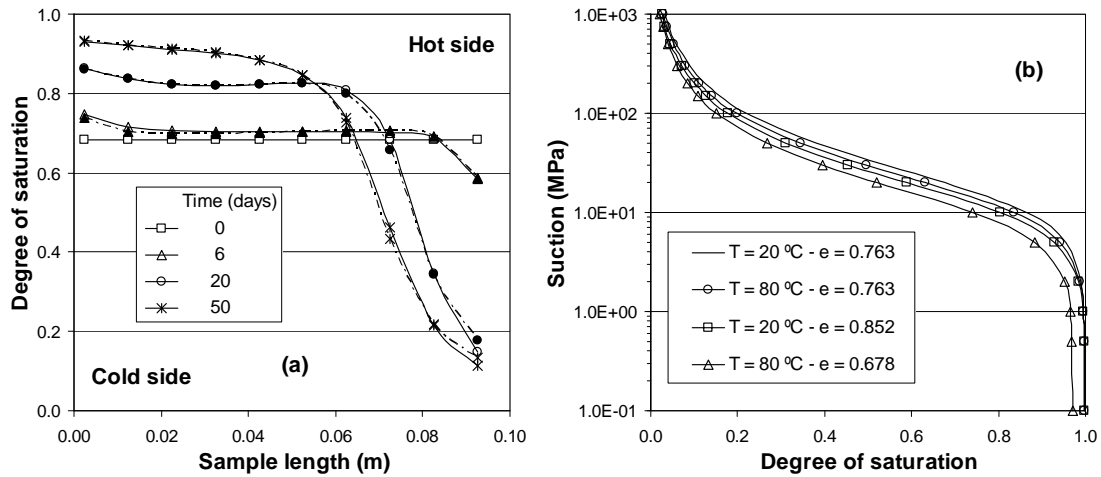

Figure 3.9. (a) Distribution of degree of saturation along the sample at different times (in days) for Case 1 (empty symbols) and Case 2 (filled symbols); (b) water retention curves at different temperatures and void ratios.

As it can be seen, there are not differences between the values of degree of saturation obtained in each case at the different time steps. Therefore, for the example considered, the influence of temperature is compensated by the change in porosity distribution along the sample.

This result can be explained analysing the water retention curves shown in Figure 3.9(b). The water retention curve used in Case 1 depends not only on the temperature but also on the density. Thus, the differences observed between the distributions of degree of saturation along the sample in the previous example because of temperature effect have almost disappeared in this example. Changes in the value of the void ratio produce changes in the parameters α_r and S_{ls} [eqs. (3.30) and (3.31) respectively]. On the hot side, the void ratio is lower than the initial one and this increases the retention capacity of the soil. The opposite is true on the cold side as porosity increases in this zone. At the end, these effects counteract those due to changes in temperature.

3.6 Concluding remarks

The influence of dry density and temperature on the water retention capacity of compacted samples of MX-80 bentonite has been analysed using experimental data reported in the literature (Villar et al., 2006; Villar & Gómez-Espina, 2007). The influence of dry density on the water retention capacity depends on the suction range. For suctions above a threshold value the retention capacity in terms of water content is slightly higher as the dry density is higher, whereas for lower suctions, the lower the dry density of the bentonite the higher its water content. The retention capacity decreases with temperature, more than predicted by the change in surface tension.

Thermodynamics of adsorption is an alternative tool to analyse the influence of temperature on the retention capacity of soils. The solution obtained using thermodynamic concepts is formally equal to that deduced from applying the capillary model. However, the former one includes the interaction between the adsorbed water and the soil particles. This last interaction is considered through the chemical potential of the solid phase, which varies as a function of the amount adsorbed. By using this concept it is possible to explain the differences between the results deduced from experimental data and those obtained using the capillary principle about the influence of the temperature on the water retention capacity of soils.

Modifications to the expression postulated by van Genuchten (1980) have been proposed in order to fit experimental values of suction and water content obtained at different temperatures and void ratios. Using thermodynamic concepts it is possible to include the effect of temperature in the same way that was made traditionally using the capillary model. The influence of void ratio on the water retention capacity was incorporated throughout an empirical law that resembles experimental evidences. By a fitting process values of the coefficients in the proposed law were determined for the material analysed in this work.

The suggested expressions were incorporated into a finite element code (CODE_BRIGHT) and simulations of theoretical coupled thermo-hydro-mechanical problems were carried out. The results show the influence of temperature and void ratio on the final water distribution along the samples when their effects are incorporated into the expression adopted for the soil water retention curve. The simulations suggest that, for the material used in this analysis and in confined cases – a situation that resembles that expected in bentonite blocks within underground

repositories - the influence of temperature on the water retention capacity can be partially compensated by the effect of changes in void ratio.

Chapter 4

Water density in expansive clays

Summary

There is increasing evidence from researchers on clay mineralogy that the density of water attached to clay minerals may be greater than 1.0 Mg/m^3. This fact becomes especially evident in compacted highly expansive clays close to water saturation. This kind of material is being considered in the design of engineered barriers for radioactive waste disposal, because of its sealing and retention properties. From a geotechnical point of view, most of the analyses required to check the performance of the barrier are sensitive to the value considered for the water density. This is the case of the unsaturated flow calculations, which depend on the water retention properties of the soil. The Chapter presents first a review of the measurements performed at a microscopic level. A description of the hydration process of an expansive clay considering the micro and macrostructure is included. Then, a method to obtain an average water density for sodium and calcium bentonites depending on suction is proposed. The method is used to correct the water retention curves expressed in terms of the degree of saturation.

4.1 Preface

Deep geological repositories are being considered as a tentative solution for the disposal of high-level radioactive waste. Bentonite, which is a clay predominantly constituted of minerals of the smectite type, has been selected as one of the sealing materials in the multi-barrier designs for nuclear waste repositories because of its low permeability when compacted, its capacity to inhibit the migration of contaminants from the waste to the surrounding environment and its swelling capacity. One option is to install the bentonite in the barrier as compacted blocks manufactured with its hygroscopic water content. Under these conditions, the clay has initially a high suction that controls the mechanical and hydraulic behaviour of the barrier.

Within the barrier the bentonite experiences a transient temperature regime which depends on the decaying heat power induced by the waste and a transient wetting phase controlled by the rate of absorption of water from the host rock (clay, granite). As a consequence, the part of the barrier close to the canister will be initially dried whereas the outer part in contact with the host rock will experience hydration and expansion. Therefore the clay buffer will be subjected to coupled processes that will affect its behaviour (Gens, 2003).

One of the fundamental properties that is required when predicting the hydration of the bentonite within the barrier is its water retention capacity. Since the bentonite inside the barrier will be mostly confined, experimental methods have been developed to determine the water retention curve keeping the volume of the tested sample constant. From these tests the relationship between the suction values and the gravimetric water content is obtained, which constitutes the "retention curve" or the "soil water retention curve" (Yahia-Aissa, 1999; Lloret et al., 2003; Lloret et al., 2004; Villar & Lloret, 2004).

In many applications the retention curve is presented in terms of the degree of saturation. In fact, from the gravimetric water content the degree of saturation can be directly evaluated. This is important when a numerical analysis is being performed, as balance equations are based on the degree of saturation instead of water content as main variable. In the case of highly expansive soils, it is systematically observed that, close to saturation (nil suction), the degree of saturation calculated from the water content is bigger than one (Villar, 2002; Marcial, 2003). This fact suggests that a systematic error is being carried out in this simple calculation. Both in the works mentioned and in this Thesis it is assumed that this error comes from the value

assigned to the density of the water in the bentonite, which must be well above 1.0 Mg/m^3 as suggested by recent publications in the field of clay mineralogy.

The Chapter presents first a review of the measurements carried out by clay mineralogists. Based on this, a description of the hydration process in typical expansive clays is shown. Then, a method to obtain an average water density for sodium and calcium bentonites depending on suction is proposed. The method is used to review published experimental results of water retention curves on compacted bentonite samples.

4.1.1 Fabric of compacted expansive clays

Mercury intrusion porosimetry (MIP) tests and environmental scanning electron microscopy (ESEM) analysis on bentonite samples statically compacted at different dry densities show that in their fabric it is possible to consider a double structure defined by the clay aggregates and the pores between them (Figure 4.1).

An aggregate includes several particles and each particle is formed by several silicate sheets (also called unit layers or clay layers). In the case of smectites these unit layers are of the TOT type (an octahedral sheet between two tetrahedral sheets, i.e. a 2:1 layer phyllosilicate). The porosity inside an aggregate (or "microporosity", or intra-aggregate porosity) is not homogeneous, but includes the pores inside each particle (ranging between 0.2 and 2.0 nm) constituting the intra-particle (or interlayer) porosity and also includes the pores between particles or inter-particle porosity. It is commonly assumed that the porosity inside the aggregates is not affected by compaction when the water content is not too close to saturation (Delage et al., 2006). Consequently, the microporosity distribution is initially independent of the dry density of the compacted sample (Lloret & Villar, 2007). On the other hand, the pores between the aggregates (macropores) define the inter-aggregate porosity or "macroporosity" (Mitchell, 1993).

These observations correlate with the results obtained on montmorillonite (a kind of smectite) powder samples (Mooney et al., 1952a; Bihannic et al., 2001; Tournassat et al., 2003; Stepkowska et al., 2004) which suggest that the clay layers are ordered in stacks forming particles which are grouped in larger particles (aggregates). The number of layers in the particles depends partly on the exchangeable cation type and on the water content of the sample.

Figure 4.1 presents a sketch of the fabric of a compacted bentonite sample where the different structures commented above can be identified. An environmental scanning electron microscopy (ESEM) image corresponding to the fabric of a compacted FEBEX bentonite sample is shown in the same figure.

(a)   (b)
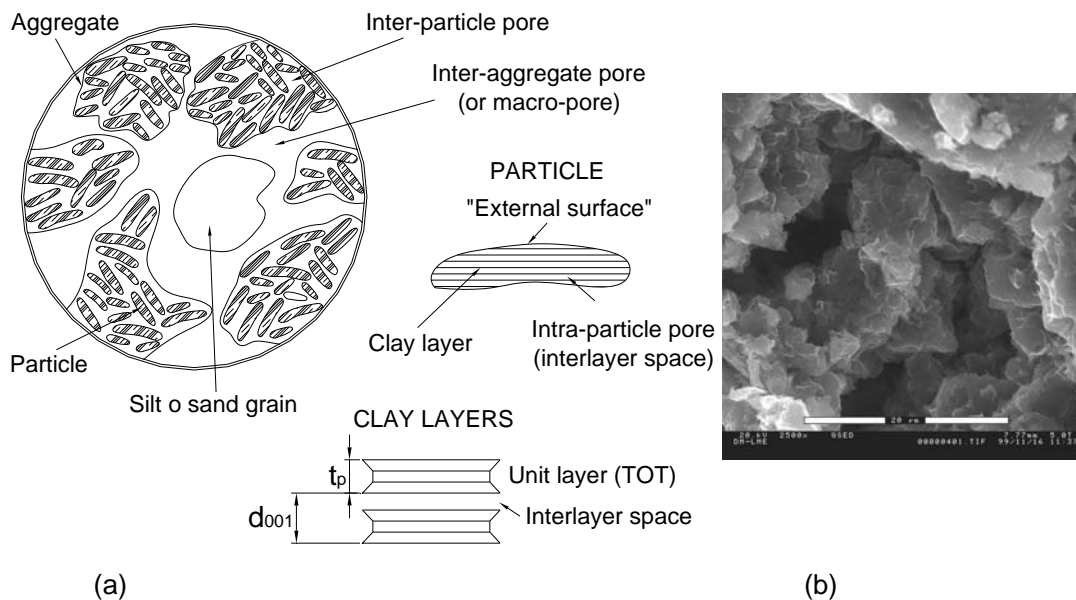
Figure 4.1. (a) Sketch of the fabric of a compacted bentonite sample; (b) microphotograph of a compacted bentonite sample obtained by ESEM [from Lloret et al. (2003)].

4.1.2 Water in expansive clays

The interaction between smectite, which is the main mineral of bentonite, and water has been the object of studies during many years (Mooney et al., 1952a-b; Keren & Shainberg, 1975, 1979; Kraehenbuehl et al., 1987; Cases et al., 1992; Cuadros, 1997; Dios Cancela et al., 1997; Tournassat et al., 2003; Stepkowska et al., 2004; Ferrage et al., 2005a-b; Devineau et al., 2006, among others). In fine soils it is possible to define different types of water that affect their behaviour (Kézdi, 1974). In the case of expansive soils, it is possible to distinguish between the water in the macropores, which has the physical and chemical properties of ordinary liquid water, and the water attracted to the external surfaces of clay minerals or held as interlayer water in the spaces between clay layers.

The sorption of water into the interlayer space of smectites depends on the size and charge of the exchangeable cations, and the value and localization of the layer charge

of the silicate sheet (Keren & Shainberg, 1975, 1979; Sposito & Prost, 1982; Ferrage et al., 2005a-b; Laird, 2006). Many experimental results suggest that the water confined in small pores or in the proximity of the clay layers of expansive materials presents properties that differ from those of free water. Low (1979) showed that these differences are related to changes in intermolecular bonding influenced by the surfaces of montmorillonite layers, and they are significant and persist at appreciable water contents. Neutron diffraction experiments on Na-montmorillonite revealed that the way in which the interlayer water is ordered increases its density approximately 5 % over that of free water (Hawkins & Egelstaff, 1980). Studies by near-infrared spectroscopy (NIR) indicate the existence of several mechanisms affecting water molecules in the space between silicate layers which depend on the exchangeable cations and hydration conditions (Cariati et al., 1981). Derjaguin et al. (1986) showed that the water density in thin pores (about 50 Å in size) at room temperature is 2 % higher than that of free water. Push et al. (1990) obtained values of interlayer water density in Na-montmorillonite between 1.0 Mg/m^3 and 1.05 Mg/m^3. They indicated that the interlayer water represents around 10 % of the total water volume in pure Na- and Ca-montmorillonte at low dry density (0.35 Mg/m^3) and more than 90 % at dry densities exceeding 1.60 Mg/m^3. Different neutron diffraction experiments on Ni- and Na-vermiculite confirm the existence of complexes between the water molecules and the exchangeable cations (Skipper et al., 1991). Quasielastic neutron scattering (QENS) studies on Na-vermiculite clay showed that both the confinement of water and the presence of Na ions affect the water dynamics (Swenson et al., 2000). Villar & Lloret (2004) showed that the average density of the water in saturated samples of compacted bentonite depends on the specimen density and water content, and values higher than 1.05 Mg/m^3 and up to 1.22 Mg/m^3 were obtained for bentonite dry densities between 1.3 and 1.8 Mg/m^3. Also experiments in granulated Ca-Mg bentonite (FEBEX bentonite) indicated an interlayer water density higher than 1.0 Mg/m^3 (Fernández & Rivas, 2005).

During the hydration of montmorillonite from the dry state, the exchangeable cations placed in the interlayers are initially hydrated according to their hydration energy. Subsequently, the spaces between particles are filled with free water. The former step is associated with the crystalline swelling and the latter one to the osmotic swelling, since it is in these spaces where the diffuse double layers develop. These mechanisms

Most of water is on the external
surface of the particles

Particle
(12-14 layers)

Aggregate

Inter-aggregate pore

——— Clay layer
– – – External water
∘ ∘ ∘ ∘ ∘ Interlayer water

0 % < RH < 16 %

Particles with
interlayer water

Particle
(6-7 layers)

Particles without
interlayer water

Inter-layer pore
(Intra-particle pore)

16 % < RH < 50 %

Intra-aggregate pore
(Inter-particle pore)

Most of water is
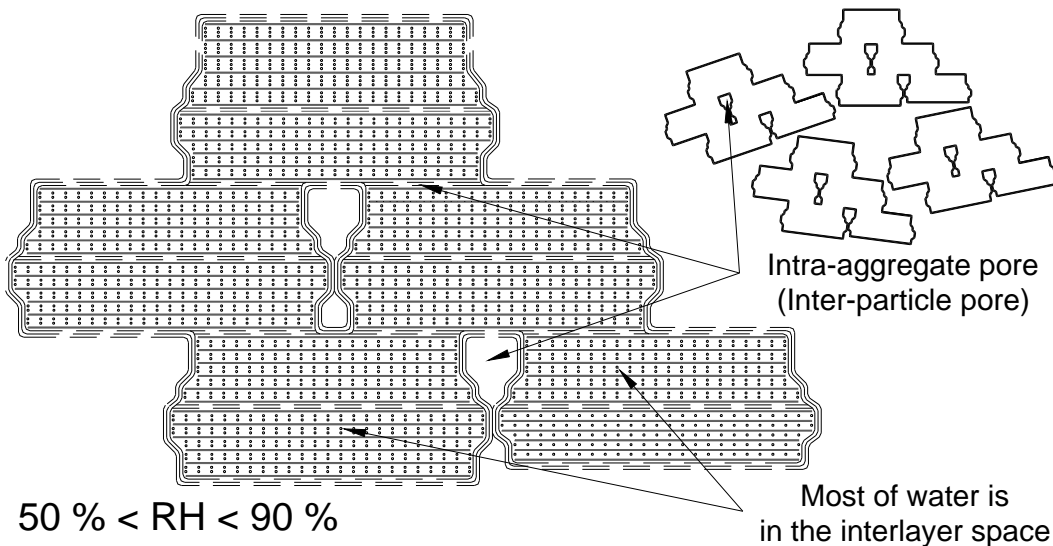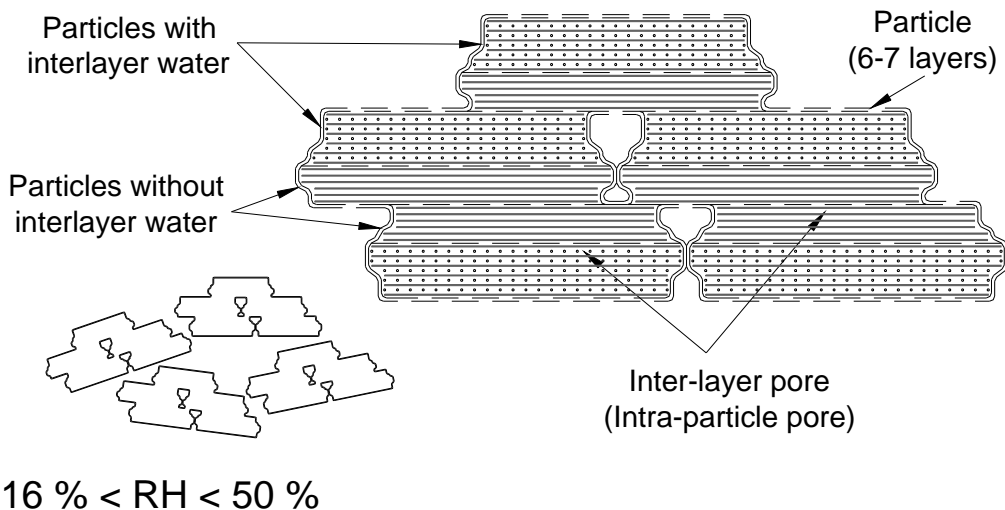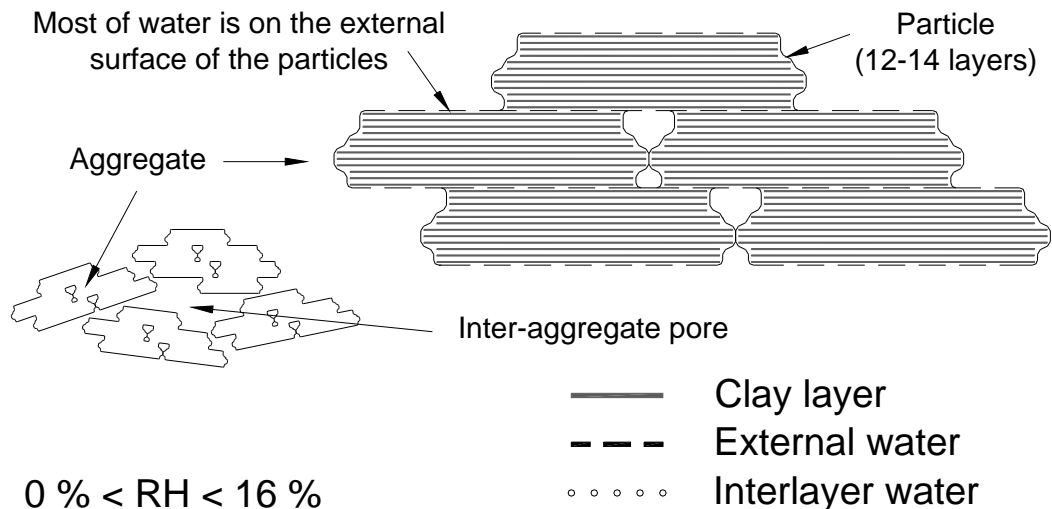in the interlayer space

50 % < RH < 90 %

Figure 4.2. Sketch of the adsorption mechanism on Na-montmorillonite powder [based on Cases et al. (1992)].

produce changes in the microstructure of the material associated with variations in the basal distance (d_{001}) and specific surface area.

At low and moderate relative humidity, the swelling develops at particle level and occurs without any important global volume change. On the other hand, in the range of high relative humidity the changes of volume are appreciable in the case of samples hydrated under free volume conditions (Delage et al., 1998; Villar, 2005). For confined samples, macroscopic swelling is prevented and porosity redistribution occurs, which results in microporosity invading macroporosity (Villar & Lloret, 2001; Lloret et al., 2004; Devineau et al., 2006).

Figure 4.2 presents a simple sketch of the hydration mechanism of a Na-montmorillonite powder, based on the work by Cases et al. (1992). For low values of relative humidity (below 16 %), water is just present on the external surface of the particles. As the relative humidity increases, water occupies gradually the available interlayer spaces. Eventually, more layers of water are arranged on the external surface of the particles. Close to water saturation the macropores are also filled with free water. From the measurements at microscopic level, it can be assumed that the water adsorbed on the external surface and the water in the macropores have both a density of 1.0 Mg/m^3, but the water in the interlayer space has a greater density (Hawkins & Egelstaff, 1980; Derjaguin et al., 1986; Swenson et al., 2000).

4.1.3 Water retention curve of compacted bentonite samples

The retention capacity of compacted bentonite samples depends on complex mechanisms defined by the interaction of water, clay layers and exchangeable ions in the interlayer.

In order to predict the hydration of the bentonite within an engineered barrier it is necessary to know, among other properties, its water retention capacity or soil water retention curve (SWRC). Figure 4.3(a) shows experimental results of suction as a function of the gravimetric water content for wetting paths followed by compacted bentonite samples kept at constant volume and room temperature (Lloret et al., 2004). The results are not dependent on the dry density for suction values larger than 10 MPa, because for highly active soils in the range of high suction values, the water is mainly retained in the intra-aggregate pores (Al-Mukhtar et al., 1999; Romero et al., 1999;

Yahia-Aissa et al., 2001). In fact, in the retention curve of a compacted bentonite sample it is possible to define two zones (Romero et al., 1999; Lloret et al., 2003). On the one hand, there is a zone, corresponding to the low water content, where the water is mainly in the intra-aggregate space and the suction depends on the specific surface area and mineralogical composition of the clay. The quantity of water retained in this zone is independent on the dry density, and in a wetting process the intra-aggregate space becomes saturated before the macropores. On the other hand, in the inter-aggregate zone, the main mechanism of water retention is capillarity. However, if the sample saturates under confined conditions, the intra-aggregate pore volume increases at the expense of the macroporosity (Lloret et al., 2004), and thus the capillary effect would still be negligible. Close to saturation the samples with a higher porosity (lower dry density) will logically have higher water contents for a given suction.
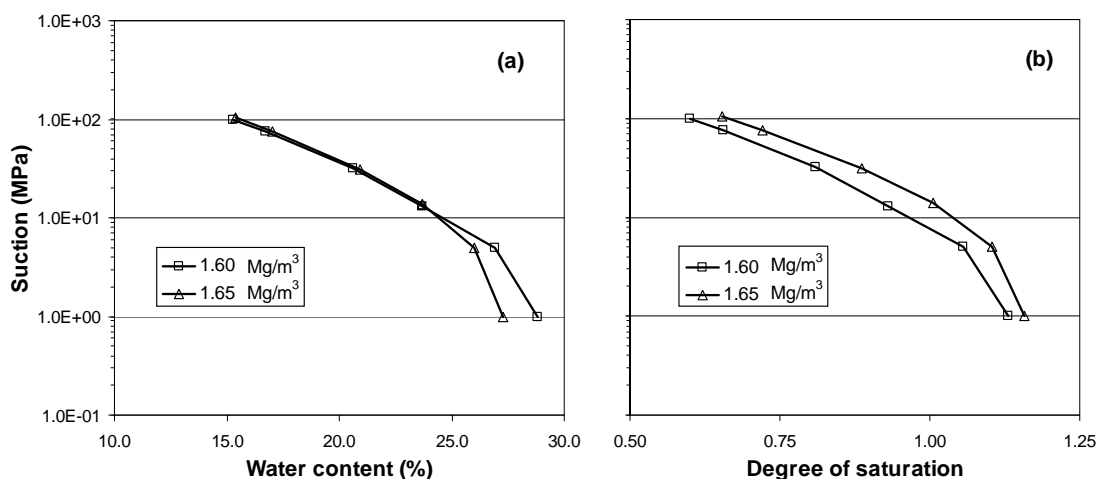
Figure 4.3. Water retention curves under constant volume conditions for FEBEX bentonite samples compacted at different dry densities [from Lloret et al. (2004)]. (a) Suction against water content; (b) suction against degree of saturation.

In many practical cases, however, it may be of interest to express suction as a function of the degree of saturation. That is the case in numerical analyses where the degree of saturation becomes one of the main variables. Usually this relationship is applied

$$S_l = \frac{w\rho_s}{e\rho_w} \qquad\qquad (4.1)$$

where S_l is the degree of saturation, w is the gravimetric water content, e is the void ratio, and ρ_s and ρ_w are the solid particle density and the water density, respectively. Void ratio is related to dry density and solid particle density.

Using equation (4.1), the measurements presented in Figure 4.3(a) are depicted in Figure 4.3(b) with the degree of saturation as main variable. Comparing Figure 4.3(a) and 4.3(b), it is evident that the retention curves for different dry densities are not coincident when the degree of saturation instead of the water content is considered. Another important observation is that, for low suction values, the degree of saturation is bigger than one. It is important to note that the degree of saturation has been calculated considering the conventional value for the free water density (1.0 Mg/m^3). The value of ρ_s used in this case was 2.70 Mg/m^3 (Lloret et al., 2004).

4.2 Estimation of the average water density

In the previous section, a literature review suggesting that some of the liquid water held in expansive clays exhibits physical properties quite different from those of the free water has been presented. In particular there is increasing evidence that its density is greater than 1.0 Mg/m^3. It should be pointed out, however, that there are different types of water in a compacted sample and only a portion of the water held in the pores has a density equal to 1.0 Mg/m^3 whereas much of water would have density higher than 1.0 Mg/m^3. This change in the conventional value of water density is assumed to be responsible of the degrees of saturation greater than one found by several authors [Figure 4.3(b)].

The method proposed in this Chapter takes into account that in expansive soils there is a difference between the water held as interlayer water and the water in the rest of the pores. Thus, the total water content w in a sample is given by

$$w = w_i + w_e + w_f \tag{4.2}$$

where w_i is the water in the interlayer space, w_e is the water adsorbed on the external surface of the clay particles, and w_f is the free water. There is not an easy way to separate the different kinds of water in a sample. In general, it could be assumed that at relative humidity lower than 90 % the water is held in the interlayer zone (interlayer water) and adsorbed on the external surface of the particles (Cases et al., 1997; Salles

et al., 2008). At higher relative humidity (lower suction) it is expected that some capillary condensation occurs in the macropores. As mentioned before, when compacted samples are hydrated under confined conditions, porosity redistribution takes place and the macroporosity volume decreases as suction decreases. As a consequence, the pore volume available to accommodate free water reduces. For the sake of simplicity, it is assumed in this work that free water is negligible (i.e. w_f = 0) and water in the sample is only held as interlayer water w_i, and external water w_e. A certain error, which could be more noticeable at low suctions and at very low densities, is implicit in this simplification. However, in the context of radioactive waste clay barriers (confinement and highly compaction conditions), it has been shown that the amount of free water is very small in practice. Bradbury & Baeyens (2003) estimated that only 1.1 % of the water in compacted MX-80 bentonite was free water for samples of dry density 1.8 Mg/m^3. Also Fernández et al. (2004) estimated a value of free water around 1.5 % of the total amount of water in samples of FEBEX bentonite compacted at dry density 1.65 Mg/m^3.

Because of the different types of water in a compacted bentonite sample, it is not straightforward to define a fixed value for the water density. This will depend on the amount of water in the soil (degree of saturation) and on the clay minerals, as the hydration process depends on the exchangeable cations and the specific surface area of the smectite. Therefore, an average value rather than a homogeneous constant value should be adopted for the water density. If m_w^i and m_w^e are the mass of interlayer water and the mass of external water in the sample respectively, and V_w^i and V_w^e are the volume of the interlayer and external water respectively, the average water density ρ_w can be obtained as

$$\rho_w = \frac{m_w^i + m_w^e}{V_w^i + V_w^e} = \frac{w}{\dfrac{w_i}{\rho_w^i} + \dfrac{w_e}{\rho_w^e}}$$

(4.3)

where the external water is assumed to have properties of the free water, that is, ρ_w^e = 1.0 Mg/m^3. Equation (4.3) is obtained dividing the numerator and denominator by the mass of solids. Therefore, to compute the average water density, it is necessary to estimate the amount of external and interlayer water and the value of the interlayer water density. In this section, a general method to estimate these values is proposed.

A first difficulty arises when the water density in the interlayer space ρ_w^i is analysed. Different types of water exist in that space depending on the hydration state, and that requires considering different water densities for each state. Eventually, an average value of ρ_w^i should also be used when computing equation (4.3).

The total specific surface area of a montmorillonite sample comprises the external and interlayer specific surface areas. The external area includes both the external faces and the edges of the montmorillonite particles (Kraehenbuehl et al., 1987). The total specific surface area is determined through the analysis of the sorption isotherms of different polar molecules (water, ethylene glycol monoethyl ether), whereas the external surface area is usually obtained through sorption of gases (nitrogen) or the calorimetric method (Mooney et al., 1952a; Kraehenbuehl et al., 1987; Cases et al., 1992; Cuadros, 1997; Fernández & Rivas, 2005). The interlayer specific surface area is computed as the difference between the total and external areas.

From experimental sorption results, it seems that the water adsorbed in the interlayer space increases continuously as the relative humidity rises, while the distance between the clay layers changes in steps (Mooney et al., 1952a-b; Keren & Shainberg, 1975, 1979; Cases et al., 1992; Dios Cancela et al., 1997; Saiyouri et al., 2004; Ferrage et al., 2005a; Devineau et al., 2006). The basal distance (d_{001}, Figure 4.1) value for a given relative humidity (i.e. water activity) depends on the exchangeable cations and corresponds to none, one, two, three or four water layers that define the different hydration states which can be found in the interlayer space.

For each hydration state it is possible to determine a theoretical density for the water in the interlayer space through the following equation (Martin, 1962)

$$\rho_w^j = \frac{w_j}{S_{int,j} \, \Delta_j} \tag{4.4}$$

with w_j being the theoretical interlayer water content, $S_{int,j}$ the interlayer specific surface area, and Δ_j the half distance between clay layers defined as

$$\Delta_j = \frac{(d_{001})_j - t_p}{2} \tag{4.5}$$

where $(d_{001})_j$ is the basal distance and t_p is the clay layer thickness (Figure 1). The theoretical interlayer water content can be estimated considering the area occupied by a water molecule in the different hydration states (Cases et al., 1992, 1997; Bérend et al., 1995) and the interlayer specific surface area

$$w_j = \frac{jS_{\text{int},j}M_w}{2\sigma_j N_A}$$ (4.6)

with σ_j the area of an adsorbed water molecule, M_w the molecular mass of water, and N_A the Avogadro's number. In equations (4.4) to (4.6) the subscript j is used to indicate the different hydration states.

The analysis of X-ray measurements on hydrated montmorillonite shows that the hydration state is never homogeneous (Pons et al., 1981; Moore & Hower, 1986; Kraehenbuehl et al., 1987; Cases et al., 1992; Saiyouri et al., 2004; Ferrage et al., 2005a-b). Thus, the basal distance obtained from an X-ray analysis corresponding to a given relative humidity is, in fact, an average of the different hydration states in the sample interlayers. The fitting of experimental X-ray results of pure minerals using different methods allows to determine a distribution of the different hydration states and to define the participation of each one for a given relative humidity.

Taking these observations into account, it would be possible to obtain an actual value for the interlayer water density ρ_w^i as a function of the relative humidity

$$\rho_w^i = \frac{\displaystyle\sum_{j=1}^{n} p_j w_j}{\displaystyle\sum_{j=1}^{n} p_j \frac{w_j}{\rho_w^j}}$$ (4.7)

where p_j is the contribution of each hydration state for a given relative humidity, obtained from the simulation of X-ray measurements, ρ_w^j is the corresponding theoretical interlayer water density as obtained from equation (4.4), and n is the number of hydration states corresponding to that relative humidity. In fact, w_j could be considered as the maximum interlayer water content corresponding to the state j. However, the actual interlayer water content for a given suction would only be a fraction of the maximum water content and this is taken into account through the term

p_j. Values of the average interlayer water density for two different montmorillonites as a function of the suction are presented in the next section.

To evaluate equation (4.3), the amount of external and interlayer water content is also required. The water adsorbed on the external surface of the aggregates varies as the montmorillonite is hydrated and it is possible to compute the external water w_e for each suction value using the equation (Cases et al., 1992, 1997; Bérend et al., 1995)

$$w_e = \theta \frac{S_{ext} M_w}{\sigma N_A} \tag{4.8}$$

where θ is the external coverage defined as a function of the heat of adsorption of water on the considered clay (Hagymassy et al., 1969), S_{ext} represents the measured external specific surface area, M_w is the molecular mass of water, σ is the area of an adsorbed water molecule, and N_A is the Avogadro's number.

Therefore, using equation (4.2) it is possible to determine the internal water w_i, from the difference between the total amount of adsorbed water measured in the laboratory w, and the water adsorbed on the external surfaces w_e, assuming that w_f is negligible. Finally, the average water density ρ_w corresponding to each water content within the bentonite sample can now be calculated by means of equation (4.3).

4.3 Analysis of experimental soil water retention curves

4.3.1 MX-80 bentonite

The proposed methodology has been applied to analyse published experimental results obtained in MX-80 bentonite samples. This commercial material has been considered as sealing material for the barrier design of high-level waste repositories by several Agencies dealing with radioactive waste disposal [e.g. ANDRA (France), SKB (Sweden)]. This bentonite contains montmorillonite (65-82 %) as main mineral phase and it is supplied homoionised in sodium (Pusch, 1982; Delage et al., 2006). It can be thus considered a Na-montmorillonite.

Many authors have analysed the mechanism of adsorption and desorption of water vapour in Na-montmorillonite through the water sorption isotherm on powder samples. Mooney et al. (1952a) and Cases et al. (1992) indicate that at dry state, particles are formed by 21 to 29 unit layers. At low water content the water adsorption occurs predominantly on the external surface of the stacks and to some extent in the interlayers as well (Kraehenbuehl et al., 1987; Cases et al., 1992). As the water content increases, the basal distance (d_{001}) increases (Mooney et al., 1952b; Cases et al., 1992; Tournassat et al., 2003; Saiyouri et al., 2004; Ferrage et al., 2005a; Devineau et al., 2006). Results suggest that, at the beginning of the Na-montmorillonite hydration process, particles subdivide into smaller ones increasing the external specific surface. This structural change is partially responsible for the marked hysteresis in the initial adsorption-desorption cycle of the sorption isotherms (Mooney et al., 1952a; Keren & Shainberg, 1975; Kraehenbuehl et al., 1987; Cases et al., 1992; Stepkowska et al., 2004). Later, as hydration proceeds, water fills the interlayer space and the basal distance increases without major changes in the value of the specific surface area. This mechanism applies to powder as well as to compacted samples hydrated under free volume conditions.

Most of the measurements reported in the literature refer to basal spacings in bentonite powder. However, an important aspect to take into account when analysing the water retention capacity of expansive clays is the effect of compaction and volumetric constraints on the hydration process. Recent works suggest that compaction does not affect the intra-aggregate porosity, at least in samples compacted at water contents not too close to saturation (Romero et al., 1999; Lloret et al., 2003; Delage et al., 2006). These volumetric or stress constraints influence mainly the macropores (Saiyouri et al., 2004; Devineau et al., 2006). Measurements of basal distances in MX-80 bentonite pellets hydrated under free volume conditions and tested at 28 ± 2 ºC suggest that the compression of the sample does not affect the hydration process at the microstructural level. Also, Villar (2007) determined the basal distance as a function of the relative humidity in samples of MX-80 bentonite compacted at different dry densities (1.3 and 1.6 Mg/m^3) and tested at 20 ºC. The experiments were carried out at constant volume and the relative humidity was varied between 88 % and 99 % (suction between 20 MPa and 1.3 MPa). The results show that the average distance for this range of suction values corresponds approximately to two water layers in the interlayer space, as other authors have found for powder samples of similar clays in the same range of relative humidity. Saiyouri et al. (2004) examined the evolution of the basal distance with relative humidity (suction between 1 kPa and 100 MPa) in pellets of MX-

80 bentonite compacted at a dry density of 1.6 Mg/m^3 and tested under unconfined conditions at room temperature. At suction values lower than 0.1 MPa the basal distances correspond predominantly to four-layer hydrates in the interlayer space, probably because the samples were allowed to swell during hydration, whereas the basal distances coincide with those obtained by Villar (2007) when the same suction range is considered.

In order to apply the proposed methodology to estimate the average water density, the first step is to define the theoretical interlayer water density for each hydration state using equation (4.4). Different values are suggested in the literature for the basal distance of each hydration state; because of that, it was decided to consider average values of 12.4, 15.4, 18.4 and 21.6 Å for the one-, two-, three-, and four-layer hydrate state, respectively (Mooney et al., 1952b; Cases et al., 1992; Tournassat et al., 2003; Saiyouri et al., 2004; Ferrage et al., 2005a; Devineau et al., 2006). For the clay layer thickness t_p an average value of 9.5 Å was adopted (Cases et al., 1992; Bourg et al., 2006). The interlayer specific surface area $S_{int,j}$ changes as the water content changes and it was calculated using the expression proposed by Cases et al. (1992) for Na-montmorillonite samples

$$S_{int,j} = 801.3 - \left(S_{ext} - S_{ext\,lat,j}\right) \tag{4.9}$$

where S_{ext} in m^2/g represents the total external specific surface area and $S_{ext\,lat,j}$ stands for the lateral external specific surface area. For the latter, values of 5.1 m^2/g in the dry state, 6.7 m^2/g in the one-layer hydrate state and 8.3 m^2/g in the two-layer hydrate state were obtained by Cases et al. (1992) and Bérend et al. (1995) in samples tested at 25 °C. In the present work, this last value was also adopted for the lateral external specific surface area in the three- and four-layer hydrate state. For values of relative humidity higher than 16 %, Cases et al. (1992) determined a value for the external specific surface area of 105 m^2/g. Finally, values of the area occupied by a water molecule in the different hydration states (7.8 Å^2 in the one-layer hydrate and 8.7 Å^2 in the two- and three-layer hydrate) have been adopted from the literature (Cases et al., 1992; Bérend et al., 1995). This last value is also considered, if necessary, for the four-layer hydrate state. It is believed that the difference between the value of the area occupied by a water molecule adsorbed on the external surface and that in the interlayer space can be attributed to the interaction between the water molecules and the interlayer cations.

Using equations (4.4) and (4.9), and the values for the basal spacing and the water molecule area indicated above, it is possible to determine a theoretical interlayer water density for each hydration state in a Na-montmorillonite sample (Table 4.1).

Water layers j	$\rho_w^{\ j}$ (Mg/m^3)
1	1.32
2	1.17
3	1.16
4	1.14

Table 4.1. Theoretical interlayer water density for each hydration state j in Na-montmorillonite obtained using equation (4.4).

The next step is to define the proportion of each hydration state p_j corresponding to a given relative humidity (or suction value), and as it was commented before, there exist different methods to estimate these values. Table 4.2 presents the results obtained by Saiyouri et al. (2004), showing the proportion of zero-, one-, two-, three- or four-layer hydrates found in the interlayer at a particular suction.

Suction (MPa)	RH	Layers				
		0	1	2	3	4
0.01	1.00	0.0	0.0	0.32	0.32	0.20
0.03	1.00	0.0	0.0	0.32	0.32	0.20
0.10	1.00	0.0	0.0	0.20	0.60	0.20
1.0	0.99	0.0	0.0	0.33	0.33	0.33
2.8	0.98	0.0	0.0	0.33	0.33	0.33
6.9	0.95	0.0	0.22	0.50	0.28	0.0
15.0	0.89	0.0	0.15	0.70	0.15	0.0
26.0	0.82	0.0	0.23	0.60	0.17	0.0
33.0	0.78	0.0	0.30	0.50	0.20	0.0
56.0	0.66	0.10	0.30	0.50	0.10	0.0
107.0	0.45	0.18	0.64	0.18	0.0	0.0

Table 4.2. Participation of each hydration state as a function of the total suction (RH) during the hydration of an MX-80 bentonite sample [from Saiyouri et al. (2004)].

Using these results and considering the theoretical interlayer water density value for each hydration state (Table 4.1), it is possible to obtain an average value for the interlayer water density ρ_w^i as a function of the relative humidity using equation (4.7). The results obtained are shown in Figure 4.4, together with the linear relationship adopted to define ρ_w^i for intermediate values of relative humidity. This relation was defined for relative humidity higher than 16 %, which corresponds to the beginning of the interlayer hydration (Cases et al., 1992).
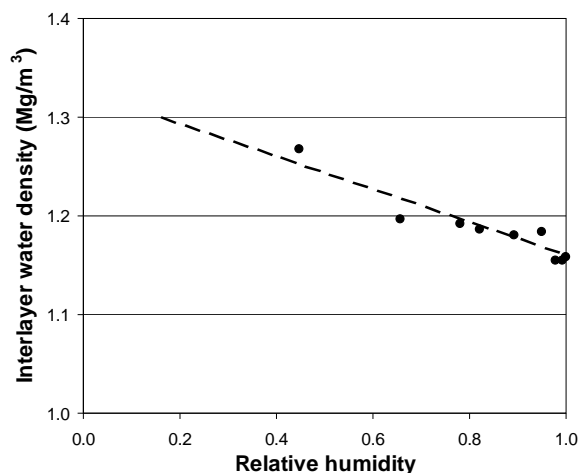

Figure 4.4. Average interlayer water density against relative humidity in MX-80 bentonite. Dashed line represents the linear fitting adopted.

Finally, the value of the external water has to be defined as a function of the relative humidity. Cases et al. (1992) calculated the external water for relative humidity lower than 16 %. For higher values of relative humidity, equation (4.8) was used and the external coverage θ was obtained from Table 4.3 (Hagymassy et al., 1969). For the area of an absorbed water molecule σ a value of 14.8 Å^2 reported by Harkins & Jura (1944) was used.

RH	θ	RH	θ
0.2	0.79	0.7	1.96
0.3	0.99	0.8	2.30
0.4	1.21	0.9	3.03
0.5	1.43	1.0	6.06
0.6	1.67		

Table 4.3. External coverage θ as a function of relative humidity [from Hagymassy et al. (1969)].

The variation of the average water density with suction for the MX-80 bentonite sample compacted at 1.60 Mg/m^3 and obtained with the methodology described above is shown in Figure 4.5. A value of 1.09 Mg/m^3 for the average water density was obtained for the lower suction value recorded in the tests (1.3 MPa). The results suggest that, as the sample becomes saturated, the average water density decreases.
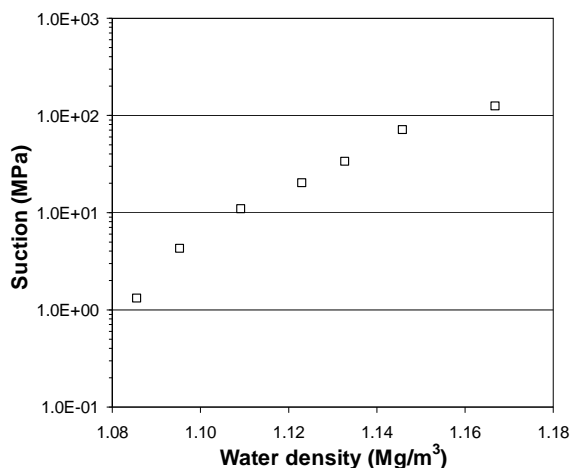
Figure 4.5. Estimated relationship between suction and average water density for a MX-80 bentonite sample compacted at a dry density of 1.60 Mg/m^3.

Figures 4.6 show experimental results for an MX-80 bentonite sample compacted at dry density 1.60 Mg/m^3 and tested at 20 °C (Villar, 2005).

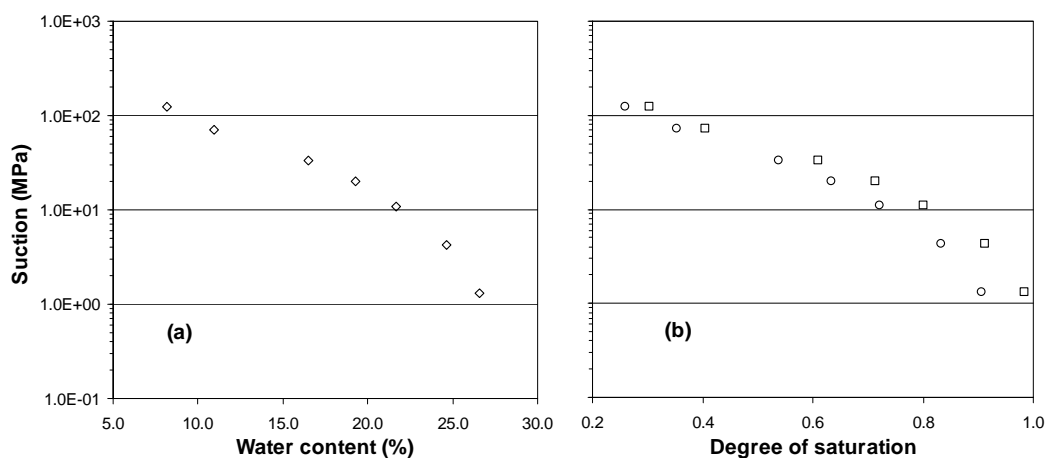**Figure 4.6. Water retention curve under constant volume conditions for a MX-80 bentonite sample compacted at a dry density of 1.60 Mg/m^3 [from Villar (2005)]. (a) Suction against water content; (b) suction against degree of saturation. Values determined using ρ_w = 1.0 Mg/m^3 (squares) and using the water density values obtained with the proposed method (circles).**

Figure 4.6(a) shows the water retention curve as a function of the gravimetric water content while Figure 4.6(b) shows the same results but as a function of the degree of saturation. These values were computed both using a water density of 1.0 Mg/m^3 and that obtained following the proposed method (Figure 4.5). Note that for low suctions, although the average water density is close to 1.0 Mg/m^3, the water content is large. Therefore changes in the degree of saturation value computed by means of equation (4.1) are more important at lower suctions.

4.3.2 FEBEX bentonite

The proposed methodology was also applied to the analysis of previous experimental results of water retention curves obtained in FEBEX bentonite samples. This material was considered as sealing material in the engineered barrier design for high-level radioactive waste proposed by ENRESA (Spanish Agency for Management of Radioactive Waste). The major mineral phase of this bentonite is montmorillonite (92 %) and Ca and Mg are the dominant exchangeable cations (ENRESA, 2000; Fernández & Rivas, 2005).

The adsorption and desorption of water vapour in Ca-montmorillonite has been studied using the water sorption isotherms on powder samples by Mooney et al. (1952b), Keren & Shainberg (1975), Kraehenbuehl et al. (1987), Dios Cancela et al. (1997), Ferrage et al. (2005a-b) and Devineau et al. (2006).

The basal distance in Ca-montmorillonite powder samples varies with water content (Mooney et al., 1952b; Keren & Shainberg, 1975; Dios Cancela et al., 1997; Ferrage et al., 2005a). Villar (2007) determined the basal distance as a function of relative humidity in samples of FEBEX bentonite compacted at different dry densities and tested at constant volume and at 20 °C. The results show that the basal distances for relative humidity varying between 60 % and 95 % correspond approximately to two-layer hydrate. The results for compacted samples coincide with those obtained for FEBEX bentonite powder in the same relative humidity range by Fernández & Rivas (2005). Fernández (2003) determined that the basal distance in saturated samples of FEBEX bentonite under constant volume corresponds almost to the three-layer hydrate.

Again, it seems that compaction does not affect the interlayer swelling in the case of samples hydrated under free volume conditions. However, although there are not

experimental results available for compacted samples hydrated under confined conditions at very low suction values, it is expected some dependence between the contribution of each hydration state and the density of the sample.

The method described above was applied to the analysis of the water retention curves of compacted samples of FEBEX bentonite shown in Figure 4.3. These values were obtained at constant volume and at 20 °C (Lloret et al., 2004).

Fernández & Rivas (2005) analysed the hydration of the FEBEX bentonite using different methods. In the present work the values of the interlayer water density for each hydration state calculated by these authors following the method proposed by Cases et al. (1992), were adopted. The values of w_j are 132.5, 239.0, and 358.5 mg/g for the one-, two-, and three-layer hydrate state, respectively. On the other hand, the average values of the basal distance (d_{001}) are 11.2, 15.5, and 18.8 Å for the one-, two-, and three-layer hydrate state, respectively. A value of 9.8 Å was assumed for the clay layer thickness, t_p (Fernández & Rivas, 2005). The values of the theoretical interlayer water density for each hydration state in a FEBEX bentonite sample are indicated in Table 4.4 (Fernández & Rivas, 2005). When comparing these results with those corresponding to Na-smectite (Table 4.1) it is possible to conclude that, for the same hydration state, the density of the interlayer water is higher when the interlayer cations are predominantly divalent (FEBEX bentonite).

Water layers j	$\rho_w{}^j$ (Mg/m^3)
1	1.51
2	1.23 – 1.13
3	1.11

Table 4.4. Theoretical interlayer water density for each hydration state j in FEBEX bentonite [from Fernández & Rivas (2005)].

Ferrage et al. (2005a) have determined the participation of each hydration state p_j as a function of the relative humidity for a Ca-montmorillonite powder sample (Table 4.5). Using these results and those corresponding to the theoretical interlayer water density for each state (Table 4.4) an average value for the interlayer water density ρ_w^i as a function of the relative humidity is obtained from equation (4.7). The results are shown in Figure 4.7 together with a fitting function adopted for the calculation of the intermediate values of ρ_w^i.

Suction (MPa)	RH	Layers		
		0	1	2
30.0	0.80	0.07	0.10	0.85
68.0	0.60	0.08	0.13	0.80
122.0	0.40	0.09	0.15	0.77
140.0	0.35	0.14	0.40	0.47
214.0	0.20	0.23	0.68	0.09

Table 4.5. Participation of each hydration state as a function of the total suction (RH) during the hydration of a Ca-montmorillonite sample [from Ferrage et al. (2005a)].
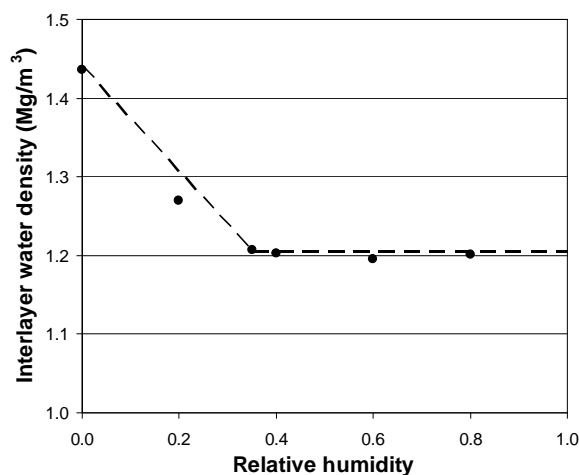

Figure 4.7. Average interlayer water density against relative humidity in FEBEX bentonite. Dashed line represents the fitting adopted.

The external water in the FEBEX bentonite was determined by interpolation of the values given in Table 4.6 (Fernández & Rivas, 2005), corresponding to bentonite powder. These authors have applied the procedure proposed by Cases et al. (1992) and described when introducing equation (4.8). Using these values of external water it is possible to determine the values of interlayer water, and using equation (4.3) a relation between the average water density and relative humidity is obtained.

Figure 4.8 presents the relation between water density and suction for FEBEX bentonite samples compacted at two dry densities. The differences between water density values for each case are very small because both dry densities are in fact very close. In this case, the influence of dry density on the results depicted in Figure 4.8 comes from the retention curves presented previously in Figure 4.3, where two curves for dry densities 1.60 and 1.65 Mg/m^3 were shown. The total water content is different for both samples and as the external water content is the same (independent on dry

density), the difference is assigned to the interlayer water and thus the average water density becomes also different. This effect is more important close to saturation, since the proportion of interlayer water increases when the samples are hydrated at constant volume. However, for high suctions (e.g. more than 10 MPa) the effect of dry density on the average water density should be small. As in the case of the MX-80 bentonite, the results suggest that the average water density decreases as suction decreases. This must be attributed to the predominance of high hydration states for which the density of the interlayer water is lower (Table 4.4).

RH	w_e
0.00	0.000
0.20	0.010
0.45	0.018
0.58	0.026
0.75	0.032
0.85	0.041
1.00	0.077

Table 4.6. External water content w_e as a function of relative humidity in powder FEBEX bentonite [from Fernández & Rivas (2005)].

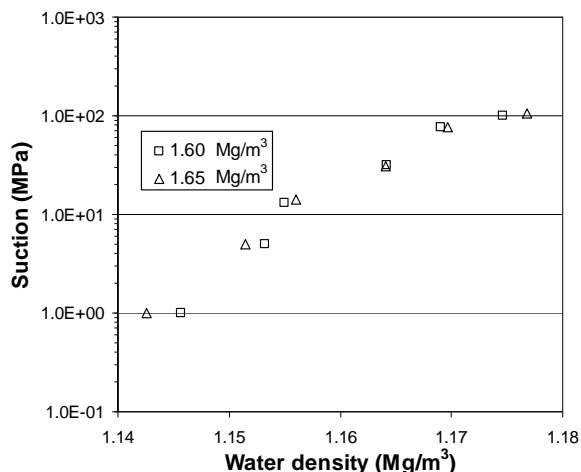**Figure 4.8. Estimated relationship between suction and average water density for FEBEX bentonite samples compacted at different dry densities.**

Figure 4.9 shows the suction values as a function of the degree of saturation when they are calculated either considering the free water density (empty symbols) or the proposed method (filled symbols). The change in the water density produces changes

in the retention curve, which are more important in the low suction range. That was also the case for the MX-80 bentonite.
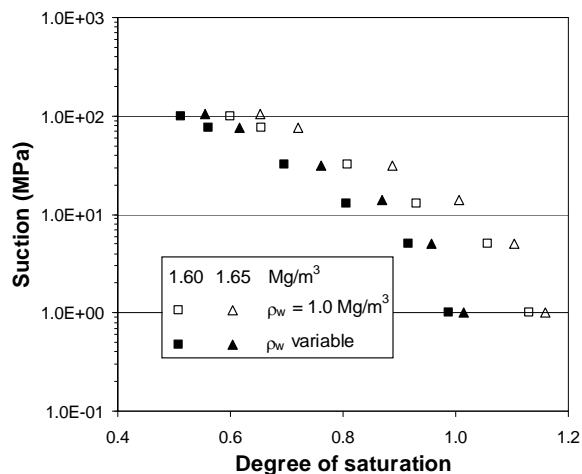

Figure 4.9. Suction against degree of saturation for compacted FEBEX bentonite samples. Values determined using ρ_w = 1.0 Mg/m^3 (empty symbols) and using the water density values obtained with the proposed method (filled symbols).

The comparison between the results in Figures 4.6 and 4.9 shows that the correction in the degree of saturation values for the FEBEX bentonite is more important than in the case of the MX-80 bentonite. This water density effect is due to the higher water density found for the FEBEX bentonite, which can be partially associated to the predominant exchangeable cations in the clay and the difference in the interaction mechanisms between each cation and the interlayer water, which influence the hydration process.

4.4 Application

To solve coupled problems in partially saturated soil it is necessary to know, among others constitutive laws, the soil water retention curve. In general, numerical codes are formulated using the degree of saturation as the variable to indicate the water content within the porous medium. Because of that, it is common to express the retention capacity as a relation between suction and degree of saturation. To apply the concepts previously developed the hydration of a sample made up of expansive soil is analysed. The objective of this study is to evaluate how the law adopted for water density affects the results obtained.

Two cases were analysed and in order to simplify the evaluation of the results only the hydraulic problem was considered. Temperature and gas pressure were fixed equal to 20 ºC and 0.1 MPa respectively. Initial suction and water content were defined equal to 53 MPa and 11.3 % respectively. It is assumed that the sample is made up of MX-80 bentonite compacted at a dry density of 1.60 Mg/m^3. The sample is hydrated throughout one of its boundary by applying a small water flux. The imposed hydraulic boundary condition guarantees that the water injected within the sample is the same in both cases analysed. Case 1 represents a situation where coefficients in the liquid density law are determined using the method proposed in this Chapter. In the other case (Case 2), parameters commonly used to define the density of liquid free water are considered.

The soil water retention curves are defined using the expression proposed by van Genuchten (1980) [see eq. (3.29)]. Parameters in that expression were defined using the values presented in Figure 4.6. As it can be seen in that figure, degrees of saturation higher than one are obtained at lower suction values in Case 2. In that case, the maximum degree of saturation S_{ls} was fixed equal to 1.0 and automatically the fitting process forces values of degree of saturation lower than one in all those cases where this value is surpassed. Values of the parameters defining the water retention curve used in each case considered are indicated in Table 4.7. As it can be seen, taking into account the appropriate estimation of water density results in a reduction of the degree of saturation for a particular value of suction. From a practical point of view this reduces the air entry value in the water retention curve.

With respect to the liquid density ρ_l, a generic expression for this law can be written as a function of the liquid pressure P_l and temperature T

$$\rho_l = f\left(P_l, T\right) \tag{4.10}$$

Additionally, derivatives of equation (4.10) with respect to the independent variables are needed in the general formulation used to solve coupled problems. In general, in the analysis of coupled processes as those considered in this Thesis, species in liquid phase are liquid water and dissolved air. However, it is generally accepted that some properties of the liquid phase are equal to those corresponding to the liquid water. In particular, the law used to define the liquid phase density is assumed equal to that of the liquid water.

Different alternatives were evaluated to fit the results shown in Figure 4.5. However, some of them should be rejected because derivatives obtained from those expressions could become undefined at some values of the liquid pressure. Because of that, the following law was finally adopted (Olivella et al., 1996)

$$\rho_l = \rho_{l0} \exp\left[\beta(P_l - P_{l0}) + \alpha_l T\right] \tag{4.11}$$

where ρ_{l0} is a reference liquid density, β and α_l are the compressibility and the volumetric thermal expansion of the liquid respectively, and P_{l0} is a reference liquid pressure. Coefficients for the hydraulic laws used in each case are indicated in Table 4.7.

In both cases, the value of the coefficient α_l was adopted equal to that usually considered for liquid free water. As it was already indicated, values of coefficients ρ_{l0} and β in Case 2 were also assumed equal to those used for liquid free water. In Case 1, on the other hand, those coefficients were derived for liquid density data corresponding to experimental results of retention capacity obtained for a sample compacted at a dry density of 1.6 Mg/m^3 (Figure 4.5).

	Case 1	Case 2
Coefficient	Soil water retention curve	
α (MPa^{-1})	0.16	0.08
m	0.29	0.32
	Liquid density	
ρ_{l0} (Mg/m^3)	1106.0	1000.0
β (MPa^{-1})	-6.5x10^{-4}	4.5x10^{-4}
α_l (^{o}C^{-1})	-3.4x10^{-4}	

Table 4.7. Coefficients defining the hydraulic constitutive laws used in each case analysed.

With respect to coefficients adopted in Case 1 for the liquid density law, two pertinent comments have to be made. First, it is thought that the influence of sample density on coefficients could be marginal at high values of that variable. However, it should be verified when more experimental data of retention capacity for samples compacted at different densities and tested at the same conditions become available. Second, the values of those coefficients have been deduced for liquid pressures lower than 0.1

MPa (i.e. when the soil sample is in unsaturated state). Thus, when the soil is saturated, one option is to assume that the volumetric expansion of water in expansive soils coincides with that of the free water. The other possibility is to consider that the water density is independent of the liquid pressure (i.e., the value of the liquid density is constant and equal to the value corresponding to nil suction). This last option was adopted in the example described below.

Figure 4.10(a) presents the distribution of degree of saturation along the sample at different time steps and for each case considered. Continuous lines represent results obtained in Case 1 while doted lines correspond to those obtained in Case 2. The final time (300 days) corresponds to a water content which is 98 % of the water content at saturation in Case 2.

Figure 4.10(b) shows how the relation between the water content in different zones within the sample in Case 1 respect to the corresponding one in Case 2 varies as the hydration proceeds. The zone close to the hydration boundary is designed as "wet" in the figure whereas that far away of the injection point as "dry". In the same figure, the relation between the overall water content corresponding to each case considered at a given time is indicated as "average".
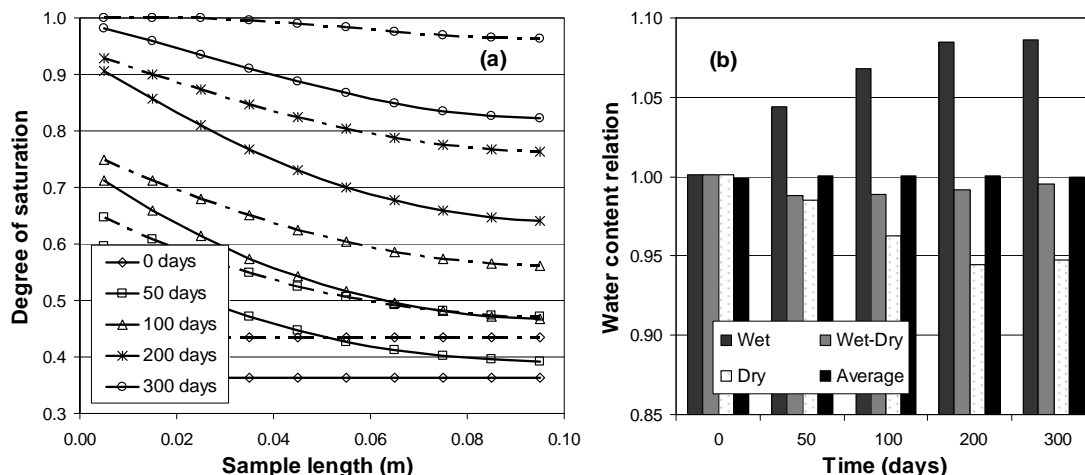
Figure 4.10. (a) Evolution of the degree of saturation at different times and for each case considered; continuous lines correspond to Case 1 and dotted lines to Case 2; (b) temporal evolution of the relation between values of water content at different zones within the sample.

Values in Figure 4.10(a) suggest that the sample becomes saturated earlier in Case 2 than in Case 1. Results indicate that only in the zone close to the injection boundary

the sample saturates approximately at the same time in both cases considered. However, at the time when sample in Case 2 becomes almost saturated (300 days), the difference in degree of saturation between both cases approximates to 15 % in the zone opposed to the injection boundary. In other words, calculations suggest that more time will be needed to saturate the sample in Case 1.

As it can be seen in Figure 4.10(b), until the time when sample nearly saturates for Case 2 (300 days), the global water content within the sample at a given time is the same in both cases (black bars). However, as the hydration proceeds, the relation between the water content in Case 1 with respects to that in Case 2 increases in the zone close to the injection point (gray bars) whereas this ratio decreases in the opposed zone (white zone).

Other aspect to be highlighted is the difference in the quantity of water needed to saturate the sample in each case analysed. For the dry density considered, the gravimetric water content at saturation is about 27 % in Case 2 whereas it is close to 30 % in Case 1. Clearly, it will be needed to inject more water in the latter case to saturate the sample.

4.5 Concluding remarks

The water in the interlayer zone of clayey soils has several features that are quite different from those of free water. This is suggested by experimental studies on the characteristics of water in the interlayer zone and measurements of the water retention capacity of compacted and confined samples of expansive clays. In the latter case, degrees of saturation higher than one have been systematically obtained close to saturation when they are calculated using the density of free water (1.0 Mg/m^3).

In this Chapter a methodology that permits to consider the fact that the water density in expansive clays changes as a function of relative humidity (suction) has been presented. If this aspect is considered, it is possible to obtain retention curves in which the values of degree of saturation in the range of low suctions are not higher than one. The method allows to estimate an average value of the water density taking into account, on the one hand, the water adsorbed at the external surface of the aggregates, and on the other hand, the water between clay layers for which densities greater than 1.0 Mg/m^3 have been deduced.

It seems that the exchangeable cation in the interlayer space plays a central role in the values that result for the water density at different suctions. Thus, water density is higher, and consequently the effect of water density is more important, in bentonites with predominant divalent cations in the interlayer space (FEBEX bentonite) than in those with monovalent exchangeable cations (MX-80 bentonite).

The curves "suction – average water density" obtained for two bentonites (Figures 4.5 and 4.8) can be used in those geotechnical analyses that are sensitive to water density. In particular, when analysing the performance of engineered clay barriers, the unsaturated flow calculations should consider this effect on the water retention curves. Taking into account the appropriate estimation of water density results in a reduction of the degree of saturation for a particular value of suction. From a practical point of view this reduces the air entry value of the material and increases the time required for saturation. It should be pointed out that in the context of compacted expansive clays, these "suction – average water density" curves are not very sensitive to dry density or to compaction conditions for high suction values (e.g. higher than 10 MPa).

Finally it must be highlighted that the values used in this work and adopted from the literature, although considered "state of the art values", have possibly some uncertainty in their determination, which is very difficult to accomplish. Because of that, the method proposed in the present work will be more accurate as more detailed and improved results become available.

Chapter 5

Coupled analysis of a laboratory experiment under high temperatures

Summary

The Temperature Buffer Test is a heated full-scale field experiment carried out at the Äspö Hard Rock Laboratory in Sweden, simulating repository conditions for radioactive waste. The initial thermo-hydro-mechanical (THM) evolution in the clay barrier was investigated in a separate mock-up test. The Chapter describes this laboratory experiment and the corresponding numerical simulations. Most of the related work refers to THM analyses of bentonite barriers well below 100 ⁰C, but here higher temperatures are considered. A 0.20 m closed specimen of compacted MX-80 bentonite was subjected to a temperature gradient (84 ⁰C and 120 ⁰C at the boundaries). The evolution of temperature, relative humidity, pore pressure and stresses was monitored at several points. The test was allowed to reach steady-state conditions. The specimen was then sampled and analysed in terms of water content and bulk density.

Several finite element analyses considering different coupled THM interactions were performed, and compared with measurements. Bentonite properties were obtained from independent tests. Additionally, retention properties were also obtained from measured saturation ratios and steady-state suction values. For the mechanical problem the Barcelona Expansive Model was used, which includes explicitly the two structural levels that actually exist in expansive clays (macro- and microstructure). This model made it possible to simulate the evolution of stresses as well as the expansion of bentonite at the cold side and the compression at the hot side using a single set of parameters.

5.1 Preface

A current approach for radioactive waste disposal involves surrounding canisters containing the waste by expansive clay in deep repositories. The clay barrier, initially unsaturated, is subjected to high thermal and hydraulic gradients, and because of its expansive nature it is expected to swell close to the host rock as a result of the water inflow, but it may shrink close to the canister because of high temperature. One of the current full-scale field experiments reproducing this approach is the Temperature Buffer Test (TBT), carried out at the SKB Äspö Hard Rock Laboratory in Sweden (Sandén et al., 2007). Temperatures of about 140 ºC are reached at some particular points of the compacted bentonite blocks used in this test. For this reason, the thermo-hydro-mechanical analysis of the clay barrier constitutes a challenging problem, as most of the previous studies involved temperatures well below 100 ºC (Gens et al., 1998; Chen & Ledesma, 2007). Additionally, some laboratory tests were carried out in order to understand the physical processes involved, and to compare measurements with numerical simulations. This Chapter presents one of those experiments in detail: a mock-up test denoted as TBT_3, performed at the CEA laboratory in Saclay, France.

The objective of the TBT_3 test was to apply a thermal gradient similar to that measured in the TBT field experiment to a confined sample of MX-80 bentonite. The evolution of temperature, relative humidity and stress during a well-defined thermal loading sequence was measured at several points. Because of the high temperatures reached, and the expected development of vapour pressure during the test, the confining cell was designed to be airtight as well as watertight.

Under a thermal gradient the initially unsaturated compacted bentonite sample develops both liquid water and vapour flows, which in turn contribute to a heat redistribution by advection. Also, the thermal conductivity increases with the amount of water in the soil pores: that is, with the degree of saturation (Knutsson, 1983; Börgesson et al., 1994; Hökmark, 2004). The hydraulic behaviour of the bentonite is also influenced by temperature. In particular, the water retention capacity of clay minerals seems to decrease when the temperature increases (Romero et al., 2001; Villar & Lloret, 2004; Tang & Cui, 2005; Villar et al., 2005; Villar & Gómez-Espina, 2007). In general, this effect is larger than that predicted by the decrease of water surface tension with temperature as suggested by Philip & de Vries (1957). Additionally, the corresponding water content for nil suction seems to decrease for high

temperatures. A comprehensive description of the effects of temperature on retention properties is found in Jacinto et al. (2009).

The above dependences highlight the physical couplings between the thermal and the hydraulic problem in this case. Additionally, the mechanical behaviour of bentonite is governed by the distribution of water and temperature within the sample. Thus a coupled thermo-hydro-mechanical analysis of the experiment becomes necessary to simulate the variables measured in the test.

Regarding the mechanical model, an important effort has been developed by many researchers following the work by Alonso et al. (1990). The elasto-plastic model (the Barcelona Basic Model or BBM) was appropriate for low-expansive unsaturated soils. In the context of the TBT_3 experiment, however, this model would hardly reproduce the complex behaviour of the bentonite. In recent years the fabric of compacted expansive clays has been studied in detail, and a double structure made up of clay aggregates and large macrostructural pores has been recognised. Gens & Alonso (1992), Alonso (1998), Yong (1999) and Cui et al. (2002) indicate that the behaviour of this material is very complex: it results from the interaction between the volume change of aggregates made up of a highly expansive clay mineral (microstructural level) and the rearrangement of the granular-like skeleton formed by the aggregates (macrostructural level). Based on these observations, and on the conceptual model introduced by Gens & Alonso (1992), an extension of the original BBM model was implemented to solve boundary value problems (Sánchez, 2004; Sánchez et al., 2005). This new constitutive law (the Barcelona Expansive Model or BExM) has been adopted here to simulate the mechanical variables of the test.

The Chapter describes the TBT_3 experiment in detail. Data obtained after dismantling the test have been used to perform an interpretation of the TH behaviour of the bentonite under steady-state conditions. Temperature effects on water retention properties are described as well. Finally, a THM analysis using a double-structure mechanical model is presented. Measured stresses are compared with the corresponding simulated values, and the swelling and shrinkage of the bentonite at the cold side and at the hot side of the sample are reasonably reproduced with the model.

5.2 TBT_3 mock-up experiment

5.2.1 Materials and methods

A cylindrical rigid cell was equipped with heaters for temperature control at the two circular faces of a contained bentonite specimen. The cell was densely instrumented with sensors for measurement of temperature, relative humidity, pore pressure, radial stress and the axial stress through the mobile piston.

The design of the cell is illustrated in Figure 5.1. The base, the cell body, the back and upper flange, as well as the piston were made of stainless steel. The sleeve on the inside of the cell body was made of pure PTFE and had a thickness of 17 mm. The joints between the base and the cell body, and between the back flange and the piston, were sealed with Viton® O-rings.
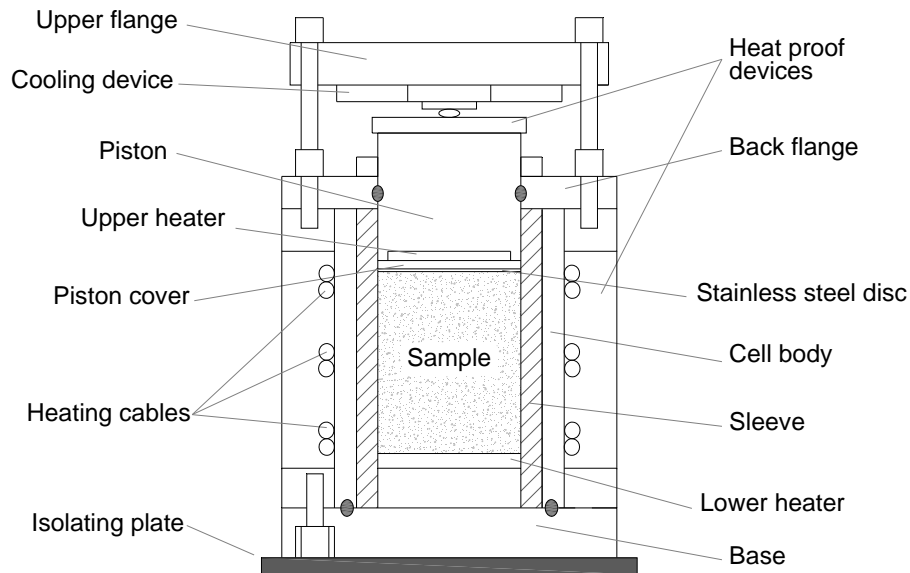
Figure 5.1. Schematic view of the cell equipped for TBT_3 experiment [after Gatabin & Guillot (2006)].

The wafer heaters used for temperature control at the upper and lower faces of the specimen consisted of hollow copper plates in which heating cables were wound. Each heater was fitted with two temperature probes embedded in the coil: one in the centre and the other at 60-70 mm from the centre. The central probes were used for temperature regulation. Three heating cables were rolled up around the cell body at a

quarter, a half, and three quarters of the height of the specimen. The temperature at each height was measured by a thermocouple. Each heater and cable was supplied by a direct-current stabilized power device controlled by a process regulator, which was set independently.

The specimen was made of MX-80 bentonite powder, which was conditioned in a climate chamber in order to increase its water content to 13.3 %. The cold isostatic procedure of compaction (CIP) was selected to obtain a core that was homogeneous in density. This method is a well-known procedure in the field of ceramics and metallurgy to prepare isotropic homogeneous samples from powder material at room temperature (ASTM, 2008). Its use in soil mechanics is convenient when the requirements for isotropy and homogeneity of the sample are particularly strict (Gatabin & Guillot, 2006). The core was isotropically compacted at a pressure of 3.2 MPa following a slow rate of pressure increase and a de-aerating process. It was assumed that the specimen was reasonably homogeneous in density and degree of saturation at the initial state. A final average dry density of 1.70 Mg/m^3 was achieved, which corresponds to a degree of saturation of 58.6 % for a particle density of 2.78 Mg/m^3. The core was then machined to a diameter of 202.5 mm and a height of 202 mm, to fit within the total available volume in the PTFE containment sleeve.

The bentonite specimen was fitted with 14 resistance temperature probes, 11 capacitive relative humidity (RH) sensors, and four pore pressure sensors. The RH sensors were miniature sensors, 7 mm in diameter, provided by Rotronic AG and modified to avoid vapour leakage through their cables (Gatabin & Guillot, 2006). Within the specimen, a cylindrical zone 50 mm in diameter along the vertical axis was preserved without any sensor so that it could be cored at the end of the test for analysis purposes. One relative humidity sensor (RH10) acted as peripheral sensor, its sensitive end being close to the cylindrical envelope. All sensors were positioned perpendicularly to the vertical axis of the cell. Three strain gauge total pressure sensors were installed in the cell body for monitoring of radial stresses. A list of sensors and their locations is given in Table 5.1. A load cell was used for monitoring the axial stress through the mobile piston.

The cell was thermally isolated with 50 mm thick rock-wool strips enveloping the cell body. The base was placed on a low-conductivity plate, consisting of Portland cement reinforced with synthetic products and wollastonite.

Temperature							
T0	T1	T2	T3	T4	T5	T6	T7
0.0	2.5	18.75	35.0	51.25	67.5	83.75	100.0
T8	T9	T10	T11	T12	T13	Piston*	
116.25	132.5	148.75	165.0	181.25	197.5	206.0	
Relative humidity[†]							
RH1		RH2		RH3	RH4	RH5	RH6
22.5		37.5		52.5	72.5	92.5	112.5
RH7		RH8		RH9	RH10[‡]	RH11	
132.5		152.5		172.5	172.5	190.0	
Pore pressure					Radial pressure		
PP1	PP2		PP3	PP4	PT1	PT2	PT3
52.0	84.0		116.0	148.0	135.0	159.0	183.0

* Taking into account a stainless-steel plate of 3.0 mm.

[†] A temperature measurement is associated with a relative humidity measurement.

[‡] Sensor located near the wall of the cell, in order to measure RH at the interface bentonite-casing.

Table 5.1. Sensor locations for TBT_3. Heights (in mm) are measured from the lower heater.

The defined thermal protocol was divided in three phases: (a) an initial homogeneous thermal ramping over 15 days from room temperature at 22 ºC to 84 ºC; (b) a temperature increase at the hot face over 15 days to 120 ºC, with cold face temperature constant at 84 ºC; and (c) an equilibration phase with constant thermal gradient. The final phase was continued for 72 days. In total, the experiment was run for 102 days. The target temperatures for the heating cables were set to correspond to a linear temperature distribution: that is, for a temperature gap between 84 ºC and 120 ºC, the target temperatures were 93 ºC, 102 ºC and 111 ºC respectively.

After switching off the heaters and removing the external layer of heat insulation, the specimen was allowed to cool for approximately 20 h. The experiment was dismantled by removing the upper flange, the back flange, the piston and the stainless steel disc. Bentonite samples were finally recovered by coring a vertical cylinder 50 mm in diameter in the centre of the specimen. This core was sampled, and analysed for water content and bulk density by weighing in petroleum.

5.2.2 Results

The original thermal protocol was followed in detail and the registered temperatures show that the heating system worked as planned (Figure 5.2). The temperature at the cold end of the specimen (T13) was, however, slightly lower (by up to 3 ⁰C) than at the hot end (T0) during the initial phase with respect to the prescribed homogeneous temperature. This difference was due to the design of the metallic cell. The hot end rested on an isolating plate, whereas the cold end was subjected to ambient air exchange. Although the metallic cell was carefully insulated, some of the heat produced by heaters at the hot and cold faces was lost, with more in the upper part of the cell than in the lower part. This heat loss was minimised by the addition of heating cables fixed on the external wall of the cell. Moreover, to maintain the load sensor at constant temperature, the upper part of the piston was cooled at 25 ⁰C. The variation in temperature was expected to create a temperature gradient able to modify the water balance in the specimen slightly.

At the end of the measurements, the heaters were turned off so that the sample could cool for 20 h. Data were recorded during the post-cooling period until the cell was opened. A temperature difference of 10 ⁰C, from 40 ⁰C at the hot end to 30 ⁰C at the cold end, remained present in the specimen at the beginning of the sampling phase.
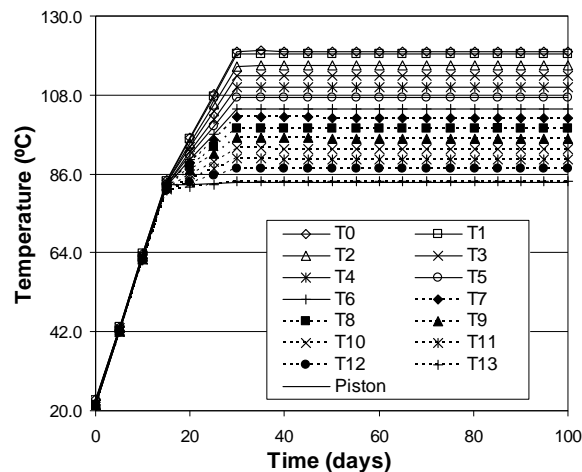

Figure 5.2. Evolution of temperature at different locations within the sample.

The evolution and distribution of relative humidity, at steady state and after cooling, are shown in Figure 5.3. During the initial phase the relative humidity values increased generally from 60 % to values between 67 % and 79 %. This separation of relative humidity levels is probably due to the minor temperature difference noticed during the

initial phase (the temperature varied between 84.2 ºC and 81.3 ºC). This is essentially a step towards the final steady-state condition, when the temperature varied between 120 ºC and 84 ºC, and the RH values were between 40 % and 100 %. This indicates that a redistribution of moisture had already occurred after 15 days.

A more significant separation was registered during the second phase, when the thermal gradient was applied. At the end of the phase the values ranged from 60 % to 96 %. The RH6 sensor failed during this phase. The separation continued during the final phase, with relative humidity values at steady state ranging from 40 % to 100 %. The four uppermost sensors at the cold side (RH8–RH11) showed 100 % or slightly higher values of relative humidity. In the following analyses, a maximum value of 100 % is assumed for these sensors.
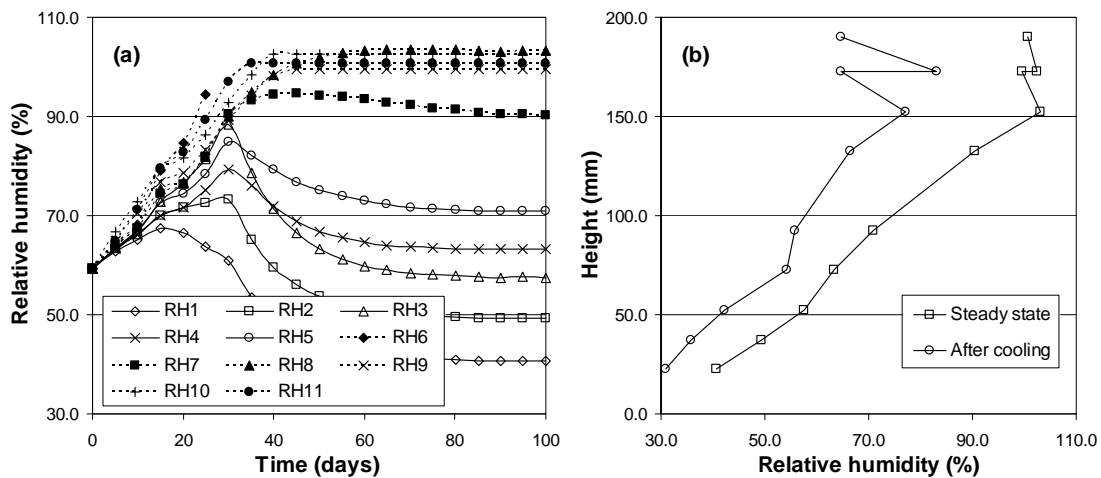

Figure 5.3. (a) Relative humidity evolution at different position within the sample. (b) Relative humidity distribution at steady state condition (quadrilaterals) and after cooling (circles).

The build-up of stresses is shown in Figure 5.4(a). The radial sensor closest to the cold side (PT3) registered the highest stress, with a peak value of 6.5 MPa. The axial stress and the radial stress closest to the mid-section (PT1) equilibrated at 2.0–3.0 MPa. The PT2 sensor was located between PT1 and PT3, and it could therefore be expected that the stress level at this point would fall between 3.0 and 6.0 MPa. Instead, the stress was lower (< 1.0 MPa). This deviation was probably caused by a bad contact between the sensor membrane and the specimen. Pore pressures were generally around absolute atmospheric pressure [Figure 5.4(b)]. A small but significant peak was detected at the time when the maximum thermal gradient was reached (day 30).

At the end of the test, after cooling, samples were taken from 13 different levels in the specimen, and measured values of water content and dry density are shown in Figure 5.5.
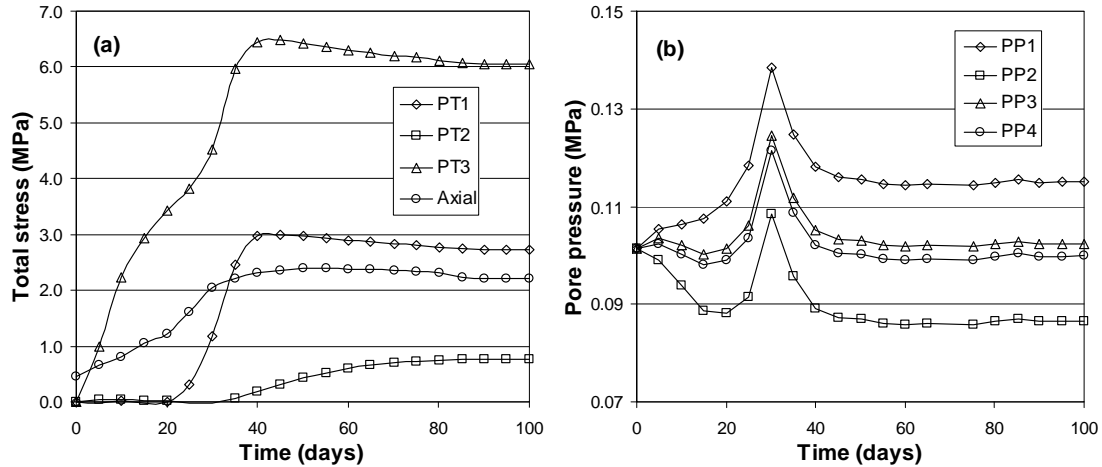
Figure 5.4. Temporal evolution of (a) radial and axial stress and (b) pore pressure at different locations within the sample.

Figure 5.5. Water content and dry density distribution along the sample at the end of the test.

5.3 Analysis and simulation of the experiment

In this section experimental data are analysed and some results are used to define constitutive laws used in the numerical simulations. Calculations were carried out using the finite element program CODE_BRIGHT, developed by Olivella et al. (1996).

Balance equations that govern the non-isothermal multiphase flow through deformable porous media are formulated following the compositional approach (Olivel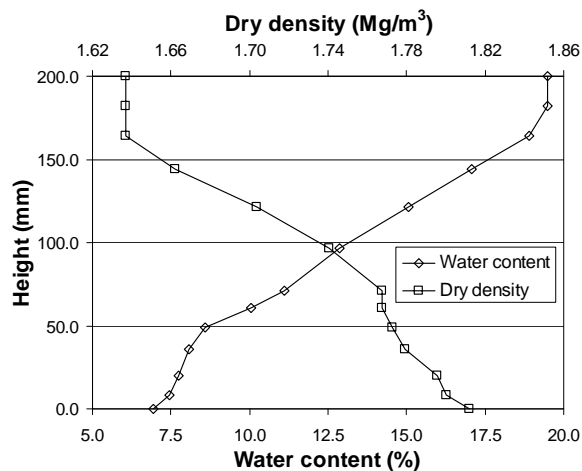la et al., 1994). That is, mass balance is performed for each species in the medium (solid, water, air). In addition to that, an equation for energy balance is established for the medium as a whole and the equation of momentum balance reduces to the conventional stress equilibrium equation. The general balance equations are presented in Chapter 2.

5.3.1 Thermo-hydraulic analysis

5.3.1.1 Vapour pressure and suction

The Clausius-Clapeyron equation defines the relationships between the saturated vapour pressure of water and the temperature (Atkins, 1998)

$$P_v^0 = P_v^{ref} \exp\left[\frac{-\Delta H_{vap}}{R} \left(\frac{1}{T} - \frac{1}{T^{ref}} \right) \right] \tag{5.1}$$

where P_v^0 and P_v^{ref} are the saturated vapour pressure and the saturated reference vapour pressure respectively, ΔH_{vap} is the enthalpy of vaporization, R the universal gas constant, and T and T^{ref} are the absolute temperature and the absolute reference temperature respectively. The dependence of the water vapour pressure on total gas pressure can be neglected for small values of the latter variable (Guggenheim, 1967; Castellan, 1972).

There are different mechanisms for binding of water to the soil matrix, such as direct adhesion of water molecules to solid surfaces, osmotic binding of water in double layers, and capillary binding of water. As a result of these attractive forces, the pressure of the vapour in equilibrium with pore water is less than that defined by equation (5.1). The relative humidity RH defines the relation between those values of the vapour pressure, and it can be expressed in terms of the thermodynamics relationship (Edlefsen & Anderson, 1943)

$$RH = \frac{P_v}{P_v^0} = \exp\left[\frac{M_w s}{\rho_l RT} \right] \tag{5.2}$$

where M_w is the molar mass of water, s is the suction, and ρ_l is the liquid density.

The time evolution of the vapour pressure at different sensor locations is shown in Figure 5.6(a). Vapour pressures start to separate within the range 0.06-0.12 MPa when the thermal gradient is applied. The peak values above absolute atmospheric pressure appear to correspond with the measured pore pressures [Figure 5.4(b)], which suggests that the cell was not totally gastight, but allowed a minor pressure build-up at this point. The spatial distribution of vapour pressure is further illustrated in Figure 5.6(b). Here it can be clearly seen that the vapour pressure at both ends never exceeded 0.1 MPa. The steady-state distribution (100 days curve) shows lower values at the ends of the sample. In the central part of the specimen, between 50 and 150 mm height, the vapour pressures were found in a narrow interval between 0.076 and 0.080 MPa.
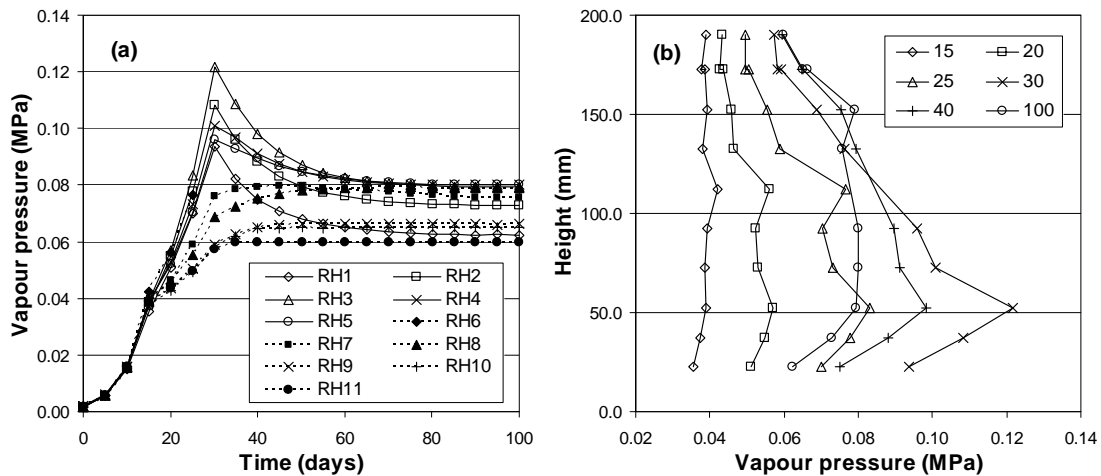
Figure 5.6. (a) Evolution of the vapour pressure obtained from RH-sensor values and equations (5.1) and (5.2). (b) Vapour pressure distribution at different times (in days).

Suction values calculated using equation (5.2) and the relative humidity measurements at different sensor positions are shown in Figure 5.7(a). Note that suctions within the sample show a wide variation, from 0.0 to 160.0 MPa. Figure 5.7(b) presents the spatial distribution of suction after 100 days, when steady-state conditions can be assumed, and before the sample was dismantled. Suction values equal to 0.0 MPa were assumed when the relative humidity registered by the sensor was equal to or higher than 100 % (RH8 to RH11).

Figure 5.7. (a) Evolution of the suction values (obtained from RH measurements) at different positions within the sample. (b) Suction distribution at steady state conditions and before of dismantling.
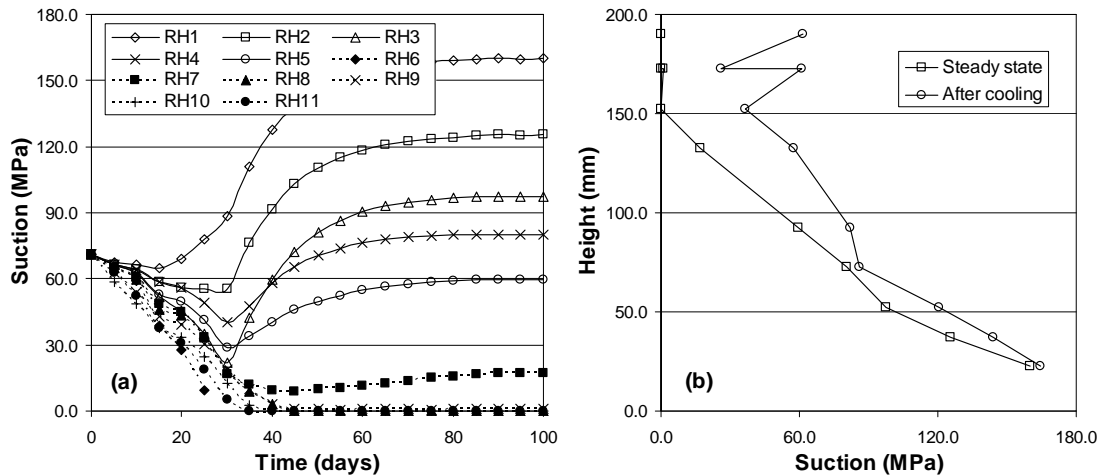
5.3.1.2 In situ retention curve

Measured water contents and corresponding degrees of saturation when dismantling the test, together with the calculated suction values, allow the evaluation of an 'in situ retention curve'. Such relations are shown in Figure 5.8(a), both for steady-state conditions and after the 20 h cooling period. It is assumed that water content does not change during the cooling period before dismantling of the test, as it is measured only at the end of this process. Numerical simulations have shown that water content does not change too much after cooling, although liquid degree of saturation may change owing to water condensation.

The relation between water contents and the post-cooling suction values are generally in accordance with retention data for free-swelling samples (Dueck, 2004). In the same figure are also shown experimental results obtained on compacted blocks made up of bentonite previously mixed with the desired water quantity (Villar, 2005). It can be also observed that suction values for the steady-state condition are significantly lower than those corresponding to free-swelling samples and compacted blocks [Figure 5.8(a)].

Figure 5.8(b) presents the same relations, but in terms of degree of saturation instead of water content. Note that under the experimental conditions, suction can apparently be zero - that is, the vapour is saturated - even though the bentonite is not water saturated. In Figure 5.8(b) the final dry densities measured after dismantling (in Mg/m^3)

and the temperatures measured in steady-state conditions are also indicated. Retention capacity measurements from Villar et al. (2006), obtained in samples of the same material compacted at dry densities of 1.60 and 1.75 Mg/m^3 and tested at different temperatures, are included in the same figure. It can be observed that the general trend is the same for all the experimental results.
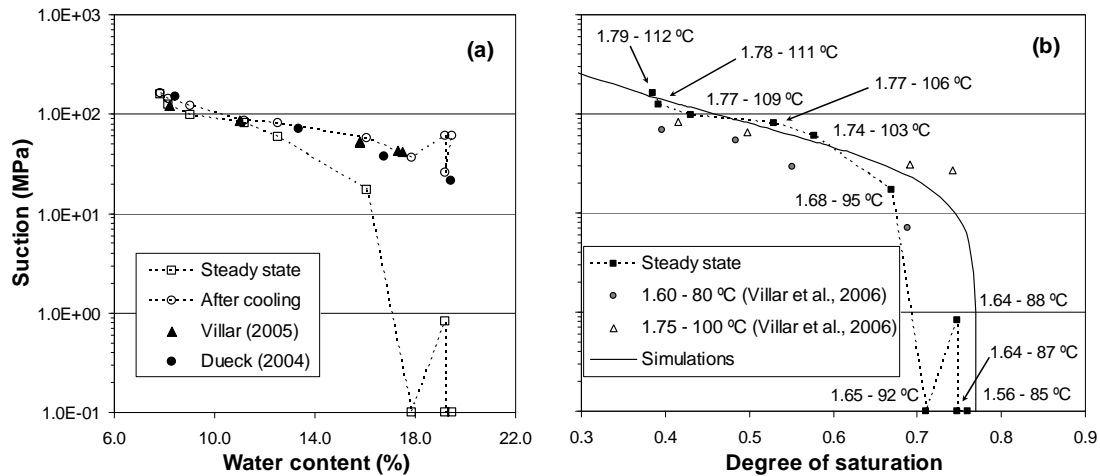

Figure 5.8. (a) Suction against water content at steady state conditions and after cooling measured in the experiment. (b) Suction against degree of saturation indicating steady state temperatures and measured dry densities (in Mg/m^3) after dismantling. Continuous line represents the van Genuchten (1980) relation used in the numerical analyses.

5.3.1.3 Thermo-hydraulic numerical simulation

The objective of the thermo-hydraulic (TH) simulation is to reproduce the general trends observed in the thermal and hydraulic variables and to get an insight into the behaviour of the clay in the test. An aspect of interest is to evaluate the relative influence of each water flow component at different times of the experiment. The total mass balance of water in a porous media is given by equation (2.69). In the case of a TH analysis (mechanical terms are not considered) the following equation applies

$$\phi \frac{D_s}{Dt}\left(\theta_l^w S_l + \theta_g^w S_g\right) + \nabla \cdot \left(\mathbf{j}_l'^w + \mathbf{j}_g'^w\right) = f^w \tag{5.3}$$

where ϕ is the porosity of the medium, θ_α^w is the mass of water per unit volume of the α phase [$\alpha = l$ (liquid), g (gas)], S_α is the volumetric fraction of pores occupied by the α phase, $\mathbf{j}_\alpha'^w$ is the flux of water in the α phase respect to the solid phase, and

f^w is a water supply. $D_S(\bullet)/Dt$ means the material derivative with respect to the solid phase [eq. (2.66)].

The first term on the left-hand side of equation (5.3) corresponds to the storage term while the second one is the gradient of water flux. If f^w = 0 (i.e., closed system), the gradient of the fluxes is equal to the change of the storage term. When steady state conditions are reached, the first term in equation (5.3) is nil and using equations (2.70), (2.74) and (2.76) the following expression is obtained (gravity terms have been neglected)

$$-\theta_l^w \frac{\mathbf{k}k_{rl}}{\mu_l} \nabla P_l = \theta_g^w \frac{\mathbf{k}k_{rg}}{\mu_g} \nabla P_g + \mathbf{D}_g^w \nabla \omega_g^w \tag{5.4}$$

with $\mathbf{k}$ the tensor of intrinsic permeability, $k_{r\alpha}$ the relative permeability of the α phase, μ_α the dynamic viscosity, P_α the pressure in the α phase, $\mathbf{D}_g^w$ the diffusion coefficient, and ω_g^w the mass fraction of water in the gas phase.

In this simulation, the model proposed by van Genuchten (1980) was adopted for the soil water retention curve

$$S_{le} = \frac{S_l - S_{lr}}{S_{ls} - S_{lr}} = \left[\frac{1}{1 + (\alpha s)^{\frac{1}{1-m}}} \right]^m \tag{5.5}$$

where S_{le} is the effective degree of saturation, S_{lr} and S_{ls} are the minimum and maximum degree of saturation respectively, and m and α are fitting parameters. Table 5.2 presents the parameters used in equation (5.5) and the curve obtained is shown in Figure 5.8(b) (continuous line).

α (MPa)	2.2 x 10^{-1}	m	0.35
S_{ls}	0.77	S_{lr}	0.0

Table 5.2. Parameters of the water retention curve used in the analyses.

The conductive flux of heat is simulated using the Fourier´s law [eq. (2.73)]. Based on experimental results (Börgesson et al., 1994; Tang, 2005) the following law was adopted for the current soil thermal conductivity λ_T

$$\lambda_T = \lambda_{dry}\left(1 - S_l\right) + \lambda_{sat}S_l \qquad (5.6)$$

where values of λ_{dry} and λ_{sat} are the thermal conductivity in dry and saturated state respectively.

For the tensor of intrinsic permeability $\mathbf{k}$, which is a function of the pore structure, the Kozeny´s model (Bear, 1972) was adopted

$$\mathbf{k} = \mathbf{k}_0 \frac{\phi^3}{\left(1 - \phi\right)^2} \frac{\left(1 - \phi_0\right)^2}{\phi_0^3} \qquad (5.7)$$

with $\mathbf{k}_0$ the tensor of intrinsic permeability corresponding to a reference porosity ϕ_0 .

It is assumed that the relative permeability of the α phase depends on the effective degree of saturation $S_{\alpha e}$ according to the law

$$k_{r\alpha} = A_\alpha \left(S_{\alpha e}\right)^{n_\alpha} \qquad (5.8)$$

with A_α and n_α parameters to be defined form experimental data.

Table 5.3 indicates the values adopted for the coefficients in the thermal and hydraulic constitutive equations (5.6) to (5.8).

λ_{dry} [W/(m·K)]	λ_{sat} [W/(m·K)]	$\mathbf{k}_0$ (m^2)	ϕ_0
0.3	1.3	3.6 x 10^{-21}	0.37
A_l	n_l	A_g	n_g
1.0	3.0	2.2 x 10^8	4.17

Table 5.3. Parameters defining thermal and hydraulic constitutive equations.

The diffusive flow of water in the gas phase is given by equation (2.76). The dispersion tensor $\mathbf{D}_\alpha^i$ in that equation is given by the expression (Olivella & Gens, 2000)

$$\mathbf{D}_\alpha^i = \tau\phi\rho_\alpha S_\alpha D_m^i \mathbf{I} \qquad (5.9)$$

where τ is the tortuosity parameter, ϕ is the porosity of the medium, ρ_α and S_α are the mass density and degree of saturation, respectively, of the α phase, D_m^i is the molecular diffusion coefficient, and $\mathbf{I}$ is the identity matrix.

One of the parameters to be defined in equation (5.9) is the molecular diffusion coefficient D_m^w. The binary diffusivity is a function of the temperature and pressure, and near standard temperature and pressure conditions it can be expressed as (Massman, 1998)

$$D_m^w = D_0 \frac{P_0^g}{P_g} \left(\frac{T}{T_0} \right)^n \tag{5.10}$$

where D_0 is the diffusivity at T_0 = 273.15 K and P_g^0 = 101.325 kPa, T is the absolute temperature, P_g the gas pressure, and n is a coefficient. For the diffusivity of water vapour in air, Massman (1998) proposes a D_0 value of 2.178x10^{-5} m^2/s and n equal to 1.81. The expression obtained is valid in a range of temperatures between -20 ºC and 100 ºC. Marrero & Masson (1972) (in Massman, 1998) suggest values of 2.090x10^{-5} m^2/s and 2.072, respectively, for D_0 and n. This expression is also valid for temperatures above 100 ºC. Values for the n coefficient between 1.5 and 2.3 are also indicated in the literature (Chen & Othmer, 1962; Seager et al., 1963; Pollock, 1986). An n coefficient equal to 2.2 and a D_0 value of 2.1x10^{-5} m^2/s were used in the analyses carried out in this work. This results in a variation with the temperature similar to that suggested by other researchers.

Philip & de Vries (1957) consider a value of 0.66 for the tortuosity coefficient τ, while Bear (1972) indicates that values varying in the range 0.56-0.8 can be considered. Hökmark (2004) obtains a value of 1.0 by fitting results of temperature gradient tests on MX-80 bentonite samples. A coefficient τ equal to 0.65 was adopted in the calculation. It is important to emphasise that a combination of different values for the parameters n, D_0 and τ result in a similar variation of the dispersion coefficient [eq. (5.9)] with temperature.

A one-dimensional geometry was used in the simulation. Twenty-two linear elements were used to represent the geometry, and the temporal discretisation was defined according to the thermal protocol applied in the test. The thermal boundary conditions

applied at the upper (cold) and lower (hot) boundaries are the same as those in the experiment. The objective of the heating cables was to minimise the heat lost along the cell body. Temperatures in the sensors located at the same height as the heating cables coincide with those imposed by the cables. However, it was difficult to discern whether the heating cables avoided any heat loss, or whether they supplied heat into the sample and thereby controlled the temperature of the soil. Therefore it was assumed that no heat exchange occurred along the lateral part of the cell body (adiabatic boundary). This hypothesis was then confirmed by the results obtained for the temperature gradient along the sample [Figure 5.12(a)]. The boundaries of the model are considered impervious to liquid. Experimental results show that, as the temperature gradient was applied, the gas pressure increased throughout the whole sample [Figure 5.4(b)]. After the maximum temperature gradient was reached, it seems that a gas escape might have occurred. It looks probable that the gas escape was at the hot end, because the gas pressure should have been higher in that part of the sample. Consequently, for the simulation, a gastight system was considered until day 30, and then a gas pressure of 0.1 MPa was imposed at the hot end.

In CODE_BRIGHT the boundary condition for balance equations are incorporated by adding a flux (Olivella et al., 1996). For the case of an applied gas pressure the mass flux of a species i as a component of the gas phase is

$$j_g^i = \left(\omega_g^i\right)^0 \gamma_g (P_g^0 - P_g) \tag{5.11}$$

where ω_g^i is the mass fraction of the species i in the gas phase, and the superscript zero indicates prescribed values. The coefficient γ_g is a leakage coefficient that allows the prescribed pressure to be applied with more or less strength. For the analyses a low transfer coefficient was used.

An initial gas pressure of 0.1 MPa and an initial temperature of 22 ºC were applied on the sample. The initial water content (13.3 %) and the adopted water retention curve define the initial suction value. Main results of the TH variables are presented in section 5.3.2.2 as a part of the THM numerical simulation carried out. At this point, only aspects related to the evolution of the different fluxes present in the test are analysed.

Figures 5.9(a)-(d) show the water flux components and the balance between them for different days. During the transient stage, the water flux components due to the diffusive flux [Figure 5.9(c)] and the advective gas flow [Figure 5.9(b)] are bigger than

that due to the liquid phase movement [Figure 5.9(a)]. Figure 5.9(d) shows the net water movement from the hot to the cold side during that state, which is balanced by the storage term [eq. (5.3)]. During the application of the temperature gradient the diffusive flux dominates and it is the main mechanism of water transport. However, at steady state conditions the water flow component due to the nonadvective flow is the lower one. This result is consistent with the low vapour pressure gradient observed along the sample at the end of the experiment [Figure 5.6(b)]. On the other hand, although the gas pressure gradient along the sample is small, the water flow component due to the gas movement is important because of the high gas relative permeability of the material.
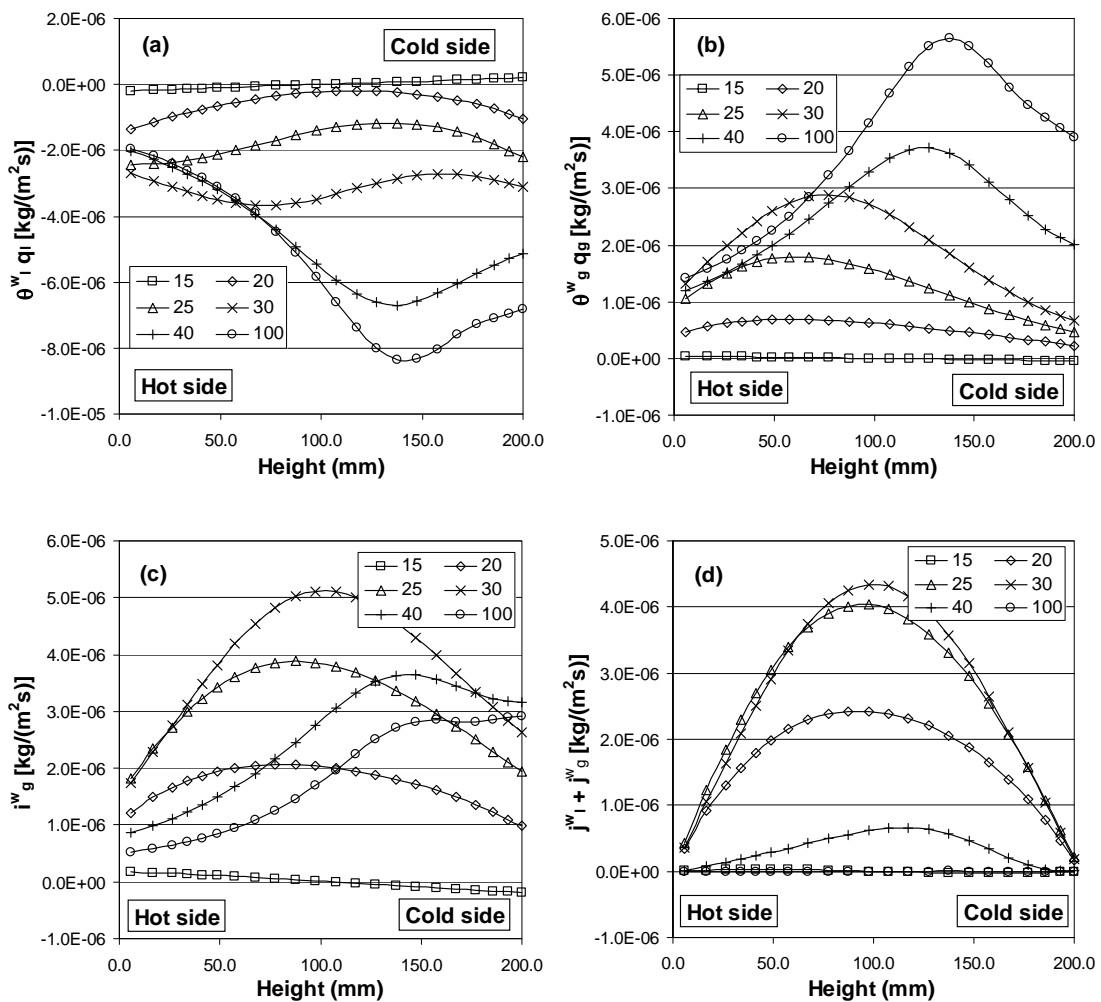

Figure 5.9. (a) Advective water flux component in the liquid phase. (b) Advective water flux component in the gas phase. (c) Nonadvective water flux components in the gas phase. (d) Balance of those water flux components. Labels indicate different times (in days). Positive values mean flux from the hot (bottom) to the cold (top) side.

5.3.2 Thermo-hydro-mechanical analysis

5.3.2.1 Mechanical model

The Barcelona Expansive Model (BExM) originally proposed by Gens & Alonso (1992) has been used in this work to simulate the mechanical behaviour. The model was implemented in the finite element program CODE_BRIGHT (Sánchez, 2004; Sánchez et al., 2005). It assumes that in the material fabric it is possible to define the macrostructural level that is responsible for major structural rearrangements and the microstructural level where swelling of the active minerals takes place [Figure 5.10(a)]. Only a general overview of the whole model is given below, while a more detailed description is presented elsewhere (Gens & Alonso, 1992; Alonso et al., 1999; Sánchez, 2004; Sánchez et al., 2005).

The Barcelona Basic Model (BBM) developed by Alonso et al. (1990) has been adopted to simulate the macrostructural behaviour. This model is able to reproduce many of the basic mechanisms observed in unsaturated non-expansive soils. The independent stress variables used to simulate the unsaturated soil behaviour are the net stress σ_{ij}, and the suction s, defined as

$$\sigma_{ij} = \sigma_{ij,t} - P_g \qquad\qquad s = P_g - P_l \qquad\qquad (5.12)$$

where $\sigma_{ij,t}$ is the total stress, P_g the gas pressure, and P_l the liquid pressure.

The BBM was extended to include the effect of temperature on the mechanical response (Gens, 1995). This model considers that the thermal effect is only volumetric and also includes a dependence of the pre-consolidation pressure (hardening parameter of the model) on temperature. In this way, it is assumed that as temperature increases the size of the yield surface reduces.

The elastic volumetric strain increment is given by

$$\dot{\varepsilon}_v^e = \frac{\kappa}{1+e}\frac{\dot{p}}{p} + \frac{\kappa_s}{1+e}\frac{\dot{s}}{s+0.1} + \alpha_T \dot{T} \qquad\qquad (5.13)$$

with κ defined as

$$\kappa = \left(\frac{\kappa_p}{1+e} + \alpha_{pT} \Delta T \right)(1+e) \qquad (5.14)$$

and where p is the net mean stress, κ_p is the elastic stiffness parameter for changes in net mean stress, κ_s is the elastic stiffness parameter for changes in suction, e is the void ratio, and α_{pT} and α_T are isotropic thermal expansion coefficient of the solid skeleton. Theses last two parameters are defined as a function of temperature and pressure (Appendix B).
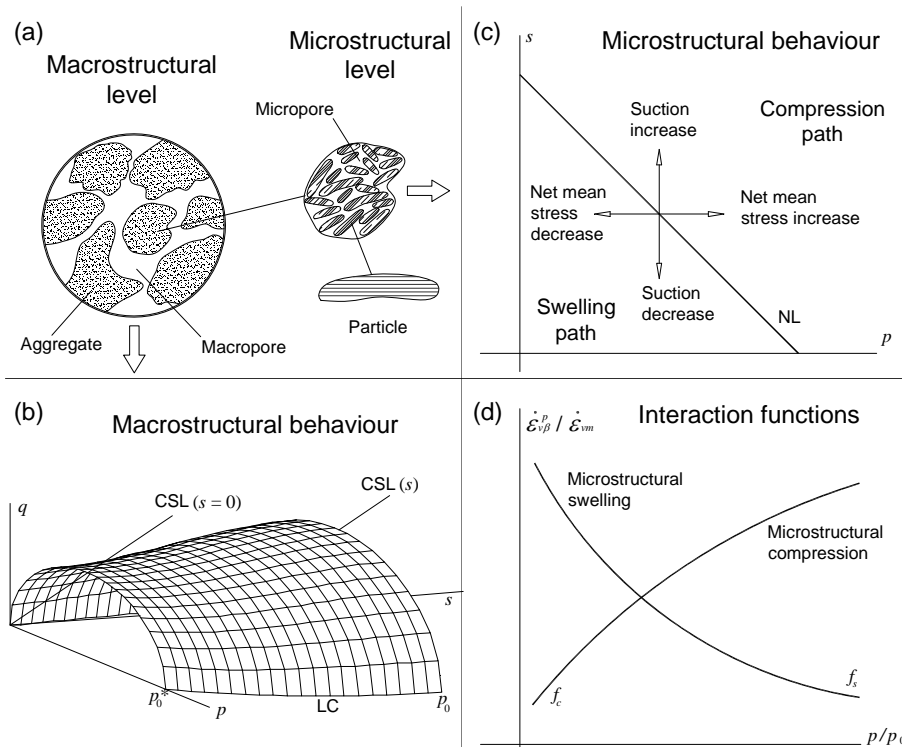

Figure 5.10. (a) Structural levels in a fabric of a compacted bentonite. (b) Three-dimensional view of the BBM yield surface (macrostructural behaviour). (c) Compression and swelling regions separated by the NL (Neutral Loading) line (microstructural behaviour). (d) Interaction functions (coupling between micro and macrostructure).

The thermal effect on the pre-consolidation stress has been included considering a dependence of the pre-consolidation stress at saturated state p_0^* with the temperature (Gens, 1995)

$$p_c = p_0^* + \gamma_T \Delta T \qquad (5.15)$$

where p_c is the pre-consolidation stress for a saturated state at the current temperature, ΔT is the temperature increment defined as the difference between the current temperature T and the reference temperature T_0, and γ_T is a coefficient (usually negative) corresponding to a reduction of the yield surface due to temperature increments. The expression adopted for γ_T is given in Appendix B.

It is assumed that the evolution of the hardening parameter depends only on plastic volumetric strains ε_v^p according to (Gens, 1995)

$$\dot{p}_0^* = \frac{1+e}{\lambda_0 - \kappa} p_0^* \dot{\varepsilon}_v^p \tag{5.16}$$

where λ_0 is the slope of the virgin consolidation line at saturated state.

The Loading-Collapse (*LC*) curve represents the locus of the yield points in the plane defined by the net mean stress and the suction at the reference temperature. The pre-consolidation pressure p_0 at different values of suction and at the current temperature is defined in the same way as postulated by Alonso et al. (1990)

$$p_0 = p_r \left(\frac{p_c}{p_r} \right)^{\frac{\lambda_0 - \kappa}{\lambda_s - \kappa}} \tag{5.17}$$

where p_r is a reference stress.

The dependence on suction of the slope of the virgin consolidation line λ_s can be expressed as follow

$$\lambda_s = \lambda_0 [(1-r)\exp(-\beta s) + r] \tag{5.18}$$

with β and r model parameters.

The formulation has been extended to the triaxial stress space considering the deviatoric stress q, and assuming different yield surfaces for each suction value. Figure 5.10(b) is a three-dimensional view when the yield surface adopted is the modified Cam-clay model. The dependence of strength with suction and temperature is accounted for by allowing the Critical State Line (*CSL*) to vary in the following way

$$p_s = -ks\exp(-\xi\Delta T) \hspace{4cm} (5.19)$$

with k a parameter that defines the intersection value of the *CSL* at zero volumetric net stress (related to cohesion), and ξ a coefficient which takes into account the variation of strength due to temperature changes.

In the general framework developed by Gens & Alonso (1992), it is assumed that physico-chemical phenomena occurring at microstructural level are basically reversible and independent of the macrostructure. The microstructural deformations are considered elastic and volumetric, and its increment is given by

$$\dot{\varepsilon}_{vm} = \frac{\dot{\hat{p}}}{K_m} = \frac{\dot{p}}{K_m} + \chi\frac{\dot{s}}{K_m} \hspace{3cm} (5.20)$$

where the subscripts m and v refer to the microstructural level and volumetric strain respectively, and K_m is the microstructural bulk modulus. The latter one is defined by the following law (Alonso, 1998)

$$K_m = \frac{\exp(-\alpha_m\hat{p})}{\beta_m} \hspace{3.5cm} (5.21)$$

where α_m and β_m are material parameters.

The microstructural mean effective stress is defined as (Alonso, 1998)

$$\hat{p} = p + \chi s \hspace{4cm} (5.22)$$

where χ can be considered a function of the degree of saturation. In this work χ was assumed equal to 1.0 and in that case the microstructural volumetric strain only depends on the increment of the mean effective stress (Alonso et al., 1999).

The curve corresponding to a constant microstructural effective stress is called Neutral Loading (*NL*) line because no microstructural deformations take place along it. For χ equal to 1.0 it becomes a straight line [Figure 5.10(c)]. The *NL* separates stress paths originating swelling from that causing compression. Therefore, a reduction in suction or mean stress will produce microstructural expansion, whereas an increase in suction or mean stress will lead microstructural compression (Gens & Alonso, 1992).

The interaction between structural levels is a key point in the model formulation. Microstructural deformation is considered independent of the macrostructure, but the reverse is not true (Gens & Alonso, 1992). Therefore, macrostructural behaviour can be affected by microstructural deformations in an irreversible way. The framework postulates that the plastic macrostructural strain produced by microstructural strains can be calculated through the following expression (Sánchez et al., 2005)

$$\dot{\varepsilon}_{v\beta}^{p} = f_{\beta}\dot{\varepsilon}_{vm} \tag{5.23}$$

where f_{β} is a coupling function, and $\varepsilon_{v\beta}^{p}$ is the macrostructural plastic strain arising from the interaction mechanisms between both structural levels. Sánchez et al. (2005) define two interaction functions: f_{c} for microstructural contraction and f_{s} for microstructural swelling [Figure 5.10(d)]. It is assumed that the interaction functions depend on the ratio p/p_{0}, where p_{0} is the apparent preconsolidation stress at the current value of suction and temperature (Gens & Alonso, 1992; Alonso et al., 1999).

The increment in the total volumetric plastic strain ε_{v}^{p}, due to both mechanisms considered in the model is obtained as (Sánchez et al., 2005)

$$\dot{\varepsilon}_{v}^{p} = \dot{\varepsilon}_{vLC}^{p} + \dot{\varepsilon}_{v\beta}^{p} \tag{5.23}$$

where ε_{vLC}^{p} is the plastic volumetric strain induced by the macrostructural behaviour, obtained from the BBM model.

5.3.2.2 Thermo-hydro-mechanical numerical simulation

A set of thermo-hydro-mechanical (THM) simulations were also performed using the same geometry, boundary conditions and TH parameters as considered previously. Now the stress equilibrium equation and the mechanical terms were considered in the analyses.

Initial thermal and hydraulic conditions are equals to those used in TH analyses. The cold isostatic pressing (CIP) procedure guarantees homogeneity of the sample. However, during the mounting process, a small vertical stress was applied on the upper piston to close the cell. Therefore some initial stresses were transferred to the sample, which are more evident in the axial than in the radial direction [Figure 5.4(a)]. This situation may have a small influence on the absolute stress values obtained in the

test, but not on the trend observed in the experimental results. Because the main objective of this study was to simulate the general path observed in the test, and because it is common practice to consider an initial isotropic stress state in this kind of simulation, it was decided to adopt an initial isotropic stress value of 0.2 MPa (average value between those initially recorded in the experiment) for the axial and radial directions.

The initial void ratio values assumed for the micro and macrostructure were 0.460 and 0.199, respectively. These values were deduced from experimental data of porosity distribution on MX-80 bentonite samples compacted at a similar dry density and water content (Delage et al., 2006). The porosities were determined applying the reasoning used by Lloret et al. (2003) when analysing the structure of compacted samples of a Ca-bentonite (FEBEX bentonite).

Parameters that define the thermal and hydraulic behaviour are those indicated in Table 5.2 and Table 5.3. Mechanical parameters have been obtained from the interpretation of experiments performed on MX-80 bentonite samples and reported in the literature (Villar, 2005; Tang et al., 2008). The interaction functions are similar to those adopted in previous analyses to simulate the response of expansive clay (Lloret et al., 2003). Table 5.4 presents the parameters used to define the macrostructural behaviour, and Table 5.5 indicates those corresponding to the microstructural behaviour. An initial value of p_0^* equal to 13.0 MPa was considered (Villar, 2005).

κ_p	0.018	λ_0	0.25
r	0.75	β	0.10
p_r (MPa)	0.5	κ_s	0.001
α_0 (°C^{-1})	-1.0x10^{-4}	a_1 [MPa·(C°)$^{-1}$]	-1.0x10^{-4}

Table 5.4. Parameters for the mechanical model (macrostructural behaviour).

α_m (MPa^{-1})	1.8x10^{-2}	β_m (MPa^{-1})	1.8x10^{-3}
Interaction functions			
$f_c = 1.1 + 0.9\tanh[10(p/p_0 - 0.45)]$		$f_s = 0.9 - 1.1\tanh[10(p/p_0 - 0.45)]$	

Table 5.5. Parameters for the mechanical model (microstructural behaviour).

Figure 5.11(a) presents the vapour pressure results. As in the test, that variable increases as the temperature gradient between both ends is applied. At day 30, when

the gas boundary condition at the hot end is changed, the vapour pressure values begin to decrease. It is important to emphasise that these results are obtained as a consequence of the boundary condition applied. The comparison of this figure with measurements plotted in Figure 5.6(a) suggests that the main trends are well reproduced.

Figure 5.11(b) presents the relative humidity distribution within the sample. As before, the experimental tendency [Figure 5.3(a)] is well captured, although differences between the measured and calculated values are evident in some sensors, in particular during the phase of application of the temperature gradient.
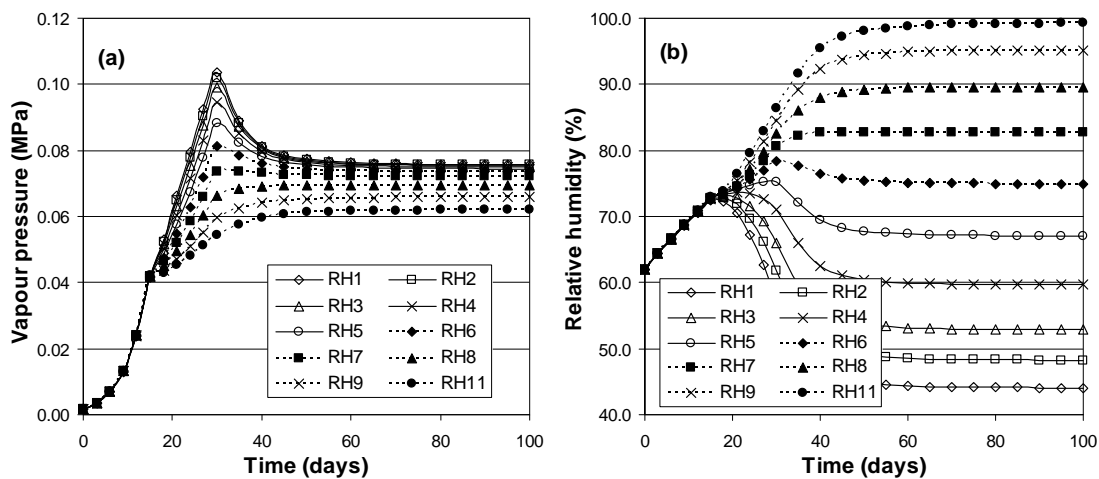

Figure 5.11. (a) Vapour pressure evolution and (b) suction evolution in the sample.

Although not shown, the computed water mass balance between the initial value and that corresponding to different times indicates that the water mass is almost constant during the calculation. That is, the water vapour lost during the test through the hot boundary is very small. This result is in agreement with the experimental finding described by Gatabin & Guillot (2006).

The calculated temperature distribution along the sample and that obtained from the experiment after 100 days are presented in Figure 5.12(a). The temperatures measured by thermocouples (T sensors) and RH sensors were generally in agreement. The linear temperature distribution, specified by the target values of the heating cables, was also evident from the thermocouple readings.

Figure 5.12(b) shows the distribution of the degree of saturation at steady-state conditions, which captures the experimental tendency quite well. Experimental degrees

of saturation were obtained after dismantling the test. The water redistribution was significant, and changed from an initial degree of saturation of 58 % to the final values, which ranged between 36 % and 77 %.
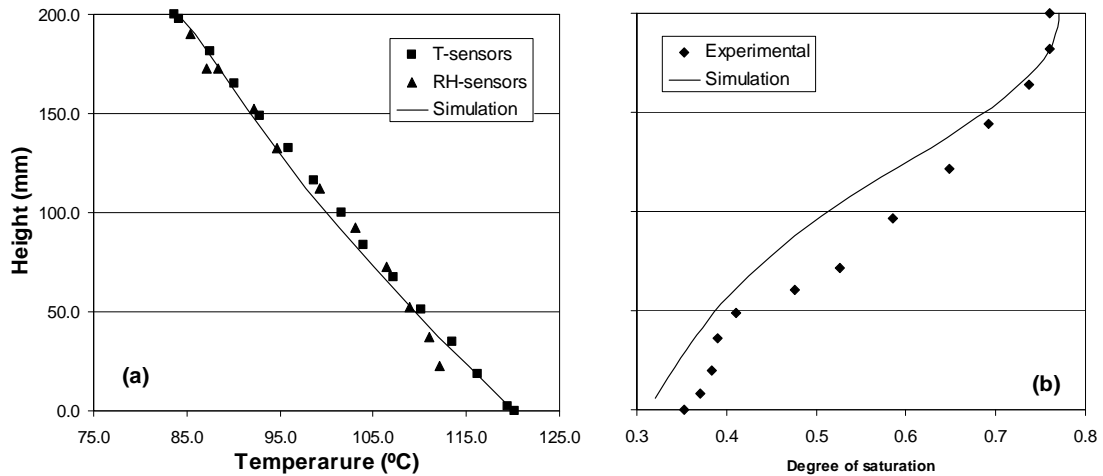

Figure 5.12. Distribution of (a) temperature and (b) degree of saturation along the sample at steady state conditions. T-sensors and RH-sensors are values from the experiment.

Figures 5.13(a) and 5.13(b) compare, respectively, the measured (continuous lines) and computed (dashed lines) axial and radial stresses.

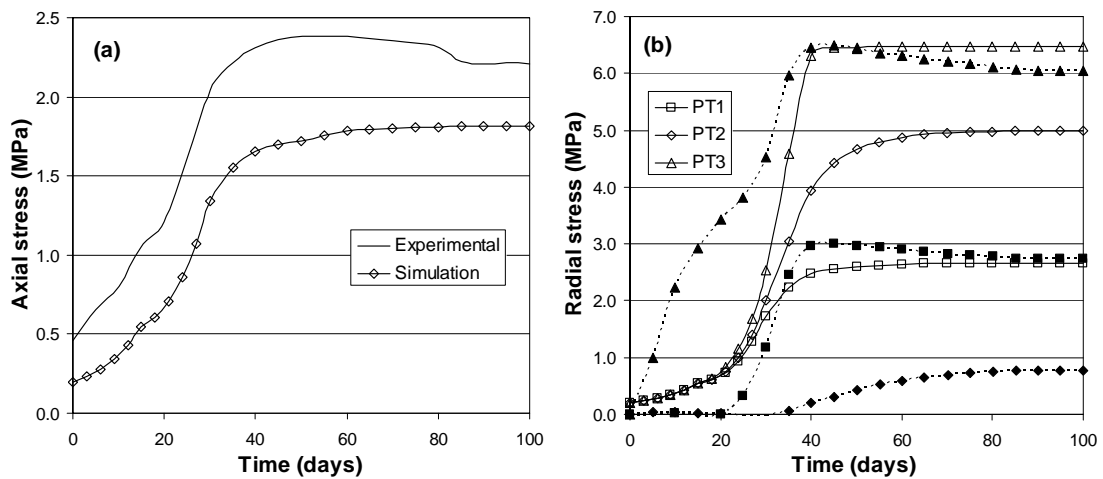**Figure 5.13. (a) Evolution of the axial stress at the top of the sample. (b) Evolution of the radial stress at different positions along the sample; filled symbols represent experimental values and empty symbols are results from the simulation.**

A reasonably good result is obtained in all sensors, considering the difficulties when predicting stresses in high expansive clays. It is thought that a problem could have

affected the registered values in the mid radial sensor (Gatabin & Guillot, 2006). However, the predicted result for this sensor is in fact a reasonable value when compared with other measurements, and when the experimental values of dry density and water content for that position are considered.

In Figure 5.14(a) the porosity distribution obtained after dismantling the sample is compared with that resulting from the calculation. Some differences can be seen between the experimental porosity values and those resulting from the simulation in the upper part of the sample (cold side). However, measured values close to that end may have been affected by the handling of the sample when dismantling the test (Gatabin & Guillot, 2006).

Figure 5.14(b) presents the porosity distribution for each structure (macro and micro) considered in the mechanical model at different times. As can be seen, the application of the homogeneous thermal ramping produces a microstructural swelling and a corresponding shrinkage at macrostructural level. As the test progresses, micro- and macroporosity increments are observed at the cold side, while at the hot side the porosity reduction is associated with shrinkage at both structural levels. However, there is a zone where the microporosity increases and the macroporosity decreases.
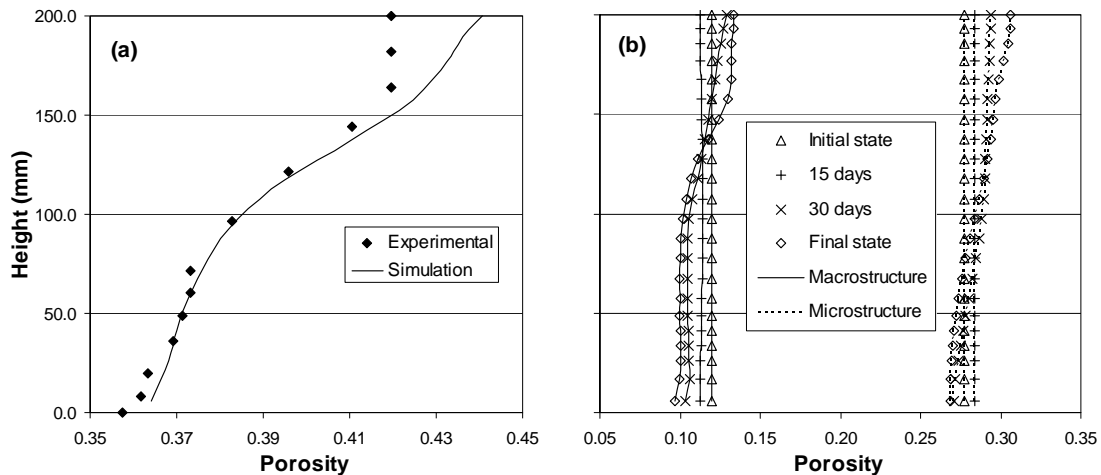
Figure 5.14. (a) Porosity distribution along the sample. Experimental values were obtained after sample dismantling. (b) Initial and final porosity distribution in the macro and microstructure (calculated values).

Figure 5.15(a) presents the values of the interaction functions at different positions within the sample, and Figure 5.15(b) describes the generalised stress paths at the same positions in the net mean stress - suction plane.

At a point close to the cold side (height of 177 mm), changes in the microstructural effective mean stress induce swelling in the microstructure. At the same time, because of the coupling between the micro- and macrostructure, that microstructural expansion induces a plastic deformation of the macrostructure. That coupling is considered through the interaction function f_s, and the path followed in this case is indicated by circles in Figure 5.15(a). As the values of the interaction function are positive, then the macrostructural deformation due to the microstructural deformation will be an expansion. This situation corresponds to the porosity increase observed in the upper part of the sample [Figure 5.14(a)].

The generalised stress path of a point close to the bottom of the sample [square symbols in Figure 5.15(b)] results in a compression of the microstructure. The interaction function f_c adopts positive values, and consequently shrinkage at the macrostructural level results, as a consequence of the coupling between both structural levels. This case represents the response of a point at the hot side where the porosity reduces [Figure 5.14(a)].
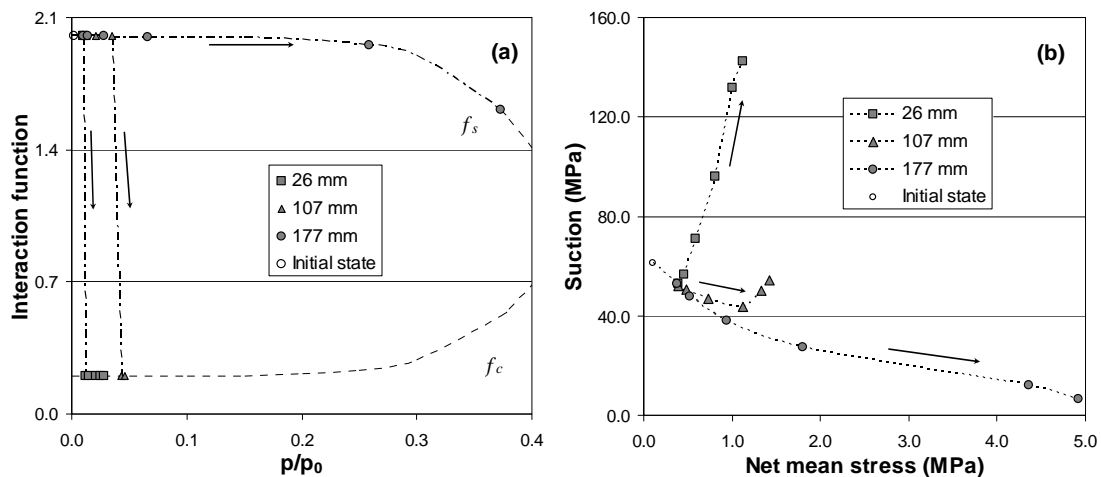

Figure 5.15. (a) Values of the interaction function at some points within the sample. Interaction functions are indicated in dashed lines. (b) Stress-suction paths at some points of the sample. Labels refer to heights with respect to the bottom of the sample.

Finally, the response of a point at mid height of the sample (triangles) is presented in Figure 5.15 as well. The generalised stress path induces a microstructural swelling deformation until day 30, and then a compression of the microstructure. These changes induce corresponding deformations at the macrostructural level as the interaction functions, f_s and f_c respectively, are positive. However, Figure 5.14(b)

indicates that the macroporosity at that level always reduces. This suggests that the changes due to the porosity redistribution along the sample are larger than those due to the coupling between both structures.

5.4 Concluding remarks

The TBT_3 mock-up test was a laboratory experiment carried out to investigate the initial thermo-hydro-mechanical (THM) evolution in a clay barrier. A cylindrical rigid cell was equipped with heaters for temperature control at the two circular faces of a contained bentonite specimen. The specimen was made of MX-80 bentonite powder conditioned to a water content of 13.3 % and isotropically compacted to an average dry density of 1.70 Mg/m^3. The cell was densely instrumented with sensors for measurement of temperature, relative humidity, pore pressure, radial stress and the axial stress. The thermal protocol was divided in three phases and the experiment was run for 102 days. After switching off the heaters, the experiment was dismantled and bentonite samples were finally recovered and analysed for water content and bulk density.

The Chapter describes the behaviour of a compacted sample of unsaturated expansive clay (MX-80 bentonite) when subjected to a thermal gradient under confined conditions in the context of engineered barriers for radioactive waste emplacement. The laboratory experiment and the corresponding numerical simulation of the thermo-hydro-mechanical (THM) processes involved are presented. Because of the complex interaction between the thermal problem, the water redistribution (in liquid and vapour form) and the stress - strain behaviour, these physical processes are highly coupled.

With respect to previous studies, the work presents a laboratory experiment that was densely instrumented, and in which temperatures above 100 ºC were involved. Most of the previous publications refer to simpler laboratory experiments, and to lower temperatures. The use of high temperatures in these types of test implies enhancement of the gas mobility, and it also requires changing some of the usual laws that were obtained for temperatures below 100 ºC. In particular, the soil water retention curve is clearly affected by temperature, as observed when measuring suctions and water content in the sample at the end of the test. The retention capacity decreases with temperature.

Numerical simulations were performed using a finite element code that solves the governing equations corresponding to THM coupled problems. Generally, the TH

results were able to reproduce the tendency of the variables measured during the experiment: temperatures and relative humidities. Additionally, the computations indicated that vapour diffusion was the predominant flux during the transient phase of the experiment. The Barcelona Expansive Model was considered as a constitutive law appropriate for simulation of the mechanical behaviour of bentonites, because it accounts for the double structure that can be found in compacted samples of this material (micro- and macrostructure). The model previously implemented in the finite element code allowed the experiment to be simulated, and reproduced the measured stresses reasonably well. The cold side of the sample showed a swelling behaviour, whereas the hot side experienced shrinkage. Measurements of porosity along the sample at the end of the test were also in good agreement with the predictions of the model. The analysis suggests that both micro- and macrostructure deform in the same manner at both ends. However, in the central part of the sample the microstructure expands, whereas the porosity of the macrostructure reduces.

The good agreement between numerical simulations and measurements indicates that the main THM mechanisms involved in the behaviour of compacted bentonite under thermal gradients have been taken into account. In particular, this analysis presents: (a) the use of the Barcelona Expansive Model for MX-80 bentonite, including the estimation of its parameters; (b) the analysis of the diffusive flow term and the parameters involved at high temperatures; (c) the use of a non-conventional retention curve for MX-80 at high temperature. These developments may be useful for future analyses in this field.

Chapter 6

Description, analysis and interpretation of the in situ Temperature Buffer Test

Summary

This Chapter describes the performance, observations and interpretation of the Temperature Buffer Test (TBT), a full-scale field experiment carried out at the Äspö Hard Rock Laboratory in Sweden, simulating repository conditions for high level radioactive waste. In the experiment, two individually powered heaters are emplaced vertically on top of each other in a pit excavated in crystalline rock and simulate the heat production of radioactive waste. The test is run at high temperatures and with controlled hydraulic boundary conditions. An extensive instrumentation of the test gives information about the thermo-hydro-mechanical (THM) behaviour of the near-field region constituted by the compacted bentonite barrier surrounding the heater and the immediately adjacent rock. The performance and analysis of the in situ test have significantly enhanced the understanding of a complex THM problem. Interpretation of experimental results is assisted by the performance of a coupled numerical analysis based on a formulation that incorporates the relevant THM phenomena. Special attention is paid to the progress of hydration in the barrier, to the effects of heating and vapour transport, and to the development of swelling pressures in the barrier. The analysis has proven the capability of the numerical formulation to provide adequate predictive capacity.

6.1 Preface

ANDRA (French National Agency for Radioactive Waste Management) and SKB (Swedish Nuclear Fuel and Waste Management Co) are performing the Temperature Buffer Test (TBT) in granitic rock at the Äspö Hard Rock Laboratory, Sweden. The overall objective of the project is to investigate how well the bentonite buffer can endure the high temperatures expected to be found around vitrified waste canisters.

The Äspö Hard Rock Laboratory is located near Oskarshamn and was built by SKB (Figure 6.1). The underground portion reaches a depth of 460 m and the total length of the tunnel is 3.600 m. Above ground, there is a research village with offices, lift and ventilation buildings. The research works at Äspö enable to develop and test all the processes involved in a final repository on a full scale and in a realistic environment.

Figure 6.1. General layout of the Äspö Hard Rock Laboratory (http://www.skb.se).

TBT simulates a full-scale KBS-3V method for deposition of high level radioactive waste (where KBS stands for Nuclear Fuel Safety in Swedish and V for vertical). The spent nuclear fuel is encapsulated in copper. The canisters will then be deposited in a deep repository consisting of a system of horizontal tunnels in the bedrock. The tunnels will be about 250 m long and spaced at a distance of about 40 m from each other. On the floor of the tunnels, deposition holes will be built at intervals of about 6 m. The copper canisters will be deposited in the deposition holes and surrounded by a buffer of bentonite. When deposition is finished, the tunnels and shafts will be sealed.

The present Chapter describes the performance, analysis and interpretation of the in situ Temperature Buffer Test, a full-scale heating test carried out at the Äspö Hard Rock Laboratory. In the first part of the Chapter, the main features of the test are described. After that, determination of material parameters and main aspects of the numerical model are presented. The Chapter continues with the simultaneous presentation of some selected observations, and the associated predictions of the numerical analysis. The comparison between predictions and observations provides a firm basis for the interpretation of the test.

6.2 Description of the in situ test

A layout of the TBT is shown in Figure 6.2 while a drawing of the experiment set up is provided in Figure 6.3. In this experiment two electrical heaters (upper and lower) of about 0.6 m diameter and 3.0 m long simulate the power generated by the radioactive waste. They are deposited in a hole of about 1.8 m diameter and with bentonite blocks as buffer material in the annular space between the heaters and the rock wall. Two possibilities for the disposal of vitrified waste are evaluated in the experiment. In the upper part a composite barrier with a sand shield between the heater and the bentonite buffer is considered, while in the lower part the traditional configuration of bentonite buffer between the heater and the rock is evaluated. The sand shield will reduce the temperature to which the bentonite will be exposed. Without this shield, the bentonite will be exposed to temperatures well over 100 °C. Finally, a retaining plug was built at the top of the hole to give confinement to the overall system.

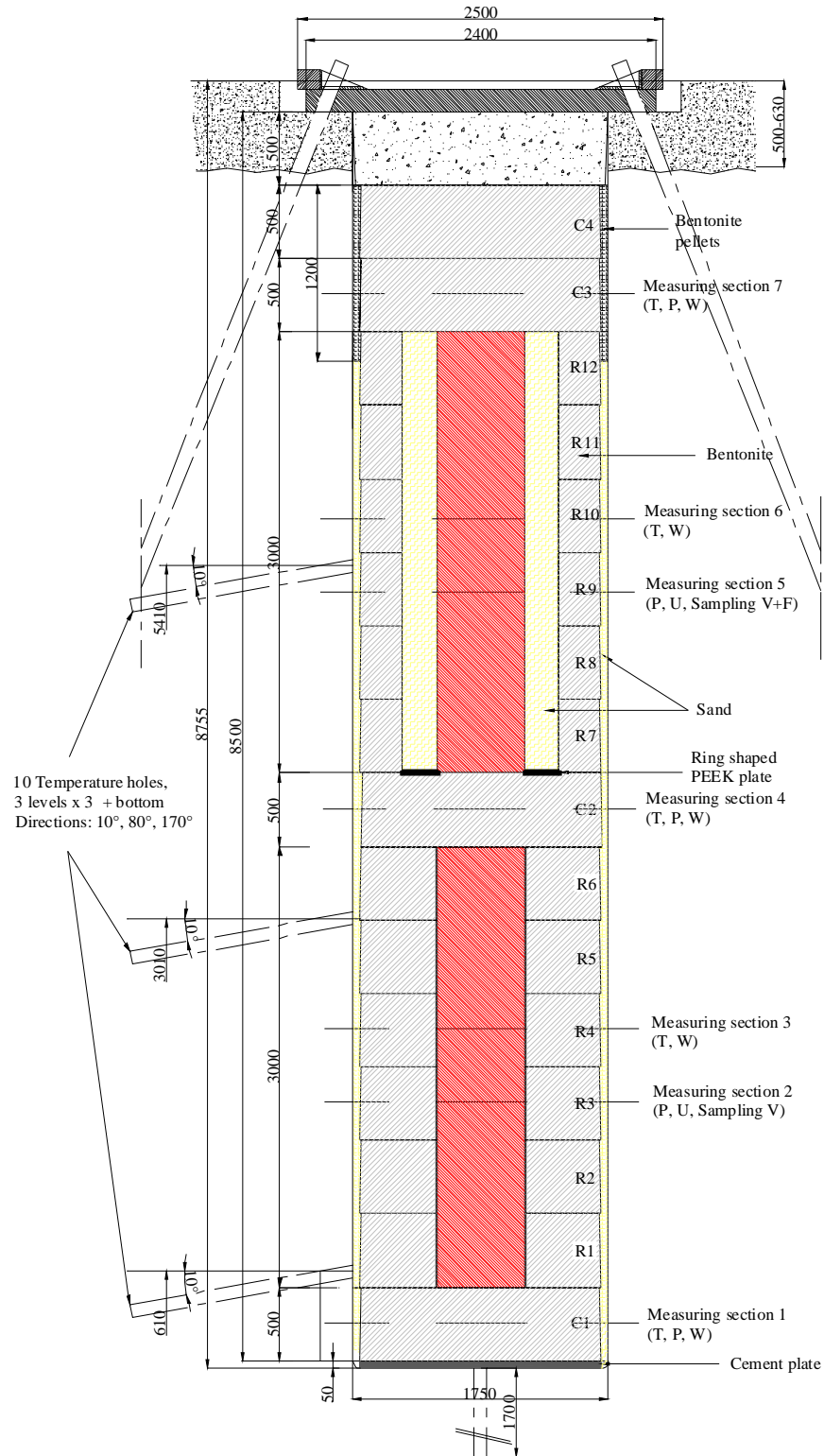**Figure 6.2. Principle design of the Temperature Buffer Test (SKB, 2005).**

Figure 6.3. Experimental set up of the Temperature Buffer Test (SKB, 2005).

The power output of the two heaters was dimensioned to evaluate the effects of a realistic thermal shock. A target temperature of about 100 ºC at 0.5 m radius has been specified for the experiment. To guarantee that a high saturation level will be reached in all parts, water was injected to the system using the slot between the bentonite blocks and the rock, which is filled with compacted sand that functions as a filter.

A complete set of experimental results is presented in a series of specific sensor data reports (Goudarzi et al., 2005, 2006, 2007, 2008). The experiment includes an extensive instrumentation to monitor temperatures, total pressures, pore pressures and relative humidity in different sections within the enginering barrier (Figure 6.3). Temperature is also measured in the rock and on the internal and external surface of the heaters. Forces and displacements of the plug are monitored as well as the water inflow and water pressure in the outer sand.

The heat generation started in March 2003 and the test has been running up to August 2009. The initially constant power of 900 W applied to both canister was raised to 1500 W during the first 15 days. After 1175 days, a power increase of 100 W was applied to compensate the loss of the thermal load due to the dismantling of the Canister Retrieval Test (CRT). To evaluate, after dismantling, possible changes in the structure of the bentonite when exposed to very high temperatures, the power in the lower heater was increased from 1600 to 2000 W after 1695 days. At the same time, the power output from the upper heater was decreased from 1600 to 1000 W. In both heaters, changes were made in steps of 100 W once a week.

The sand filter was filled through four tubes ending at the bottom of the outer sand during 377 days after the test started. The liquid pressure in the main injection tube as well as the water inflow was registered. Water began to flow through tubes connecting the uppermost parts of the sand filter with the atmosphere after about 80 days, although the outflow stopped rather early. It was necessary to apply a considerable pressure to inject water into the sand filter, while it was expected that the permeable sand should get saturated at a low (atmospheric) pressure and that it would be necessary to restrict the water supply in order to control the filling rate. The pressure in the injection system was measured but it was not effective continuously, but dropped to zero in periods during the first part of the test. This suggested that the water pressure in the sand filter was low (approximately atmospheric) and fairly uniform along the height of the column during that period.

Initially, it was not clear the origin of this flow resistance. However, the analysis of experimental results suggested that the clogging of the filters at the tips of the inflow pipes just above the bottom of the sand filter was the more probable cause of this problem. Because of that, from April 2004, water was also supplied through the tubes located in the upper parts of the sand filter. After about 1000 days, injection was also started at two pipes located between C3 and C4 (Goudarzi et al., 2005).

Relative humidity was determined using Wescor psychrometers and capacitive transducer manufactured by Vaisala and Rotronic. Geokom vibrating-wire transducers were installed to measure positive pore water pressures and total stresses. Temperatures were monitored by use of thermocouples within the enginnering barrier, at different heights and radii in the rock, and on the internal and external surfaces of the heaters. Temperature readings were also provided by the capacity relative humidity sensors, psychrometers, and the pressure cells with vibrating-wire transducers.

In addition to the in situ test, the TBT project also included some associated laboratory tests performed at CIEMAT (Research Centre for Energy, Environment and Technology) and CEA (French Atomic Energy Commission). Two mock-up tests were implemented at CEA to further investigate the role of temperature gradients and temperature levels on the phenomena of bentonite desaturation in thermo-hydro-mechanical problems (Gatabin & Billaud, 2005; Gatabin & Guillot, 2006). The aim of these experiments was to study the mechanisms of water redistribution occurring in a bentonite buffer as a consequence of an initial thermal load, with a view to get complementary data to those collected during the field test but in controlled conditions.

CIEMAT has performed different laboratory works to complement experimental data available on the MX-80 bentonite behaviour. Experimental results obtained in those works have been used to define parameters of the constitutive laws that characterize the bentonite behaviour in the numerical simulations. A detailed description of the tests carried out within the framework of the TBT project can be found in a series of documents published by CIEMAT (Villar, 2005; Villar et al., 2005, 2006; Villar & Gómez-Espina, 2007).

6.3 Description of the analysis

It is expected that a significant number of coupled THM processes will ocurr in the near field of a real high level radioactive waste repository. As a consequence, a THM formulation that incorporates the main features of this behaviour will be required to

solve this kind of problems. Olivella et al. (1994) describe a formulation which has been discretised in space (finite elements) and time (finite differences) in order to be used for numerical analysis. It constitutes the bases of the computer program CODE_BRIGHT (Olivella et al., 1996), which has been used to perform the analyses reported below.

In the context of the TBT project, an attempt was made to carry out a gas test in the upper part of the field experiment. Finally, that option was abandoned because the system was not tight. As a necessary and preliminary task, after 1505 days water started to be injected in the sand shield to guarantee full saturation of the barrier at that level. The applied protocol and experimental results suggest that considerable disturbance of prevailing conditions could have ocurred in the upper part of the field test during this operation. Due to this situation and because the main objective of this Chapter is to validate the applied formulation and the constitutive laws adopted for the materials, only 1500 days from the instant of switching the heaters on were considered in the numerical simulation.

6.3.1 Material parameters

Many materials take part in TBT and to perform analyses of the coupled processes that develop in this kind of problem, it is necessary to adopt specific constitutive laws that define the thermal, hydraulic and mechanical behaviour of those materials. As a consequence, a large number of parameters have to be determined. In this section a compilation of the experimental information used to define most of the material parameters is given.

Rock

Äspö diorite, Småland granite, greenstone and fine-grained granite make up most of the rock mass in Äspö Hard Rock Laboratory (Andersson & Johansson, 2002). The hole used to implement TBT was bored at a depth of 420 m and it has been bored in Äspö diorite with veins of fine-grained granite and minor veins of greenstone. After boring no water inflow into the deposition hole was measured. The magnitude of the major horizontal stress is approximately 25 MPa at 450 m depth. The magnitudes of the minor horizontal stress and the vertical stress at this level are 10 and 12 MPa, respectively. Young's modulus and Poisson's ratio for Äspö diorite are around 50 GPa and 0.27 respectively (Andersson & Johansson, 2002).

The rock heat conductivity specified in the predictive modeling program (Åkesson, 2006) was 2.6 W/(m·K) while the heat capacity was 800.0 J/(kg·K).

Johansson et al. (1998) present results about the porosity distribution of rock samples from Äspö. The Äspö diorite shows heterogeneous and mineral specific porosity distribution. The measured total porosity varies between 0.003 and 0.005, but porosities of 0.03 were observed near large quartz and feldspar mineral crystals. The porosity pattern of fine-grained granite was uniformly distributed although a slight foliation could be observed. The global porosity was low, between 0.002 and 0.003, but values as higher as 0.01 were determined in some points. Autio et al. (2003) determined porosity values of 0.003 and 0.008 for undamaged and damaged Äspö diorite, respectively. The corresponding intrinsic permeability values were 8.4×10^{-20} and 1.0×10^{-18} m^2. Measured hydraulic conductivity was three orders of magnitude higher than the corresponding one to the undisturbed rock in a depth of 3 mm from the wall of a tunnel bored in Äspö granite (Pusch & Liedtke, 2003).

The retention behaviour has not been measured for the host rock, but values previously used by Börgesson & Hernelind (1999) were considered to determine the parameters of the water retention curve adopted in the calculations.

Bentonite

Table 6.1 indicates the water content and bulk density obtained after compaction for the different bentonite blocks used in TBT (Åkesson, 2006). According to the data it was decided to define two kinds of bentonite with different properties; one representing blocks C1 to C4 and R1 to R6, while the other one includes blocks R7 to R12.

Block	Inner diameter (mm)	Outer diameter (mm)	Bulk density (Mg/m^3)	Water content
C1 – C4	-	1580	1.996	0.175
R1 - R6	630	1640	1.994	0.175
R7 - R12	1070	1637	2.064	0.175

Table 6.1. Water content and bulk density of bentonite blocks used in the field test.

The water retention capacity of compacted samples of MX-80 bentonite has been extensively investigated by CIEMAT (Villar, 2005; Villar et al., 2005, 2006; Villar & Gómez-Espina, 2007). Figure 6.4 presents experimental results of water retention capacity obtained on samples compacted at different densities and tested using different methodologies. Parameters that define the water retention curve adopted in the simulations have been determined using these experimental data.
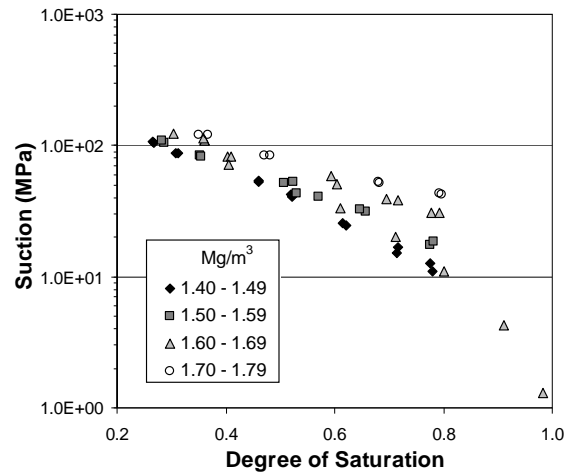
Figure 6.4. Suction as a function of degree of saturation for samples of MX-80 bentonite compacted at different densities.

Figure 6.5 shows experimental values of intrinsic permeability as a function of the sample porosity (Börgesson & Hernelind, 1999; Villar, 2005). As it can be seen there is some scatter between the reported data.
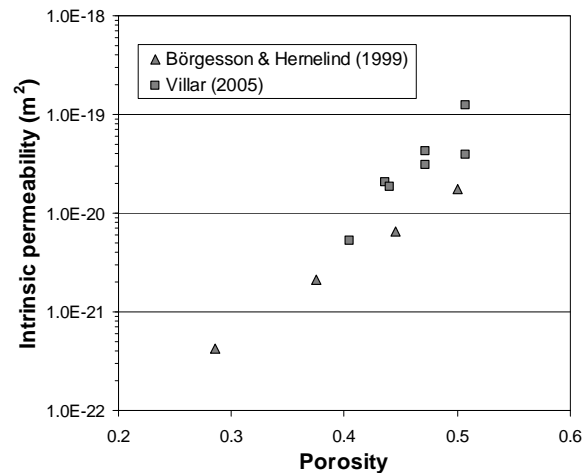

Figure 6.5. Intrinsic permeability as a function of sample porosity.

A compilation of experimental values of heat conductivity for compacted samples of MX-80 bentonite is given in Figure 6.6 (Börgesson et al., 1994; Tang, 2005). Results by Börgesson et al. (1994) have been obtained on saturated MX-80 bentonite samples with different void ratios and in samples with the same void ratio but variable degree of saturation. Knutsson (1983) concluded that heat capacity of compacted samples increases with water content and applied pressure, and reported values between 800.0 and 1050.0 J/(kg·K).
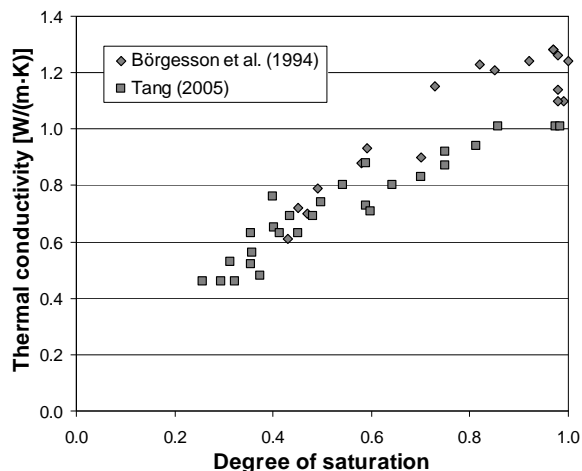
Figure 6.6. Thermal conductivity at different degrees of saturation. Sample void ratio varies between 0.55 and 1.50.

Figure 6.7 presents results of swelling pressure tests of MX-80 bentonite samples compacted at different dry densities (Pusch, 1980; Villar, 2005). As it can be seen the swelling pressure increases as the dry density increases, and values between 6.0 and 10.0 MPa are obtained in the dry density range that is expected to be found in the final state of TBT.

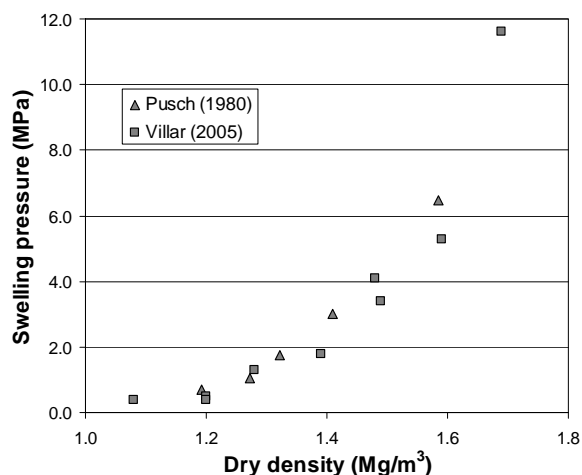**Figure 6.7. Swelling pressure for MX-80 bentonite samples compacted at different dry densities.**

Villar (2005) has done suction controlled oedometer tests on MX-80 bentonite samples compacted at nominal dry densities of 1.69 and 1.79 Mg/m^3. In one case the suction was imposed using the axis translation method while in the other case the relative humidity of the atmosphere in contact with the sample was controlled. Samples

were hydrated at a very low constant vertical load (0.1 MPa), and then this external load was increased by steps. Tang (2005) and Tang et al. (2008) evaluated the effect of changes in suction and temperature on the mechanical response of compacted samples of MX-80 betonites. Using those experimental results, parameters of the mechanical model used in the simulations were determined as indicated in Appendix B.

Sand

Initial water content of the sand was 0.03, while initial target bulk densities were 1.85 and 1.70 Mg/m^3 respectively, for the sand shield and sand filter (Åkesson, 2006).

There is small experimental information about the sand behaviour. As a consequence, values suggested in Åkesson (2006) for different parameters were adopted. The thermal conductivity varies between 0.4 W/(m·K) for the dry state to 1.7 W/(m·K) at saturated state, while a heat capacity of 900.0 J/(kg·K) was assumed.

Pellets

The bentonite pellet filling the upper part of the slot between the bentonite blocks and the rock has an initial water content of 0.1 and a bulk density of 1.20 Mg/m^3 (Åkesson, 2006).

Pusch et al. (2003) present some experimental results about the behaviour of pellets made up of MX-80 bentonite. The swelling pressure of samples prepared using pellets is higher than that corresponding to samples of the same density but prepared from powder clay. The order of magnitude of hydraulic conductivity informed by these authors is 1.0×10^{-12} m/s. Because of that, a value of intrinsic permeability equal to 2.0×10^{-18} m^2 was adopted in the numerical simulations of the TBT.

To the author knowledge, there is not information related to the water retention capacity of compacted samples of MX-80 bentonite pellets. Hoffmann et al. (2007) have determined the water retention capacity of pellet mixtures of FEBEX bentonite compacted at three dry densities. There are also experimental data about the retention capacity of compacted powder samples of the same material (ENRESA, 2000). The comparison of results permits to obtain a relation between the values of the parameters used to define the water retentiton curve for each case. Using a similar relation to that obtained for the FEBEX material, an estimation of the parameters used to define the water retention curve of the pellet mixture of MX-80 bentonite was obtained.

Thermal parameters were assumed equal to those adopted for the bentonite blocks.

6.3.2 Geometry, boundary and initial conditions

Figure 6.8 presents the axisymetic geometry used in the analyses. Boundaries were defined far enough to guarantee that they do not influence the obtained results. All materials used in the experiment have been represented. Although there was a gap between the bentonite and the heater in the lower part of the barrier, the analysis has assumed that, initially, there was contact in that interface.

For the thermal problem, a constant temperature of 20 °C was assumed throughout. Regarding the hydraulic problem, constant liquid pressures of 4.0 and 4.4 MPa were applied on the upper and lower boundaries of the model respectively, while on the right one a lineal variation between those values was assumed. Additionally, the gas equation was always taken into account, considering that some nodes at the top of the sand filter were connected to the atmosphere at the beginning, in order to account for the effect of the open pipes. A fixed gas pressure of 0.1 MPa was considered until day 377 and, after that, a water flux was applied on them. The initial stress field within the rock was assumed uniform and isotropic with a value of 15.0 MPa.

The analysis started simulating the excavation followed by the construction of the bentonite barrier and the insertion of the heater. To represent the bentonite two materials were considered because of the different initial conditions between the block used in the field test. Thus, a dry density of 1.70 Mg/m^3 has been assumed for the clay barrier in correspondence with the upper heater (R7 to R12). For the rest of bentonite a dry density equal to 1.65 Mg/m^3 was used (C1 to C4 and R1 to R6). In accordance with the measurements performed during installation, an average initial water content of 0.15 and a suction of 50 MPa have been assumed for the clay barrier. The water content is lower than that used for block compaction, probably because of some drying during storage and installation. Initial stress in the barrier is assumed isotropic and equal to 0.2 MPa.

Power was applied to the heaters in accordance with the actual test protocol (Table 6.2). The instant of switching the heaters on is taken as time zero.

Time (days)	Power (W)
0 - 8	900
8 - 15	1200
15 - 1175	1500
1175 - 1500	1600

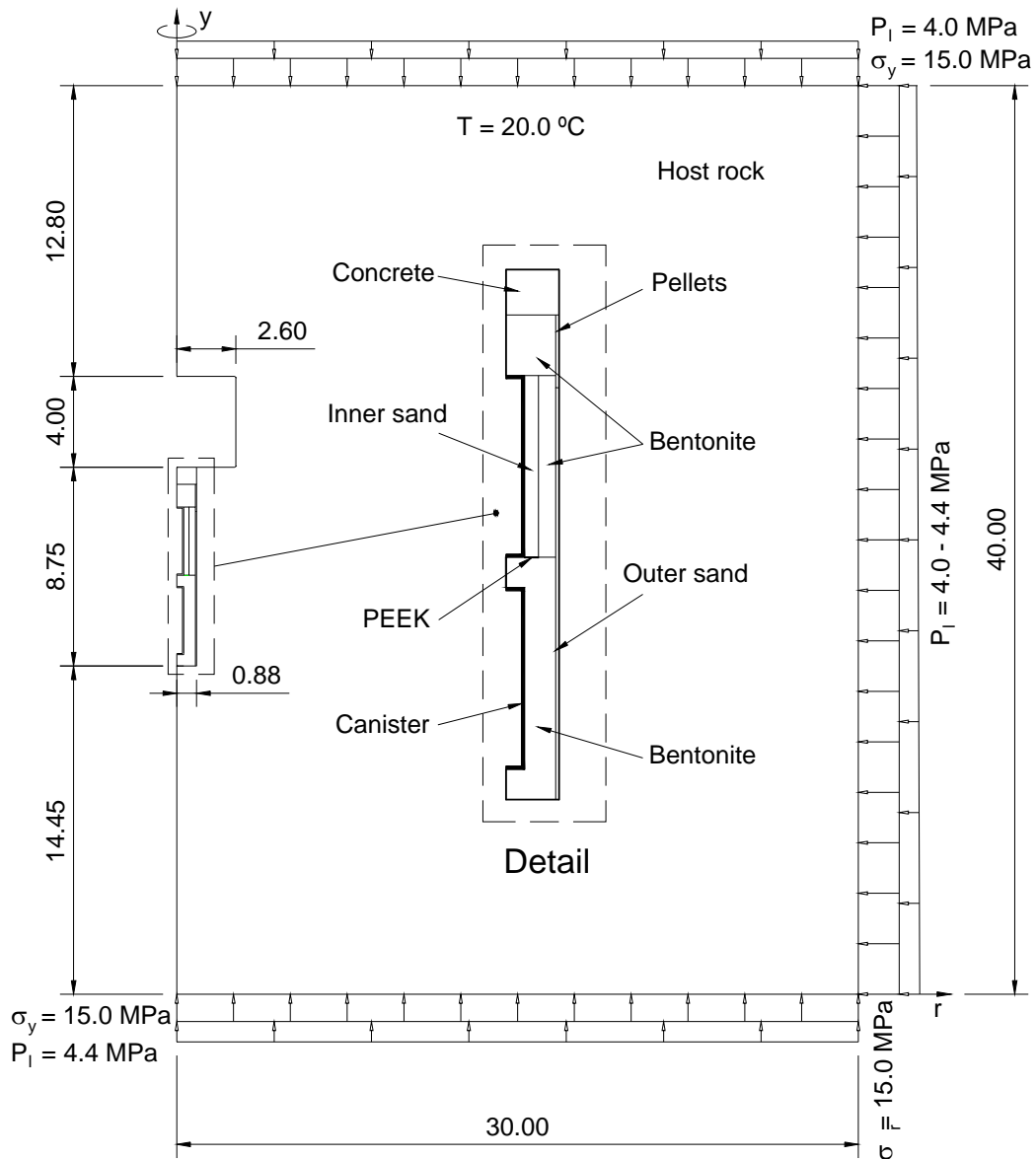**Table 6.2. Power applied on each heater in the field test.**

Figure 6.8. Axisymetric geometry for the analysis of the in situ heating test (dimensions are in meters).

On the outer sand, a water flux was applied as boundary condition. As the total water inflow instead of the inflow on each pipe was registered in the field test some assumptions were made to calculate the liquid flux applied to the nodes of the model. During the first 377 days, the water flux to be applied at the lower part of the outer sand can be well defined. Since then, it was assumed that the water flux is the same in the upper and lower pipes. After 1000 days, the total inflow was divided by the total number of injection pipes and then the water flux was applied in the upper and lower nodes of the outer sand and some nodes between C3 and C4. It is noted that the

actual water inflow distribution can be different from the distribution assumed in the analyses. Figure 6.9 shows the total volume of water injected into the system and the curves of water inflow adopted in the simulation as input data in the nodes at the bottom and top of the sand filter as well as that applied in the zone between C3 and C4 (mats).
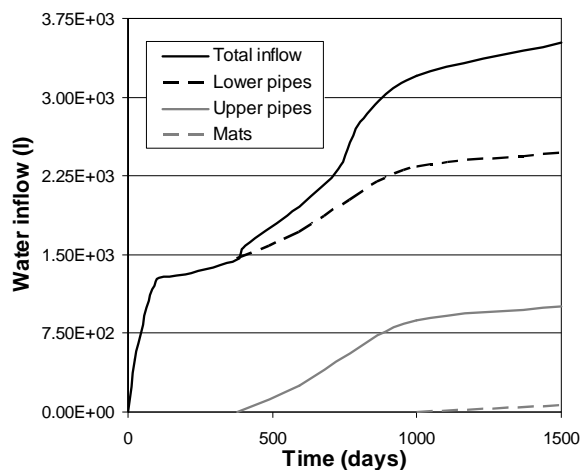

Figure 6.9. Total water injected into the engineered barrier and distribution adopted in the numerical simulation.

A complete list of the initial conditions and material parameters used in the simulation is given in Appendix B.

6.4 Test observations and interpretations

The analysis reported in this paragraph is assumed as the Base Case (BC). It corresponds to the analysis performed using the best information on initial and boundary conditions, and on material parameters at the time when the test started. Therefore the results reported below can be considered as predictions.

Representative test observations concerning the behaviour of the engineered barrier are presented. Predictions of the numerical analysis are plotted alongside the test observations to assess the performance of the model. In the figures, z indicates the vertical distance measured from the bottom of the borehole.

6.4.1 Thermal results

Figure 6.10 shows the evolution of the temperature in various sections of the engineered barrier. In each section, temperatures at different radial distances from the axis of the hole are plotted.

It can be noted that, after the initial stage, temperatures generally are constant throughout the barrier. The small increase in temperature about 1100 days after the heating started is due to the power increase applided to both heaters. The analysis reproduces the observations quite well at the level of the upper heater [Figure 6.10(c)-(d)]. On the other hand, some differences are observed in correspondence with the sensors located at the level of the lower heater.
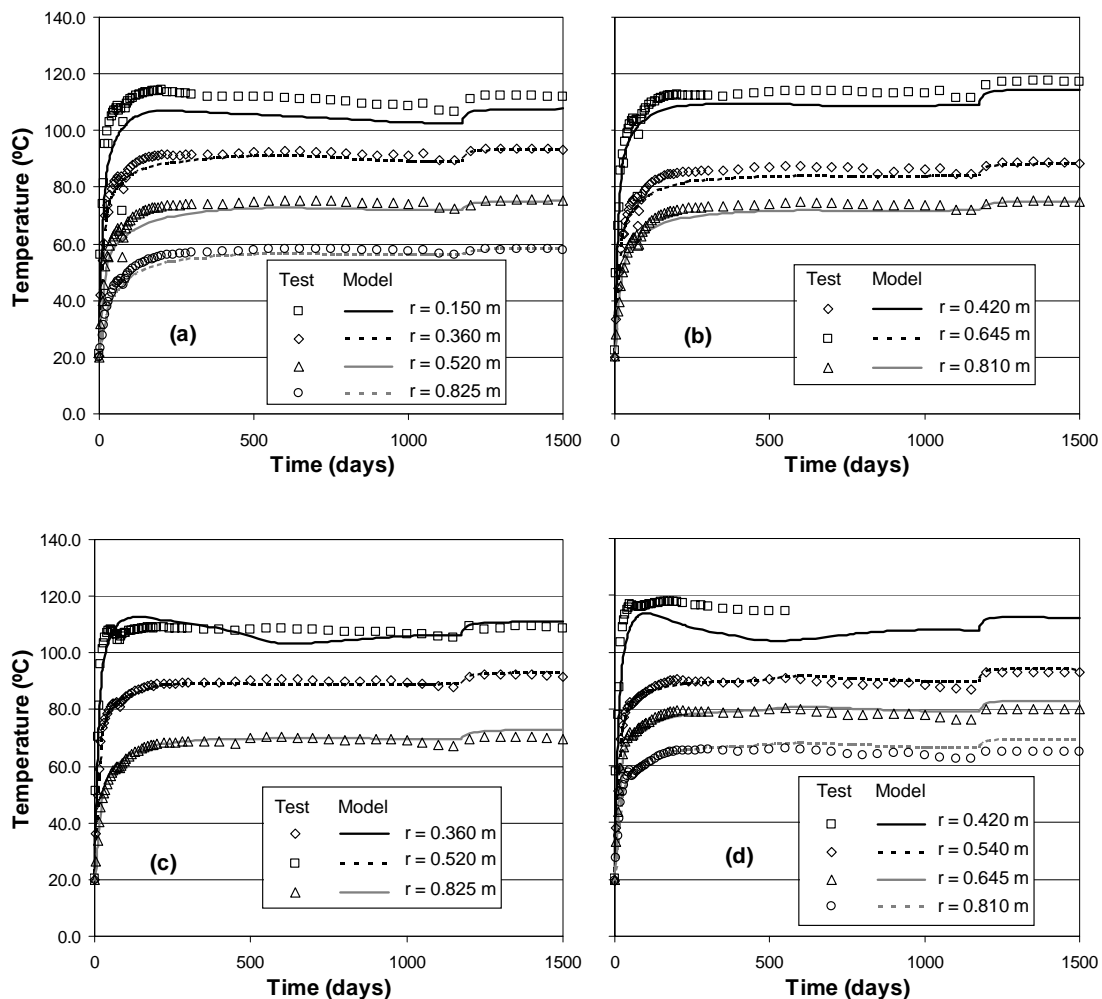

Figure 6.10. Evolution of temperature in bentonite barrier, observations and computed results. Base Case. (a) z = 0.45 m; (b) z = 2.45 m; (c) z = 3.95 m; (d) z = 5.95 m.

To get a complete picture of the near-field behaviour it is interesting to examine the response of the host rock (granite). It is subjected to a lower heat loading and therefore the observed effects are more limited. Figure 6.11 presents the evolution of temperature measured in several sensors installed at different distances form the periphery of the deposition hole and at different heights from the bottom of the borehole.
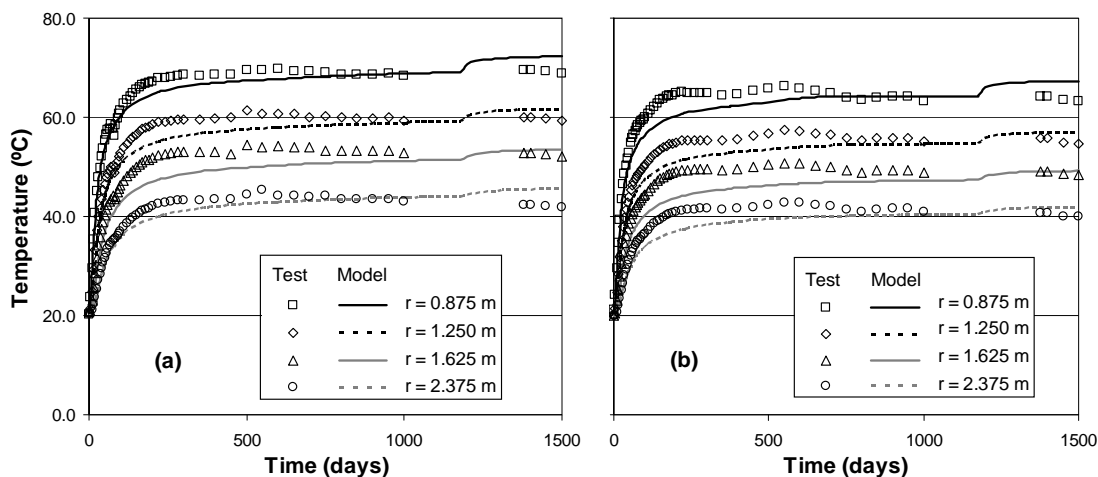
Figure 6.11. Evolution of temperature in granite, observations and computed results. Base Case. (a) z = 3.01 m; (b) z = 5.41 m.

Observed temperature at the level of the lower heater are higher than those corresponding to the level of the upper heater. The values and evolution of the temperatures are well predicted although the model is not able to reprodude the rapid increase of temperature observed at the start of the test.

It is important to note that the Canister Retrieval Test (CRT) was running in the same galery that TBT at the time when the latter was mounted. The CRT was a heating experiment running at 6.0 m distance from the TBT deposition hole. Temperature in the rock around of the TBT hole was monitored in four positions using instruments installed in vertical holes drilled at 0.3 m from the periphery of the TBT hole. Before TBT started, registered temperature was 27 ºC in the sensor facing CRT and about 23 ºC in the others ones. The influence of the CRT was not included in the simulation and therefore, it is though that part of the discrepancies between measured and simulated results can be associated to this simplification.

6.4.2 Hydraulic results

Figure 6.12 shows the variation with time of relative humidity, measured with capacitive sensors, in four sections. Relative humidity is plotted because it is the actual parameter measured by the capacitive transducers. Total suction s is related to relative humidity RH through the psychrometric law [eq. (3.3)].
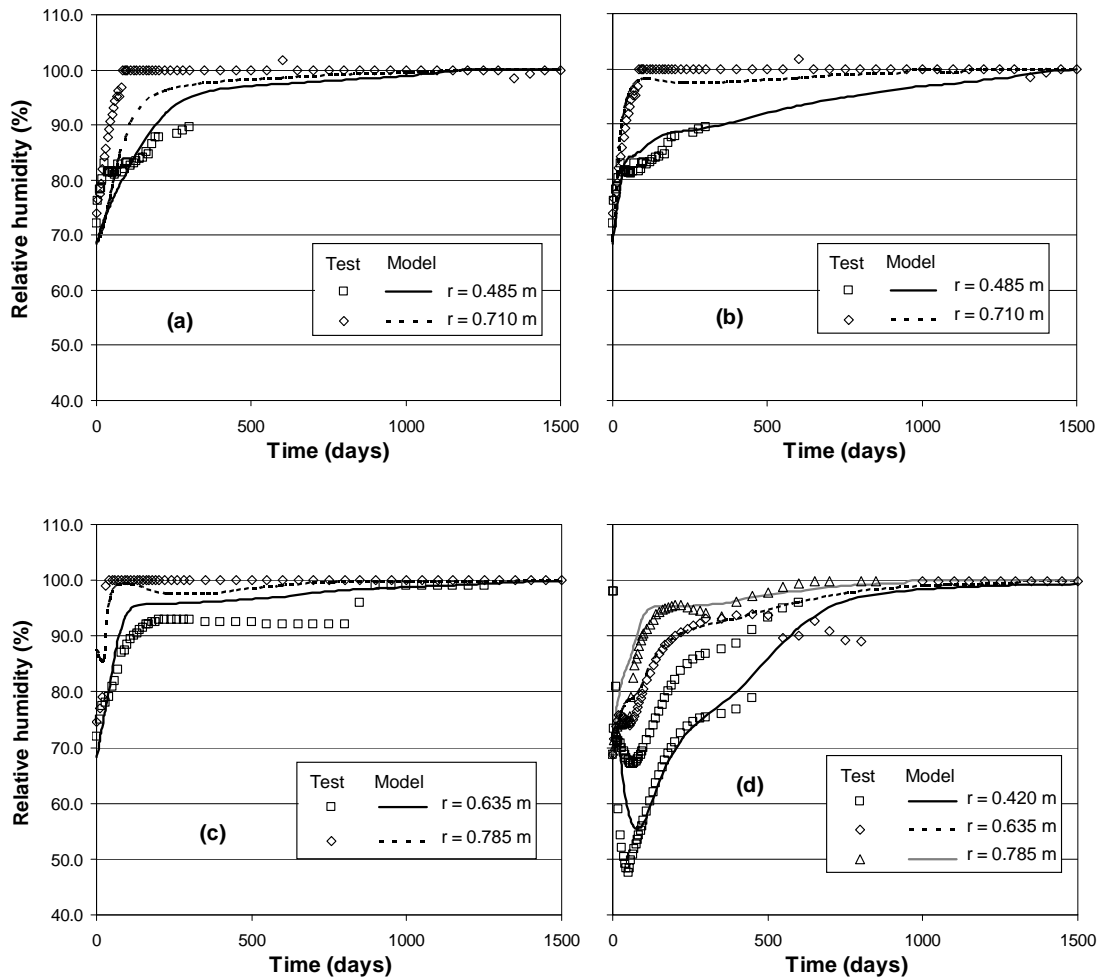
Figure 6.12. Evolution of relative humidity in bentonite barrier, observations and computed results. Base Case. (a) z = 0.25 m; (b) z = 2.25 m; (c) z = 3.75 m; (b) z = 5.25 m and 5.75 m.

In the zone near the rock, and in the middle of the barrier, there is a monotonic increase of relative humidity, reflecting the process of hydration induced principaly by the injection of water through the outer sand and in minor extent by water drawn from the host rock. However, in the region closer to the hole axis it can be observed that

there is first an increase of relative humidity followed immediately by drying; finally, a new increase of relative humidity occurs.

By examination of the numerical analysis results it is possible to identify the processes underlying this behaviour. The first relative humidity increase is due to a vapour front (driven by heating) passing through the observation point. After that, a temperature increase causes evaporation and, therefore, drying of the material. After approximately 100 days general hydration takes over, causing the final gradual increase of relative humidity. A significant part of the early hydration of the middle and outer barrier zones is due to the condensation of vapour coming from the inner region.

Figure 6.13 presents the evolution of degree of saturation at different radii within the bentonite buffer in correspondence with the mid-height of the lower and upper heater.
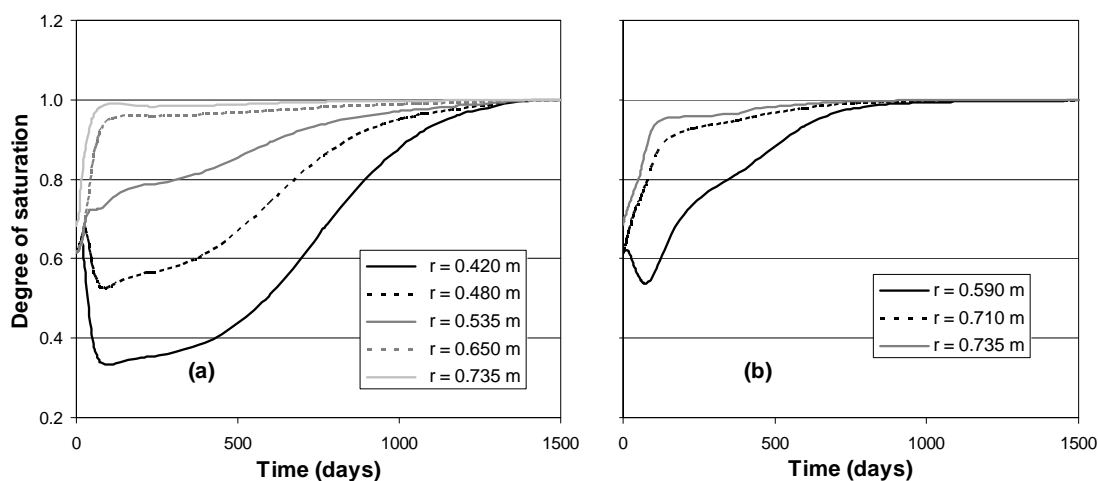
Figure 6.13. Evolution of degree of saturation in bentonite barrier, computed results. Base Case. (a) z = 2.25 m; (b) z = 5.75 m.

As in the case of the relative humidity, in the region closer to the hole axis it can be observed that there is first a small increase of degree of saturation followed immediately by a decrease of this variable; finally, as the hydration proceeds a new increase of degree of saturation occurs. On the contrary, in the zone near the rock and in the middle of the barrier, there is a monotonic increase of the degree of saturation. Results suggest that the bentontie blocks are close to full saturation after 1500 days of heating.

6.4.3 Mechanical results

As Figure 6.14 shows stresses in the barrier increase very significantly during hydration because of the high swelling of the compacted bentonite blocks. At the end of the test, values of the total stresses close to 6-8 MPa were reached.

It is possible that the slower development of the measured swelling stresses, as compared with the predictions from the analysis, may be due, at least in part, to the initial liner/barrier and rock/barrier gaps, not accounted for in the modelling. In any case, the predicted final total stress in the barrier is similar to that measured in several of total stress cells.
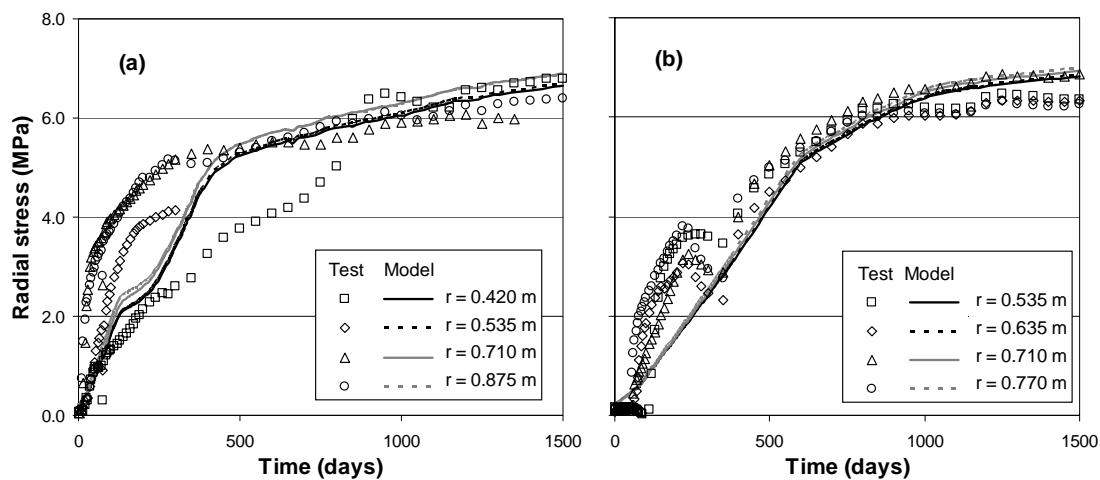
Figure 6.14. Evolution of stress in bentonite barrier, observations and computed results. Base Case. (a) z = 2.25 m; (b) z = 5.75 m.

6.5 Analysis using a different liquid density

In Chapter 4 it was analysed how the interaction between the liquid water retained in the pores of compacted bentonite samples and the smectite affect the density of the water. From a practical point of view, when simulations of coupled processes in engineered barriers are being carried out, this traduces in changes that can be introduced in the law adopted for the density of the liquid as well as in the water retention curve of the bentonite used in the buffer. The objective of the analysis described in this paragraph (Liquid Density Case, LDC) was to evaluate how the concepts developed in Chapter 4 would affect the obtained results in the case of the TBT field experiment.

The density of the liquid water is incorporated into the calculations of coupled processes through the law adopted for this variable. As it was shown in Chapter 4, in the case of engineered barriers made up of bentonites blocks, it would be necessary to consider the influence of the liquid density in the water retention curve defined in terms of degree of saturation. It is also possible that water density in expansive clays depends not only on liquid pressure (suction) but also on sample density. However, until more experimental data become available it is not possibility to quantify the influence of this last variable. Anyhow, it is thought that as a first approximation this effect could be neglected without introducing major error in the final results.

For the simulations the same geometry as shown in Figure 6.8 was used. The law for the liquid density was adopted equal to that deduced in Chapter 4 corresponding to a sample density of 1.60 Mg/m^3. Parameters of the water retention curve are indicated in Table 6.3.

P_0 (MPa)	22.0	m	0.38
P_d (MPa)	1000.0	d	1.0

Table 6.3. Parameters of the water retention curve used in the analysis of LDC.

It is important to note that CODE_BRIGHT assumes the same liquid density law for all the materials included in the model. In the case of TBT most of the external water introduced into the barrier was due to the external water supplied through the outer sand as the permeability of the host rock is very low. Therefore, it can be assumed that the total water coming into the engineered barrier in this example was similar to that of the Base Case (BC).

The initial water content of the bentonite blocks was the same in the BC and in the LDC. The initial water content in the blocks represents 97 % of the initial total water within the barrier. For the other materials that constitute the barrier the same water retention curve and initial conditions are used in both analyses (i.e. the same initial degree of saturation). As a consequence, the initial total water within the barrier is about 2 % higher in LDC than in BC, which is considered sufficiently small to influence the final results.

6.5.1 Thermal results

Figure 6.16 compares experimental and numerical values of temperature at the same locations than those considered in Figure 6.10.
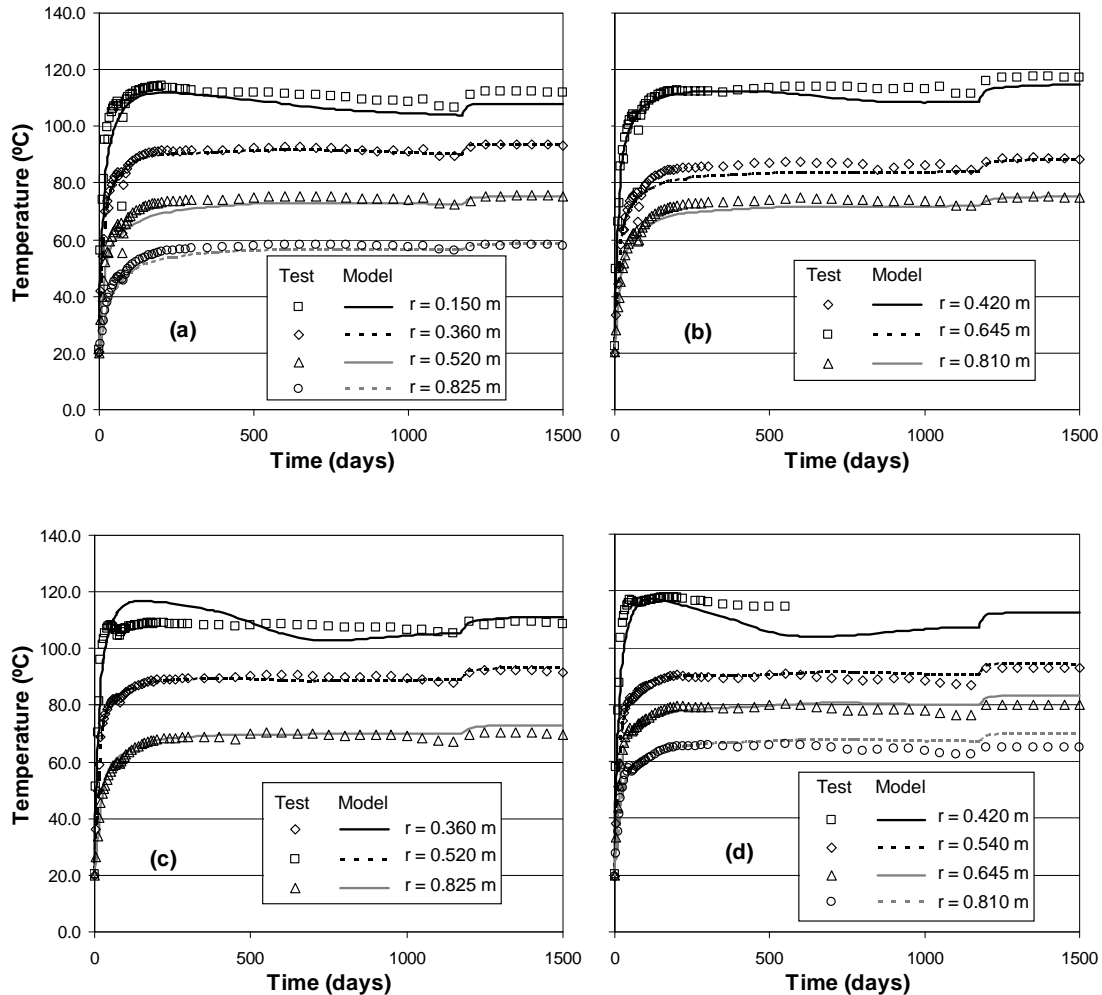
Figure 6.16. Evolution of temperature in bentonite barrier, observations and computed results. Liquid Density Case. (a) z = 0.45 m; (b) z = 2.45 m; (c) z = 3.95 m; (d) z = 5.95 m.

In general, results obtained in this case reproduce the experimental data better than in the BC. As the energy is mainly transported by conduction, the good agreement at different radial distances indicates that the value of thermal conductivity, which depends on the degree of saturation, is well captured.

6.5.2 Hydraulic results

Figure 6.17 correspond to the evolution with time of relative humidity in four sections of the experiment. The general trend is well reproduced in the zone close to the rock and in the middle of the bentonite barrier. However, calculated results suggest that hydration proceeds more slowly in the inner part of the buffer.
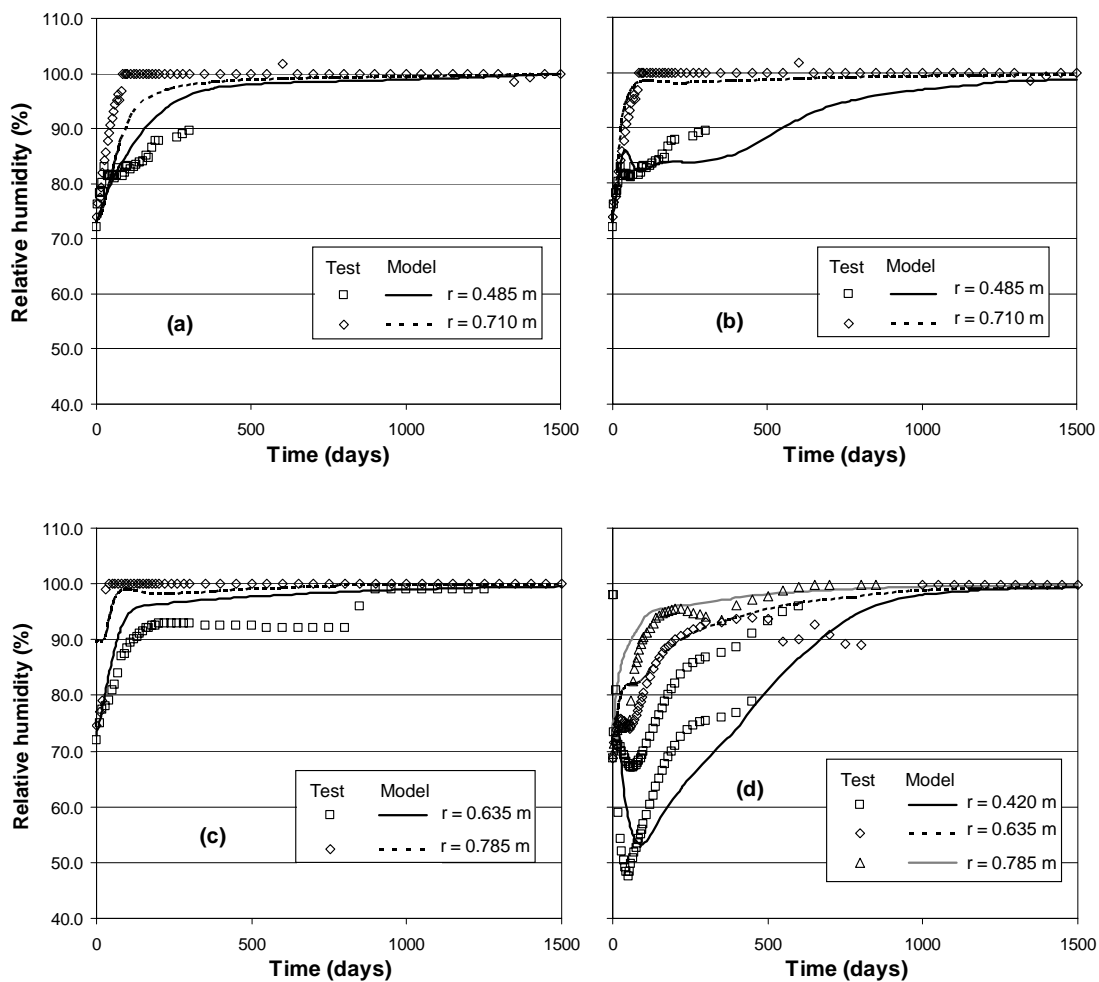
Figure 6.17. Evolution of relative humidity in bentonite barrier, observations and computed results. Liquid Density Case. (a) z = 0.25 m; (b) z = 2.25 m; (c) z = 3.75 m; (b) z = 5.25 m and 5.75 m.

Figure 6.18 presents the computed temperal evolution of degree of saturation at different raddi from the heater axis. Two major differences with respect to the results obtained in the BC can be highlighted. First, as it was already commented, initial values of deggre of saturation are lower in this case as the same initial water content was considered in both analyses. The other difference appears when the degrees of

saturation at a given radius are compared. Results suggest that the time required to get the same hydration level will be higher in the LDC than in the BC. This aspect was already commented in Chapter 4 when a simple case was analysed.
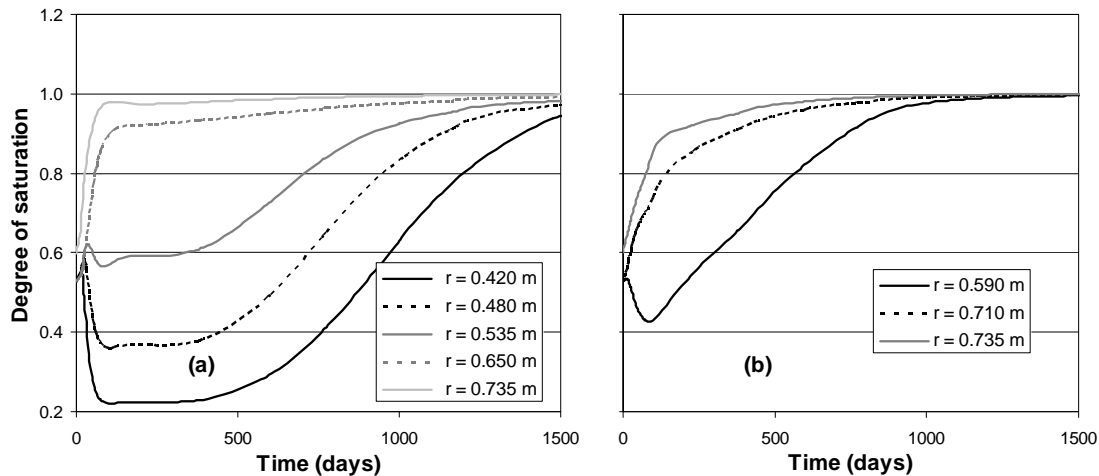
Figure 6.18. Evolution of degree of saturation in bentonite barrier, computed results. Liquid Density Case. (a) z = 2.25 m; (b) z = 5.75 m.

6.6 Concluding remarks

The Temperature Buffer Test is a large-scale in situ heating test performed to simulate the conditions of vitrified high-level radioactive waste disposal in a deep geological repository excavated in granite. Two possibilities for the disposal of vitrified waste are evaluated in the experiment by using heaters that mimic the thermal effects of nuclear waste. In the upper part a composite barrier with a sand shield between the heater and the bentonite buffer is considered, while in the lower part an engineered barrier made up of compacted swelling clay between the heater and the rock is evaluated. The test has provided a large amount of information concerning the thermo-hydro-mechanical behaviour of the bentonite barrier and of the adjacent rock. The progress of hydration, the effects of heating, vapour transport and development of swelling pressures have been identified as the major interacting phenomena underlying the observed patterns of behaviour.

An adequate interpretation of the test could be carried out using an appropriate coupled THM formulation which incorporates the relevant processes involved in the problem under consideration. The general balance equations are complemented by constitutive laws and equilibrium restrictions. Several parameters are required to define

the numerical problem and it has been possible to determine them on the basis of an extensive programme of laboratory tests.

The numerical model designed as Base Case (BC) was developed during the early stages of the test and therefore the model computations largely represent a predictive exercise. The comparison between the results of the numerical analysis and the field observations suggests that the formulation and associated computer code are able to reproduce well the main observed features of the THM behaviour of the test. Indeed, quantitative agreement is very satisfactory for a large number of variables. A good representation of the test was achieved without introducing additional complexities like the explicit consideration of the gaps between blocks and the blocks and the heaters.

The interaction between the water and the expansive clay used in engineered barriers changes some properties of the water retained in the pores. This aspect was considered in the Liquid Density Case (LDC) where a different law for the liquid density and a modified soil water retention curve were used. Numerical results show an improvement in some of the predicted thermo-hydraulic variables. Additionaly, this analysis highlights the increment in the time required to obtain a given level of saturation within the barrier.

Information obtained during the dismantling process will provide further evidence of the predictive capabilities of the numerical model. In this way, confidence in the use of these computational tools for the long-term prediction of THM problems associated with nuclear waste disposal will be significantly enhanced.

Chapter 7

Conclusions and future works

7.1 General conclusions

The main objective of this Thesis was to advance in the understanding of the effect of high temperatures in different aspects of the thermo-hydro-mechanical behaviour of expansive materials. This document has been organized in such a way that the main conclusions are presented in detail at the end of each Chapter. Because of that, in this section only some remarks and the main general conclusions are included.

This Thesis was developed in the framework of the Temperature Buffer Test (TBT) project. This project includes a full-scale field experiment that simulates repository conditions for high level radioactive waste. Deep geological disposal is by far the most likely possibility to be implemented for the safe disposal of high level radioactive waste. The repository is built placing several barriers, both natural and artificial, between the potentially harmful radionuclides and the biosphere. Within the project, laboratory tests were also carried out to evaluate the response of the bentonite selected to build the barrier. The aim of the TBT is to improve the understanding about the influence of high temperatures on different properties of the buffer material that constitutes the engineered barrier.

Bentonite is placed around the waste canister as compacted. Samples of bentonite statically compacted show a fabric where it is possible to consider a double structure defined by the clay aggregates and the pores between them. An aggregate includes several particles and each particle is formed by several silicate sheets. It is commonly assumed that the porosity of aggregates or microporosity is independent of the dry density of the compacted sample. On the other hand, the pores between the aggregates define the macroporosity.

Compacted expansive clay plays an important role in the general performance of the engineered barrier. At the beginning, the main actions that affect the bentonite within the barrier are the heating arising from the canisters and the hydration from the surrounding rock. This material is initially in an unsaturated state and a direct experimental assessment of its unsaturated properties is in general extremely demanding. The soil water retention curve (SWRC), however, has resulted in a practical and sufficient estimation tool from which to derive unsaturated soil property functions. The SWRC defines the constitutive relationship between the amount of water in the soil and its energy status. In Geotechnical Engineering, the suction has been traditionally used as the measure of the water energy in the soil.

Because of the characteristic of the TBT project, the effect of high temperatures on the water retention capacity of expansive soils was one of the aspects to be investigated in this Thesis. As suggested by experimental results, for low and medium values of suction, water retention in soil is also affected by changes in the soil fabric. The density (or void ratio) can be assumed as a first order approximation to the description of the soil fabric. In the context of high waste underground repositories, bentonite within the barrier will be mostly confined. However, porosity redistribution will take place during the hydration process. Therefore, the effect of the sample density on the water retention capacity was also analysed in this work.

The first approximation to analyse the influence of variables like temperature and sample density on the water retention capacity of soil is through the capillary model. This model expresses the water retention capacity as a function of the surface tension of water, the contact angle between the solid and the liquid phases, and the radius of the capillary. Philip & de Vries (1957) postulated that changes in the retention capacity due to temperature variations could be explained by concurrent changes in the surface tension of water. This approximation, however, has systematically failed to explain the experimental results obtained in different kind of soils. As indicated in Chapter 3, various alternatives have been suggested to explain the larger than expected changes in the water retention capacity due to temperature increases. Grant & Salehzadeh (1996) suggested that the temperature also affect the contact angle. By using thermodynamics concepts these authors defined a dependence of that variable on temperature changes. This approximation could be considered as an improvement of that proposed by Philip & de Vries (1957). However, the analyses of experimental results suggest that the contact angle also depends on the water content of soil.

Although very intuitive, the capillary model only explains partially the effect of variables like temperature and density on the water retention capacity of fine-grained soils. However, thermodynamic of interfacial phenomena seems to be a more useful tool to interpret the physical adsorption of water by soils. Two approaches within this framework were presented and their advantages and drawbacks when applied to the analysis of the water adsorption in clays were considered in Chapter 2. In one approach the solid adsorbent is assumed inert and a measure of the free energy of the solid phase is given by the spreading pressure. In the case of deformable solids this energy is called to the surface potential of the solid phase. In both cases, the variables change as the adsorption progress and they represent a quantity similar to the surface tension.

The influence of dry density and temperature on the water retention capacity of compacted samples of MX-80 bentonite has been studied in Chapter 3 of this Thesis. Experimental data reported in the literature (Villar et al., 2006; Villar & Gómez-Espina, 2007) were analysed by using concepts of thermodynamic of adsorption and the approach deduced from the capillary model. Interestingly, both cases resulted formally equal and a direct comparison of the results obtained could be carried out. As it is reported in the literature, results from the capillary model are not able to explain the higher than expected changes in the retention capacity with the temperature. These discrepancies could be explained by using the definition of spreading pressure. By using this concept it is shown that the capillary model represents the energy of adhesion of the water with the surface of the solid particles already covered with a film in equilibrium with the saturated vapor of the liquid. This energy is a very much smaller value than the real adhesion energy between the clean particles of clayey soils and the liquid water. Consequently, part of the mechanisms that define the interaction between the soil particles and the water retained in the porous are not considered.

To incorporate the effect of temperature and porosity in the numerical analysis of coupled thermo-hydro-mechanical processes, an empiric expression which defines the SWRC must be adopted. Parameters in these empirical expressions are determined by fitting experimental data. The inclusion of the temperature and density effects into the equation proposed by van Genuchten (1980) was analysed in Chapter 3. This particular law was adopted because of its applicability to fit experimental results for a wide variety of soils. For this law a direct relationship between parameters in the expression of the SWRC and the thermodynamic variables deduced from thermodynamic of adsorption was obtained.

The interaction between smectite, which is the main mineral of bentonite, and water is complex problem that has been intensely studied during many years. In general, it is assumed that in expansive soils different kinds of water can be identified. Thus, it is possible to distinguish between the water in the macropores, which can be considered as water with physical and chemical properties similar to those of the liquid free water, and the water that exists attracted to the external surfaces of clay minerals or held as interlayer water in the spaces between clay layers. There is not an easy way to separate the different kinds of water that can be identified in a compacted sample of bentonite. This will depend on the amount of water in the soil (degree of saturation) and on the clay minerals, as hydration process depends on the exchangeable cation of the

expansive clay. Because of that, it is not straightforward to define a fixed value for the water density.

From an experimental point of view, different methods are used to determine the water retention capacity of soils. The basis for all of them is that the moisture within the soil is brought to thermodynamic equilibrium with liquid water or a gas at a known reference energy. In many applications, however, it is needed to express these results (i.e. the soil water retention curve) in terms of degree of saturation. This is the case of coupled formulations as that used in this Thesis where balance equations are based on degree of saturation instead of water content as main variable to indicate the moisture content of the porous material. In the case of highly expansive soils, it is systematically observed that, close to saturation (nil suction) the degree of saturation calculated from the water content is bigger than one. This fact suggests that a systematic error is being carried out in this simple calculation. In this Thesis it was assumed that this error comes from the value assigned to the density of the water in the bentonite, which must be well above 1.0 Mg/m^3 as suggested by recent publications in the field of clay mineralogy.

In this Thesis a methodology was developed to calculate the density of the water in compacted samples of bentonite. This method permits to obtain a relationship between the water density and the suction. When this aspect is considered, it is possible to obtain in a natural way a water retention curve where the values of degree of saturation are lower than one in the range of low suctions. The methodology was applied to the analysis of experimental data corresponding to a bentonite with predominant monovalent (MX-80 bentonite) and bivalent (FEBEX bentonite) exchangeable cations in the interlayer space. Results suggest that the exchangeable cation in the interlayer space plays a central role in the values that result for the water density at different suctions. In both cases, the density of water increases as suction increases and values higher than 1.0 Mg/m^3 were deduced. Also, taking into account the appropriate estimation of water density, results in a reduction of the degree of saturation for a particular value of suction. From a practical point of view this reduces the air entry value of the material and increases the time required for saturation. Finally, from the methodology described in Chapter 4 it would be possible to get a soil water retention curve for each structure present in a compacted sample of bentonite. This fact could be interesting when an analysis considering a material with double porosity is carried out.

Other aspects to be considered in the analysis of thermo-hydro-mechanical processes are the hydro- and thermo-mechanical couplings. Experimental results on

the hydro-mechanical behaviour of compacted expansive soils at ambient temperature indicate that swelling is produced during wetting under low stresses and collapse is induced under high stresses. When wetting under a confined condition (constant volume), swelling pressure is generally developed. This behaviour is the result of complex mechanisms appearing from the interaction between the volume change of aggregates made up of a highly expansive clay minerals (microstructural level) and the rearrangement of the granular-like skeleton formed by the aggregates (macrostructural level). With respect to the thermo-mechanical behaviour of unsaturated expansive soils, experimental works showed that, as in the case of saturated samples, heating may induce expansion under large over-consolidation ratio (OCR) and contraction under small OCR. Therefore, the mechanical model used in the simulation of coupled processes should include most of the dependences indicated above.

Chapter 5 describes the behaviour of a compacted sample of MX-80 bentonite in unsaturated state when subjected to a thermal gradient under confined conditions. The laboratory experiment was densely instrumented and temperatures above 100 ºC were involved. In order to improve the understanding of the different phenomena occurring in the test, numerical simulations were performed using a finite element code that solves THM coupled problems. The analyses indicated the necessity to use a special water retention curve where a degree of saturation lower than one must be considered at nil suction. This fact corresponds with the analysis of experimental results which revealed that the soil water retention curve is clearly affected by temperature, as observed when suction and water content measured within the sample at the end of the test were drawn. Also, a revision of the different coefficients adopted in the diffusion law of the water vapour was needed due to the enhancement of the gas mobility.

For the mechanical simulation of the mock-up laboratory test (TBT_3) the Barcelona Expansive Model (BExM) was adopted. The BExM assumes that physico-chemical phenomena occurring at microstructural level are basically reversible and independent of the macrostructure. The macrostructural behaviour, on the other hand, is simulated using the BBM. The key point in the model formulation is the interaction between structural levels. Thus, microstructural deformation is considered independent of the macrostructure, but the reverse is not true. The Barcelona Expansive Model was considered as a constitutive law appropriate for the simulation of the mechanical behaviour of the bentonite, because it accounts for the double structure that can be found in compacted samples of this material (micro- and macrostructure). The model previously implemented in the finite element code allowed the experiment to be

simulated, and reproduced the measured stresses reasonably well. The cold side of the sample showed a swelling behaviour, whereas the hot side experienced shrinkage. Measurements of porosity along the sample at the end of the test were also in good agreement with the predictions of the model. The analysis suggests that both micro- and macrostructure deform in the same manner at both ends. However, in the central part of the sample the microstructure expands, whereas the porosity of the macrostructure reduces. The good agreement between numerical simulations and measurements indicates that the main THM mechanisms involved in the behaviour of compacted bentonite under thermal gradients have been taken into account.

Chapter 6 describes the performance, observations and interpretation of the Temperature Buffer Test (TBT), a full-scale in situ heating test performed to simulate the conditions of vitrified high-level radioactive waste disposal in a deep geological repository excavated in granite. Two possibilities for the disposal of vitrified waste are evaluated in the experiment by using heaters that mimic the thermal effects of nuclear waste. In the upper part a composite barrier with a sand shield between the heater and the bentonite buffer is considered, while in the lower part an engineered barrier made up of compacted swelling clay between the heater and the rock is evaluated. The test has provided a large amount of information concerning the thermo-hydro-mechanical behaviour of the bentonite barrier and of the adjacent rock. The progress of hydration, the effects of heating, vapour transport and development of swelling pressures have been identified as the major interacting phenomena underlying the observed patterns of behaviour. The analyses confirm the capabilities of the coupled formulation used in this Thesis. Several parameters are required to define the numerical problem and it has been possible to determine them on the basis of an extensive programme of laboratory tests.

In general, predictions of the thermo-hydraulic variables are in good agreement with experimental data for both cases considered. The numerical model designed as Base Case (BC) was developed during the early stages of the test and therefore the model computations largely represent a predictive exercise. The comparison between the results of the numerical analysis and the field observations suggests that the formulation and associated computer code are able to reproduce well the main observed features of the TH behaviour of the test. The influence because of the interaction between the water and the expansive clay used in engineered barriers on the hydration process was evaluated in the Liquid Density Case (LDC). A different law for the liquid density and a modified soil water retention curve were used. Numerical

results show an improvement in some of the predicted thermo-hydraulic variables. Additionally, this analysis highlights the increment in the time required to obtain a given level of saturation within the barrier.

For the mechanical analysis of the in situ experiment an extension of the original version of the Barcelona Basic Model (BBM) was used. This model was developed using the net stress as the mechanical independent variable and the suction as the hydraulic independent variable. It is assumed that the hydraulic effect is volumetric by postulating a dependence of the pre-consolidation pressure on the suction. Also, a dependence of the plastic stiffness coefficient on the suction is assumed. The formulation has been extended to the triaxial stress space considering different yield surfaces for each suction value. This model assumes that the thermal effect on the mechanical response is volumetric and includes a dependence of the pre-consolidation pressure (hardening parameter of the model) on temperature. In this way, it is assumed that as temperature increases the size of the yield surface reduces. To take into account experimental evidences with respect to the behaviour of highly expansive materials modifications were introduced in the elastic stiffness parameters of the model. Thus, the elastic stiffness coefficient for changes in net mean stress depends on suction while the elastic stiffness coefficient for changes in suction depends on net mean stress. In general, the stress level at different positions is well captured although some specific aspects of the response will require a more sophisticated model in order to be reproduced.

7.2 Future works

Some possible aspects for further investigation are indicated below. They are grouped according to the areas studied in this Thesis.

As shown in Chapter 3 of this Thesis, concepts derived from thermodynamics of interfacial phenomena give a powerful tool to analyse the effect of temperature increments on the water retention capacity of expansive soils. However, it is though that temperature effects are different at each structural level as each one has its main mechanism of water retention. As more experimental data become available it would be possible, by using the method presented in Chapter 4, to estimate the water content for each structural level at a given water energy and temperature. Then, using the concepts introduced in Chapter 2 it would be possible to quantify the temperature effect

on the retention capacity of the micro and macrostructure. Finally, this effect could be incorporated into the numerical simulations as indicated in Chapter 3.

Experimental data suggest that soil deformability and external loads are variables that affect the water retention capacity of soils. An analysis of experimental results of the water retention capacity of bentonite samples compacted at different densities and tested at variable temperature was carried out in Chapter 3. By using thermodynamic concepts presented in Chapter 2, a coefficient χ that depends on the differential enthalpy and the differential entropy of the adsorbed water was defined. First results suggest that this coefficient varies with the sample density. However, because of the lack of experimental data it was not possible to obtain a clear tendency about the relationship between the coefficient χ and the sample porosity. An analysis of the same experimental results using a commonly adopted expression for the soil water retention curve was also included in Chapter 3. From this analysis a relation between the air entry value in the SWRC (a parameter typically associated to the sample density) and the coefficient χ was deduced. In the same Chapter, a way to take into account the influence of sample void ratio on the water retention curve was given. This approach is essentially empirical as are other proposed in the literature. However, as more experimental data become available a relationship between the sample void ratio and the coefficient χ could be defined and consequently, the dependence of the water retention capacity on sample density could be straightforwardly incorporated in numerical simulations.

It seems that the interaction between the active clay minerals present in expansive soils and the water retained in the porous space of the samples made up of these materials changes the density of the water. A first approach to consider this effect was put forward in this Thesis. However, as it was already indicated, it is though that the sample density also plays a role in the value of the water density inside soil pores. As more experimental data related to the water retention capacity of expansive soil including a wide range of densities become available it would be interesting to evaluate and quantify the magnitude of this effect.

After the dismantling of the field test a complete program of laboratory experiments is planned. It considers, among other, determination of bulk density, water content, swelling pressure, hydraulic conductivity and retention properties on samples of bentonite obtained at different levels and radii within the barrier. Also, some tests as electron microscopy and X-ray diffraction analysis will be carried out to evaluate

changes in the mineralogy of the material. When post-mortem experimental data become available it will be possible to compare some of these results with those obtained from the numerical simulations. Eventually, these data could be a tool to newly estimate the parameters of the constitutive laws adopted to define the behaviour of the MX-80 bentonite blocks.

Studies performed on samples of bentonite subjected to high temperatures (Pusch & Karnland, 1988; Pusch & Güven, 1990; Neaman et al., 2003; Pusch et al., 2003) indicate that transformations are experienced in the fabric of the material. In general, treated samples show denser aggregates and larger voids that untreated samples which indicate a contraction of the clay layers that constitute the particles. Results suggest that the collapse at the level of arrangements of clay layers seems to be irreversible. Additionally, precipitation of silicious cementing compounds with a consequent reduction of the swelling potential is observed. Temperatures higher than 150 ºC were reached in the bentonite close to the lower heater in the TBT field experiment. It would be interesting to evaluate the fabric of samples obtained at different radii from the heater and to compare with experimental finding reported by other authors.

The Barcelona Expansive Model has shown its capabilities to simulate the behaviour of expansive materials. In the original version of this model the effect of temperature on the soil response is incorporated at the macrostructural level. Sánchez & Gens (2006) proposed to consider an increment in the microstructural bulk modulus with temperature to take into account the diminution in the swelling capacity of expansive clays because of temperature increments. This traduces in a reduction in the volumetric deformation at that structural level. Pusch et al. (1998) proposed a conceptual model where the effect of temperature depends on the value of this variable and basically affects the swelling capacity of the microstructure in an irreversible way. A possible way to include these concepts in the BExM would be to consider that from a temperature level on plastic volumetric strains develop at the microstructure of the material.

References

Abu-Zreig M.M., Al-Akhras N.M., Attom M.F. (2001). Influence of heat treatment on the behavior of clayey soils. *Applied Clay Sci.*, **20**, 129–135.

Abuel-Naga H.M., Bergado D.T., Bouazza A., Ramana G.V. (2007). Volume change behaviour of saturated clay under drained heating conditions: experimental results and constitutive modeling. *Can. Geotech. J.*, **44**, 942-956.

Adamson A.W. (1990). Physical chemistry of surfaces. Fifth edition. John Wiley & Sons, New York.

Åkesson M. (2006). Äspö Hard Rock Laboratory. Temperature Buffer Test. Evaluation modeling – Mock-up test. International Progress Report. IPR-06-11. SKB, Stockholm, 121 pp.

Åkesson M. (2008). Temperature Buffer Test. Evaluation modeling – TBT_3 Mock-up test. International Progress Report IPR-08-09, SKB, Stockholm. 143 pp.

Al-Mukhtar M., Qi Y., Alcover J-F., Bergaya F. (1999). Oedometric and water-retention behavior of highly compacted unsaturated smectites. *Can. Geotech. J.*, **36**, 675-684.

Alonso E.E (1998). Modelling expansive soil behaviour. *Proc. Second Int. Conference Unsaturated Soils, Beijing*, Vol. 1, 37-70.

Alonso E.E., Gens A., Josa A. (1990). A constitutive model for partially saturated soils. *Géotechnique*, **40**, No. 3, 405-430.

Alonso E.E, Vaunat J., Gens A. (1999). Modelling the mechanical behaviour of expansive clays. *Eng. Geol.*, **54**, 173-183.

Assouline S. (2006). Modeling the relationship between soil bulk density and the water retention curve. *Vadose Zone J.*, **5**, 554-563.

ASTM (2008). ASTM B925-08 Standard Practices for Production and Preparation of Powder Metallurgy (PM) Test Specimens. American Society for Testing and Materials, ASTM International, PA, USA.

Assouline S., Tavares-Filho J., Tessier D. (1997). Effect of compaction on soil physical and hydraulic properties: experimental results and modeling. *Soil Sci. Soc. Am. J.*, **61**, 390-398.

Atkins P.W. (1998). Physical chemistry. Sixth edition. Oxford University Press, Oxford.

Bachmann J., Horton R., Grant S.A., van der Ploeg R.R. (2002). Temperature dependence of water retention curves for wettable and water-repellent soils. *Soil Sci. Soc. Am. J.*, **66**, 44-52.

Barbour S.L. (1998). Nineteenth Canadian Geotechnical Colloquium: The soil-water characteristic curve: a historical perspective. *Can. Geotech. J.*, **35**, 873-894.

Bear J. (1972). Dynamics of fluids in porous media. Dover Publications, New York.

Bérend I., Cases J.M., François M., Uriot J.P., Michot L., Masion A., Thomas F. (1995). Mechanism of adsorption and desorption of water vapor by homoionic montmorillonites: 2. The Li+, Na+, K+, Rb+ and Cs+-exchanged forms. *Clay Clay Miner.*, **43**, No. 3, 324-336.

Bihannic I., Tchoubar D., Lyonnard S., Besson G., Thomas F. (2001). X-ray scattering investigation of swelling clay fabric. 1. The dry state. *J. Colloid Interface Sci.*, **240**, 211-218.

Bolzon G., Schrefler B. (2005). Thermal effects in partially saturated soils: a constitutive model. *Int. J. Numer. Anal. Meth. Geomech.*, **29**, No. 9, 861-877.

Börgesson L., Fredrikson A., Johannesson L-E (1994). Heat conductivity of buffer materials. Technical Report 94-29, SKB, Stockholm. 51 pp.

Bourg I.C., Sposito G., Bourg A.C.M. (2006). Tracer diffusion in compacted, water-saturated bentonite. *Clay Clay Miner.*, **54**, No. 3, 363-374.

Box J.E., Taylor S.A. (1962). Influence of soil bulk density on matric potential. *Soil Sci. Soc. Proc.*, **26**, 119-122.

Boyd G.E., Livingston H.K. (1942). Adsorption and the energy changes at crystalline solid surfaces. *J. Am. Chem. Soc.*, **64**, 2383-2388.

Bradbury M.H., Baeyens B. (2003). Porewater chemistry in compacted re-saturated MX-80 bentonite. *J. Contam. Hydrol.*, **61**, 329-338.

Burghignoli A., Desideri A., Miliziano S. (2000). A laboratory study on the thermomechanical behaviour of clayey soils. *Can. Geotech. J.*, **37**, 764-780.

Cariati F., Erre L., Micera G., Piu P., Gessa C. (1981). Water molecules and hydroxyl groups in montmorillonites as studied by near infrared spectroscopy. *Clay Clay Miner.*, **29**, No. 2, 157-159.

Cases J.M., Bérend I., Besson G., François M., Uriot J.P., Thomas F., Poirier J.E. (1992). Mechanism of adsorption and desorption of water vapor by homoionic montmorillonite. 1. The sodium-exchanged form. *Langmuir*, **8**, 2730-2739.

Cases J.M., Bérend I., François M., Uriot J.P., Michot L.J., Thomas F. (1997). Mechanism of adsorption and desorption of water vapor by homoionic montmorillonite: 3. The Mg^{2+}, Ca^{2+}, Sr^{2+} and Ba^{2+} exchanged forms. *Clay Clay Miner.*, **45**, No. 1, 8-22.

Castellan G.W. (1972). Physical chemistry, Second edition. Addison-Wesley Publishing Company, Reading (Massachusetts).

Cekerevac C., Laloui L. (2004). Experimental study of thermal effects on mechanical behaviour of a clay. *Int. J. Numer. Anal. Meth. Geomech.*, **28**, 209-228.

Chahal R.S. (1964). Effect of temperature and trapped air on the energy status of water in porous media. *Soil Sci.*, **98**, 107-112.

Chahal R.S. (1965). Effect of temperature and trapped air on matric suction. *Soil Sci.*, **100**, No. 4, 262-266.

Chen N.H., Othmer D.F. (1962). New generalized equation for the gas diffusion coefficient. *J. Chem. Eng. Data*, **7**, No. 1, 37-41.

Chen G.J., Ledesma A. (2007). Coupled solution of heat and moisture flow in unsaturated clay barriers in a repository geometry. *Int. J. Numer. Anal. Meth. Geomech.*, **31**, No. 8, 1045-1065.

Chen G.J., Ledesma A. (2008). Coupled thermohydromechanical modeling of the full-scale in situ test "Prototype Repository". *J. Geotech. Geonv. Eng.*, **135**, No. 1, 121-132.

Constantz J. (1991). Comparison of isothermal and isobaric water retention paths in nonswelling porous materials. *Water Resour. Res.*, **27**, No. 12, 3165-3170.

Cornelis W.M., Khlosi M., Hartmann R., van Meirvenne M., de Vos B. (2005). Comparison of unimodal analytical expressions for the soil-water retention curve. *Soil Sci. Soc. Am. J.*, **69**, 1902-1911.

Coussy O. (2004). Poromechanics. John Wiley & Sons, Chichester.

Cuadros J. (1997). Interlayer cation effects on the hydration state of smectite. *Am. J. Sci.*, **297**, 829-841.

Cui Y.J., Sultan N., Delage P. (2000). A thermomechanical model for saturated clays. *Can. Geotech. J.*, **37**, 607-620.

Cui Y.J., Yahia-Aissa M., Delage P. (2002). A model for the volume change behavior of heavily compacted swelling clays. *Eng. Geol.*, **64**, No. 2-3, 233-250.

Delage P., Howat M.D., Cui Y.J. (1998). The relationship between suction and swelling properties in heavily compacted unsaturated clay. *Eng. Geol.*, **50**, 31-48.

Delage P., Sultan N., Cui Y.J. (2000). On the thermal consolidation of Boom clay. *Can. Geotech. J.*, **37**, 343-354.

Delage P., Marcial D., Cui Y.J., Ruiz X. (2006). Ageing effects in a compacted bentonite: a microstructure approach. *Géotechnique*, **56**, No 5, 291-304.

Demars K.R., Charles R.D. (1982). Soil volume changes by temperature cycling. *Can. Geotech. J.*, **19**, 188-194.

Derjaguin B.V., Karasev V.V., Khromova E.N. (1986). Thermal expansion of water in fine pores. *J. Colloid Interface Sci.*, **109**, No. 2, 586-587.

Devineau K., Bihannic I., Michot L., Villiéras F., Masrouri F., Cuisinier O., Fragneto G., Michau N. (2006). In situ neutron diffraction analysis of the influence of geometric confinement on crystaline swelling of montmorillonite. *Appl. Clay Sci.*, **31**, 76-84.

Dios Cancela G., Huertas F.J., Romero Taboada E., Sánchez-Rasero F., Hernández Laguna A. (1997). Adsorption of water vapor by homoionic montmorillonites. Heats of adsorption and desorption. *J. Colloid Interface Sci.*, **185**, 343-354.

Dixon D., Chandler N., Graham J., Gray M.N. (2002). Two large-scale sealing tests conducted at Atomic Energy of Canada´s underground research laboratory: the buffer-container experiment and the isothermal test. *Can. Geotech. J.*, **39**, 503-518.

Dueck A. (2004). Hydro-mechanical properties of a water unsaturated sodium bentonite. Laboratory study and theoretical interpretation. PhD thesis, Division of Soil Mechanics and Foundation Engineering, Lund Institute of Technology, Lund.

Edlefsen N.E., Anderson A.B.C. (1943). Thermodynamics of soil moisture. *Hilgardia*, **15**, No 2, 31-298.

ENRESA (2000). FEBEX project: full-scale engineered barriers experiment for a deep geological repository for high level radioactive waste in crystalline host rock. Final Report, ENRESA 1/2000, Madrid, 354 pp.

Feddes R.A., Kabat P., van Bakel P.J.T., Bronswijk J.J.B., Halbertsma J. (1988). Modelling soil water dynamics in the unsaturated zone - State of the art. *J. Hydrol.*, **100**, 69-111.

Fernández A.M. (2003). Caracterización y modelización del agua intersticial de materiales arcillosos: estudio de la bentonita de Cortijo de Archidona. PhD thesis (in Spanish). Universidad Autónoma de Madrid, Madrid.

Fernández A.M., Baeyens B., Bradbury M., Rivas P. (2004). Analysis of the pore water chemical composition of a Spanish compacted bentonite used in an engineered barrier. *Phys. Chem. Earth*, **29**, 105-118.

Fernández A.M., Rivas P. (2005). Analysis and distribution of waters in the compacted FEBEX bentonite: pore water chemistry and adsorbed water properties. In *Advances in Understanding Engineered Clay Barriers* (E.E. Alonso & A. Ledesma eds), A.A. Balkema, Leiden, 257-275.

Ferrage E., Lanson B., Sakharov B.A., Drits V.A. (2005a). Investigation of smectite hydration properties by modeling experimental X-ray diffraction patterns: Part I. Montmorillonite hydration properties. *Am. Mineral.*, **90**, 1358-1374.

Ferrage E., Lanson B., Malikova N., Plançon A., Sakharov B.A., Drits V.A. (2005b). New insights on the distribution of interlayer waterr in bi-hydrated smectite from X-ray diffraction profile modeling of 00l reflections. *Chem. Mater.*, **17**, 3499-3512.

Fredlung D.G, Rahardjo H. (1993). Soil Mechanics for Unsaturated Soils. Wiley-Interscience, New York.

Fredlund D.G., Xing A. (1994). Equations for the soil-water characteristic curve. *Can. Geotech. J.*, **31**, 521-532.

Fredlung D.G. (2006). Unsaturated soil mechanics in engineering practice. *J. Geotech. Geoenv. Eng.*, **132**, No. 3, 286-321.

Gatabin C., Guillot W. (2006). TBT_3 mock-up test. Final report. Technical Data Report, NT DPC/SCCME 06-345-A, CEA, Saclay, 26 pp.

Gardner R. (1955). Relation of temperature to moisture tension of soil. *Soil Sci.*, **79**, 257-265.

Gawin D., Baggio P., Schrefler B.A. (1995). Coupled heat, water and gas flow in deformable porous media. *Int. J. Numer. Meth. Fluid*, **20**, No. 8-9, 969-987.

Gens A., Alonso E.E. (1992). A framework for the behaviour of unsaturated expansive clays. *Can. Geotech. J.*, **29**, 1013-1032.

Gens A. (1995). Constitutive laws. In *Modern issues in non-saturated soils* (A. Gens, P. Jouanna & B. Schrefler eds), 129-158, Wien, Springer-Verlag.

Gens A., Garcia-Molina A.J., Olivella S., Alonso E.E., Huertas F. (1998). Analysis of a full scale in situ test simulating repository conditions. *Int. J. Numer. Anal. Meth. Geomech.*, **22**, 515-548.

Gens A. (2003). The role of Geotechnical Engineering for nuclear energy utilisation. In *Proceedings of XIII European Conference of Soils Mechanics and Geotechnical Engineering* (Vanícek, Barvínek, Bohác, Jettmar, Jirásko & Salák eds), Vol. 3, 25 - 67, Prague, Czech Geotechnical Society.

Gens A., Sánchez M., Do N. Guimarães L., Alonso E.E., Lloret A., Olivella S., Villar M.V., Huertas F. (2009). A full-scale in situ heating test for high-level nuclear waste disposal: observations, analysis and interpretation. *Géotechnique*, **59**, No. 4, 377-399.

Gens A., Olivella S. (2001). THM phenomena in saturated and unsaturated porous media. Fundamentals and formulation. *Revue Française de Génie Civil*, **5**, No 6, 693-717.

Gitirana G.F.N., Fredlund D.G. (2004). Soil-water characteristic curve equation with independent properties. *J. Geotech. Geoenv. Eng.*, **130**, No 2, 209-212.

Graham J., Tanaka N., Crilly T., Alfaro M. (2001). Modified Cam-Clay modelling of temperature effects in clays. *Can. Geotech. J.*, **38**, 608–621.

Grant S.A. (2003). Extension of temperature effects model for capillary pressure saturation relations. *Water Resour. Res.*, **39**, No. 1, 1003, doi: 10.1029/2000WR000193.

Grant S.A., Salehzadeh A. (1996). Calculation of temperature effects on wetting coefficients of porous solids and their capillary pressure functions. *Water Resour. Res.*, **32**, No. 2, 261-270.

Gregg S.J., Sing K.S.W. (1967). Adsoprtion, surface area and porosity. Academic Press, London.

Groenevelt P.H., Bolt G.H. (1972). Water retention in soil. *Soil Sci.*, **113**, No 4, 238-245.

Groenevelt P.H., Grant C.D. (2004). A new model for the soil-water retention curve that solves the problem of residual water contents. *Eur. J. Soil Sci.*, **55**, 479–485.

Guggenheim E.A. (1967). Thermodynamics. An advanced treatment for chemists and physicists. Fifth edition. North-Holland Publishing, Amsterdam.

Hagymassy J., Brunauer S., Mikhail R.Sh. (1969). Pore structure analysis by water vapour adsorption. I. t-curves for water vapour. *J. Colloid Interface Sci.*, **29**, No. 3, 485-491.

Harkins W.D., Jura G. (1944). Surfaces of solids. XIII. A vapor adsorption method for the determination of the area of a solid without the assumption of a molecular area, and the areas occupied by Nitogen and other molecules on the surface of a solid. *J. Am. Chem. Soc.*, **66**, 1366-1373.

Harkins W.D., Livingston H.K. (1942). Energy relation of the surface of solids. II. Spreading pressure as related to the work of adhesion between a solid and a liquid. *J. Chem. Phys.*, **10**, 342-356.

Haridasan M., Jensen R.D. (1972). Effect of temperature on pressure head-water content relationship and conductivity of two soils. *Soil Sci. Soc. Amer. Proc.*, **36**, 703-708.

Hawkins R.K., Egelstaff P.A. (1980). Interfacial water structure in montmorillonite from neutron diffraction experiments. *Clay Clay Miner.*, **28**, No. 1, 19-28.

Hill T.L. (1949). Statistical mechanics of adsorption. V. Thermodynamics and heat of adsorption. *J. Chem. Physics*, **17**, No 6, 520-535.

Hill T.L. (1950). Statistical mechanics of adsorption. IX. Adsorption thermodynamics and solution thermodynamics. *J. Chem. Physics*, **18**, No. 3, 246-256.

Hillel D. (1980). Fundamentals of soil physics. Academic Press, New York.

Hökmark H. (2004). Hydration of the bentonite buffer in a KBS-3 repository. *Appl. Clay Sci.*, **26**, 219-233.

Hökmark H., Ledesma A., Lassabatere T., Fälth B., Börgesson L., Robinet J.C., Sellali N., Sémété P. (2007). Modelling heat and moisture transport in the ANDRA/SKB temperature buffer test. *Phys. Chem. Earth*, **32**, No. 8-14, 753-766.

Hopmans J.W., Dane J.H. (1986). Temperature dependence of soil water retention curves. *Soil Sci. Soc. Am. J.*, **50**, 562-567.

Huang W.L., Bassett W.A., Wu T.C. (1994). Dehydration and hydration of montmorillonite at elevated temperatures and pressures monitored using synchrotron radiation. *Am. Mineral.*, **79**, 683-691.

Hueckel T., Baldi G. (1990). Thermoplasticity of saturated clay: experimental constitutive study. *J. Geotech. Eng.*, **116**, No. 12, 1778-1796.

Hueckel T., Borsetto M. (1990). Thermoplasticity of saturated soils and shales: constitutive equations. *J. Geotech. Eng.*, 116, No. 12, 1765-1777.

Iwata S., Tabuchi T., Warkentin B.P. (1995). Soil-water interactions. Mechanism and applications. Marcel Dekker, New York.

Jacinto A.C., Villar M.V., Gómez-Espina R., Ledesma A. (2009). Adaptation of the van Genuchten expression to the effects of temperature and density for compacted bentonites. *Appl. Clay Sci.*, **42**, 575–582.

Jura G., Harkins W.D. (1944). Surfaces of solids. XI. Determination of the decrease of free surface energy of a solid by an adsorbed film. *J. Am. Chem. Soc*, **66**, 1356-1362.

Jury W.A., Horton R. (2004). Soil physics. John Wiley & Sons, Hoboken (New Jersey).

Keren R., Shainberg I. (1975). Water vapor isotherms and heat of immersion of Na/Ca-montmorillonite systems – I: Homoionic clay. *Clay Clay Miner.*, **23**, No. 3, 193-200.

Keren R., Shainberg I. (1979). Water vapor isotherms and heat of immersion of Na/Ca-montmorillonite systems – II: Mixed systems. *Clay Clay Miner.*, **27**, No. 2, 145-151.

Keren R., Shainberg I. (1980). Water vapor isotherms and heat of immersion of Na- and Ca-montmorillonite systems. III. Thermodynamics. *Clay Clay Miner.*, **28**, No. 3, 204-210.

Kézdi Á. (1974). Handbook of soil mechanics. Soil physics. Elsevier Scientific Publishing Company, Amsterdam.

Kraehenbuehl F., Stoeckli H.F., Brunner F., Kahr G., Muller-Vonmoos M. (1987). Study of the water-bentonite system by vapour adsorption, immersion calorimetry and X-ray techniques: I. Micropore volumes and internal surface areas, following Dubinin´s theory. *Clay Miner.*, **22**, No. 1, 1-9.

Koster van Gross A.F., Guggenheim S. (1984). The effect of pressure on the dehydration reaction of interlayer water in Na-montmorillonite (SWy-1). *Am. Mineral.*, **69**, 872-879.

Koster van Gross A.F., Guggenheim S. (1986). Dehydration of K-exchanged montmorillonite at elevated temperatures and pressures. *Clay Clay Miner.*, **34**, No. 3, 281-286.

Knutsson S. (1983). On the thermal conductivity and thermal diffusivity of highly compacted bentonite. SKBF Technical Report 83-72, Stockholm, 43 pp.

Koorevaar P. Menelik G., Dirksen C. (1983). Elements of soil physics. Elsevier Science Publishing, Amsterdam.

Kuntiwattanakul P., Towhata I., Ohishi K., Seko I. (1995). Temperature effects on undrainded shear characteristics of clay. *Soils Found.*, **35**, No 1, 147-162.

Laird D.A. (2006). Influence of layer charge on swelling of smectites. *Appl. Clay Sci.*, **34**, 74-87.

Leong E.C., Rahardjo H. (1997). Review of soil-water characteristic curve equations. *J. Geotech. Geonv. Engrg.*, **123**, No. 12, 1106-1117.

Liu H.H., Dane J.H. (1993). Reconciliation between measured and theoretical temperature effects on soils water retention curves. *Soil Sci. Soc. Am. J.*, **57**, 1202-1207.

Lloret A., Villar M.V. (2007). Advances on the knowledge of the thermo-hydro-mechanical behaviour of heavily compacted FEBEX bentonite. *Phys. Chem. Earth*, **32**, No. 8-14, 701-715.

Lloret A., Romero E., Villar M.V. (2004). FEBEX II Project. Final report on thermo-hydro-mechanical laboratory tests. Publicación Técnica ENRESA 10/2004. Madrid. 165 pp.

Lloret A., Villar M.V., Sánchez M., Gens A., Pintado X., Alonso E.E. (2003). Mechanical behaviour of heavily compacted bentonite under high suction changes. *Géotechnique*, **53**, No. 1, 27-40.

Low P.F. (1979). Nature and propeties of water in montmorillonite-water system. *Soil Sci. Soc. Am. J.*, **43**, 651-658.

Ma C., Hueckel T. (1992). Stress and pore pressure in saturated clay subjected to heat from radioactive waste: a numerical simulation. *Can. Geotech. J.*, **29**, 1087-1094.

Ma C., Hueckel T. (1993). Thermomechanical effects on adsorbed water in clays around a heat source*. Int. J. Numer. Anal. Meth. Geomech.*, **17**, 175-196.

MacDonald A., Rogner H-H, Gritsevskyi A. (2008). Great expectations. Projections of nuclear power around the world show an upward trend. IAEA Bulletin 50-1, 28-31.

Marcial D. (2003). Comportement hydromécanique et microstructural des matériaux de barrière ouvragée. Ph.D. thesis (in French). École Nationale des Ponts et Chausées, Paris, 316 pp.

Martin T.R. (1962). Adsorbed water on clay: A review. In *Proceedings of the 9th National Conference on Clay and Clay Minerals* (Swineford, Ada and Franks eds.), New York, Pergamon Press, 23-70.

Massman W.J. (1998). A review of the molecular diffusivities of H_2O, CO_2, CH_4, CO, O_3, SO_2, NH_3, N_2O, NO, and NO_2 in air, O_2 and N_2 near STP. *Atmos. Environ.*, **32**, No. 6, 1111-1127.

Mbonimpa M., Aubertin M., Maqsoud A., Bussière B. (2006). Predictive model for the water retention curve of deformable clayey soils. *J. Geotech. Geoenv. Eng.*, **132**, No. 9, 1121-1132.

Mitchell J.K. (1993). Fundamentals of soils behaviour. Second edition. John Wiley & Sons, New York.

Modaressi H., Laloui L. (1997). A thermo-viscoplastic constitutive model for clays. *Int. J. Num. Anal. Meth. Geomech.*, **21**, 313-335.

Mohamed ElBaradei (2007). Nuclear power´s changing picture. The world´s rising demand for electricity will take a mix of energy sources. IAEA Bulletin 49-1, 18-21.

Mooney R.W., Keenan A.G., Wood L.A. (1952a). Adsorption of water vapor by montmorillonite. I. Heat of desorption and application of BET theory. *J. Am. Chem. Soc.*, **74**, No. 6, 1367-1371.

Mooney R.W., Keenan A.G., Wood L.A. (1952b). Adsorption of water vapor by montmorillonite. II. Effect of exchangeable ions and lattice swelling as measured by X-ray diffraction. *J. Am. Chem. Soc.*, **74**, No. 6, 1371-1374.

Moore D.M, Hower J. (1986). Ordered interstratification of dehydrated and hydrated Na-Smectite. *Clay Clay Miner.*, **34**, No. 4, 379-384.

Myers A.L. (2002).Thermodynamics of adsorption in porous materials. *Am. Inst. Chem. Eng.*, **48**, No 1, 145-160.

Myers A.L., Monson P.A. (2002). Adsorption in porous materials at high pressure: theory and experiment. *Langmuir*, **18**, 10261-10273.

Neaman A., Pelletier M., Villieras F. (2003). The effects of exchanged cation, compression, heating and hydration on textural properties of bulk bentonite and its corresponding purified montmorillonite. *Appl. Clay Sci.*, **22**, 153-168.

Ng C.W.W., Pang Y.W. (2000). Influence of stress state on soil-water characteristics and slope stability. *J. Geotech. Geonv. Eng.*, **126**, No. 2, 157-166.

Nimmo J.R., Miller E.E. (1986). The temperature dependence of isothermal moisture vs. potential characteristics of soils. *Soil Sci. Soc. Am. J.*, **50**, 1105-1113.

Olivella S., Carrera J., Gens A., Alonso E.E. (1994). Nonisothermal multiphase flow of brine and gas through saline media. *Trans. Porous Media*, **15**, 271-293.

Olivella S., Gens A., Carrera J., Alonso E.E (1996). Numerical formulation for a simulator (CODE_BRIGHT) for the coupled analysis of saline media. Engineering Computations, **13**, No. 7, 87-112.

Olivella S., Carrera J., Gens A., Alonso E.E (1996). Porosity variations in saline media caused by temperature gradients coupled to multiphase flow and dissolution/precipitation. *Trans. Porous Media*, **25**, 1-25.

Olivella S., Gens A. (2000). Vapour transport in low permeability unsaturated soil with capillary effects. *Trans. Porous Media*, **40**, 219-241.

Or D, Tuller M. (1999). Liquid retention and interfacial area in variably saturated porous media: upscaling from single-poro to sample-scale model. *Water Resour. Res.*, **35**, 3591-3605.

Pham H.Q., Fredlund D.G. (2008). Equations for the entire soil-water characteristic curve of a volume change soil. *Can. Geotech. J.*, **45**, 443-453.

Philip J.R. (1969). Hydrostatics and hydrodynamics in swelling soils. *Water Resour. Res.*, **5**, No. 5, 1070-1077.

Philip J.R., de Vries D.A. (1957). Moisture movement in porous materials under temperature gradients. *Trans. Am. Geophys. Union*, **38**, No. 2, 222-232.

Pollock D.W. (1986). Simulation of flow and energy transport processes associated with high-level radioactive waste disposal in unsaturated alluvium. *Water Resour. Res.*, **22**, No. 5, 765-775.

Pons C.H., Rousseaux F., Tchoubar D. (1981). Utilisation du rayonnement synchrotron en diffusion aux petits angles pour l'etude du gonflement des smectites: I. Etude du systeme eau-montmorillonite-Na en fonction de la temperature. *Clay Miner.*, **16**, 23-42.

Pusch R. (1982). Mineral-water interactions and their influence on the physical behavior of highly compacted Na bentonite. *Can. Geotech. J.*, **19**, 381-387.

Push R., Karnland O. (1988). Hydrotermal effects on montmorillonite. A preliminary study. SKB Technical Report 88-15, Stockholm, 64 pp.

Pusch R., Güven N. (1990). Electron microscopic examination of hydrothermally treated bentonite clay. *Eng. Geol.* , **28**, 303-314.

Pusch R., Karnland O., Hökmark H. (1990). GGM – A general microstructural model for qualitative and quantitative studies of smectite clays. SKB Technical Report 90-43, Stockholm, 94 pp.

Pusch R., Takase H., Benbow S. (1998). Chemical processes causing cementation in heat-affected smectite – the Kinnekulle bentonite. SKB Technical Report TR-98-25, Stockholm.

Pusch R., Bluemlingb P., Johnson L. (2003). Performance of strongly compressed MX-80 pellets under repository-like conditions. *Appl. Clay Sci.*, **23**, 239-244.

Rao S.M., Revanasiddappa K. (2005). Role of microfabric in matix suction of residual soils. *Eng. Geol.*, **80**, 60-70.

Reeves P.C., Celia M.A. (1996). A functional relationship between capillary pressure, saturation, and interfacial area as revealed by a pore-scale network model. *Water Resour. Res.*, **32**, 2345-2358.

Robinet J-C., Rahbaoui A., Plas F., Lebon P. (1996). A constitutive thermomechanical model for saturated clays. *Eng. Geol.*, **41**, 145-169.

Romero E., Vaunat J. (2000). Retention curve of deformable clays. In *Experimental Evidence and Theoretical Approaches in Unsaturated Soils* (Tarantino and Mancuso eds), Balkema, Rotterdam, 91-106.

Romero E., Gens A., Lloret A. (1999). Water permeability, water retention and microstructure of unsaturated compacted Boom clay. *Eng. Geol.*, **54**, 117-127.

Romero E., Gens A., Lloret A. (2001). Temperature effects on the hydraulic behaviour of an unsaturated clay. *Geotech. Geol. Eng.*, **19**, 311-332.

Romero E., Gens A., Lloret A. (2003). Suction effects on a compacted clay under non-isothermal conditions. *Géotechnique*, **53**, No. 1, 65-81.

Saiyouri N., Tessier D., Hicher Y. (2004). Experimental study of swelling in unsaturated compacted clays. *Clay Miner.*, **39**, 469-479.

Salles F., Beurroies I., Bildstein O., Jullien M., Raynal J., Denoyel R., Van Damme H. (2008). A calorimetric study of mesoscopic swelling and hydration sequence in solid Na-montmorillonite. *Appl. Clay Sci.*, **39**, 186-201.

Sánchez M. (2004). Coupled Thermo-Hydro-Mechanical analysis in low permeability media. Ph.D. Thesis, Geotechnical Engineering Department, Technical University of Catalunya, Barcelona, 281 pp.

Sánchez M., Gens A., Guimaraes L., Olivella S. (2005). A double structure generalized plasticity model for expansive materials. *Int. J. Numer. Anal. Meth. Geomech.*, **29**, 751–787.

Sánchez M., Gens A. (2006). Progress report on numerical analysis of laboratory experiments incorporating new THM phenomena - WP3.2 (NF-PRO C-3). Technical Report CIMNE/DETCG 01/06, 41 pp.

Sandén, T., Goudarzi, R., de Combarieu, M., Åkesson, M., Hökmark, H. (2007). Temperature buffer test – design, instrumentation and measurements. *Phys. Chem. Earth*, **32**, 77-92.

Seager, S.L., Geertson, L.R., Giddings, J.C. (1963). Temperature dependence of gas and vapour diffusion coefficients. *J. Chem. Eng. Data*, **8**, No. 2, 168-169.

She H.Y., Sleep B.E. (1998). The effect of temperature on capillary pressure-saturation relationships for air-water and perchloroethylene-water systems. *Water Resour. Res.*, **34**, No. 10, 2587-2597.

Skipper N.T., Soper A.K., McConnell J.D.C. (1991). The structure of interlayer water in vermiculite. *J. Chem. Phys.*, **94**, No. 8, 5751-5760.

Smith J.M., Van Ness H.C., Abbott M.M. (2001). Introduction to chemical engineering thermodynamics, McGraw-Hill, New York.

Sposito G., Prost R. (1982). Structure of water adsorbed on smectites. *Chem. Rev.*, **82**, No. 6, 553-573.

Stange F., Horn R. (2005). Modeling the soil water retention curve for conditions of variable porosity. *Vadose Zone J.*, **4**, 602-613.

Startsev A.D., McNabb D.H. (2001). Skidder traffic on water retention, pore-size distribution, and van Genuchten parameters of boreal forest soils. *Soil Sci. Soc. Am. J.*, **65**, 224-231.

Stepkowska E.T., Pérez-Rodriguez J.L., Maqueda C., Starnawska E. (2004). Variability in water sorption and in particle thickness of standard smectites. *Appl. Clay Sci.*, **24**, 185-199.

Sultan N., Delage P., Cui Y.J. (2002). Temperature effects on the volume change behaviour of Boom clay. *Eng. Geol.*, **64**, 135-145.

Swenson J., Bergman R., Howells W.S. (2000). Quasielastic neutron scattering of two-dimensional water in a vermiculite clay. *J. Chem. Phys.*, **113**, No. 7, 2873-2879.

Tanaka N., Graham J., Crilly T. (1997). Stress-strain behaviour of reconstituted illitic clay at different temperatures. *Eng. Geol.*, **47**, 339-350.

Tang A.M., Cui Y.J. (2005). Controlling suction by the vapour equilibrium technique at different temperatures and its application in determining the water retention properties of MX-80 clay. *Can. Geotech. J.*, **42**, 287-296.

Tang A.M., Cui Y.J. (2009). Modelling the thermomechanical volume change behaviour of compacted expansive clays. *Géotechnique*, **59**, No. 3, 185–195.

Tang A.M., Cui Y.J., Barnel N. (2008). Thermo-mechanical behaviour of a compacted swelling clay. *Géotechnique*, **58**, No. 1, 45-54.

Taylor S.A. (1965). Measuring soil-water potential. In *Methodology of plant eco-physiology* (Eckardt ed.), Imprimerie Firmin-Didot, Paris, 149-157.

Taylor S.A, Box J.E. (1961). Influence of confining pressure and bulk density on soil water matric potential. *Soil Sci.*, **91**, 6-10.

Taylor S.A., Stewart G.L. (1960). Some thermodynamic properties of soil water. *Soil Sci. Soc. Am. J.*, **24**, 243-247.

Thomas H.R., He Y., Onofrei C. (1998a). An examination of the validation of a model of the hydro/thermo/mechanical behaviour of engineered clay barriers. *Int. J. Num. Anal. Meth. Geom.*, **22**, 49-71.

Thomas H.R., Rees S.W., Sloper N.J. (1998b). Three-dimensional heat, moisture and air transfer in unsaturated soils. *Int. J. Num. Anal. Meth. Geom.*, **22**, 75-95.

Tindall J.A., Kunkel J.R. (1999). Unsaturated zone hydrology for Scientist and Engineers. Prentice-Hall, Upper Saddle River (New Jersey).

Tournassat C., Neaman A., Villiéras F., Bosbach D., Charlet L. (2003). Nanomorphology of montmorillonite particles: Estimation of the clay edge sorption site density by low-pressure gas adsorption and AFM observations. *Am. Mineral.*, **88**, 1989-1995.

Tolman R.C. (1948). Consideration of the Gibbs theory of surface tension. *J. Chem. Phys.*, **16**, No. 8, 758-774.

Tuller M., Or. D., Dudley L.M. (1999). Adsorption and capillary condensation in porous media: liquid retention and interfacial configurations in angular pores. *Water Resour. Res.*, **35**, 1949-1964.

Vanapalli S.K., Fredlund D.G., Pufahl D.E. (1999). The influence of soil structure and stress history on the soil-water characteristic of a compacted till. *Géotechnique*, **49**, No. 2, 143-149.

van Genuchten M.Th. (1980). A closed-form equation for predicting the hydraulic conductivity of unsaturated soils. *Soil Sci. Soc. Am. J.*, **44**, 892-898.

Villar M.V. (2002). Thermo-hydro-mechanical characterisation of a bentonite from Cabo de Gata. A study applied to the use of bentonite as sealing material in high level radioactive waste repositories. Publicación Técnica ENRESA 01/2002, Madrid. 258 pp.

Villar M.V. (2005). MX-80 Bentonite. Thermo-Hydro-Mechanical Characterisation Performed at CIEMAT in the Context of the Prototype Project. Technical Report 1053, Ciemat, Madrid, 45 pp.

Villar M.V. (2007). Water retention of two natural compacted bentonites. *Clay Clay Miner.*, **55**, No. 3, 311-322.

Villar M.V., Lloret A. (2001). Variation of the intrinsic permeability of expansive clays upon saturation. In *Clay Science for Engineering* (Adachi and Fukue eds.), Balkema, Rotterdam, 259-266.

Villar M.V., Lloret A. (2004). Influence of temperature on the hydro-mechanical behaviour of a compacted bentonite. *Appl. Clay Sci.*, **26**, 337-350.

Villar M.V., Gómez-Espina R. (2007). Retention curves of two bentonites at high temperature. Experimental Unsaturated Soil Mechanics. Springer Proceedings in Physics, **112**, 267-274.

Villar M.V., Martín P.L., Lloret A. (2005). Determination of water retention curves of two bentonites at high temperature. In *Advanced experimental unsaturated soil mechanics. Experus 2005.* (Tarantino, Romero and Cui eds.), A.A. Balkema Publishers, London, 77-82.

Villar M.V., Gómez-Espina R., Martín P.L. (2006). Behaviour of MX-80 bentonite at unsaturated conditions and under thermo-hydraulic gradient. Technical Report 1081, Ciemat, Madrid, 51 pp.

Yahia-Aissa M. (1999) Comportement hydromécanique d'une argile gonflante fortement compactée. Ph.D. thesis (in French). École Nationale des Ponts et Chaussées, CERMES, Paris, 241 pp.

Yahia-Aissa M., Delage P., Cui Y.J. (2001). Suction – water content relationship in swelling clays. In *Clay Science for Engineering* (Adachi and Fukue eds), Balkema, Rotterdam, 65-68.

Yong R.N. (1999). Soil suction and soil-water potentials in swelling clays in engineered clay barriers. *Eng. Geol.*, **54**, 3-13.

Appendix A

A.1 Preface

An unsaturated soil can be considered as a porous medium where it is possible to indentify a solid, liquid and gaseous phase. General physical concepts applicable to the different phases are included in this section. They were used in the analysis of the temperature dependence of the water retention capacity in samples of compacted bentonite.

A.2 Liquid phase

The average energy of the particles in a liquid is governed by the temperature. As the temperature increases the average energy becomes higher. But within that average, some particles have energies higher than the average, and others have energies lower than the average. Some of the more energetic particles on the surface of the liquid can escape from the attractive forces holding the liquid together and evaporate. That evaporation only takes place on the surface of the liquid. That is quite different from boiling which happens when there is enough energy to disrupt the attractive forces throughout the liquid.

Although the liquid is in a closed container there will be a constant evaporation from the surface. Particles continue to break away from the surface of the liquid, but this time they are trapped in the space above the liquid. As the vapour particles bounce around, some of them will hit the surface of the liquid again and be trapped there. There will be an equilibrium set up in which the number of particles leaving the surface is exactly balanced by the number rejoining it. In this equilibrium, there will be a fixed number of the gaseous particles in the space above the liquid. When these particles hit the walls of the container, they exert a pressure. This pressure is called the saturated vapour pressure of the liquid.

In the case of water its saturated vapour pressure increases with the temperature. When the space above the liquid water is saturated with vapour particles there is a dynamic equilibrium on the surface of the liquid. The change of liquid water to vapour is endothermic; it needs heat to convert the liquid into vapour. According to the principle of Le Chatelier, increasing the temperature of a system in a dynamic equilibrium favours the endothermic change. That means that increasing the temperature increases the amount of vapour present, and so increases the saturated vapour

pressure. The equation of Clausius-Clapeyron defines the relationships between the saturated vapour pressure of water and the temperature (Atkins, 1998)

$$P_v^0 = P_v^{ref} \exp\left[\frac{-\Delta H_{vap}}{R}\left(\frac{1}{T} - \frac{1}{T^{ref}}\right)\right] \qquad (A.1)$$

where P_v^0 and P_v^{ref} are the saturated vapour pressure and the saturated reference vapour pressure respectively, ΔH_{vap} is the enthalpy of vaporization, R the universal gas constant, and T and T_{ref} are the absolute temperature and the absolute reference temperature respectively. The dependence of the water vapour pressure on total gas pressure can be neglected for small values of the latter variable (Guggenheim, 1967; Castellan, 1972).

A liquid boils when its saturated vapour pressure becomes equal to the external pressure on the liquid. When that happens, it enables bubbles of vapour to form throughout the liquid. The temperature at which liquid boils is called boiling temperature. If the external pressure is higher than the saturated vapour pressure, these bubbles are prevented from forming, and there is just evaporation at the surface of the liquid. If the liquid is in an open vessel and exposed to normal atmospheric pressure, the liquid boils when its saturated vapour pressure becomes equal to 0.1 MPa. In the case of the water, this happens when the temperature reaches 100 °C and it is called the normal boiling temperature. But at different pressures, liquid will boil at different temperatures.

A.3 Gas phase

An ideal gas is defined as one in which all collisions between atoms or molecules are perfectly elastic and in which there are no intermolecular attractive forces. It can be visualized as a collection of perfectly hard spheres which collide but which otherwise do not interact with each other. In such a gas, all the internal energy is in the form of kinetic energy and any change in internal energy is accompanied by a change in temperature. The sate of an ideal gas can be characterized by the pressure P, volume V, and absolute temperature T. The relationship between them is called the ideal gas law

$$PV = nRT \qquad (A.2)$$

with n the number of moles.

In general, in coupled THM formulations, it is assumed that the gas phase behaves as an ideal gas and that it is composed by water vapour and dry air. Dry air is considered a single species and is the main component of the gaseous phase. In general, the mass fraction of the species i in the α phase ω_α^i, is defined as

$$\omega_\alpha^i = \frac{m_i}{m_\alpha} \tag{A.3}$$

where m_i and m_α represent the mass of species i and phase α respectively. That is, m_g^w represents the mass of water in the gas phase (i.e. vapour in the gas phase).

The density of the species i in the α phase ρ_α^i, is obtained as the relation between the mass of species i in the α phase m_α^i, and the volume of the α phase V_α

$$\rho_\alpha^i = \frac{m_\alpha^i}{V_\alpha} \tag{A4}$$

Again, in the case of water, ρ_g^w represents the water density in the gas phase (vapour density).

The law of partial pressure or Dalton's law states that the total pressure exerted by a gaseous mixture is equal to the sum of the partial pressures of each individual component in a gas mixture. Mathematically, the total pressure P of a mixture of gases can be defined as the summation of the partial pressure P_i of each component i

$$P = \sum_{i=1}^{n} P_i \tag{A5}$$

If this law is applied to the gas phase, the following relation is obtained

$$P_g = P_g^w + P_g^a \tag{A6}$$

where P_g is the pressure in the gaseous phase, and P_g^w and P_g^a are the partial pressure of water and air in the gas phase respectively. The water partial pressure in the gas phase or the vapour pressure is defined by equation (A.1).

A.4 Soil retention capacity at different temperatures

The following figures present the analysis of experimental results using the concepts described above. Experiments were performed on compacted samples of MX-80 bentonite with different initial water contents and dry densities of 1.60 and 1.75 Mg/m^3 (Villar et al., 2005, 2006; Villar & Gómez-Espina, 2007). Tests were performed at constant volume. The samples were heated by steps and the relative humidity for different temperatures was registered.

Figures A.1(a)-(d) correspond to a dry density of 1.60 Mg/m^3 and they indicate how the total water in the sample distributes between liquid and gaseous phases as the suction decreases because of the temperature increments. As it can be seen the water content in the gas phase (liquid phase) increases (decreases) as the sample is heated.
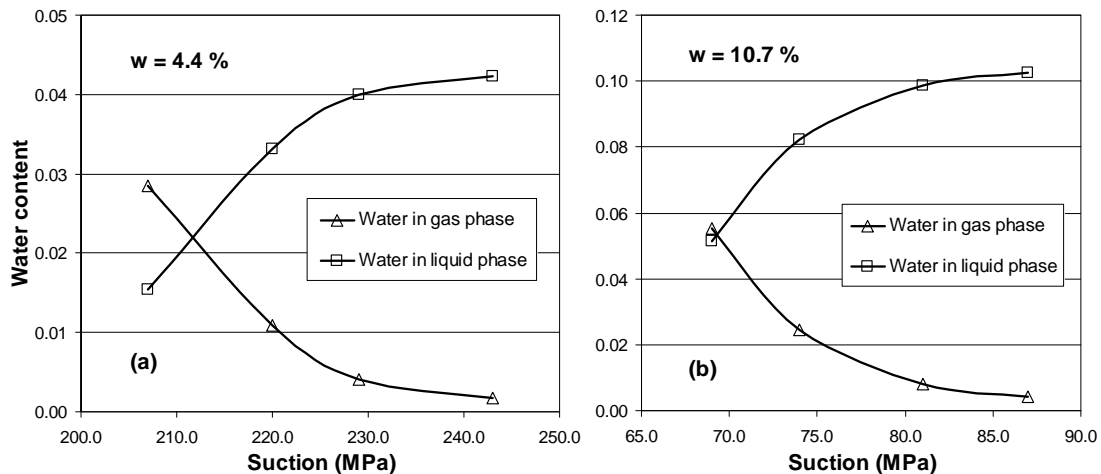

Figure A.1. Water distribution between liquid and gas phases as the temperature in the sample is increased. Sample dry density is 1.60 Mg/m^3.
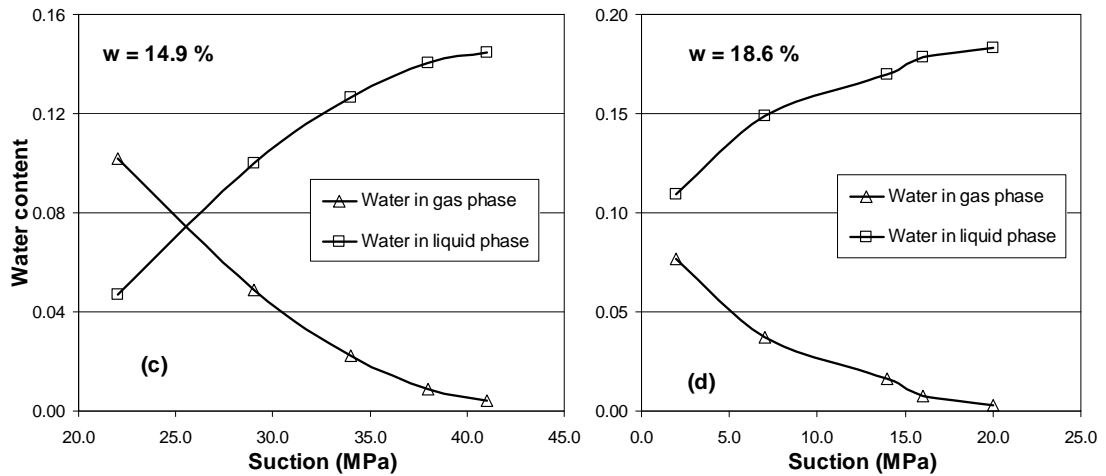
Figure A.1 (continuation). Water distribution between liquid and gas phases as the temperature in the sample is increased. Sample dry density is 1.60 Mg/m^3.

A similar analysis was carried out using experimental results corresponding to samples compacted at a dry density of 1.75 Mg/m^3. Figures A.2(a)-(d) present the distribution of the water between gas and liquid phase as the suction in the sample varies as a consequence of the temperature increment.
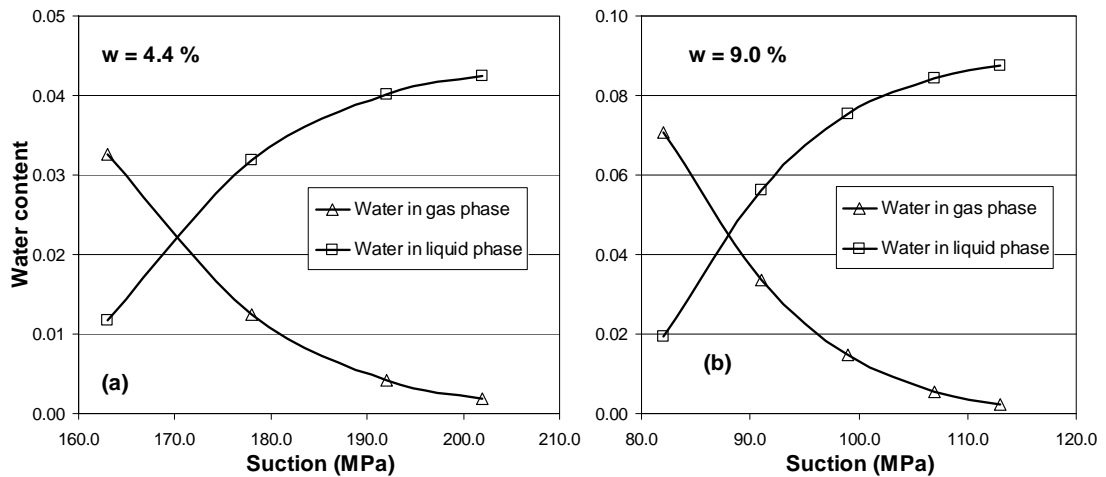

Figure A.2. Water distribution between liquid and gas phases as the temperature in the sample is increased. Sample dry density is 1.75 Mg/m^3.
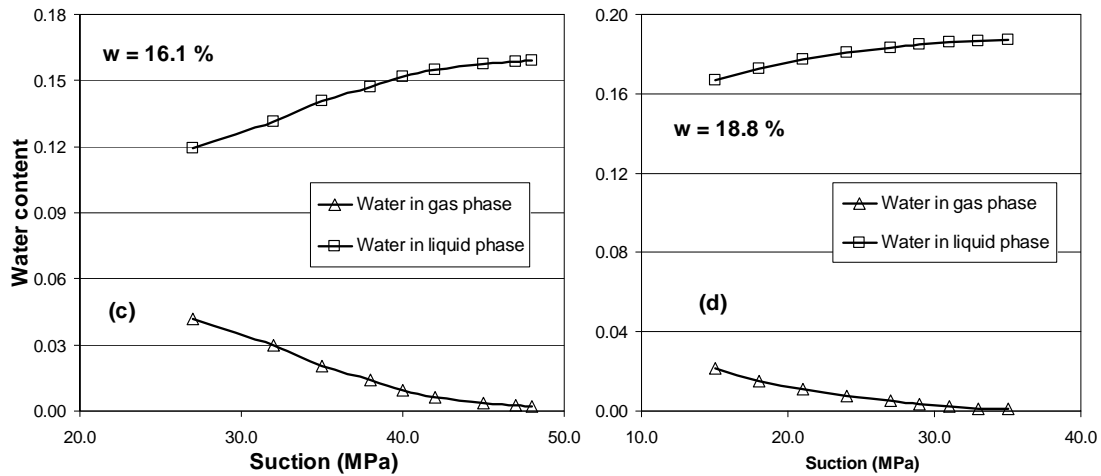
Figure A.2 (continuation). Water distribution between liquid and gas phases as the temperature in the sample is increased. Sample dry density is 1.75 Mg/m^3.

Figure A.3 shows the variation of the mass of liquid water with the temperature in samples tested at different total water contents and dry densities. For a dry density of 1.60 Mg/m^3, the water content corresponding to a degree of saturation equal to one is 27.0 %, while for the higher density that value is 21.6 %. These values where calculated using a water density equal to 1.0 Mg/m^3.
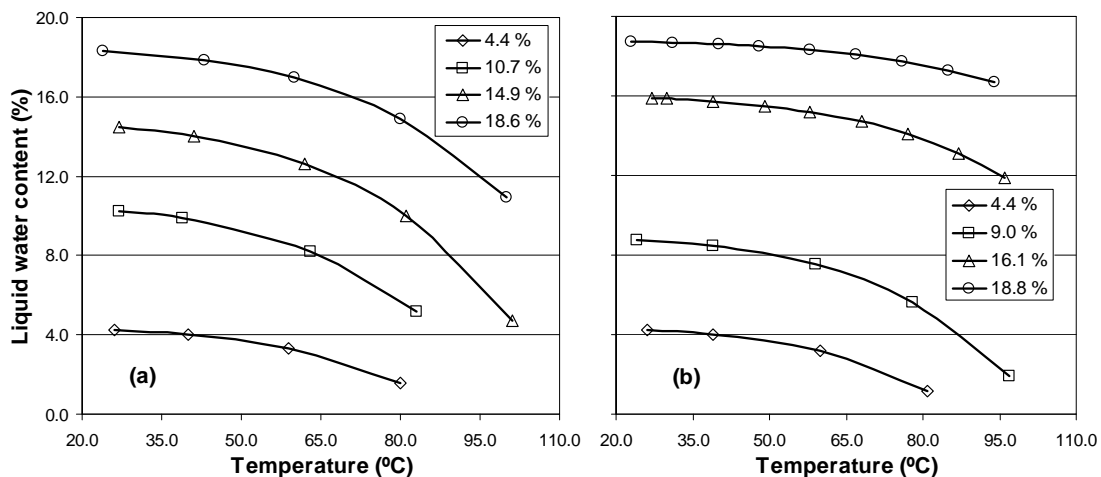
Figure A.3. Liquid water content against temperature for different total water contents. Dry density equal to (a) 1.60 Mg/m^3 and (b) 1.75 Mg/m^3.

Using the values obtained for the liquid water content at each temperature, the degree of saturation was determined for each sample at different total water contents. Figure A.4 presents results of water retention capacity at different temperatures and dry densities. They indicate the suction as a function of the degree of saturation at

different temperatures. Clearly, as the temperature increases the degree of saturation diminished for a given suction. It is important to note that, as results suggest, it is possible to obtain suction values close to zero while the saturation degree is lower that one. On the other hand, it seems that in the region of low suction the retention capacity, in terms of degree of saturation, is larger at the higher density.
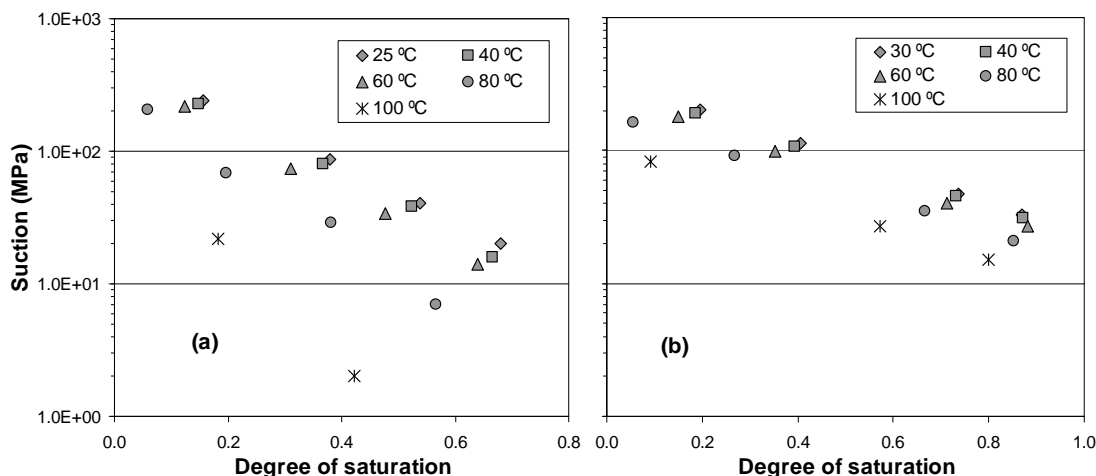
Figure A.4. Suction against degree of saturation at different temperatures. Dry densities are equal to (a) 1.60 Mg/m^3 and (b) 1.75 Mg/m^3.

A.5 Saturated water content as a function of temperature and sample void ratio

This section uses the theoretical background derived by Campanella & Mitchell (1968) to analyse the volume changes in saturated soil samples under non-isothermal conditions.

The soil is taken to be fully saturated. The changes of volume of the pore water dV_w, and of the soil grains dV_s, due to an infinitesimal temperature change dT are given by

$$dV_w = \alpha_w V_w dT \tag{A.7}$$

$$dV_s = \alpha_s V_s dT \tag{A.8}$$

where V_w and V_s are the volume and α_w and α_s the coefficients of thermal expansion of pore water and soil grains respectively.

It is assumed that the thermal loads are applied in drained conditions. The volume of pore water drained from a soil element due to a thermal loading is dV_{dr}. Using this value and the water volume change it is possible to calculate the void volume change. In mathematical form results

$$dV_v = dV_w - dV_{dr} \tag{A.9}$$

On the other hand, an infinitesimal volume change of the specimen can be written as

$$dV = dV_s + dV_v \tag{A.10}$$

It is assumed that the total volume of the sample is constant under a temperature increment. From equations (A.7) to (A.10) it follows that

$$dV_{dr} = \alpha_w V_w dT + \alpha_s V_s dT \tag{A.11}$$

The soil is taken to be fully saturated and therefore, the void volume V_v, coincides with the water volume in the soil sample. Equation (A.11) can be rewritten as

$$dV_{dr} = \left(\alpha_w + \frac{\alpha_s}{e} \right) V_w dT \tag{A.12}$$

An expression for the infinitesimal mass of drained water is obtained by multiplying the water volume in equation (A12) by the water density ρ_w

$$dm_{dr} = \left(\alpha_w + \frac{\alpha_s}{e} \right) m_w dT \tag{A.13}$$

Integration of equation (A.13) defines the mass of water that exits from a saturated soil sample due to a temperature change

$$m_{dr} = \left(\alpha_w + \frac{\alpha_s}{e} \right) m_w^r (T - T_r) \tag{A.14}$$

where m_w^r is the water mass at a reference temperature T_r and at a void ratio e. In deriving equation (A.14) it is assumed that the coefficients of thermal expansion of water and soil grains are temperature independent. The mass of water at the temperature T is obtained as the difference between the reference mass of water and the drained water

$$m_w^T = m_w^r \left[1 - \left(\alpha_w + \frac{\alpha_s}{e} \right) (T - T_r) \right] \tag{A.15}$$

Then, dividing by the soil mass (constant) an expression for the variation of the saturated water content as a function of the temperature is deduced

$$w_T = w_r \left[1 - \left(\alpha_w + \frac{\alpha_s}{e} \right) (T - T_r) \right] \tag{A.16}$$

where w_T and w_r are the water content at temperature T and T_r respectively. Under saturated conditions, the water content w at void ratio e and temperature T can be related to the water content w_T at void ratio e_r and the same temperature by the equation

$$w = w_T \frac{e}{e_r} \tag{A.17}$$

Finally, an expression for the water content at saturated conditions as a function of temperature and void ratio can be obtained

$$w = w_r \frac{e}{e_r} \left[1 - \left(\alpha_w + \frac{\alpha_s}{e} \right) (T - T_r) \right] \tag{A.18}$$

Campanella & Mitchell (1968) considered the thermal properties of free water to predict its thermal expansion in a saturated soil subjected to an increment of temperature. In low porosity plastic clays, Baldi et al. (1988) assume that the molecules of adsorbed water are under the action of a pressure exponentially decreasing with the distance between the water molecule and the clay platelet. The effect of temperature and pressure on the volume change of the adsorbed water results in a lower water thermal expansion. Delage et al. (2000) apply both methodologies to analyse experimental results of a stiff plastic clay and, additionally, combine the coefficient of water thermal expansion proposed by Baldi et al. (1988) with the formulation of Campanella & Mitchell (1968). The conclusion is that the simpler model of Campanella & Mitchell (1968) is satisfactory to reproduce experimental results.

By considering the precedent evidences it seems that the coefficient of thermal expansion of free water defines an upper limit value of this coefficient for the adsorbed water presents in expansive clays. Therefore, under a temperature increment (at

constant void ratio) an upper limit value for the saturated water content can be defined using equation (A.18). This equation also suggests that the saturated water content is higher in soil samples whose density is lower than a reference density.

Appendix B

B.1 Preface

This Appendix summarizes the complementary work carried out in the context of the analysis and simulation of the TBT field experiment. The constitutive model used to simulate the mechanical response of bentonite blocks is briefly described. Experimental data of the mechanical response of MX-80 bentonite samples under thermal and hydraulic actions were obtained from a literature review. These data together with the procedure followed to define the different parameters of the mechanical constitutive model are also presented. Finally, parameters used to characterize the thermo-hydro-mechanical behaviour of the different materials used in the simulations of the TBT in situ experiment are given.

B.2 Mechanical constitutive model of bentonite blocks

Experimental results on the hydro-mechanical behaviour of compacted expansive soils at ambient temperature suggest that the soil mechanical properties are influenced by the soil suction (Komine & Ogata, 1994; Delage et al., 1998; Al-Mukhtar et al., 1999; Villar, 1999; Cui et al., 2002; Lloret et al., 2003; Villar, 2005; Tang et al., 2008). Swelling is produced during wetting under low stresses and collapse is induced under high stresses. When wetting under a confined condition (constant volume), swelling pressure is generally developed.

Most of the work about the thermo-mechanical behaviour of clays has been done on saturated samples (Campanella & Mitchell, 1968; Demars & Charles, 1982; Baldi et al., 1988; Tidfors & Sallfors, 1989; Hueckel & Baldi, 1990; Towhata et al., 1993; Kuntiwattanakul et al., 1995; De Bruyn & Thimus, 1996; Del Olmo et al., 1996; Burghignoli et al., 2000; Delage et al., 2000; Laloui, 2001; Sultan et al., 2002; Cekerevac & Laloui, 2004). It has been observed that heating may induce expansion under large over-consolidation ratio (OCR) and contraction under small OCR. The effect of temperature on the mechanical properties is quite small. Recent experimental works on the thermo-mechanical behaviour of unsaturated expansive soils showed similar behaviour to that of saturated clays (Romero et al., 2005; Lloret & Villar, 2007; Tang et al., 2008).

In the numerical analysis of the TBT, the mechanical behaviour of bentonite blocks was simulated using a constitutive model based on the Barcelona Basic Model (BBM). The BBM was initially developed to represent the hydro-mechanical response of low

and moderate expansive soils in unsaturated state (Alonso et al., 1990). Gens (1995) extended the original version of this model to include the effect of temperature in the mechanical response of unsaturated soils. The model described below has been also applied in the simulation of other heating field tests (Chen & Ledesma, 2009; Gens et al., 2009).

In the adopted model, the yield surface depends on stresses, suction and temperature

$$f = f\left(p, J, \theta, \varepsilon_v^p, s, \Delta T\right)$$

(B.1)

where p is the net mean stress, J is the square root of the second invariant of deviatoric stress tensor, θ is the angle of Lode, ε_v^p is the plastic volumetric strain, s is the suction, and ΔT is the difference between the current temperature T and a reference temperature T_0.

The elastic volumetric strain increment is given by

$$\dot{\varepsilon}_v^e = \left(\frac{\kappa_p}{1+e} + \alpha_{pT}\Delta T\right)\frac{\dot{p}}{p} + \frac{\kappa_s}{1+e}\frac{\dot{s}}{s+0.1} + \alpha_T\dot{T}$$

(B.2)

where κ_p is the elastic stiffness parameter for changes in net mean stress, κ_s is the elastic stiffness parameter for changes in suction, e is the void ratio, and α_{pT} and α_T are isotropic thermal expansion coefficients of the solid skeleton.

The elastic deviatoric strain increment is defined as

$$\dot{\varepsilon}_s^e = \frac{\dot{J}}{G}$$

(B.3)

with G the shear modulus.

To take into account experimental evidences about the behaviour of highly expansive materials some modifications were introduced in the elastic stiffness parameters with respect to the original version of the BBM. Thus, the elastic stiffness parameter for changes in net mean stress depends on suction through the law

$$\kappa_p = \kappa_{p0}\left(1 + \alpha_{ps}s\right)$$

(B.4)

where κ_{p0} is the elastic stiffness parameter in saturated conditions and α_{ps} is a material parameter. The elastic stiffness coefficient for changes in suction depends on net mean stress according to the expression

$$\kappa_s = \kappa_{s0}\left(1 + \alpha_{sp} \ln \frac{p}{p_{ref}}\right) \tag{B.5}$$

where κ_{s0} and α_{sp} are material parameters.

The variation of the compressibility coefficient with suction is given by the law (Alonso et al., 1990)

$$\lambda_s = \lambda_0\left[(1 - r)\exp(-\beta s) + r\right] \tag{B.6}$$

where r and β are material parameters.

The pre-consolidation pressure p_0 is assumed a function of suction and temperature. The dependence on temperature is adopted equal to that proposed by Hueckel & Borsetto (1990)

$$p_c = p_0^* + \gamma_T \Delta T \tag{B7}$$

where p_0^* is the pre-consolidation stress for saturated state at the reference temperature, and γ_T is a material parameter that govern the evolution of the yield surface with temperature. For the dependence on suction the same relationship as postulated by Alonso et al. (1990) is considered

$$p_0 = p_r\left(\frac{p_c}{p_r}\right)^{\frac{\lambda_0 - \kappa_{p0}}{\lambda_s - \kappa_{p0}}} \tag{B8}$$

where p_r is a reference stress, and λ_0 is the slope of the virgin consolidation line at saturated state.

Some experimental results indicate that coefficient α_T depends on temperature and, slightly, on pressure (Baldi et al., 1988; Hueckel & Baldi, 1990; Cekerevac & Laloui, 2004). Hueckel & Borsetto (1990) have suggested the following expression

$$\alpha_T = \alpha_0 + 2\alpha_2\Delta T + (\alpha_1 + 2\alpha_3\Delta T)\ln\frac{p}{p_0} \tag{B.9}$$

where α_i are coefficients related to the thermal expansion of the soil skeleton.

For the coefficient γ_T the expression suggested by Hueckel & Borsetto (1990) was adopted

$$\gamma_T = 2(a_1 + a_2|\Delta T|) \tag{B10}$$

where and a_1 and a_2 are parameters (usually negative).

The hardening law depends on plastic volumetric strain according to the following expression

$$\dot{p}_0^* = \frac{1+e}{\lambda_0 - \kappa}p_0^*\dot{\varepsilon}_v^p \tag{B.11}$$

with κ defined as

$$\kappa = \left(\frac{\kappa_p}{1+e} + \alpha_{pT}\Delta T\right)(1+e) \tag{B.12}$$

and α_{pT} given by

$$\alpha_{pT} = \alpha_1 + \alpha_3\Delta T \tag{B.13}$$

Experimental data of the thermo-hydro-mechanical response obtained on compacted samples of MX-80 bentonite were used to define the parameters of the adopted model.

B.2.1 Behaviour at ambient temperature

Figure B.1 presents experimental data obtained on compacted samples of MX-80 bentonite tested at different temperatures and suctions (Villar, 2005; Tang et al., 2008). Figure B.1(a) shows the variation of pre-consolidation stress on suction while Figure B.1(b) defines the dependence of coefficients κ_p and λ_s on suction. These results were used to determine parameters in equations (B.4) and (B.6).
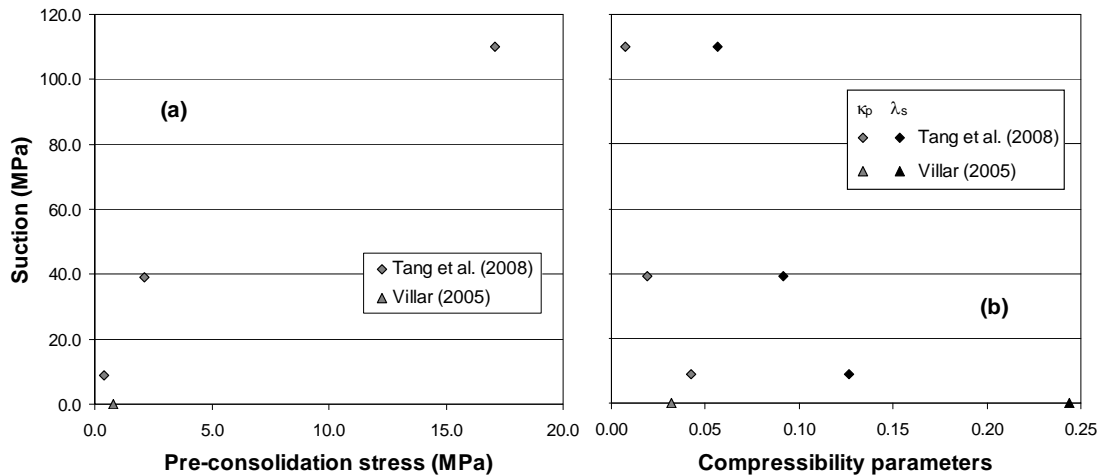
Figure B.1. (a) Pre-consolidation stress as a function of suction; (b) compressibility parameters against suction.

Villar (2005) has done suction controlled oedometer tests on MX-80 bentonite samples compacted at nominal dry densities of 1.69 and 1.79 Mg/m^3. In one case the suction was imposed using the axis translation method while in the other case the relative humidity of the atmosphere in contact with the sample was controlled. Samples were hydrated at a very low constant vertical load (0.1 MPa). Figure B.2 presents experimental results of the evolution of void ratio as a function of the suction. In order to use a logarithmic scale a constant value of 0.1 MPa has been added to all suction values plotted in this figure. These experimental results were used to define parameters in equation (B.5).

Figure B.2. Evolution of void ratio as a function of suction [from Villar (2005)].

B.2.2 Volumetric response under variable temperature

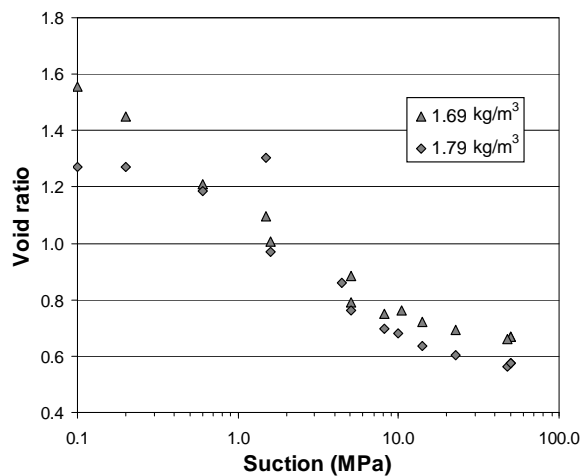Experimental results obtained by Tang et al. (2008) have been used to characterize the response of compacted bentonite samples under temperature variations. Samples of MX-80 bentonite were compacted in an isotropic cell with a water content of 10.0 % and at a dry density of 1.78 Mg/m^3.

Initial conditions in all cases were mean total stress equal to 0.1 MPa, suction 110 MPa, and temperature 25 ºC. Table B.1 indicates the paths followed in the simulated tests; each path corresponds to a loading at constant suction and temperature, or a temperature change at constant suction and total stress.

Four tests were simulated that includes different OCR of the samples. Thus T1 corresponds to a case where OCR is equal to 21 while T4 represents a situation where the sample is normally consolidated (OCR equal to 1). More interesting are the results obtained in tests T2 and T3. The OCR is similar in both cases (3.8 and 3.4 respectively) but while the behaviour in T3 corresponds with that expected in over-consolidated samples the response in T2 is similar to that observed in normally consolidated samples. This indicates that the volumetric thermal behaviour is affected by stress and suction (Tang et al., 2008).

Step	1			2			3		
Test	p (MPa)	s (MPa)	T (ºC)	p (MPa)	s (MPa)	T (ºC)	p (MPa)	s (MPa)	T (ºC)
T1	0.1	39	25	0.1	39	80			
T2	0.1	9	25	0.1	9	80			
T3	5	110	25	5	110	80			
T4	0.1	39	25	5	39	25	5	39	80

Table B.1. Steps followed in the simulation of laboratory experiments carried out by Tang et al. (2008).

Figure B.3 shows experimental data obtained by Tang et al. (2008) and results of the simulations. As it can be seen, the adopted model is able to reproduce the main trend observed in the tests. Even from a quantitative point of view, predictions agree quite well with experimental observations.
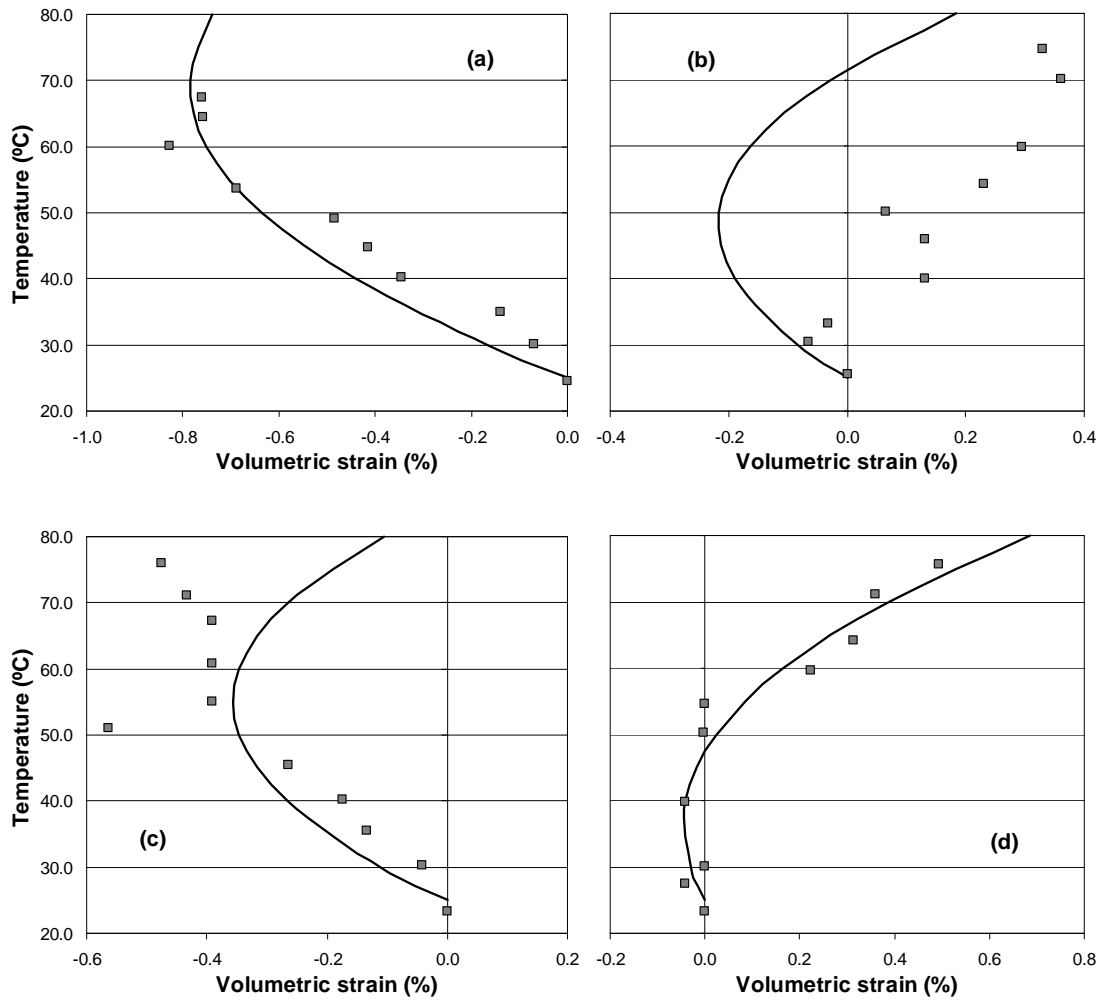
Figure B.3. Volumetric strain due to heating under constant stress and suction; (a) test T1; (b) test T2; (c) test T3; (d) test T4. Symbols are experimental data and continuous lines numerical results.

B.2.3 Mechanical response at constant suction and temperature

Figure B.4 shows experimental results of the pre-consolidation stress as a function of suction and temperature (Tang et al., 2008). In all cases, the increase in temperature reduces the values of the pre-consolidation stress. These results were used to define parameters a_1 and a_2 appearing in equation (B.10).
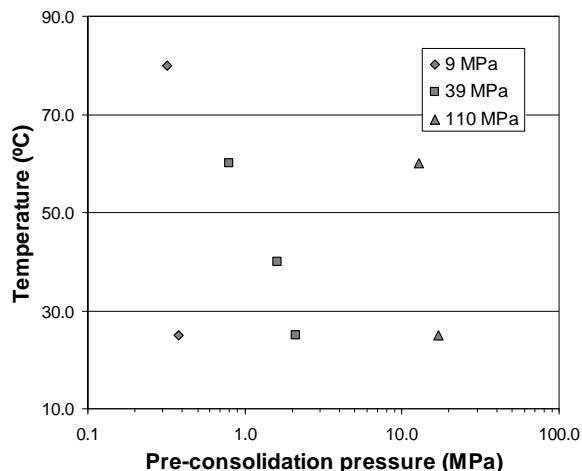
Figure B.4. Pre-consolidation pressure obtained at different suctions as a function of temperature [from Tang et al. (2008)].

B.2.4 Parameters of the mechanical constitutive model

Table B.2 summarizes the parameters of the constitutive model adopted to simulate the mechanical behaviour of the bentonite blocks used in the engineered barrier of the TBT field experiment.

| κ_{p0}	α_{ps} (MPa^{-1})	κ_{s0}	α_{sp}	p_{ref} (MPa)
0.045	-0.007	0.15	0.0	-
α_0 (ºC^{-1})	α_1 (ºC^{-1})	α_2 (ºC^{-2})	α_3 (ºC^{-2})	a_1 [MPa·(Cº)$^{-1}$]
-1.0x10^{-4}	7.0x10^{-5}	4.0x10^{-6}	0.0	-1.0x10^{-4}
a_2 [MPa·(Cº)$^{-2}$]	λ_0	β (MPa^{-1})	r	p_r (MPa)
0.0	0.25	0.05	0.35	0.05

Table B.2. Parameters of the mechanical constitutive model adopted for bentonite blocks.

B.3 Parameters, boundary and initial conditions used in the analysis of TBT

Parameters presented below describe the thermo-hydro-mechanical behaviour of the different materials used in the Base Case of the numerical analysis of the TBT in situ experiment. Most of these parameters were determined using experimental data reported in Chapter 6.

Boundary conditions were defined according to guidelines given in Åkesson (2006). Initial conditions were determined using experimental data of the different variables measured in the test at the time when the heating was started.

B.3.1 Thermal parameters

Thermal conductivity

Material	Law	λ_{dry} [W/(m·K)]	λ_{sat} [W/(m·K)]
Rock		2.6	2.6
Steel		50.2	50.2
PEEK		0.25	0.25
Concrete	$\lambda_T = \lambda_{sat}\sqrt{S_l} + \lambda_{dry}\left(1 - \sqrt{S_l}\right)$	1.7	1.7
Pellets		0.3	1.3
Sand		0.4	1.7
Bentonite		0.3	1.3

Specific heat

Material	Rock	Steel	PEEK	Concrete	Pellets	Sand	Bentonite
c [J/(kg·K)]	800.0	460.0	2000.0	750.0	950.0	900.0	950.0

B.3.2 Hydraulic parameters

Retention curve

Material	Law	P_0 (MPa)	m	P_d (MPa)	d
Rock		10.0	0.55	-	-
Steel	$S_e = \dfrac{S_l - S_{lr}}{S_{ls} - S_{lr}} = \left[1 + \left(\dfrac{P_g - P_l}{P_0}\right)^{\frac{1}{1-m}}\right]^{-m}$	1.0×10^{-4}	0.50	-	-
PEEK		1.0×10^{-4}	0.50	-	-
Concrete		10.0	0.55	-	-
Pellets		0.50	0.19	1000.0	1.5
Inner sand	$S_e = \dfrac{S_l - S_{lr}}{S_{ls} - S_{lr}} = \left[1 + \left(\dfrac{P_g - P_l}{P_0}\right)^{\frac{1}{1-m}}\right]^{-m} f_{rc}$	0.20	0.39	700.0	1.1
Outer sand		0.15	0.39	700.0	1.1
Bentonite 1[†]	$f_{rc} = \left(1 - \dfrac{P_g - P_l}{P_d}\right)^{d}$	35.0	0.42	1000.0	1.0
Bentonite 2[‡]		35.0	0.42	1000.0	1.0

[†] Bentonite for blocks C1 to C4 and R1 to R6.   [‡] Bentonite for blocks R7 to R12.

<u>Intrinsic permeability</u>

Material	Law	$\mathbf{k}_0$ (m^2)	ϕ_0
Rock		1.0x10^{-19}	0.015
Steel		1.0x10^{-22}	0.010
PEEK		1.0x10^{-22}	0.010
Concrete	$\mathbf{k} = \mathbf{k}_0 \dfrac{\phi^3}{(1-\phi)^2} \dfrac{(1-\phi_0)^2}{\phi_0^3}$	1.0x10^{-19}	0.015
Pellets		1.0x10^{-19}	0.61
Sand		1.0x10^{-15}	0.25
Bentonite		3.0x10^{-21}	0.35

B.3.3 Mechanical parameters

Parameters of the mechanical constitutive model adopted for the bentonite blocks are given in Table B.2. The other materials were assumed elastic and parameters defining their behaviour are indicated in the table below.

Material	E (MPa)	ν
Rock	5.0x10^4	0.25
Steel	2.1x10^5	0.20
PEEK	20.0	0.25
Concrete	3.0x10^4	0.20
Pellets	20.0	0.25
Inner sand	55.0	0.25
Outer sand	25.0	0.25

B.3.4 Boundary conditions

<u>Heat flux</u>

The same protocol as that applied in the test field was used (Table 6.2).

<u>Water flux</u>

Fluxes indicated below were calculated following the assumptions described in paragraph 6.3.2.

Time interval	Water flux (kg/s)		
(days)	Lower pipes	Upper pipes	Mats
1 ~ 25	2.411×10^{-4}		
25 ~ 75	1.424×10^{-4}		
75 ~ 90	7.176×10^{-5}		
90 ~ 108	4.308×10^{-5}	-	
108 ~ 223	3.724×10^{-6}		-
223 ~ 377	1.037×10^{-5}		
377 ~ 594	1.349×10^{-5}	1.349×10^{-5}	
594 ~ 766	2.062×10^{-5}	2.062×10^{-5}	
766 ~ 1000	1.561×10^{-5}	1.561×10^{-5}	
1000 ~ 1500	1.505×10^{-6}	1.505×10^{-6}	1.505×10^{-6}

B.3.5 Initial conditions

Material	P_l (MPa)	P_g (MPa)	T (ºC)	ϕ
Rock	Figure 6.8			0.010
Steel				0.010
PEEK				0.010
Concrete				0.010
Pellets	-49.9	0.1	20.0	0.613
Inner sand				0.302
Outer sand				0.358
Bentonite 1				0.415
Bentonite 2				0.397